AD-A133 206 INVESTIGATION OF FATIGUE CRACK-GROWTH RESISTANCE OF ALUMINUM ALLOYS UNDER.. (U) NORTHROP CORP HAWTHORNE CA AIRCRAFT DIV G V SCARICH ET AL. APR 83 NOR-83-84 1/2

UNCLASSIFIED N00019-81-C-0550 F/G 11/6 NL

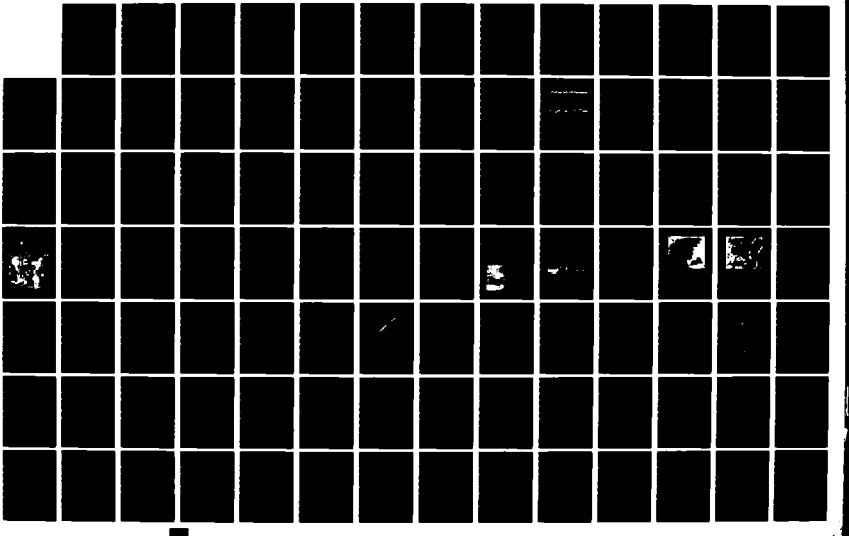

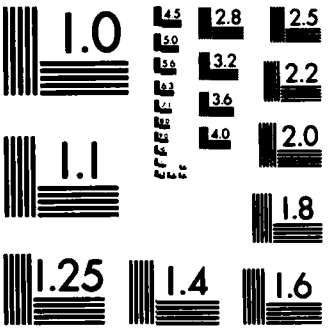

INVESTIGATION OF FATIGUE CRACK-GROWTH RESISTANCE OF ALUMINUM ALLOYS UNDER SPECTRUM LOADING

G.V. Scarich
P.E. Bretz

NORTHROP CORPORATION
AIRCRAFT DIVISION
ONE NORTHROP AVENUE
HAWTHORNE, CALIFORNIA 90250

APRIL 1983

TECHNICAL REPORT
FINAL REPORT FOR PERIOD 30 SEPTEMBER 1981-30 OCTOBER 1982

APPROVED FOR PUBLIC RELEASE: DISTRIBUTION UNLIMITED

DEPARTMENT OF THE NAVY
NAVAL AIR SYSTEMS COMMAND
WASHINGTON, D.C. 20361

UNCLASSIFIED

SECURITY CLASSIFICATION OF THIS PAGE (When Data Entered)

REPORT DOCUMENTATION PAGE		READ INSTRUCTIONS BEFORE COMPLETING FORM
1. REPORT NUMBER	2. GOVT ACCESSION NO. AD-A133206	3. RECIPIENT'S CATALOG NUMBER
4. TITLE (and Subtitle) Investigation of Fatigue Crack-Growth Resistance of Aluminum Alloys under Spectrum Loading		5. TYPE OF REPORT & PERIOD COVERED Final 1 Oct 81 – 30 Nov 1982 ✓
		6. PERFORMING ORG. REPORT NUMBER NOR-83-84
7. AUTHOR(s) G.V. Scarich (Northrop) P.E. Bretz (Alcoa)		8. CONTRACT OR GRANT NUMBER(s) N00019-81-C-0550
9. PERFORMING ORGANIZATION NAME AND ADDRESS Northrop Corporation, Aircraft Division One Northrop Avenue Hawthorne, California 90250		10. PROGRAM ELEMENT, PROJECT, TASK AREA & WORK UNIT NUMBERS N00019-81-PR-RL127
11. CONTROLLING OFFICE NAME AND ADDRESS Department of the Navy Naval Air Systems Command Washington, D.C. 20361		12. REPORT DATE April 1983
		13. NUMBER OF PAGES
14. MONITORING AGENCY NAME & ADDRESS(if different from Controlling Office)		15. SECURITY CLASS. (of this report) Unclassified
		15a. DECLASSIFICATION/DOWNGRADING SCHEDULE

16. DISTRIBUTION STATEMENT (of this Report)

Approved for public release; distribution unlimited

17. DISTRIBUTION STATEMENT (of the abstract entered in Block 20, if different from Report)

18. SUPPLEMENTARY NOTES

19. KEY WORDS (Continue on reverse side if necessary and identify by block number)

Aluminum Alloys	Spectrum Loading
2024 7475	Retardation
2124 Microstructure	Fracture Toughness
7050 Temper	Constant-Amplitude Loading
7075 Fatigue Crack Growth	Variable-Amplitude Loading

20. ABSTRACT (Continue on reverse side if necessary and identify by block number)

The purpose of this program is to obtain metallurgical guidelines and test methodologies for selection and development of spectrum fatigue resistant, high strength aluminum alloys for application to aircraft structures. Described in this report are the results of baseline characterizations of ten high strength aluminum alloys. Also described are results of fatigue crack-growth tests under two F-18 load spectra and under modifications of these spectra.

DD FORM 1 JAN 73 1473 EDITION OF 1 NOV 65 IS OBSOLETE

UNCLASSIFIED

SECURITY CLASSIFICATION OF THIS PAGE (When Data Entered)

Ten commercial 2XXX and 7XXX aluminum alloys were chosen and characterized for chemical composition, microstructure, tensile properties, and fracture toughness. Fatigue crack propagation (FCP) tests were conducted on specimens of each alloy for both constant-amplitude loading (including the near-threshold region) and two F-18 load spectra. One of the spectra was dominated by tension loads and the other contained tension and compression loads of nearly equal magnitude. The spectrum FCP testing was performed at maximum peak stress of 145 MPa (21 ksi) with limited testing at 103 and 169 MPa (15 and 24.5 ksi) to obtain additional data at the low and high end of the crack-growth range. Pertinent fracture surface features were documented on the spectrum fatigue specimens. For completeness, this report on the second phase of the program includes the results from the first phase.

For fatigue crack-growth testing under constant amplitude loading, the significant observations were that: 1) the differences in fatigue crack-growth rates were greatest in the near-threshold regime, where 2024-T351 and 7475-T651 showed the highest resistance to FCP and 2) FCP resistance varied with stress intensity factor range (ΔK). For example, in contrast to its excellent near threshold crack-growth resistance, 7475-T651 had the lowest resistance to FCP for ΔK greater than 6 MPa $\sqrt{m}$.

For spectrum testing at the maximum peak stress of 145 MPa (21 ksi):

1. The ranking of the alloys by spectrum life is the same for both spectra, except for 2020-T651. The alloys ranked as follows with their percentage of life relative to 2024-T351, averaged for both spectra, shown in parenthesis: 2024-T351 (100%), 7475-T651 (91%), 2324-T39 (87%), 2020-T651 (84%), 7475-T7351 (77%), 7050-T73651 (76%), 7075-T7351 (64%), 2124-T851 (55%), 7075-T651 (53%), and 2024-T851 (42%).
2. For each material the tension-dominated spectrum consistently resulted in longer lives than the tension-compression spectrum.

Seven of the ten alloys were spectrum fatigue tested using two independent modifications of the baseline spectra. One modification, the racetrack method, was used to eliminate 43 percent of the low-amplitude cycles to reduce testing time. The differences in spectrum fatigue lives between the modified and baseline spectra were probably small enough so that the selection of one alloy over another would not be significantly affected.

The second modification was made to determine the importance of compressive load cycles. To accomplish this, all compression load points were eliminated from the tension-compression spectrum. There were significant increases in spectrum lives compared to the baseline spectrum, but the ranking of the seven alloys for this modified spectrum was identical to that for the two baseline spectra.

In general, the spectrum performance rankings could not be correlated with yield strength or constant-amplitude FCP resistance. However, spectrum performance could be correlated with fracture toughness; specifically for the testing at 145 and 169 MPa, FCP life for both spectra generally increased with increased fracture toughness. Also the alloys that deform by planar slip generally had longer spectrum fatigue lives than those that deformed more homogeneously. The effects of deformation mode and grain structure will be addressed in the next phase where special heats will be produced and fatigue behavior determined.

PREFACE

This report was prepared by the Northrop Corporation, Aircraft Division, Hawthorne, California, under Naval Air Systems Command Contract N00019-81-C-0550. Mr. M. Valentine of Naval Air Systems Command (Code AIR-5304B4) was the project engineer.

Northrop Corporation, Aircraft Division, was the prime contractor, with Mr. G.V. Scarich serving as the program manager. Mr. S. Hsu and Mr. J. Steele were responsible for all the spectrum testing and data reduction while Mr. P.G. Porter was responsible for spectrum selection, generation and modification.

Aluminum Company of America, Alcoa Technical Center was a major participant in the program. Dr. P.E. Bretz served as the Alcoa program manager with Mr. R.R. Sawtell responsible for microstructural analyses. Alcoa was intimately involved in all the phases of the program and was primarily responsible for determining baseline mechanical properties and microstructural characterization.

The contractor report number is NOR 83-84. This report covers work from 30 September 1981 through 31 October 1982.

The authors also wish to acknowledge R. Schmidt of NAVAIR, and B.J. Mays, A.H. Freedman, G.R. Chanani, S.W. Averill, R.J. Kar, A.A. Sheinker, D.R. Drott, I.E. Sedor and K.S. Bond-Bates of Northrop for their cooperation and support during the various phases of the program.

TABLE OF CONTENTS (Concluded)

TABLE OF CONTENTS

LIST OF ILLUSTRATIONS

LIST OF ILLUSTRATIONS (Concluded)

LIST OF TABLES

ABBREVIATIONS AND SYMBOLS

a	Crack-length
a_i	Initial crack length
a_c	Current crack length
a_f	Final crack length
B	Specimen thickness
COD	Crack opening displacement
da/dH	Spectrum crack-growth rate
da/dN	Crack-growth rate (constant amplitude)
F	Failure
FCGR	Fatigue-crack growth rate
FCP	Fatigue-crack propagation
H	Simulated flight hours or half height of compact tension specimen
K	Stress-intensity factor
K_{hmax}	Stress-intensity factor at largest (highest) peak of spectrum
K_{hmin}	Stress-intensity factor at smallest (lowest) valley of spectrum
K_{max}	Maximum stress intensity factor
K_{Ic}	Plane strain fracture toughness
K_Q	Conditional fracture toughness, test did not meet all the ASTM E399 validity criteria
L-T	Crack growth on plane normal to the rolling direction (L) of the plate in a direction transverse (T) to the rolling direction (per ASTM E399)
N	Number of cycles
P_{hmax}	Load at largest (highest) peak of a spectrum
P_{hmin}	Load at smallest (lowest) valley in a spectrum
P_{max}	Peak Load
P_{sm}	Mean spectrum load
R	Stress or load ratio = P_{min}/P_{max}
SEM	Scanning electron microscope/microscopy
SFCGR	Spectrum fatigue crack growth rate

ABBREVIATIONS AND SYMBOLS (Concluded)

TC	Tension-compression, horizontal hinge tail moment spectrum
TCR	Racetrack-modified, tension-compression spectrum
TCZ	Tension-compression-zero spectrum
TD	Tension-dominated, lower wing root spectrum
TDR	Racetrack-modified, tension-dominated spectrum
TEM	Transmission electron microscope/microscopy
T/2	Mid-thickness (center) location in a plate
T/4	Quarter-thickness location in a plate
3T/4	Three-quarter thickness location in a plate
W	Specimen width
YS	Yield strength
ΔK	Stress-intensity range
ΔK_h	Overall stress-intensity range of a spectrum
ΔP	Load range
ΔP_h	Overall load range of a spectrum
$\Delta\sigma$	Stress range: Algebraic difference between successive valley and peak (positive or increasing) or between successive peak and valley (negative or decreasing).
$\Delta\sigma_h$	Overall stress range in a spectrum
σ	Applied stress
σ_{hmax}	Stress at largest (highest) peak of spectrum
σ_{hmin}	Stress at smallest (lowest) valley of a spectrum
σ_{sm}	Spectrum mean stress

I. INTRODUCTION

Fatigue crack growth behavior under variable amplitude loading is increasingly being used in the selection of materials for aircraft structures and their design, particularly for fatigue critical structures. This is supplanting the selection of materials based on constant-amplitude fatigue crack growth resistance because the life of an aircraft structure cannot be predicted reliably using constant-amplitude fatigue crack growth data and existing life prediction techniques. Research in the last decade[1-12] has shown that load sequences have a considerable effect on fatigue-crack propagation (FCP) behavior. In particular, the application of overloads or a few cycles at high tensile loads may cause retardation; that is, a temporary decrease in fatigue-crack growth rate during subsequent lower-amplitude cycles. Most of the work in the last decade was focused on understanding the effects of single overloads on fatigue crack growth rates.[1-10] Recently more emphasis is being placed upon the evaluation of fatigue crack growth under complex spectrum loading[11-14] simulating the loading experienced by aircraft structures.

The nature of a spectrum can vary widely depending on a particular component and type of aircraft. Depending on the specific details of load spectra, FCP resistance for a given material also can vary widely. The reasons for differences in FCP resistance for the same material in different spectra are generally unknown, since the load spectra are complex and the interactions between alloy microstructure and variable amplitude load histories are not well understood.

Research in the last decade[1-4, 15-19] on high strength aluminum alloys has identified several metallurgical factors which influence FCP resistance for constant amplitude loading: alloy purity (Fe, Si content), temper, alloy content (e.g., Cu content), and dispersoid type (e.g., $Al_{12}Mg_2Cr$ in 7075 vs. Al_3Zr in 7050). However, the influence of these microstructural features

on crack growth is not the same at intermediate and high growth rates ($\geq 10^{-8}$m/cycle (2.5×10^{-7}in./cycle)) as it is at near-threshold rates ($<10^{-8}$m/cycle). For example, overaging from a T6 temper to a T7 temper reduces FCP rates by a factor of two at intermediate stress intensities (ΔK) but can increase crack growth rates by a factor of ten at low ΔK. These studies demonstrate that different microstructural features control constant-amplitude FCP behavior at different ΔK values. Details of these microstructural/FCP behavior relationships will be addressed in Sections 3.6 and 3.7 of this report.

The same level of understanding regarding microstructural effects on FCP under variable amplitude loading does not exist. Whereas constant amplitude loading characterizes the steady state FCP response of an alloy, FCP under variable amplitude loading includes transient material responses not present in constant amplitude FCP. Therefore, the understanding of microstructural effects on constant amplitude FCP behavior is not sufficient to rationalize spectrum fatigue performance. In particular, the ability of an alloy to retard crack growth following a tensile overload is an important transient characteristic for assessing FCP life. However, since the present knowledge regarding the effect of microstructure on retardation behavior of aluminum alloys is limited to studies involving simple overload spectra, the results under spectrum loading at present cannot be understood.

Several mechanisms have been proposed to explain the observed retardation behavior following simple overloads. These include residual compressive stresses at the crack-tip,[20, 21] crack closure,[22-24] changes in the crack-tip plastic zone size,[1, 20, 25] crack-blunting,[1, 26] or combinations of these. A number of empirical models, based on either the crack closure[22, 23] or plastic zone size[20, 21] concepts, have been proposed that quantitatively take retardation into account in predicting FCP behavior. These models achieve satisfactory results only under certain specified conditions. However, when the test conditions are changed or broadened to include additional variables such as those existing in real spectra, the models usually fail to predict observed crack-growth lives.

The major weakness of all of these models is that they do not take into account either metallurgical or the environmental factors that influence FCP. For instance the Willenborg model predicts that materials with the same yield

strength will exhibit similar retardation behavior.[20] Chanani[1] found that this was not the case for 2024-T8 and 7075-T73 heat treated to the same yield strength. He concluded that metallurgical variables such as precipitate morphology, dislocation interactions, and cyclic hardening exponent, have to be taken into account to explain the differences between the crack growth rates. Sanders, et al.,[2] had identified microstructural features such as precipitate morphology, intermetallic constituent particles, and dispersoid size as influencing FCP. Improved analytical life prediction capabilities would result if microstructure/load history interactions for spectrum FCP are understood and incorporated in such models.

The purpose of the multiphase NAVAIR program (N00019-80-C-0427,[27] N00019-81-C-0550, and N00019-82-C-0425) is to perform a detailed metallurgical investigation of fatigue behavior and to simplify complex load histories into generic spectra. These spectra will be representative of certain classes of applications and will provide information for development of fatigue resistant alloys. As a major part of this effort, attention will be given to identifying metallurgical factors in high strength aluminum alloys which control FCP behavior under spectrum loading. This knowledge of load history/microstructure interactions is essential to the development of criteria by which complex load histories can be standardized and simplified for materials evaluation.

The development of standardized and/or simplified load spectra offers several advantages in characterizing the fatigue performance of engineering materials and designing fatigue resistant alloys. It is presently not cost-effective to develop alloys for high resistance to FCP under spectrum loading, since a wide variety of load histories must be considered. If a small number of standardized spectra existed, more meaningful tests which consider spectrum loading could be included in alloy development/selection programs. Standardized load spectra also would provide a common data base for comparisons of fatigue performance among various materials. Selected existing life prediction tools will be evaluated, and the incorporation of metallurgical factors in these models will be examined.

This report describes the work completed in Phase II of this program and includes pertinent results from Phase I[27] of this program for

completeness. Fourteen commercial 2XXX and 7XXX aluminum alloys (Figure 1) were chosen for analysis so that the influence of both purity and temper on FCP could be evaluated. In Phase I seven of the alloys were evaluated and in Phase II three additional alloys were evaluated as described below. The other four alloys and special heats will be evaluated in future phases (Figure 1). To date, ten alloys have been characterized with respect to chemical composition, microstructure, tensile properties, and fracture toughness. FCP tests were conducted on specimens of each of the ten alloys for both constant amplitude loading (including the low ΔK region) and two F-18 load spectra. One F-18 load spectrum is a tension-dominated spectrum representing the lower wing root load history, and the other is a tension-compression spectrum representing the horizontal tail hinge moment load history. In the spectrum testing, one primary stress level was used for FCGR testing, while two other stress levels were used to obtain data at the low and high ends of the crack-growth range. Fractographic examination of the spectrum fatigue specimens was used to document pertinent fracture features for each alloy.

Also described are the results of the tests performed using modified spectra. Two different types of modifications were performed independently on the baseline spectra. One modification had two goals: 1) to eliminate low amplitude cycles to reduce testing time without changing the ranking (relative life) of the alloys, and 2) to determine the importance of low amplitude cycles on the overall spectrum life. The second modification was made to determine the importance of compression cycles. Seven alloys (marked with + in Figure 1) were chosen for spectrum fatigue testing using the modified spectra. These seven alloys were chosen from the 2XXX and 7XXX aluminum alloys so that the influence of purity, temper and different alloy approaches are represented.

INVESTIGATION OF FATIGUE CRACK GROWTH OF ALUMINUM ALLOYS UNDER SPECTRUM LOADING

MATERIALS

PREVIOUS PROGRAM*	CURRENT PROGRAM**	FUTURE PROGRAMS
2024-T351 +	2020-T651	TMT2020-TX
2024-T851 +	2324-T39	2124-T351
2124-T851	7075-T651 +	7150-T6E189
7050-T73651 +		7091-T7E69
7075-T7351 +		SPECIAL HEATS WITH SELECTED MICROSTRUCTURES
7475-T651 +		
7475-T7351 +		

SPECIFIC COMPARISONS

- ALLOY PURITY (FRACTURE TOUGHNESS)
  7075 vs 7475 and 2024 vs 2124
- PRECIPITATE STRUCTURE (TEMPER)
  2024-T351 vs T851, 2124-T351 vs T851, 7475-T651 vs T7351, and 7075-T651 vs T7351
- GRAIN SIZE***
  P/M (FINE) vs I/M (COARSE) and TMT 2020 (FINE) vs CONVENTIONAL 2020 (COARSE)
- EXISTING ALLOYS vs NEW ALLOYS AND APPROACHES***
  7XXX vs 7091 P/M and 7150, and 2XXX vs 2324 and Al-Li (2020 TYPE)

GENERAL COMPARISONS

MICROSTRUCTURE
TENSILE
FRACTURE TOUGHNESS
CONSTANT-AMPLITUDE FATIGUE CRACK GROWTH

LOAD HISTORY

TWO F-18 SPECTRA (TENSION-DOMINATED AND TENSION-COMPRESSION)
THREE STRESS LEVELS
MODIFICATIONS OF THE F-18 SPECTRA – SEVERAL ITERATIONS
CRITICAL EXPERIMENTS***

SPECTRUM TEST SPECIMEN

CENTER CRACKED PANEL-6mm THICK X 100mm WIDE
L-T ORIENTATION

SPECTRUM LIFE PREDICTIONS***

* PREVIOUS PROGRAM, CONTRACT NO. N00019-80-C-0427
** CURRENT PROGRAM, CONTRACT NO. N00019-81-C-0550
*** FUTURE PLANNED EFFORT
\+ MATERIALS TESTED WITH MODIFIED SPECTRA

FIGURE 1. PROGRAM OUTLINE

The information obtained in the first two phases represents a baseline characterization of the ten alloys on which subsequent program phases will build, as well as the first steps in developing simplified spectra. In succeeding programs, alloys with systematically controlled microstructural variations will be produced and evaluated. The results of these tests as well as analyses of fatigue data, microstructural analysis, fractography, and life prediction models will be used to identify metallurgical factors and isolate those portions of each spectrum which dominate FCP behavior. From these results, guidelines and test methodologies for selection and development of fatigue resistant, high strength aluminum alloys for complex aircraft loading will be obtained.

II. EXPERIMENTAL PROCEDURE

Commercially produced 2XXX and 7XXX aluminum alloy plates in various tempers, as shown in Figure 1, and ranging in thickness from 19 to 32 mm (0.75 to 1.3 in.) were utilized in the program. Plates up to 38-mm (1.5-in) thick were evaluated in Phase I.[27]

The acceptability of each alloy was verified by chemical composition analysis and by tensile and fracture toughness (K_{Ic}) tests as described in this section. Also described in this section are the fatigue crack growth test procedures, the background on the spectra selected for use in the program and the modifications of these spectra. The plates were characterized for their tensile properties at the T/4, 3T/4, and T/2 locations (and near surface locations in Phase I). Constant load amplitude and spectrum FCP testing was performed on specimens obtained for the T/4 and 3T/4 locations of the plates to be consistent with Phase I of this study.

2.1 CHEMICAL ANALYSIS

The chemical composition of each of the plates was determined on remelt samples of material (about 65 g each) cut from the plates. A quantometer interfaced with a minicomputer was used to obtain the analyses.

2.2 METALLOGRAPHY AND FRACTOGRAPHY

Specimens for optical metallography were taken from the T/4 location in each alloy plate to insure that the observed microstructures were typical of those in the spectrum specimens. Standard metallographic procedures were used in preparing all the specimens. The specimens were examined both in the as-polished condition and following etching with Keller's reagent. Specimens for fractographic analysis were cleaned ultrasonically in an acetone bath, rinsed in alcohol, and gold-coated to improve resolution. Fractographs of the fracture surface of each specimen were obtained at crack lengths, a, of 6.4 mm (0.25 in.) and 19 mm (0.75 in.), using a scanning electron microscope (SEM).

2.3 TENSILE TESTS

Tensile tests were conducted in accordance with ASTM Standard Method B557. All tests were performed at room temperature in laboratory air on specimens taken in the longitudinal (L) orientation with respect to the rolling direction. Specimen location, nominal diameter, and gage length are listed below. It was necessary to vary specimen size in order to locate the reduced test section of each specimen at the appropriate location through the plate: center (T/2), quarter thickness (T/4), and three-quarter thickness (3T/4).

Specimen Location	No. of Specimens	Nominal Diameter		Gage Length	
		mm	(in.)	mm	(in.)
T/2	2	12.7	(0.500)	50.8	(2.00)
T/4, 3T/4	1 each	6.4	(0.250)	25.4	(1.00)

2.4 FRACTURE TOUGHNESS (K_{Ic}) TESTS

Fracture toughness tests were conducted in accordance with ASTM Standard Method E399. All tests were performed at room temperature in laboratory air on compact, C(T), specimens taken in the longitudinal (L-T) orientation with respect to the rolling direction. Two specimens were taken from each plate; the nominal thickness and nominal width of the specimens for each plate are listed below.

Nominal Plate Thickness		Nominal Specimen Thickness (B)		Nominal Specimen Width (W)	
mm	(in.)	mm	(in.)	mm	(in.)
19.0	(0.75)	19.0	(0.75)	38.1	(1.50)
31.8	(1.25)	31.8	(1.25)	63.5	(2.50)

2.5 FATIGUE CRACK PROPAGATION (FCP) TESTS UNDER CONSTANT LOAD AMPLITUDE

Constant load amplitude FCP tests were conducted over low, intermediate, and high stress intensity (ΔK) ranges on modified C(T) specimens (B = 6.35mm (0.25 in.), W = 64.8mm (2.55 in.), and H/W = 0.486) in the longitudinal (L-T) orientation. Specimens were taken from the T/4 and 3T/4 locations in each plate. All testing was performed on closed loop, servo-hydraulic test machines at a load ratio ($R = P_{min}/P_{max}$) equal to 0.33 and at a test frequency of 25 Hz. Test environment was room temperature laboratory air with high humidity (relative humidity > 90 percent).

The precracking of each specimen was conducted at R of 0.33 with visual crack length measurement. Upon attaining the desired precrack length, a, an automated test system utilizing a computer for data acquisition and machine control was used to obtain the crack growth rate (da/dN) data. Crack length was monitored continuously by an elastic compliance technique, enabling the stress intensity factor, K, to be controlled according to the equation:

$$K = K_o \exp [C (a_c - a_i)]$$

where K_o is the initial cyclic stress intensity corresponding to the starting crack length, a_i; a_c is the current crack length, and C is the constant with the dimension of 1/length.[28] A double cantilever clip-on displacement gage was used for monitoring crack opening displacements (COD). The K-decreasing tests (near-threshold) were conducted using a value for the parameter C of - 0.059 mm^{-1} (-1.5 $in.^{-1}$), and the K-increasing tests (intermediate and high K) were conducted using values of C between 0.069 mm^{-1} (1.75 $in.^{-1}$) and 0.098 mm^{-1} (2.5 $in.^{-1}$). Several visual crack length measurements were also made during each test to verify the compliance measurements.

The test procedures strictly adhered to the ASTM Standard Test Method E647 for Constant-Load-Amplitude Fatigue Crack Growth Rates Above 10^{-8} m/Cycle, and to the proposed ASTM Standard test practice for measurement of near-threshold growth rates, $da/dN < 10^{-8}$ m/cycle.[29]

2.6 SPECTRUM TESTING

Two different F-18 spectra were selected for this program. Using these two spectra, the ten materials in the program were evaluated for their spectrum fatigue crack growth behavior at three stress levels. In addition, these two spectra were modified to reveal effects of compression load cycles and small amplitude load cycles, and to shorten the testing time. Seven of the materials were selected for evaluation using these modified spectra at one stress level. The materials were selected to reveal differences in temper, purity, and microstructure. In this section, the spectra, modifications, and spectrum test procedures and analysis are described.

2.6.1 Spectrum Selection and Definition

Portions of the two F-18 spectra are shown in Figure 2, while Figure 3 shows the terminology used to describe spectrum test parameters. One is a tension-dominated spectrum representing the lower wing root load history and the other is a tension-compression spectrum representing the horizontal tail hinge moment load history. Both spectra were computer generated for the two components of the same aircraft assuming an identical sequence of events.

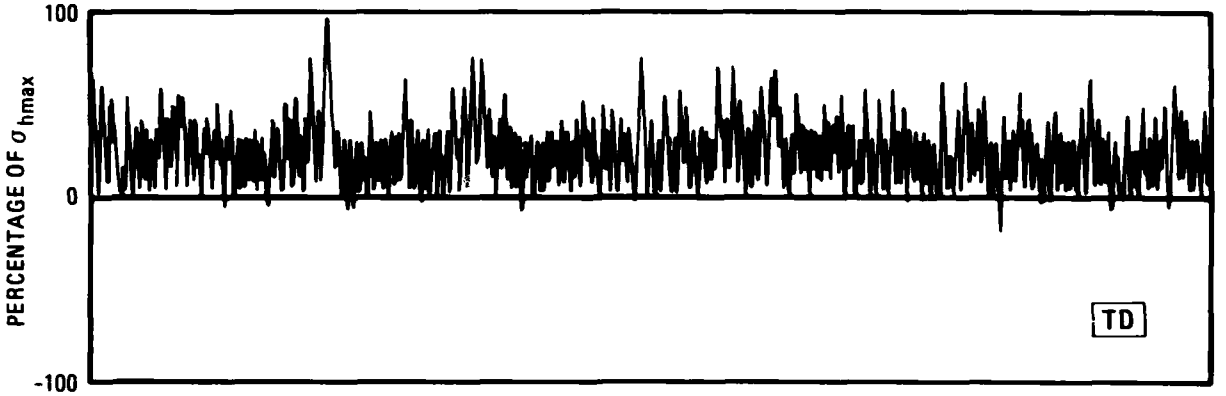

a. TENSION-DOMINATED SPECTRUM (WING ROOT)

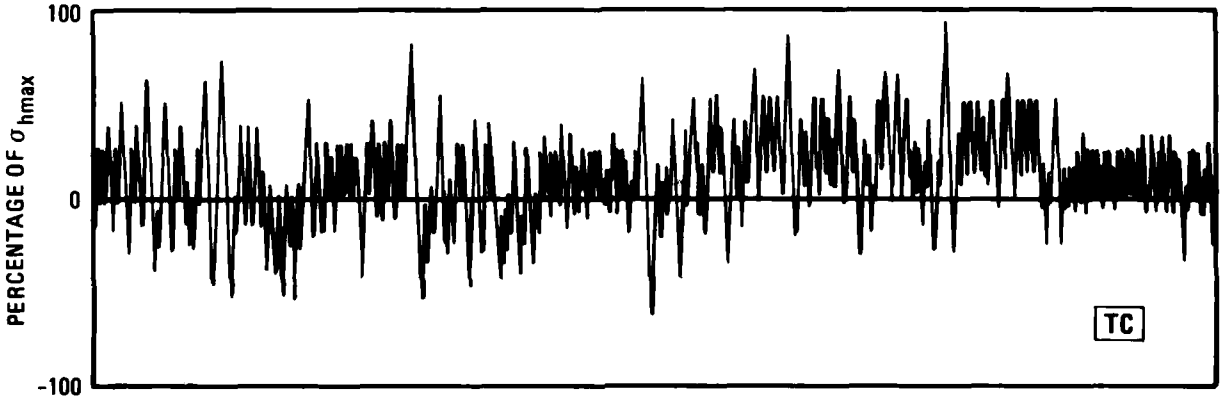

b. TENSION-COMPRESSION SPECTRUM (HORIZONTAL TAIL HINGE)

FIGURE 2. REPRESENTATIVE PORTIONS OF STRESS HISTORY OF EACH SPECTRUM

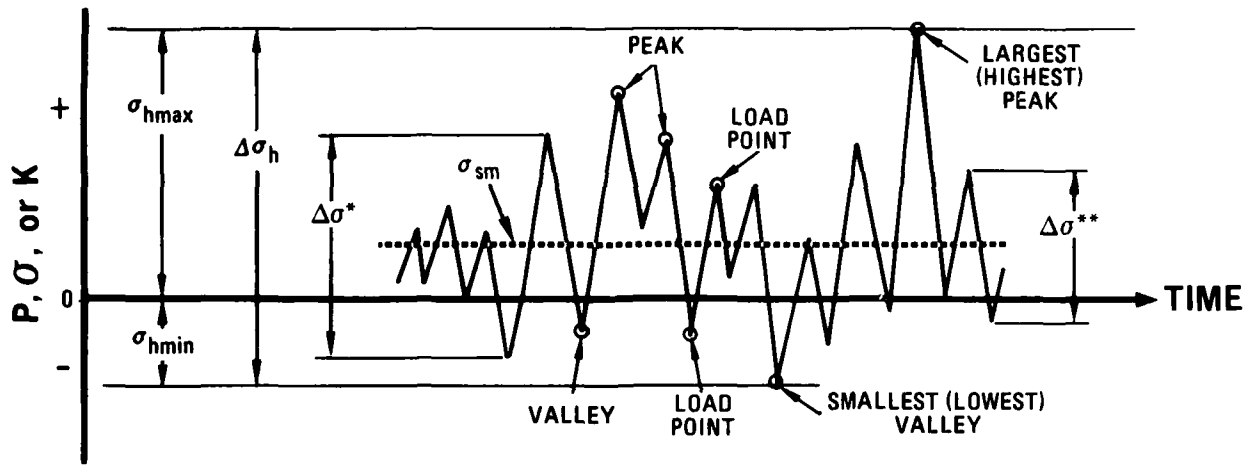

- P_{max}, σ_{max}, OR K_{max} = PEAK LOAD, STRESS, OR STRESS INTENSITY FACTOR
- P_{min}, σ_{min} OR K_{min} = MINIMUM LOAD, STRESS, OR STRESS INTENSITY FACTOR
- ΔP, $\Delta\sigma$, OR ΔK = RANGE OF LOAD, STRESS, OR STRESS INTENSITY FACTOR; ALGEBRAIC DIFFERENCE BETWEEN SUCCESSIVE VALLEY AND PEAK (POSITIVE OR INCREASING) OR BETWEEN SUCCESSIVE PEAK AND VALLEY (NEGATIVE OR DECREASING)
- P_{hmax}, σ_{hmax}, OR K_{hmax} = LOAD, STRESS, OR STRESS INTENSITY FACTOR AT LARGEST (HIGHEST) PEAK OF A SPECTRUM
- P_{hmin}, σ_{hmin}, OR K_{hmin} = LOAD, STRESS, OR STRESS INTENSITY FACTOR AT SMALLEST (LOWEST) VALLEY, I.E., THE LOWEST ALGEBRAIC VALUE IN A SPECTRUM
- ΔP_h, $\Delta\sigma_h$ OR ΔK_h = OVERALL LOAD, STRESS, OR STRESS INTENSITY RANGE, I.E., THE ALGEBRAIC DIFFERENCE BETWEEN THE LARGEST PEAK AND THE SMALLEST VALLEY OF A SPECTRUM
- P_{sm} OR σ_{sm} = SPECTRUM MEAN LOAD OR STRESS, ALGEBRAIC AVERAGE OF ALL THE PEAK AND VALLEY STRESSES OR LOADS OF A SPECTRUM

NOTES: 1. STRESS IS GROSS STRESS
2. STRESS INTENSITY IS A FUNCTION OF CRACK LENGTH
*ALSO CALLED POSITIVE OR INCREASING LOAD RANGE
**ALSO CALLED NEGATIVE OR DECREASING LOAD RANGE

FIGURE 3. DEFINITION OF TERMS

One "pass" of this basic event spectrum consists of a sequence of 250 flights representing 300 flight hours. One pass of the tension-dominated (TD) spectrum (wing root) has 4,705 load peaks and an equal number of valleys while the tension-compression (TC) spectrum (horizontal tail hinge) has 7,852 load peaks and an equal number of valleys. Since the service life of the F-18 aircraft is 6,000 hours, one service life is obtained by completion of a total of 20 passes of the above sequence. The F-18 is designed to last four lifetimes, i.e., 24,000 flight hours.

The F-18 was used as a basis for selection of spectra, stresses, and lives; therefore, a very brief and simplified description of the F-18 design follows. The F-18 (more precisely F/A-18A) is a Navy carrier-based fighter/attack aircraft. The life requirements for analysis of components are based on both durability and damage tolerance criteria. These criteria differ from the U.S. Air Force requirements of MIL-A-83444 in which the damage tolerance is based on fatigue crack growth from assumed initial flaws to various inspectability criteria. The F-18 durability and damage tolerance requirements include various combinations of fatigue crack initiation, assumed initial flaws, and growth requirements with a different number of lifetimes for each combination. The initial flaw size (or initiation) requirements are less severe than the Air Force requirements; however, the F-18 must endure more severe spectra and longer inspection intervals.

A discussion of the spectrum generation procedure follows and a schematic chart of the procedure is shown in Figure 4. The first 100 flights out of a total of 250 flights are carrier operations which initiate with a catapult launch and end with an arrested landing. The following 150 flights are field operations ending with a field landing. Field carrier landing practices are also dispersed at intervals during the field operation phase of the spectrum.

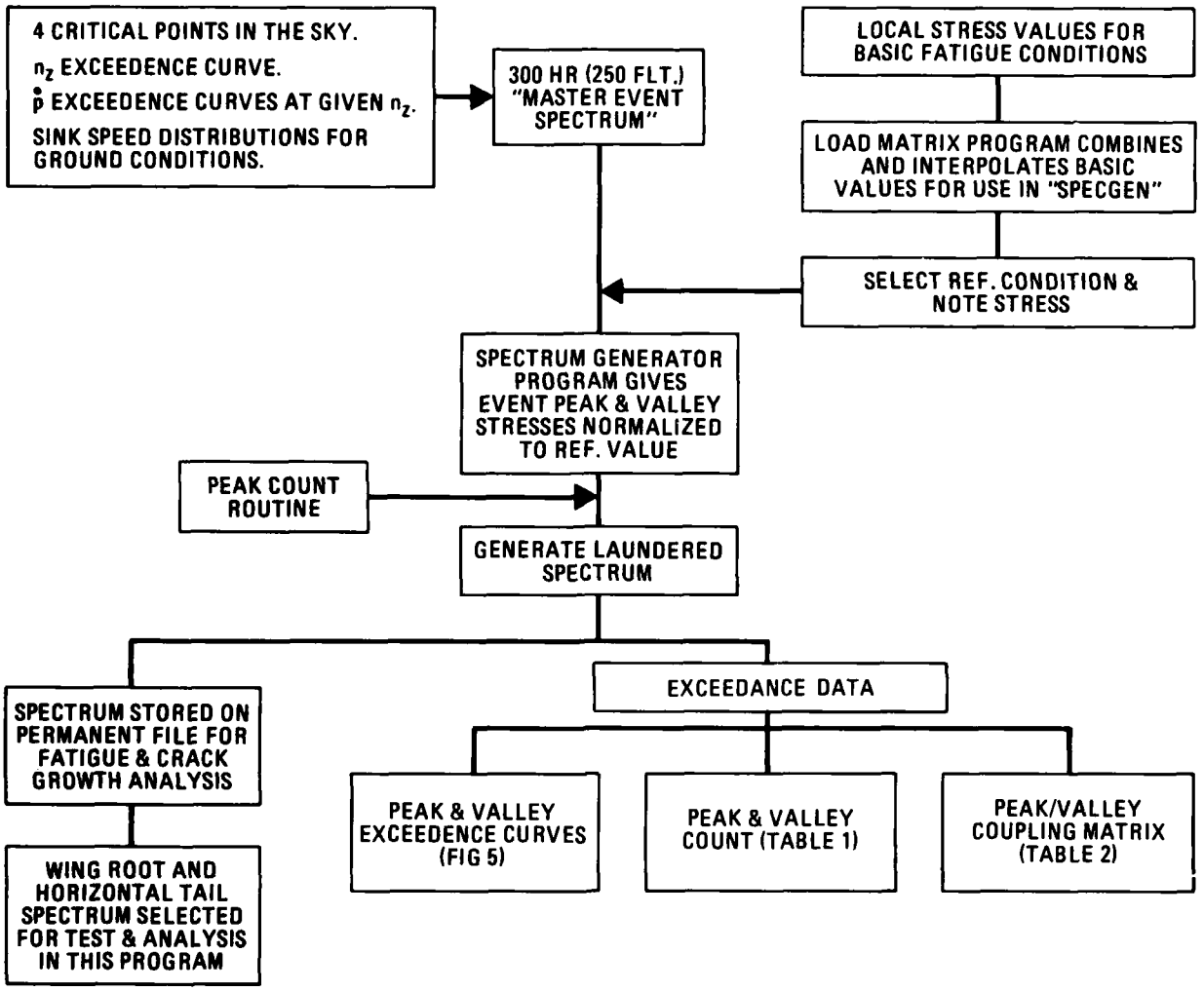

FIGURE 4. SPECTRUM GENERATION PROCEDURE

Each flight is flown at one of four critical points defined by a weight, speed, and altitude. Symmetrical events (pitch and level flight) within a flight are defined by a peak and valley load factor (n_z) sequence. Asymmetric conditions (rolls) are defined by a given roll rate (p) which gives a positive and negative load perturbation to the associated symmetrical load. Landings are defined by type (arrested landings, touch-and-go, field, etc.) and sink speed.

The load sequence for a particular location on the aircraft structure is obtained for each defined event from a table linking load magnitude with load

factor (n_z) at each critical point condition; roll rate and load factor at each critical point condition; and with sink speed for each type of landing. The table is obtained from the results of a finite element model run of the complete structure loaded by a range of unit conditions. The load values are normalized by dividing them by the load for a reference condition. This normalized load sequence is then "laundered" to eliminate small perturbations and "pass through" event peaks which are smaller than the valley of the previous event. After the laundering operation of the final load sequence is stored on a permanent file to be called up for analysis or the creation of a test tape. A listing of the spectrum is also made available in the cycle-by-cycle format. Exceedance data are summarized in the form of a graph, a table of peak and valley occurrences (spectral density function), and a tabular matrix of peak-valley couplings tabulated in increments of five percent of maximum spectrum load. These summaries for the spectra used are presented in Figure 5 and Tables 1 and 2.

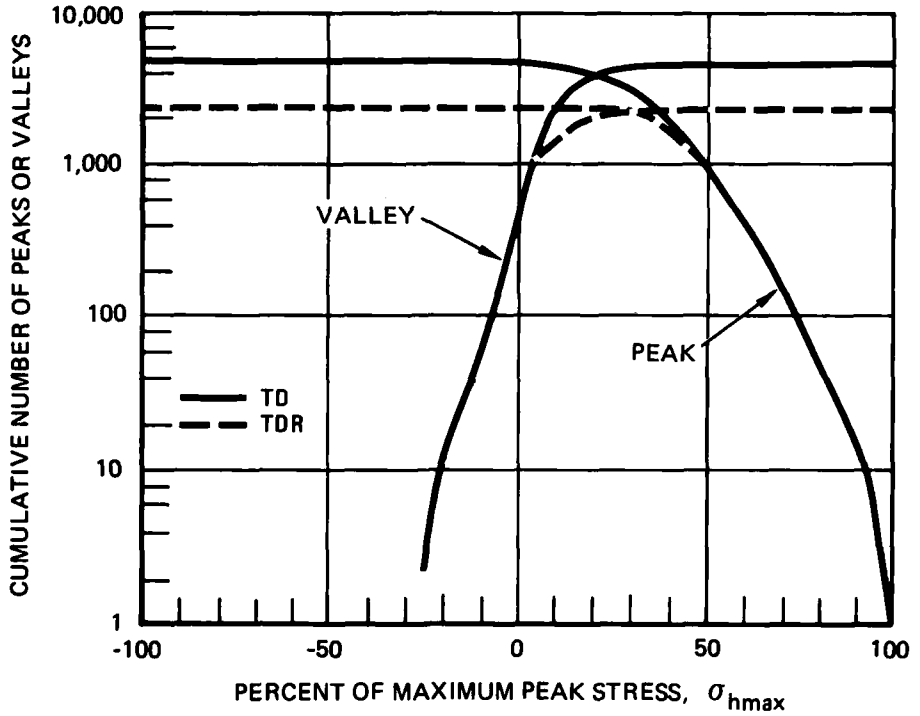

a. TENSION-DOMINATED SPECTRUM (WING ROOT)

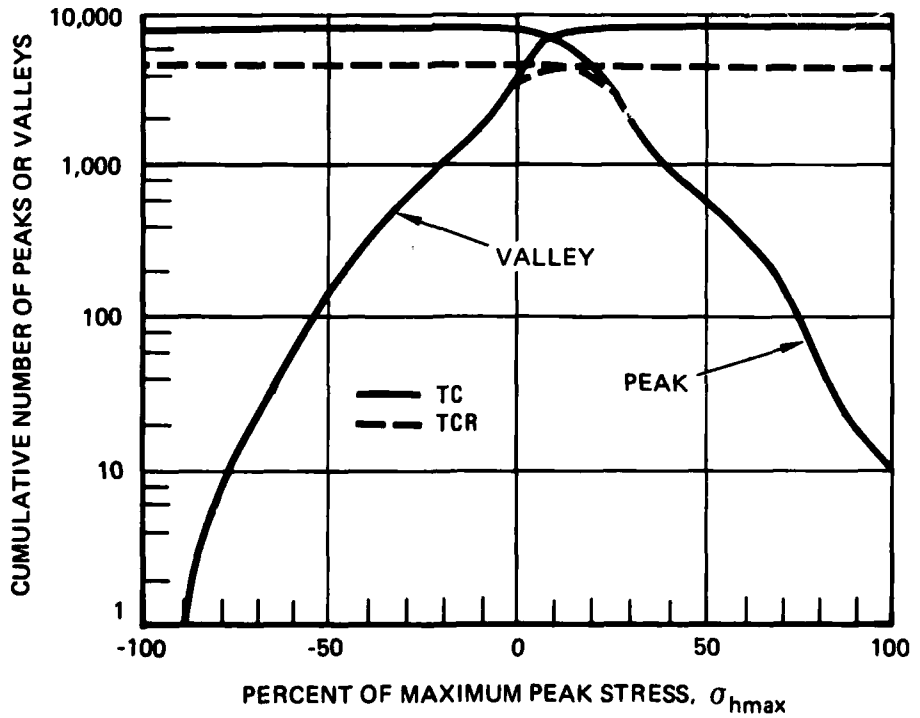

b. TENSION-COMPRESSION SPECTRUM (HORIZONTAL TAIL HINGE)

FIGURE 5. EXCEEDANCE CURVES

TABLE 1. SPECTRAL DENSITY FUNCTION

A. TENSION-DOMINATED (WING ROOT) SPECTRUM AND RACETRACK MODIFIED VERSION

PERCENT OF MAXIMUM PEAK LOAD	NUMBER OF EVENTS[a] TD (TDR)							
	PEAKS		VALLEYS		AMPLITUDES[b]		MEAN LEVELS[c]	
	TD	(TDR)	TD	(TDR)	TD	(TDR)	TD	(TDR)
P = 100	1	(1)	–	–	0	(0)	–	–
95 ≤ P < 100	7	(7)	0	(0)	0	(0)	0	(0)
90 ≤ P < 95	8	(8)	0	(0)	0	(0)	0	(0)
85 ≤ P < 90	14	(14)	0	(0)	0	(0)	0	(0)
80 ≤ P < 85	20	(20)	0	(0)	0	(0)	0	(0)
75 ≤ P < 80	42	(41)	0	(0)	0	(0)	0	(0)
70 ≤ P < 75	63	(64)	0	(0)	0	(0)	0	(0)
65 ≤ P < 70	112	(109)	0	(0)	0	(0)	5	(2)
60 ≤ P < 65	189	(182)	1	(0)	0	(0)	15	(5)
55 ≤ P < 60	123	(116)	1	(0)	0	(0)	17	(10)
50 ≤ P < 55	367	(257)	2	(0)	2	(1)	60	(26)
45 ≤ P < 50	379	(344)	3	(0)	12	(17)	144	(81)
40 ≤ P < 45	560	(788)	11	(3)	24	(34)	351	(250)
35 ≤ P < 40	770	(529)	42	(2)	89	(108)	620	(379)
30 ≤ P < 35	978	(444)	69	(4)	258	(323)	943	(700)
25 ≤ P < 30	99	(47)	169	(20)	565	(667)	1706	(1140)
20 ≤ P < 25	168	(0)	305	(45)	1085	(1219)	2198	(1438)
15 ≤ P < 20	98	(0)	437	(111)	2274	(2032)	1355	(1037)
10 ≤ P < 15	335	(0)	589	(301)	2290	(856)	453	(200)
5 ≤ P < 10	372	(0)	1192	(685)	1210	(0)	1348	(33)
0 ≤ P < 5	0	(0)	1345	(922)	1601	(0)	187	(6)
-5 ≤ P < 0	0	(0)	404	(400)	–	–	6	(0)
-10 ≤ P < -5	0	(0)	91	(91)	–	–	2	(0)
-15 ≤ P <-10	0	(0)	21	(21)	–	–	0	(0)
-20 ≤ P <-15	0	(0)	11	(11)	–	–	0	(0)
-25 ≤ P <-20	0	(0)	10	(10)	–	–	0	(0)
-30 ≤ P <-25	0	(0)	2	(2)	–	–	0	(0)
-35 ≤ P <-30	0	(0)	0	(0)	–	–	0	(0)
-40 ≤ P <-35	0	(0)	0	(0)	–	–	0	(0)
-45 ≤ P <-40	0	(0)	0	(0)	–	–	0	(0)
-50 ≤ P <-45	0	(0)	0	(0)	–	–	0	(0)
-55 ≤ P <-50	0	(0)	0	(0)	–	–	0	(0)
-60 ≤ P <-55	0	(0)	0	(0)	–	–	0	(0)
-65 ≤ P <-60	0	(0)	0	(0)	–	–	0	(0)
-70 ≤ P <-65	0	(0)	0	(0)	–	–	0	(0)
-75 ≤ P <-70	0	(0)	0	(0)	–	–	0	(0)
-80 ≤ P <-75	0	(0)	0	(0)	–	–	0	(0)
-85 ≤ P <-80	0	(0)	0	(0)	–	–	0	(0)
-90 ≤ P <-85	0	(0)	0	(0)	–	–	0	(0)
-95 ≤ P <-90	0	(0)	0	(0)	–	–	0	(0)
-100 < P <-95	0	(0)	0	(0)	–	–	0	(0)
P = -100	–	–	0	(0)	–	–	0	(0)
TOTALS	4705	(2629)	4705	(2628)	9410	(5257)	9410	(5257)

a) SEE FIGURE 3 FOR DEFINITION OF TERMS
b) ONE HALF OF LOAD RANGE
c) AVERAGE OF PEAK AND VALLEY LOADS

TABLE 1. SPECTRAL DENSITY FUNCTION (Concluded)

B. TENSION-COMPRESSION (HORIZONTAL TAIL HINGE MOMENT) SPECTRUM AND MODIFICATIONS

PERCENT OF MAXIMUM PEAK LOAD	NUMBER OF EVENTS[a], [TCZ] TC (TCR)											
	PEAKS			VALLEYS			AMPLITUDES[b]			MEAN LEVELS[c]		
	[TCZ]	TC	(TCR)	[TCZ]	TC	(TCR)	[TCZ]	TC	(TCR)	[TCZ]	TC	(TCR)
P = 100	[10]	**10**	(10)	–	–	–	[0]	**0**	(0)	–	–	–
95 ≤ P < 100	[7]	**7**	(7)	[0]	**0**	(0)	[0]	**0**	(0)	[0]	**0**	(0)
90 ≤ P < 95	[2]	**2**	(2)	[0]	**0**	(0)	[0]	**0**	(0)	[0]	**0**	(0)
85 ≤ P < 90	[22]	**22**	(22)	[0]	**0**	(0)	[0]	**1**	(1)	[0]	**0**	(0)
80 ≤ P < 85	[20]	**20**	(20)	[0]	**0**	(0)	[0]	**3**	(3)	[0]	**0**	(0)
75 ≤ P < 80	[19]	**19**	(19)	[0]	**0**	(0)	[0]	**0**	(0)	[0]	**0**	(0)
70 ≤ P < 75	[84]	**84**	(84)	[0]	**0**	(0)	[0]	**6**	(7)	[0]	**0**	(0)
65 ≤ P < 70	[47]	**47**	(47)	[0]	**0**	(0)	[0]	**19**	(21)	[0]	**0**	(0)
60 ≤ P < 65	[121]	**121**	(121)	[0]	**0**	(0)	[0]	**79**	(81)	[0]	**0**	(0)
55 ≤ P < 60	[3]	**3**	(3)	[0]	**0**	(0)	[0]	**24**	(34)	[5]	**5**	(5)
50 ≤ P < 55	[319]	**319**	(319)	[0]	**0**	(0)	[13]	**67**	(83)	[18]	**5**	(2)
45 ≤ P < 50	[84]	**84**	(84)	[0]	**0**	(0)	[18]	**154**	(187)	[27]	**16**	(12)
40 ≤ P < 45	[398]	**398**	(398)	[0]	**0**	(0)	[79]	**125**	(186)	[98]	**50**	(44)
35 ≤ P < 40	[126]	**126**	(108)	[0]	**0**	(0)	[201]	**450**	(510)	[224]	**99**	(72)
30 ≤ P < 35	[881]	**881**	(839)	[0]	**0**	(0)	[292]	**423**	(533)	[582]	**529**	(433)
25 ≤ P < 30	[2037]	**2037**	(1994)	[0]	**0**	(0)	[435]	**998**	(1163)	[494]	**214**	(152)
20 ≤ P < 25	[296]	**296**	(130)	[0]	**0**	(0)	[918]	**1896**	(1997)	[1016]	**563**	(373)
15 ≤ P < 20	[556]	**556**	(98)	[0]	**0**	(0)	[2093]	**2077**	(1862)	[2169]	**1383**	(1025)
10 ≤ P < 15	[1208]	**1208**	(63)	[237]	**237**	(134)	[4737]	**4974**	(2355)	[4479]	**4794**	(3736)
5 ≤ P < 10	[1273]	**1273**	(68)	[377]	**377**	(80)	[3069]	**2835**	(2)	[3695]	**2504**	(1355)
0 ≤ P < 5	[200]	**201**	(32)	[7099]	**1621**	(165)	[3571]	**2373**	(0)	[2619]	**3127**	(744)
-5 ≤ P < 0	[0]	**61**	(18)	[0]	**2349**	(1467)	–	–	–	[0]	**1111**	(334)
-10 ≤ P < -5	[0]	**37**	(15)	[0]	**1288**	(888)	–	–	–	[0]	**577**	(300)
-15 ≤ P < -10	[0]	**16**	(6)	[0]	**325**	(234)	–	–	–	[0]	**261**	(162)
-20 ≤ P < -15	[0]	**15**	(3)	[0]	**633**	(567)	–	–	–	[0]	**182**	(97)
-25 ≤ P < -20	[0]	**0**	(3)	[0]	**210**	(193)	–	–	–	[0]	**127**	(79)
-30 ≤ P < -25	[0]	**1**	(0)	[0]	**228**	(219)	–	–	–	[0]	**66**	(45)
-35 ≤ P < -30	[0]	**0**	(0)	[0]	**123**	(113)	–	–	–	[0]	**40**	(24)
-40 ≤ P < -35	[0]	**0**	(0)	[0]	**140**	(137)	–	–	–	[0]	**33**	(22)
-45 ≤ P < -40	[0]	**0**	(0)	[0]	**70**	(77)	–	–	–	[0]	**9**	(5)
-50 ≤ P < -45	[0]	**0**	(0)	[0]	**113**	(109)	–	–	–	[0]	**7**	(3)
-55 ≤ P < -50	[0]	**0**	(0)	[0]	**49**	(48)	–	–	–	[0]	**2**	(1)
-60 ≤ P < -55	[0]	**0**	(0)	[0]	**28**	(28)	–	–	–	[0]	**0**	(0)
-65 ≤ P < -60	[0]	**0**	(0)	[0]	**17**	(17)	–	–	–	[0]	**0**	(0)
-70 ≤ P < -65	[0]	**0**	(0)	[0]	**17**	(17)	–	–	–	[0]	**0**	(0)
-75 ≤ P < -70	[0]	**0**	(0)	[0]	**10**	(10)	–	–	–	[0]	**0**	(0)
-80 ≤ P < -75	[0]	**0**	(0)	[0]	**4**	(4)	–	–	–	[0]	**0**	(0)
-85 ≤ P < -80	[0]	**0**	(0)	[0]	**1**	(1)	–	–	–	[0]	**0**	(0)
-90 ≤ P < -85	[0]	**0**	(0)	[0]	**3**	(3)	–	–	–	[0]	**0**	(0)
-95 ≤ P < -90	[0]	**0**	(0)	[0]	**1**	(1)	–	–	–	[0]	**0**	(0)
-100 < P < -95	[0]	**0**	(0)	[0]	**0**	(0)	–	–	–	[0]	**0**	(0)
P = -100	–	–	–	[0]	**0**	(0)	–	–	–	–	–	–
TOTALS	[7713]	**7852**	(4513)	[7713]	**7852**	(4512)	[15426]	**15704**	(9025)	[15426]	**15704**	(9025)

a) SEE FIGURE 3 FOR DEFINITION OF TERMS
b) ONE HALF OF LOAD RANGE
c) AVERAGE OF PEAK AND VALLEY LOADS

TABLE 2. PEAK/VALLEY COUPLING MATRIX

A. TENSION-DOMINATED WING ROOT SPECTRUM (TD)

PERCENT OF MAXIMUM PEAK LOAD ↑ VALLEYS → / PEAKS ↓	95 TO 100	90 TO 95	85 TO 90	80 TO 85	75 TO 80	70 TO 75	65 TO 70	60 TO 65	55 TO 60	50 TO 55	45 TO 50	40 TO 45	35 TO 40	30 TO 35	25 TO 30	20 TO 25	15 TO 20	10 TO 15	5 TO 10	0 TO 5	-5 TO 0	-10 TO -5	-15 TO -10	-20 TO -15	-25 TO -20	-30 TO -25	-35 TO -30	-40 TO -35	-45 TO -40	-50 TO -45	-55 TO -50	-60 TO -55	-65 TO -60	-70 TO -65	-75 TO -70	-80 TO -75	-85 TO -80	-90 TO -85	-95 TO -90	-100 TO -95
95 TO 100														2	1		1		1	1	2																		
90 TO 95														1	1			1	3	2																				
85 TO 90														1	1			2	5	3	2																			
80 TO 85												2	2		4	2	4		6																					
75 TO 80													2		2	5	6	2	13	9	1	1																		
70 TO 75								1					3	5	6	2	7	9	17	7	7																		
65 TO 70												3	5	6	7	7	9	15	31	20	7	1																	
60 TO 65									1		1	2	5	5	9	17	21	19	64	30	11	4		1															
55 TO 60										2		1	3	7	8	8	16	22	18	23	10	3		1															
50 TO 55												4	6	8	22	21	27	48	76	48	19	5	1		3														
45 TO 50													16	14	27	23	45	65	101	77	31	7				1													
40 TO 45													1	14	41	46	68	83	152	103	55	8	1		2														
35 TO 40														6	40	59	96	122	198	162	81	20	6	1	1	1													
30 TO 35																103	96	155	137	279	154	42	7	7	3													
25 TO 30																12	2	5	19	41	22		6	1	1													
20 TO 25																	39	28	64	35	2																	
15 TO 20																		13	25	11	49																	
10 TO 15																			55	191	56																	
5 TO 10																			207	137	61																	
0 TO 5																																						
-5 TO 0																																						
-10 TO -5																																						
-15 TO -10																																						
-20 TO -15																																						
-25 TO -20																																						
-30 TO -25																																						
-35 TO -30																																						
-40 TO -35																																						
-45 TO -40																																						
-50 TO -45																																						
-55 TO -50																																						
-60 TO -55																																						
-65 TO -60																																						
-70 TO -65																																						
-75 TO -70																																						
-80 TO -75																																						
-85 TO -80																																						
-90 TO -85																																						
-95 TO -90																																						
-100 TO -95																																						

a. A VALLEY ASSOCIATED WITH THE PRECEDING PEAK

TABLE 2. PEAK/VALLEY COUPLING MATRIX (CONTINUED)

B. RACETRACK-MODIFIED TENSION-DOMINATED WING ROOT SPECTRUM (TDR)

PERCENT OF MAXIMUM PEAK LOAD[a] VALLEYS → / PEAKS ↓	95 TO 100	90 TO 95	85 TO 90	80 TO 85	75 TO 80	70 TO 75	65 TO 70	60 TO 65	55 TO 60	50 TO 55	45 TO 50	40 TO 45	35 TO 40	30 TO 35	25 TO 30	20 TO 25	15 TO 20	10 TO 15	5 TO 10	0 TO 5	-5 TO 0	-10 TO -5	-15 TO -10	-20 TO -15	-25 TO -20	-30 TO -25	-35 TO -30	-40 TO -35	-45 TO -40	-50 TO -45	-55 TO -50	-60 TO -55	-65 TO -60	-70 TO -65	-75 TO -70	-80 TO -75	-85 TO -80	-90 TO -85	-95 TO -90	-100 TO -95
95 TO 100																2			2	1	3																	
90 TO 95															1			1	3	2	1																	
85 TO 90																		1	4	6	3																	
80 TO 85															2	2	2	1	8	4	1																	
75 TO 80														1		3	6	1	13	12	4	1																
70 TO 75													1	1	3	1	7	8	20	12	11																	
65 TO 70												2	2	1	3	6	6	19	31	22	16	1																
60 TO 65														1	5	7	10	25	63	40	25	4		1	1												
55 TO 60																3	11	20	25	33	19	3	1	1													
50 TO 55															6	8	18	40	77	64	35	6	1		2												
45 TO 50																13	20	48	101	89	66	7			1	1											
40 TO 45																	31	66	137	110	84	13	1		2												
35 TO 40																		71	153	160	113	21	7	2	1	1											
30 TO 35																			48	201	146	35	5	7	2												
25 TO 30																				21	19		6		1												
20 TO 25																																					
15 TO 20																																					
10 TO 15																																					
5 TO 10																																					
0 TO 5																																					
-5 TO 0																																					
-10 TO -5																																					
-15 TO -10																																					
-20 TO -15																																					
-25 TO -20																																					
-30 TO -25																																					
-35 TO -30																																					
-40 TO -35																																					
-45 TO -40																																					
-50 TO -45																																					
-55 TO -50																																					
-60 TO -55																																					
-65 TO -60																																					
-70 TO -65																																					
-75 TO -70																																					
-80 TO -75																																					
-85 TO -80																																					
-90 TO -85																																					
-95 TO -90																																					
-100 TO -95																																					

[a]A VALLEY ASSOCIATED WITH THE PRECEDING PEAK

TABLE 2. PEAK/VALLEY COUPLING MATRIX (Continued)

C. TENSION COMPRESSION HORIZONTAL TAIL HINGE MOMENT SPECTRUM (TC)

PERCENT OF MAXIMUM PEAK LOAD + VALLEYS → / PEAKS ↓	95 TO 100	90 TO 95	85 TO 90	80 TO 85	75 TO 80	70 TO 75	65 TO 70	60 TO 65	55 TO 60	50 TO 55	45 TO 50	40 TO 45	35 TO 40	30 TO 35	25 TO 30	20 TO 25	15 TO 20	10 TO 15	5 TO 10	0 TO 5	-5 TO 0	-10 TO -5	-15 TO -10	-20 TO -15	-25 TO -20	-30 TO -25	-35 TO -30	-40 TO -35	-45 TO -40	-50 TO -45	-55 TO -50	-60 TO -55	-65 TO -60	-70 TO -65	-75 TO -70	-80 TO -75	-85 TO -80	-90 TO -85	-95 TO -90	-100 TO -95
95 TO 100																										16								1					
90 TO 95																									8	7				3	4			2					
85 TO 90																								11					1	3		2	2							
80 TO 85																								11					1	1	3	1						1		
75 TO 80																											2	4	4		55									
70 TO 75																				55							1					3	3							
65 TO 70																				32					2	9	9	67	6			1	1							
60 TO 65																			1											2										
55 TO 60																		144	1	1	1	2	9	28	18	104	2	1	2	4		1			1					
50 TO 55																		65	2	3	3	1	1		1	2			2	1	2	1								
45 TO 50																		3	4	9	41	49	57	211	2		10	1	3	3	1	3			1					
40 TO 45																		3	15	6	9	31	2	36	2	3	1	10	3	1	1			1	1					
35 TO 40																		7	76	58	36	580	13	3	10	26	7	4	7	3	3			1			1			
30 TO 35																		8	20	116	1798	20	21	77	13	11	10	7	8	6	5	3	2	3	2	1				
25 TO 30																		6	24	37	20	27	17	82	28	6	13	2	2	1	3	3	1	1						
20 TO 25																		1	18	47	36	196	18	15	98	20	7	7	3	1	1	3	1	1						1
15 TO 20																			4	356	137	280	106	29	14	10	16	7	3	4	1	1		1						
10 TO 15																				620	475	95	64	54	21	13	5	4	12	7	2		1	3	2	1				
5 TO 10																					300	32	14	41	18	21	11	5	4	7	14		1	1	1	2				
0 TO 5																						3	3	5	7	5	15	14	1	4	1	3	1							
-5 TO 0																								1	6	7	3	4	5	3	3	1	3	1				1		
-10 TO -5																										1		1	9	5										
-15 TO -10																												1	3	1	2				1				
-20 TO -15																											5		1	1	1	5		1					
-25 TO -20																																	1				1		
-30 TO -25																																							
-35 TO -30																																							
-40 TO -35																																							
-45 TO -40																																							
-50 TO -45																																							
-55 TO -50																																							
-60 TO -55																																							
-65 TO -60																																							
-70 TO -65																																							
-75 TO -70																																							
-80 TO -75																																							
-85 TO -80																																							
-90 TO -85																																							
-95 TO -90																																							
-100 TO -95																																							

a. A VALLEY ASSOCIATED WITH THE PRECEDING PEAK

TABLE 2. PEAK/VALLEY COUPLING MATRIX (Concluded)

D. RACETRACK-MODIFIED TENSION-COMPRESSION HORIZONTAL TAIL HINGE MOMENT SPECTRUM (TCR)

PERCENT OF MAXIMUM PEAK LOAD[a] VALLEYS → / PEAKS ↓	90 TO 100	80 TO 90	85 TO 80	80 TO 85	75 TO 80	70 TO 75	65 TO 70	60 TO 65	55 TO 60	50 TO 55	45 TO 50	40 TO 45	35 TO 40	30 TO 35	25 TO 30	20 TO 25	15 TO 20	10 TO 15	5 TO 10	0 TO 5	-5 TO 0	-10 TO -5	-15 TO -10	-20 TO -15	-25 TO -20	-30 TO -25	-35 TO -30	-40 TO -35	-45 TO -40	-50 TO -45	-55 TO -50	-60 TO -55	-65 TO -60	-70 TO -65	-75 TO -70	-80 TO -75	-85 TO -80	-90 TO -85	-95 TO -90	-100 TO -95
90 TO 100																										16								1					
80 TO 90																																	2						
85 TO 80																									8	7				3	4								
80 TO 85																								11					1	3		2	2						
75 TO 80																								11					1	1	3	1					1		
70 TO 75																											2	4	4		55								
65 TO 70																					51			1		2	2					3	3						
60 TO 65																					30			2	2	9	8	67	6			1	1	1					
55 TO 60																				1										2									
50 TO 55																		86	6	4	10	10	12	38	19	112	4	5	4	7		1			1				
45 TO 50																		46	4	3	6	3	7	2	3	3		1	2	1	2	1							
40 TO 45																		2	4	7	32	33	41	221	10	6	15	4	6	6	4	4	1		1	1			
35 TO 40																			9	3	8	24	2	29	2	6	2	10	4	1	2		1	1	1		1	1	
30 TO 35																			44	44	39	551	39	16	23	28	9	5	8	6	3	2	1	1			1		
25 TO 30																				60	1329	239	101	137	45	26	17	17	10	11	5	4	2	3	3	2			
20 TO 25																					2	15	13	42	21	4	10	1	3		3	1	1	1					
15 TO 20																						20	9	13	38	7	10	4	6	1	1	2		1					1	
10 TO 15																							10	14	8	4	7	5	2	2	1	1		1					
5 TO 10																								11	10	8	6	1	8	5	2	1	1	3	2				
0 TO 5																									6	9	7	5	4	4	13			1	1	1			
-5 TO 0																										1	6	5	1			2	1	1					
-10 TO -5																											3	4	1	2	2	2	2						
-15 TO -10																													5	1									
-20 TO -15																														1			1						
-25 TO -20																															1	2		1					
-30 TO -25																																							
-35 TO -30																																							
-40 TO -35																																							
-45 TO -40																																							
-50 TO -45																																							
-55 TO -50																																							
-60 TO -55																																							
-65 TO -60																																							
-70 TO -65																																							
-75 TO -70																																							
-80 TO -75																																							
-85 TO -80																																							
-90 TO -85																																							
-95 TO -90																																							
-100 TO -95																																							

[a] A VALLEY ASSOCIATED WITH THE PRECEDING PEAK

2.6.2 Spectrum Modification

Two different types of modifications were performed independently on the baseline spectra. One modification had two goals: one to eliminate low amplitude cycles to reduce testing time without changing the ranking (relative life), and the other to determine the importance of low amplitude cycles on the overall spectrum life. The second modification was made to determine the importance of compression cycles.

2.6.2.1 Racetrack Modification

The technique used to eliminate the small amplitude cycles was the "racetrack" method, which is a screening technique based on the determination of significant load reversals. The technique, shown graphically in Figure 6a, utilizes the analogy of a race course of a specified width and is represented by the load-time trace of the load spectrum.[30] The number of direction changes required to traverse the course using the shortest route depends on the width specified for the course. Significant "corners" are identified as those involving a change in the sign of the slope of the shortest route. These may be thought of as "primary" direction changes. As the course width tends towards zero a change in primary direction is indicated at every load level. As the course width increases towards the other limit, it becomes possible to traverse the course with very few changes in primary direction. This "course width" or "screening level" is given the variable name DMIN and is defined as a fraction of the load used to normalize the spectrum. In the case of the spectra used in this investigation this normalizing load has been taken to be equal to the value of the maximum tensile spectrum load (σ_{hmax}). Note that the primary load levels are identified and stored in the order that they occur and that there was a significant reduction in applied cycles.

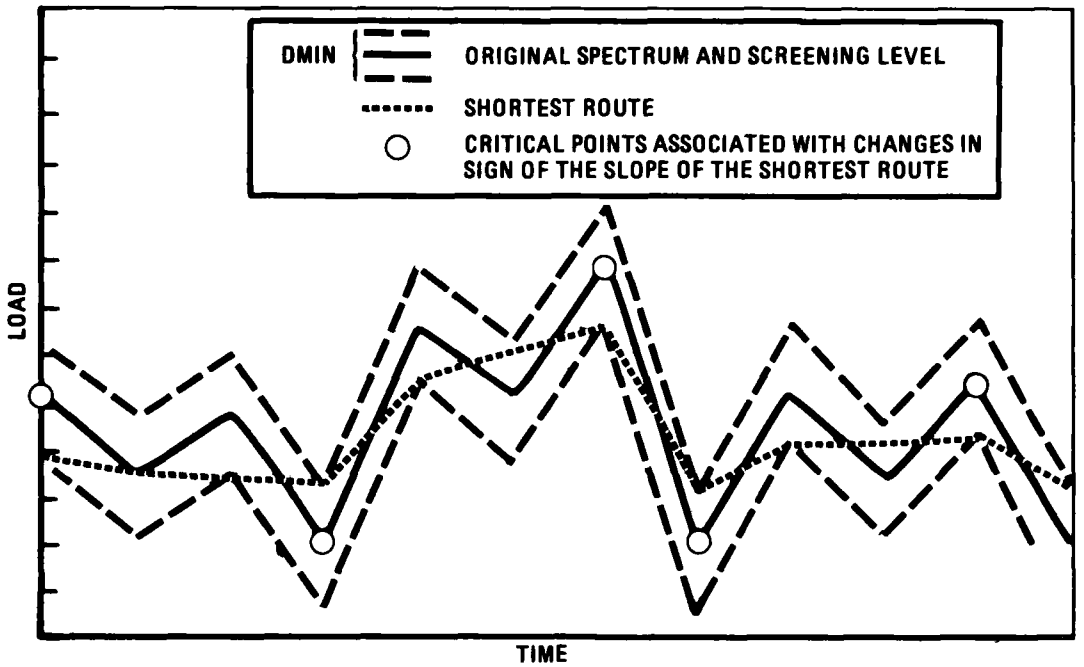

a. METHODOLOGY

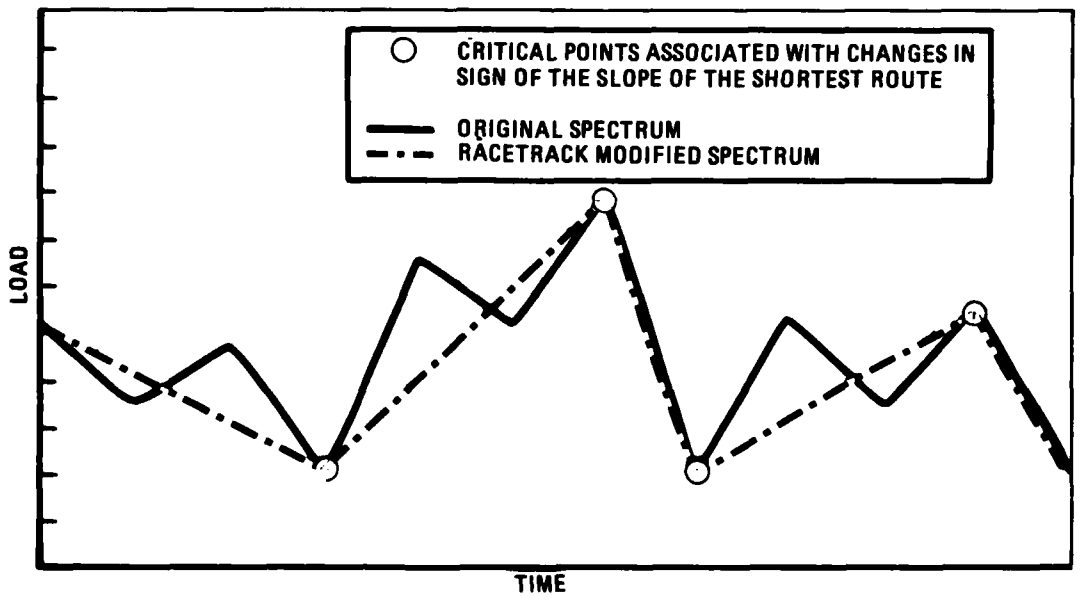

b. RESULT

FIGURE 6. RACETRACK METHOD OF SPECTRUM MODIFICATION

Little information was available to suggest appropriate levels of DMIN, and the selection was complicated by the two competing goals of this modification, one of reducing cycles and the other of determining the importance of low amplitude cycles. The results of applying the racetrack modification with a DMIN of 0.25 on the TD and TC spectra are shown in Tables 1, 2b, and 2d; and Figure 5. The racetrack modified spectra are designated TDR and TCR, respectively. As shown in Table 1 the number of load points are reduced by 44 and 43 percent, respectively (from 9410 load points for the TD spectrum to 5257 load points for the TDR spectrum and from 15704 load points for the TC spectrum to 9025 load points for the TCR spectrum). This reduces the testing time by a like amount and would also reduce spectrum prediction calculation time. The higher magnitude peaks, valleys, and amplitudes are unchanged with a gradual reduction in the number of these features at lower magnitudes and the complete elimination of the lowest magnitude features. Since little was known about the potential effects of this modification, only a single test was performed on each of the seven materials. Additional modifications are planned for future phases of the program, and then duplicate tests or tests with a smaller or larger DMIN can be performed.

2.6.2.2 Truncation of Compression Loads

The effects of tension overloads superimposed on constant-amplitude loading has been extensively evaluated,[1-10] and it has been well established that the overloads retard fatigue crack growth. Retardation has also been observed in spectrum loading, usually by comparing the spectrum fatigue behavior of a material tested under a spectrum and the behavior under that same spectrum with the highest loads truncated.[11] Some work has been done on the effects of compression loads following overloads in constant-amplitude loading. The effect of the underload is to reduce the retardation, although the resultant constant-amplitude fatigue crack growth rates are still lower than without the overload/underload combination.[31-33]

The effects of underload/overload sequencing vary for spectrum fatigue. Hsu and McGee[34] added compression underloads to two otherwise all tension spectra, a bomber and a transport spectrum. These underloads were added before or after high tension loads. Tests were performed under

essentially constant maximum peak stress intensity (K_{hmax} in the present report) conditions by load shedding, and spectrum crack growth rates were measured. For the transport spectrum, results were obtained at two different levels of K_{hmax}. For the transport spectra at the higher level of K_{hmax}, the result was the same as would be expected from constant amplitude results;[31-33] that is, a slower spectrum fatigue-crack growth rate for the underload/overload sequence than that for the overload/underload sequence. However, for both spectra at the lower value of K_{hmax}, the opposite was found. Schijve[6] reported results similar to these latter results. The high-amplitude gust-load cycles in an otherwise random spectrum were applied in either a underload/overload sequence or in a overload/underload sequence. He found that spectrum life for the underload/overload sequence of gust loads was 85 percent of that for the underload/overload sequence, which corresponds to a slower spectrum fatigue-crack growth rate for the overload/underload sequence, again opposite to the results for similar test with a constant-amplitude loading baseline. These latter results, show that applying results from constant-amplitude fatigue to spectrum fatigue can be misleading.

In the present study both baseline spectra contain significant compression loads in random spectra. The spectrum with the higher-magnitude compression loads (TC) was taken as the baseline and all loads below zero were eliminated from this spectrum by setting all loads less than zero equal to zero. This spectrum is designated TCZ. The number of load points was reduced only slightly as few linked load reversals occurred below zero load (278 load points eliminated from the 15704 load points of the TC spectrum). The summary for this spectrum is shown in Table 1. The TC spectrum contains many compressive load points with magnitudes up to about 95 percent of the maximum peak tensile load. The Phase I results showed that, for a given material and maximum peak stress, the spectrum life for the TC spectrum was always shorter than the spectrum life for the TD spectrum. It was not clear whether the more damaging effect of the TC spectrum was due to the greater proportion of compressive loads in this spectrum or a difference in the characteristics of the tensile portions of the two spectra. By comparing the fatigue lives for the TC and TCZ spectra, which are identical except for the absence of compressive loads in the latter, the effect of the compressive portion of a complex spectrum on fatigue life can be determined. It is

important to separate the effect of compressive loading on spectrum life because different material selection criteria may be needed for aircraft components which experience either a tension-dominated or a tension-compression load spectrum.

2.6.3 Specimen Preparation

The spectrum fatigue specimens (Figure 7) were machined from T/4 and 3T/4 locations of the aluminum plates in the L-T orientation. The specimen surfaces were polished and grids for measuring crack-lengths were photographically applied on both sides. The grid spacing was 1.27 mm (0.050 inch). Jeweler's saw cuts, 0.2-mm wide and 1-mm deep (0.008-inch wide by 0.04-inch deep), were made at the centrally located hole which provided an adequate "flaw" for precracking the test specimens.

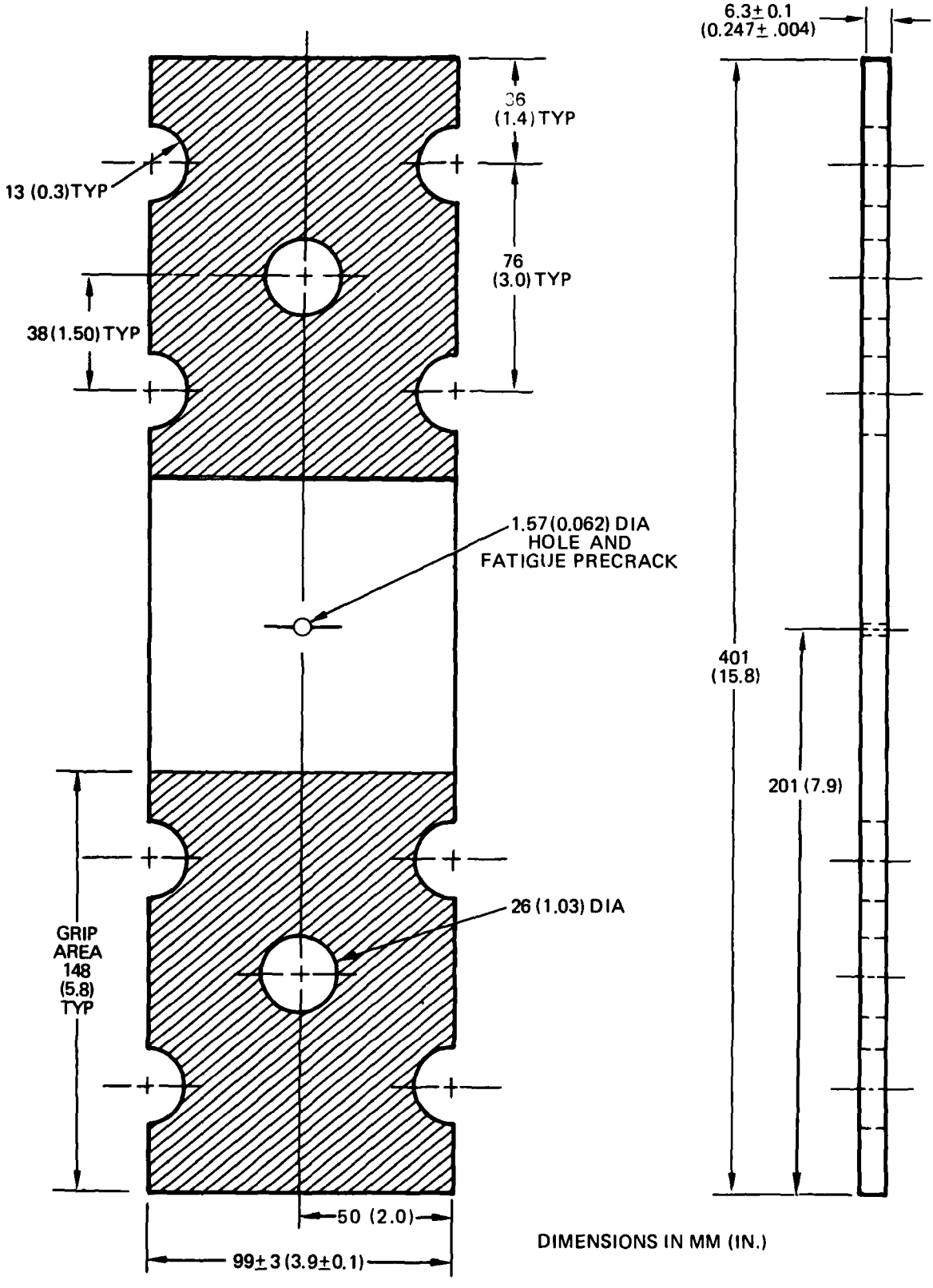

FIGURE 7. SPECTRUM SPECIMEN

2.6.4 Testing

All spectrum tests were performed on a computer controlled servo-hydraulic machine following the methods of ASTM E647 as appropriate. Precracking was performed under constant amplitude fatigue loading at a stress ratio (R) of 0.1. All of the specimens for testing at the same maximum peak (gross) stress (σ_{hmax}) were precracked with identical loads and for the final stage of precracking the maximum stress was approximately half of the subsequent maximum peak spectrum stress (σ_{hmax}). The final precrack length, a, was targeted for 3 mm (0.12 in.)* for testing at 145 MPa and 169 MPa, and was targeted for 5 mm (0.2 in.) for testing at 103 MPa. The relative humidity for all spectrum testing was between 40 and 60 percent.

The load history data were stored on a magnetic tape. The stored data contained all the necessary information, including the desired waveform, frequency, and load points, to control the test. The test setup is shown in Figure 8. Restraints were used to prevent buckling at high compressive loads.

The spectrum tests were performed using a sinusoidal waveform. The linear (theoretical) point-to-point load rate (peak to valley or valley to peak) for tests at each maximum peak stress (σ_{hmax}) was constant. The choice of load rates was governed primarily by the test system response and is shown in Table 3. The maximum frequencies shown in this table, which overrode the loading rate when necessary, insured that even the very small load excursions were applied to the specimens.

*Changed from 5.5 mm in Phase I as discussed in the footnote in Section 2.6.5.

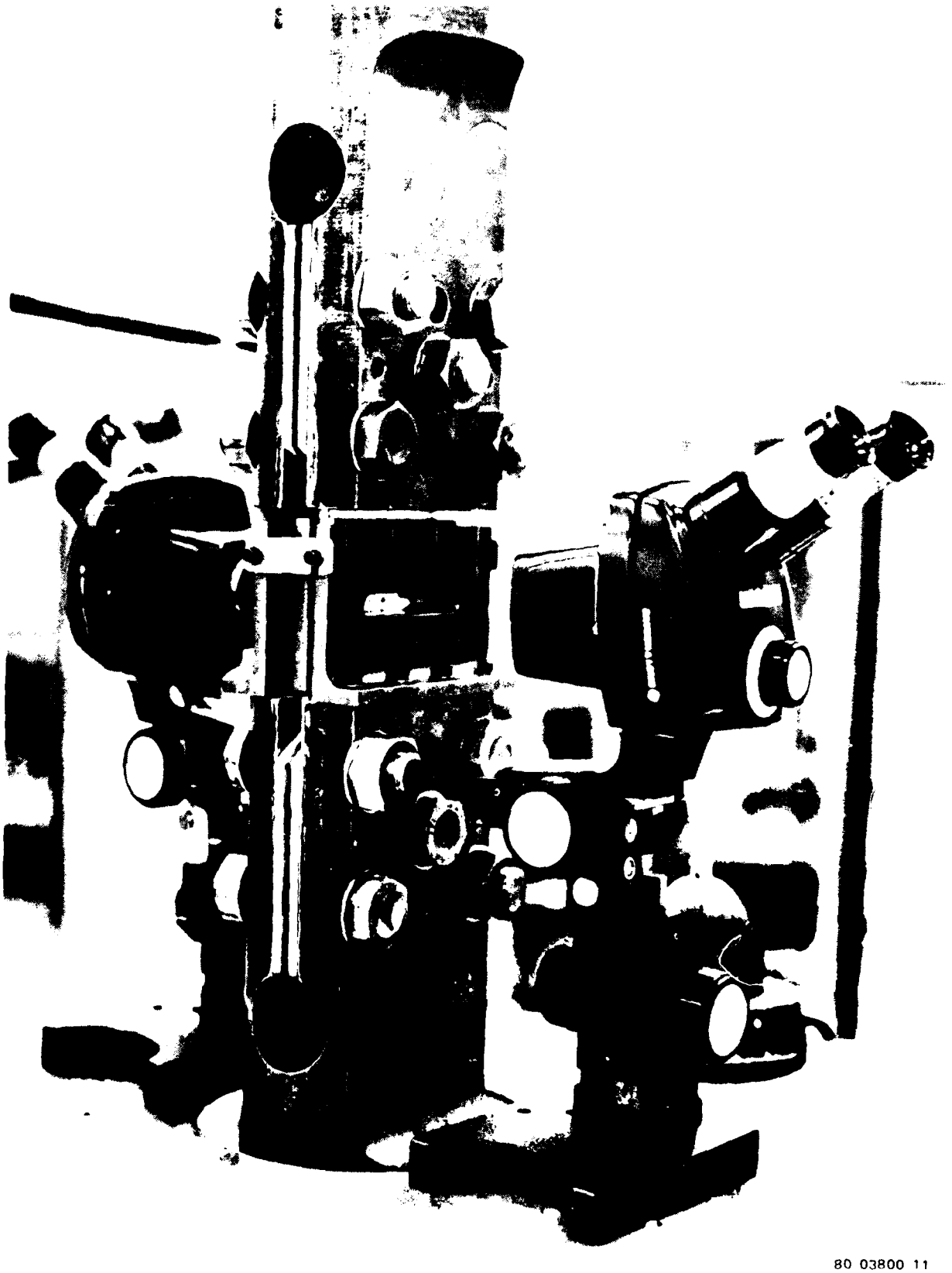

80 03800 11

FIGURE 8. SPECTRUM TEST SETUP

TABLE 3. SPECTRUM TEST CONDITIONS

MAXIMUM PEAK STRESS, σ_{hmax} MPa (ksi)	LINEAR POINT-TO-POINT LOAD RATE kN/SEC	(KIP/SEC)	OVERRIDING MAXIMUM FREQUENCY (Hz)
103 (15)	270	(60)	30
145 (21)	220	(50)	20
169 (24.5)	180	(40)	15

A special feature termed Null Pacing was used to insure that peak loads were obtained. When the error between command and feedback exceeded about one percent, computer command rate automatically slowed down so that the peak and valley loads were met and overshoots did not occur.

Spectrum testing was conducted at three maximum peak stresses (σ_{hmax}) of 103, 145, and 169 MPa (15, 21, and 14.5 ksi), selected to give a range of crack growth rates. For the F-18, the maximum peak stress level of 145 MPa corresponds to the lowest stress level that will meet test needs for design purposes. Duplicate tests were performed. To obtain more understanding of the fundamental parameters affecting spectrum FCP, tests were performed at lower and higher maximum peak stresses of 103 and 169 MPa. For Phase I testing, for the 103 MPa (15 ksi) maximum peak stress tests, the specimens were tested to a crack length of about 14 mm (0.55 in.), i.e., a total crack length, 2a, of about 28 mm (1.1 in.). Subsequently, the same specimen was tested to failure under a maximum peak stress of 169 MPa (24.5 ksi). Two such tests were performed for each alloy. For Phase II testing, only one specimen at each stress (103 and 169 MPa) was tested to failure.

Crack length measurements were visually made after each pass for the spectrum tests conducted under maximum peak stress of 145 and 169 MPa (21 and 24.5 ksi). Due to the slower crack growth rates at the 103 MPa (15 ksi) maximum peak stress, the crack length measurements were made after multiple passes. Crack length measurements were made with reference to the photographically printed grid lines at four locations on the specimen (front and rear of specimen, right and left tip of crack). The accuracy of a reading was enhanced by the use of a zoom stereo microscope (7-30X) equipped with a 0.125-mm (0.001-inch) increment reticle.

2.6.5 Test Analysis Procedure

The two-point secant method was used to determine crack growth rate per ASTM E647. To eliminate previous loading history effects, data points with crack growth rates greater than the first minimum crack growth rate were not plotted on the crack growth rate curves.

For comparison of the different materials, the lives (simulated flight hours) over the same crack length regime were used. For tests at 145 MPa (21 ksi), the number of flight hours for the crack to grow from an initial crack-length, a_i, of 6 mm (0.24 in.) to failure was used*. For tests at 103 MPa (15 ksi), the number of flight hours for the crack to grow from an initial crack-length, a_i, of 6 mm (0.24 in.) to 13 mm (0.51 in.) was used. For tests at 169 MPa (24.5 ksi), the range was from 18 mm (0.71 in.) to failure. Figure 9 shows schematically the crack-length regimes for different maximum peak stresses (σ_{hmax}). A comparison of the ranges of maximum peak stress intensities that these crack growth regimes represent is shown graphically in Figure 10.

*It was found in Phase I[27] that history effects from the precracking were affecting the spectrum crack growth rates for crack lengths longer than that expected from consideration of linear elastic fracture mechanics. To eliminate this unexplained effect, two changes were made for this phase: 1) all life comparisons were made from an initial crack length, a_i, of 6 mm instead of an a_i of 5.5 mm used in Phase I, and 2) for added assurance the final precrack length was shortened to 3 mm for testing at 145 and 169 MPa. Because of the extremely slow crack growth rates, this latter change was impractical for the testing at 103 MPa. Also in Phase I, the spectrum lives for tests at 145 and 169 MPa were reported for an initial crack length to a final crack length, a_f, to separate the effects of fracture toughness from crack growth. However other data presentations such as spectrum crack growth rates adequately allow separating these effects, so this comparison has been dropped.

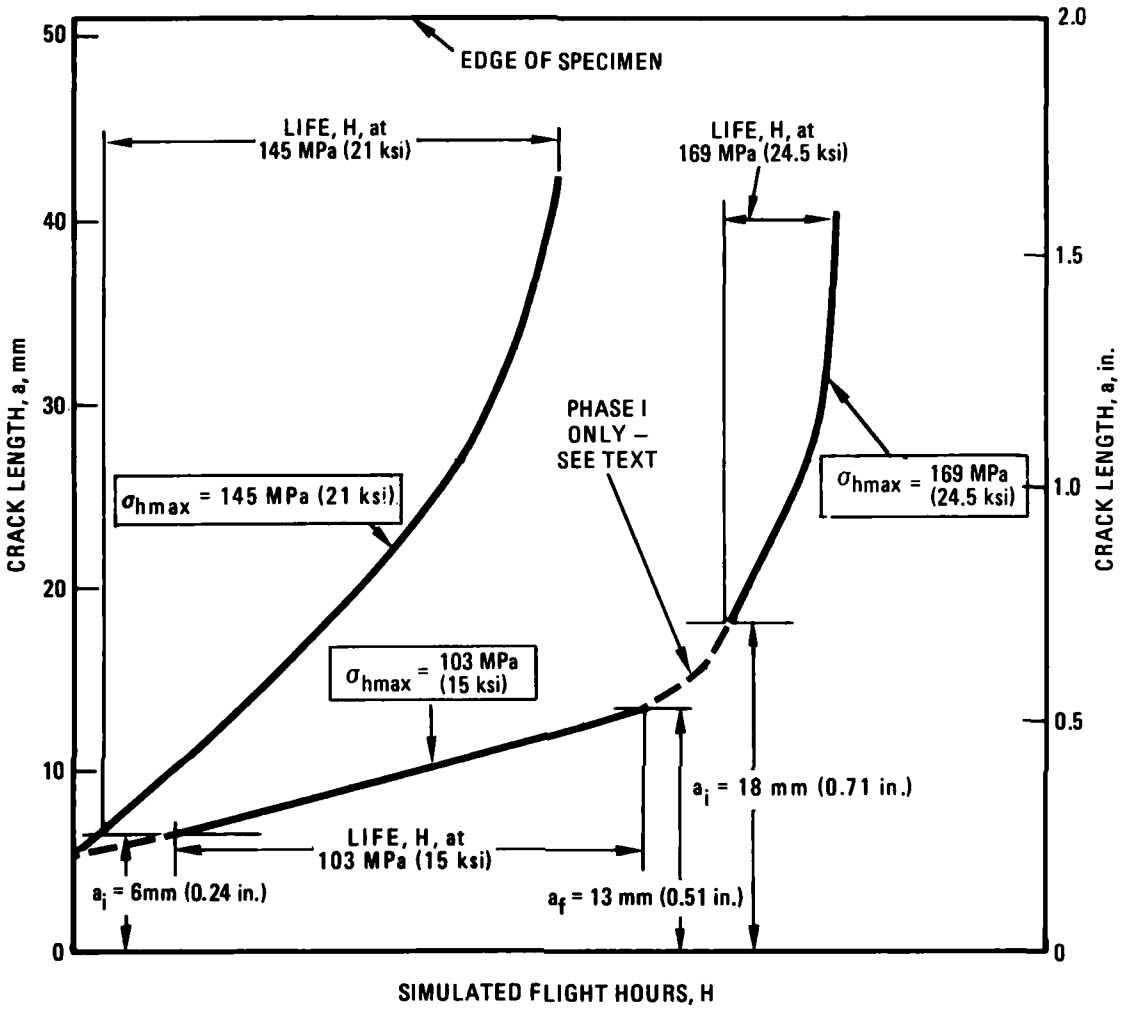

FIGURE 9. SCHEMATIC OF SPECTRUM LIFE COMPARISON PROCEDURE

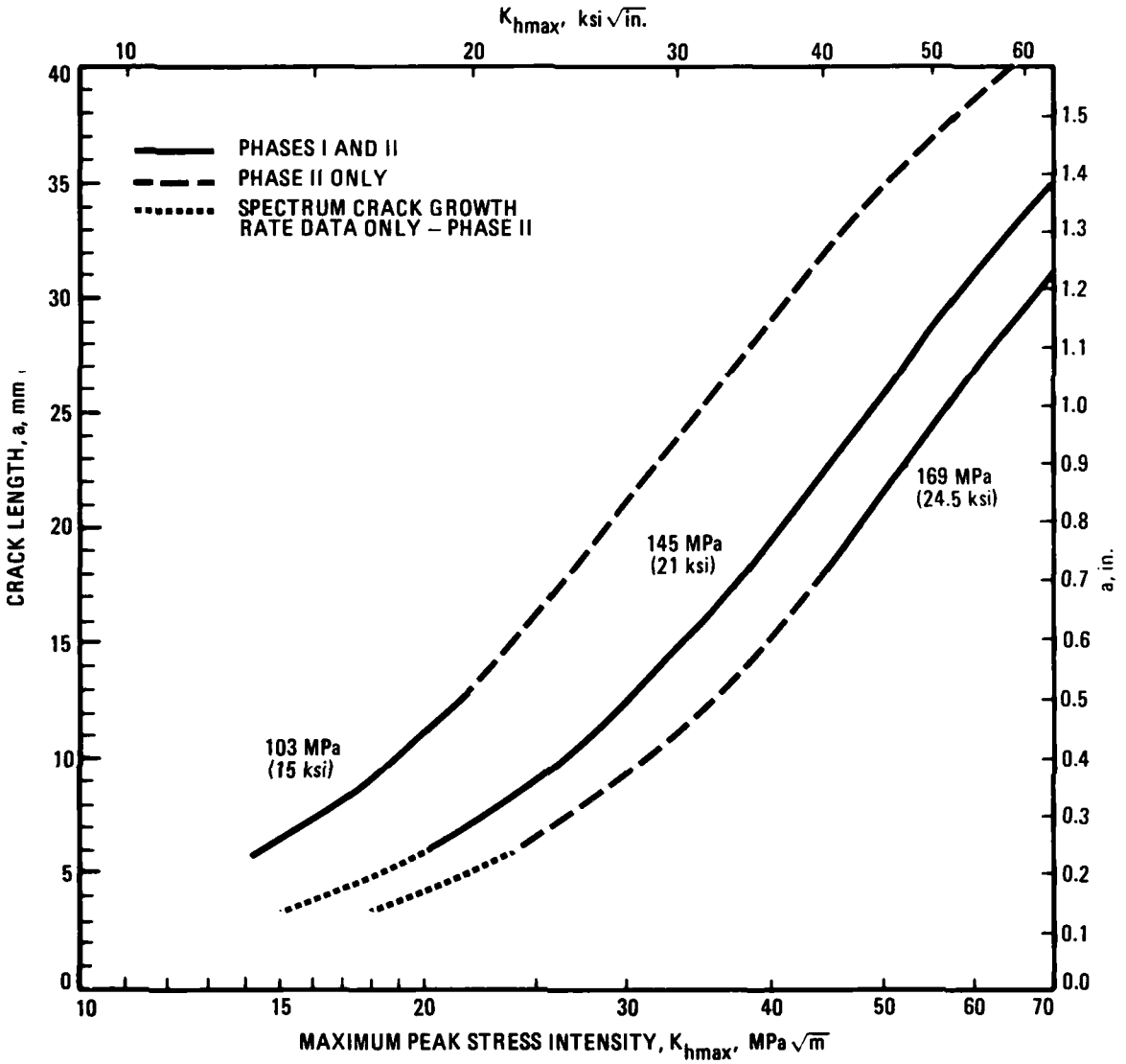

FIGURE 10. COMPARISON OF RANGES OF K_{hmax} VS a FOR THE THREE VALUES OF σ_{hmax} USED IN THE PROGRAM

III. RESULTS AND DISCUSSION

Many of the results from the Phase I effort are useful for comparison to the results of this Phase II effort and therefore are presented again in this report as necessary. The details not presented herein can be found in the Phase I report.[27]

3.1 CHEMISTRY

The chemical compositions of all alloys are listed in Table 4, along with the commercial limits for each. All ten alloys are within the appropriate composition limits.

TABLE 4. CHEMICAL COMPOSITION OF PROGRAM MATERIALS

MATERIAL	SAMPLE NO.	ELEMENT, WEIGHT PERCENT										
		LIMITS	Cu	Mg	Zn	Mn	Cr	Ti	Be	Fe	Si	OTHER
2020-T651	523713-B		4.44	–	0.03	0.52		0.02		0.20	0.09	1.09 Li 0.20 Cd
2024-T351	511338		4.35	1.54	0.07	0.51	0.00	0.03	–	0.23	0.09	–
-T851	511339		4.41	1.50	0.09	0.50	0.00	0.02	–	0.33	0.10	–
		MINIMUM	3.8	1.2	–	0.30	–	–	–	–	–	–
		MAXIMUM	4.9	1.8	0.25	0.9	0.10	0.15	–	0.50	0.50	–
2124-T851	511340		4.21	1.46	0.03	0.47	0.00	0.01	–	0.10	0.05	–
		MINIMUM	3.8	1.2	–	0.30	–	–	–	–	–	–
		MAXIMUM	4.9	1.8	0.25	0.9	0.10	0.15	–	0.30	0.20	–
2324-T39	49L513		4.23	1.52	0.01	0.51	0.00	0.01	0.002	0.08	0.05	–
		MINIMUM	3.8	1.2	–	0.3	–	–	–	–	–	–
		MAXIMUM	4.4	1.8	0.25	0.9	0.10	–	–	0.12	0.10	–
7075-T651	475332		1.70	2.41	5.62	0.05	0.20	0.06	0.002	0.26	0.12	–
-T7351	511341		1.95	2.63	5.79	0.04	0.18	0.04	–	0.27	0.09	–
		MINIMUM	1.2	2.1	5.1	–	0.18	–	–	–	–	–
		MAXIMUM	2.0	2.9	6.1	0.30	0.28	0.20	–	0.50	0.40	–
7050-T73651	511464		2.23	2.30	6.27	0.02	0.01	0.03	0.002	0.13	0.07	0.12Zr
		MINIMUM	2.0	1.9	5.7	–	–	–	–	–	–	0.08
		MAXIMUM	2.6	2.6	6.7	0.10	0.04	0.06	0.05	0.15	0.12	0.15
7475-T651	511463		1.48	2.36	5.46	0.00	0.21	0.02	0.002	0.07	0.04	–
-T7351	511630		1.6	2.43	5.67	0.00	0.17	0.02	0.001	0.06	0.05	–
		MINIMUM	1.2	1.9	5.2	–	0.18	–	–	–	–	–
		MAXIMUM	1.9	2.6	6.2	0.06	0.25	0.06	0.05	0.12	0.1	–

3.2 METALLOGRAPHY

The ten alloys investigated in Phases I and II are commercial products, many of which have been characterized extensively in the literature. The following paragraphs describe some general microstructural features of the three Phase II alloys, using appropriate micrographs from the various test samples.

As summarized in the Phase I report,[27] heat treatable aluminum alloy microstructures are characterized by grain structure and the type, size, and distribution of second-phase particles. These particles can be large, insoluble constituents (1-30 μm); smaller dispersoids (0.02-0.3 μm) formed by precipitation; and fine precipitates (0.0005 to 0.01 μm) formed during quenching or aging.

Grain structure is determined primarily by thermomechanical processing and the morphology of second-phase particles, particularly dispersoids. Grain structure and constituent morphology were examined using optical metallography. Micrographs of each alloy in the as-polished condition depict secondary phases, while micrographs in the etched condition show the grain structure.

The microstructures of 2020-T651 and 2324-T39 are shown in Figures 11 and 12, respectively. Alloy 2020 contains a relatively large amount of Fe(Mn)-bearing constituents, either Al_7Cu_2Fe or $Al_{12}(Fe,Mn)_3Si$, while 2324 contains a lesser amount of these constituents because of lower Fe and Si contents. Unlike 2020, though, 2324 does contain partially soluble Mg_2Si and Al_2CuMg constituents (the large particles in Figure 12). Etching reveals that both alloys have coarse-grained, recrystallized structures.

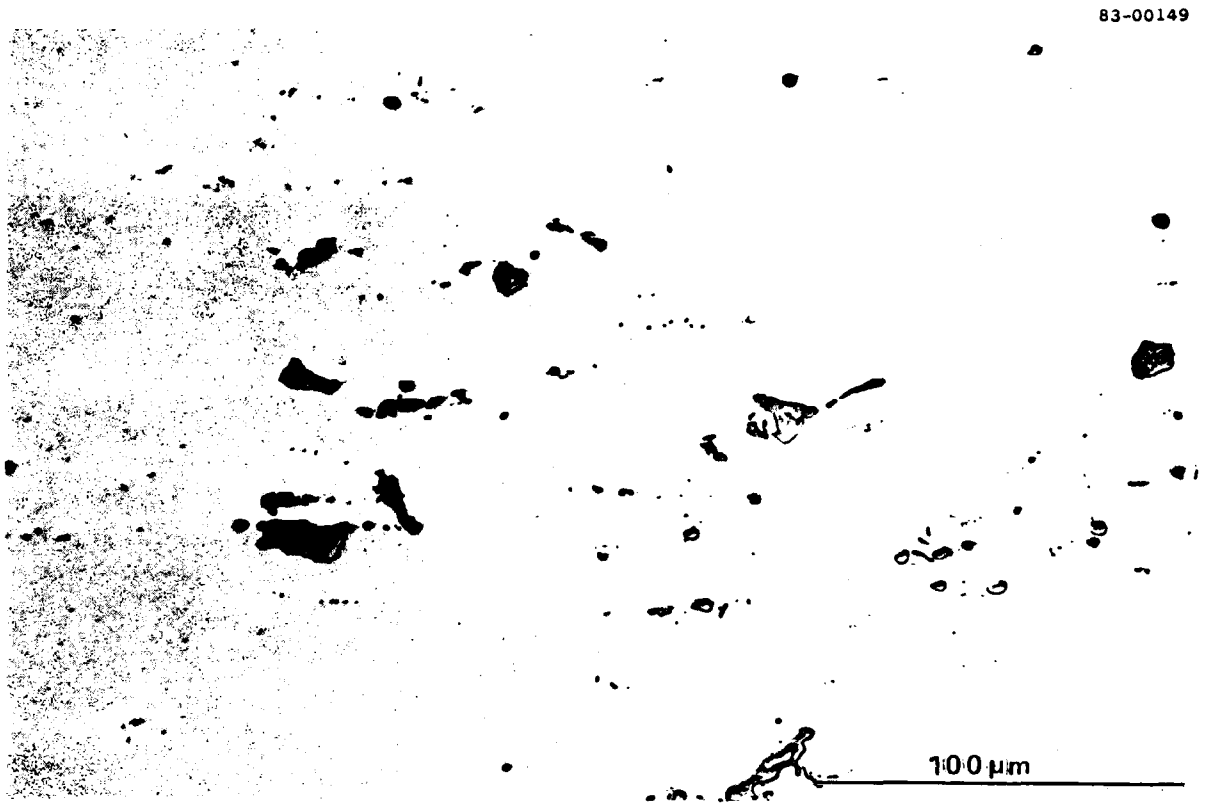

AS POLISHED 500X

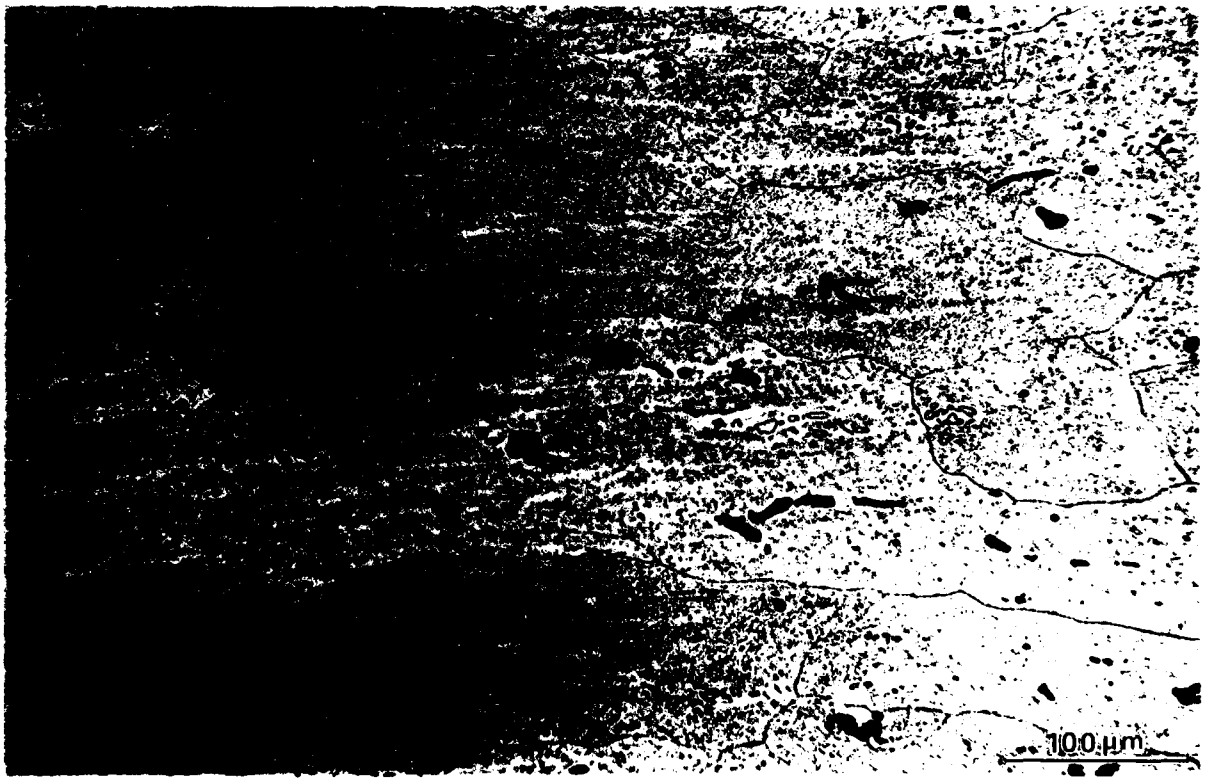

KELLER'S ETCH 250X

FIGURE 11. LONGITUDINAL MICROSTRUCTURE OF 2020-T651

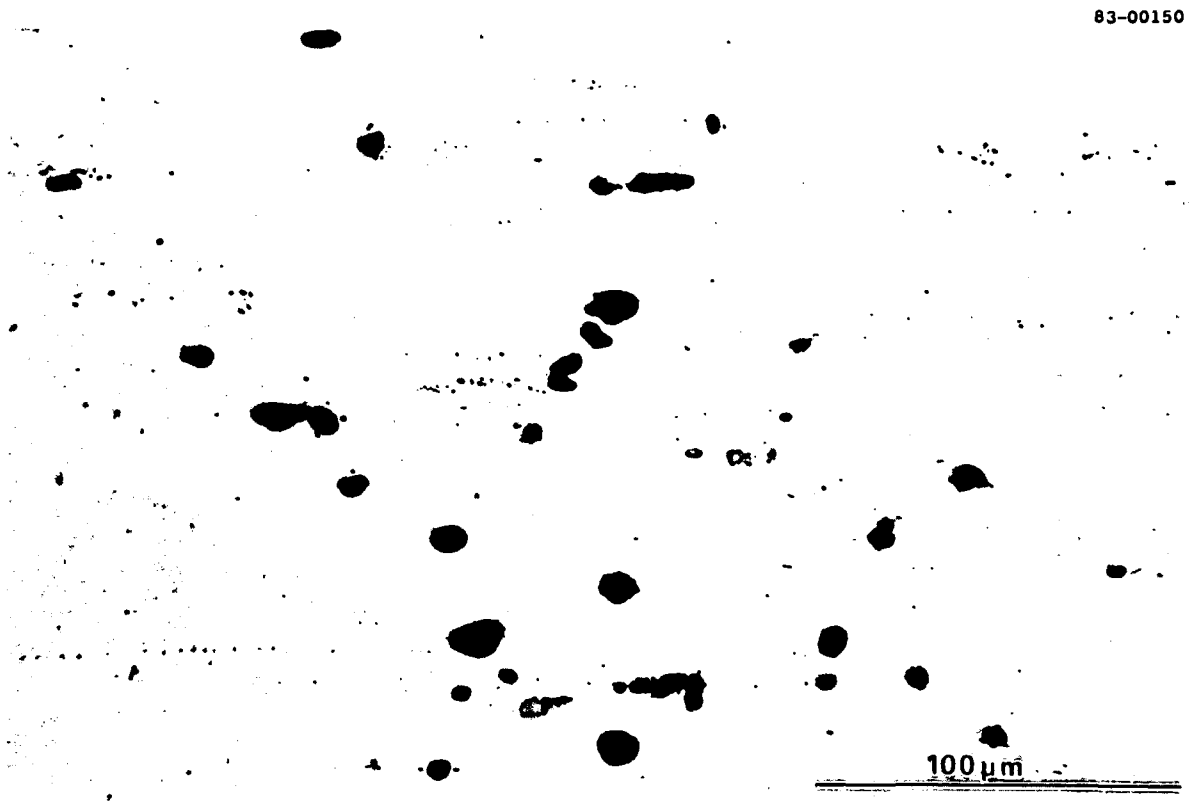

AS POLISHED 500X

KELLER'S ETCH 250X

FIGURE 12. LONGITUDINAL MICROSTRUCTURE OF 2324-T39

The fine structures of these alloys are shown in TEM micrographs presented in Figures 13 and 14. For 2020 (Figures 13), rod-like Mn-bearing dispersoids are distributed evenly throughout the microstructure, while the precipitates are barely resolved in the background. These precipitates are primarily the T_B ($Al_{15}Cu_8Li_2$), θ' (Al_2Cu) and T_1 (Al_2CuLi) phases. Small amounts of δ' (Al_3Li) also have been reported in this alloy,[35] whereas other studies have not reported δ'.[36] The precipitate free zone (PFZ) characteristic of this alloy in the T6 temper is clearly visible in this TEM micrograph (Figure 13). The Mn-bearing dispersoids in 2324-T39 (Figure 14) are surrounded by dislocation structures as a result of the alloy being cold rolled 11 percent. In this T3-type temper, strengthening precipitates are GP zones, which are too small to be seen in Figure 14.

83-00153

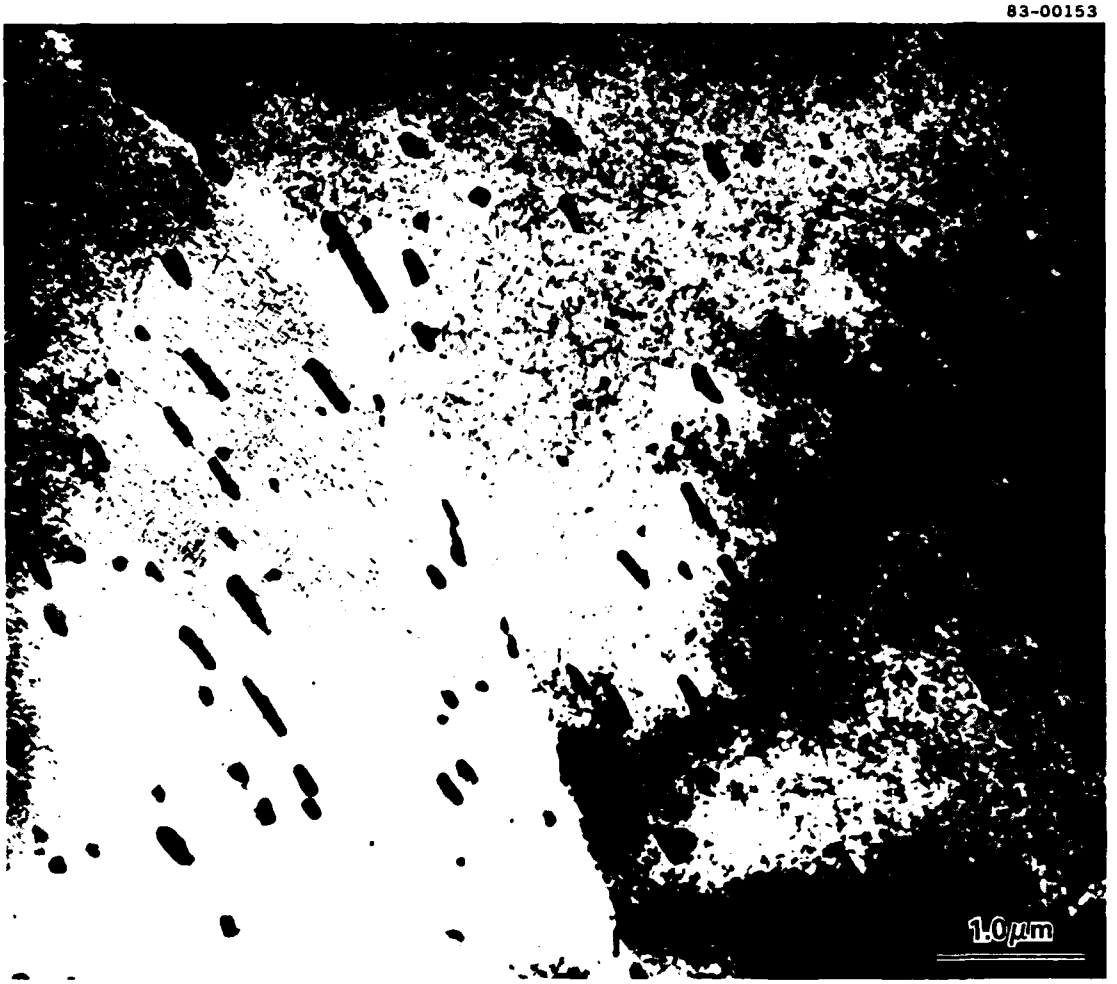

19,600X

FIGURE 13. TEM MICROGRAPH OF 2020-T651 PLATE SHOWING ROD-LIKE Mn-BEARING DISPERSOIDS WITH STRENGTHENING PRECIPITATES BARELY VISIBLE IN THE BACKGROUND

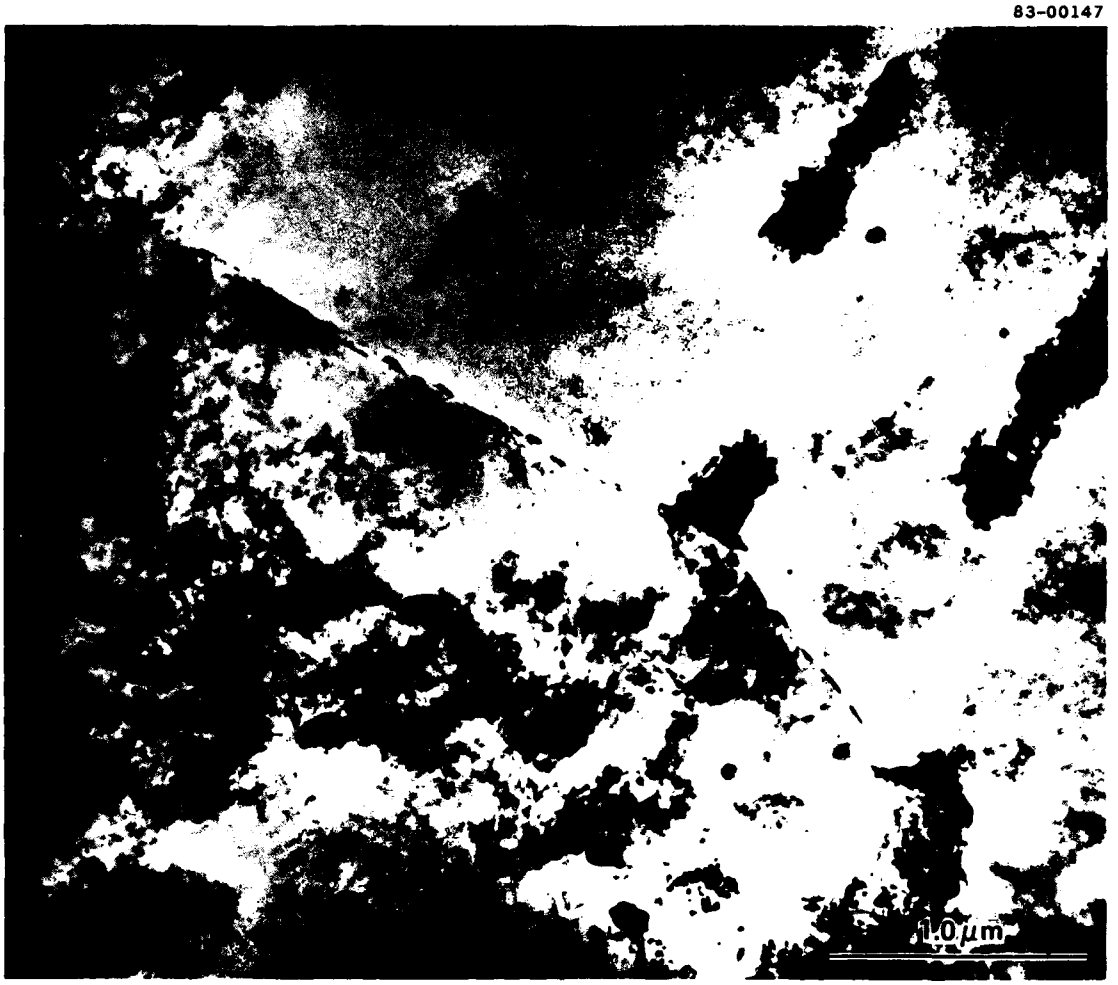

FIGURE 14. TEM MICROGRAPH OF 2324-T39 PLATE SHOWING LARGE Mn-BEARING DISPERSOIDS SURROUNDED BY DISLOCATION STRUCTURES RESULTING FROM COLD ROLLING

Optical micrographs of 7075-T651 are presented in Figure 15, and show large constituent particles including insoluble Al_7Cu_2Fe, partially soluble Mg_2Si, and soluble Al_2CuMg phases. This structure is fully recovered with a small amount of recrystallization. Previous work [15,18] indicates that 7075 contains incoherent $Al_{12}Mg_2Cr$ dispersoids and metastable strengthening precipitates, both G.P. zones and η' ($Mg(Al,Cu,Zn)_2$). A TEM micrograph of a typical 7075-T651 structure was included as Figure 18 in the Phase I report.

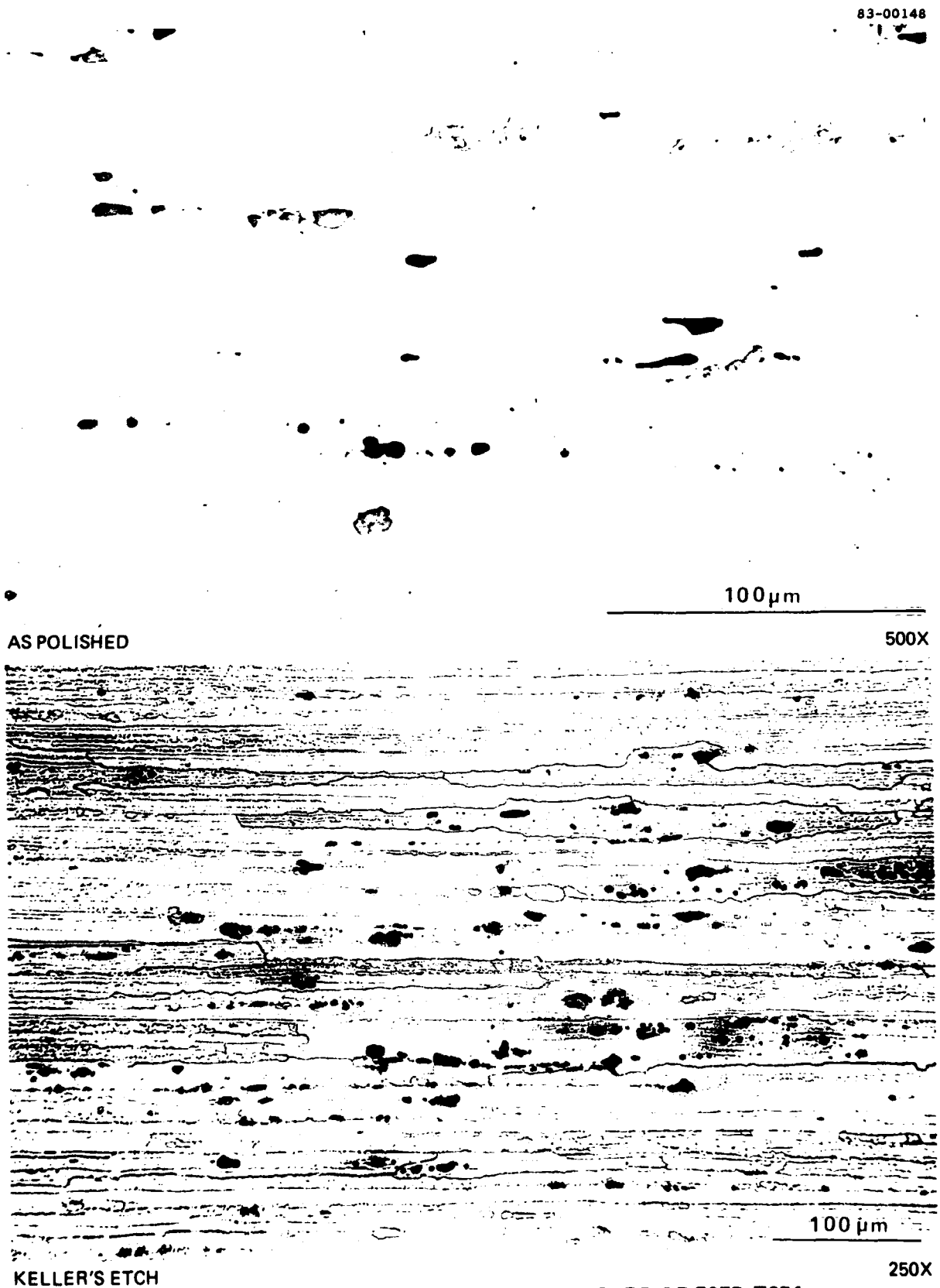

FIGURE 15. LONGITUDINAL MICROSTRUCTURE OF 7075-T651

3.3 TENSILE RESULTS

In the first phase of this study,[27] tensile tests were conducted on specimens of each alloy taken from the center (T/2), quarter thickness (T/4 and 3T/4), and near surface (top and bottom) locations. Results of these tests showed some variation in strength through the thickness in several plates. For the present contract phase, tensile specimens were taken only from the center and quarter thickness locations. These results, shown in Table 5, indicate little or no difference in either tensile or yield strength among the three test locations for any of the alloys. In all cases, the average values approximate typical properties or are well above minimum specifications.

TABLE 5. SUMMARY OF TENSILE RESULTS – LONGITUDINAL

MATERIAL PLATE THICKNESS MM (IN.)	SPECIMEN LOCATION[a b]	ULTIMATE STRENGTH		YIELD STRENGTH		ELONGATION IN 4D %[b]	REDUCTION OF AREA %[b]
		MPa	(KSI)	MPa	(KSI)		
2020-T651							
32.5 (1.28)	T/4	554	(80)	520	(75)	7	10
	T/2	551	(80)	520	(75)	6	9
		554	(80)	520	(75)	6	8
	3T/4	557	(81)	527	(76)	7	9
	AVERAGE	553	(80)	527	(76)	6	9
	AVERAGE T/4, 3T/4	555	(80)	522	(76)	7	10
	TYPICAL[c]	579	(84)	531	(77)	7	–
	MINIMUM	–	–	–	–	–	–
2024-T351	TOP SURFACE	467	(68)	364	(53)	17	20
31.8 (1.25)	T/4	450	(65)	360	(52)	19	26
	T/2	470	(68)	–	–	20	24
		470	(68)	372	(54)	19	24
	3T/4	451	(65)	361	(52)	21	24
	BOTTOM SURFACE	464	(67)	365	(53)	18	18
	AVERAGE	462	(67)	364	(53)	15	23
	AVERAGE T/4, 3T/4	451	(65)	360	(52)	20	25
	TYPICAL[c]	470	(68)	325	(47)	17[e]	–
	MINIMUM[c]	435	(63)	290	(42)	7[e]	–
2024-T851	TOP SURFACE	492	(71)	460	(67)	9	26
19.0 (0.75)	T/4	490	(71)	461	(67)	8	23
	T/2	493	(72)	465	(67)	8	22
		493	(72)	463	(67)	8	23
	3T/4	491	(71)	461	(67)	8	25
	BOTTOM SURFACE	499	(72)	465	(67)	9	23
	AVERAGE	493	(72)	463	(67)	8	24
	AVERAGE T/4, 3T/4	491	(71)	461	(67)	8	24
	TYPICAL[f]	483	(70)	448	(65)	8	–
	MINIMUM[d]	455	(66)	400	(58)	4[e]	–
2124-T851	TOP SURFACE	486	(70)	456	(66)	11	36
38.1 (1.5)	T/4	488	(71)	457	(66)	10	30
	T/2	486	(70)	457	(66)	10	28
		488	(71)	457	(66)	10	30
	3T/4	487	(71)	455	(66)	10	30
	BOTTOM SURFACE	488	(71)	454	(66)	11	35
	AVERAGE	487	(71)	455	(66)	10	32
	AVERAGE T/4, 3T/4	487	(71)	456	(66)	10	30
	TYPICAL[d.]	483	(70)	441	(64)	9	–
	MINIMUM[d]	455	(66)	395	(57)	5[f]	–
2324-T39							
37.8 (1.25)	T/4	487	(71)	450	(55)	15	25
	T/2	506	(73)	457	(66)	14	21
		507	(74)	455	(66)	14	23
	3T/4	486	(70)	453	(66)	15	24
	AVERAGE	496	(72)	454	(66)	15	23
	AVERAGE T/4, 3T/4	486	(71)	451	(65)	15	25
	TYPICAL	–	–	–	–	–	–
	MINIMUM[g]	455	(66)	386	(56)	10	–

TABLE 5. SUMMARY OF TENSILE RESULTS – LONGITUDINAL (CONTINUED)

MATERIAL PLATE THICKNESS MM (IN.)	SPECIMEN LOCATION[a b]	ULTIMATE STRENGTH		YIELD STRENGTH		ELONGATION IN 4D %[b]	REDUCTION OF AREA %[b]
		MPa	(KSI)	MPa	(KSI)		
7050-T73651	TOP SURFACE	520	(75)	462	(67)	15	40
25.4 (1.0)	T/4	535	(78)	478	(69)	15	33
	T/2	555	(80)	504	(73)	14	32
		553	(80)	500	(73)	13	32
	3T/4	534	(77)	478	(69)	15	35
	BOTTOM SURFACE	518	(75)	466	(68)	15	35
	AVERAGE	536	(78)	481	(70)	15	34
	AVERAGE T/4, 3T/4	534	(77)	478	(69)	15	34
	TYPICAL [h]	510	(74)	455	(66)	11	–
	MINIMUM [h]	490	(71)	427	(62)	9	–
7075-T651	T/4	588	(85)	533	(77)	12	16
19.1 (0.75)	T/2	593	(86)	540	(78)	11	14
		590	(86)	537	(78)	11	14
	3T/4	589	(85)	533	(77)	11	16
	AVERAGE	590	(86)	536	(78)	11	15
	AVERAGE T/4, 3T/4	589	(85)	533	(77)	12	16
	TYPICAL [d]	572	(83)	503	(78)	11	–
	MINIMUM [d]	538	(78)	469	(68)	7	–
7075-T7351	TOP SURFACE	486	(70)	409	(59)	14	33
25.4 (1.0)	T/4	502	(73)	429	(62)	12	28
	T/2	526	(76)	453	(66)	11	24
		527	(76)	454	(66)	11	24
	3T/4	502	(73)	431	(63)	13	28
	BOTTOM SURFACE	488	(71)	408	(59)	14	31
	AVERAGE	505	(73)	431	(62)	13	28
	AVERAGE T/4, 3T/4	502	(73)	430	(62)	13	28
	TYPICAL [f]	503	(73)	434	(63)	13	–
	MINIMUM [d]	475	(69)	390	(57)	6 [e]	–
7475-T651	TOP SURFACE	532	(77)	501	(73)	15	27
19.0 (0.75)	T/4	605	(88)	548	(79)	13	21
	T/2	585	(85)	541	(78)	12	17
		586	(85)	542	(79)	12	17
	3T/4	606	(88)	551	(80)	13	21
	BOTTOM SURFACE	537	(78)	506	(73)	15	22
	AVERAGE	575	(83)	531	(77)	14	21
	AVERAGE T/4, 3T/4	605	(88)	549	(80)	13	21
	TYPICAL	–	–	–	–	–	–
	MINIMUM [i]	531	(77)	469	(68)	8	–
7475-T7351	TOP SURFACE	493	(71)	423	(61)	17	51
38.1 (1.5)	T/4	511	(74)	441	(64)	17	47
	T/2	529	(77)	464	(67)	15	39
		527	(76)	461	(67)	14	37
	3T/4	514	(75)	444	(64)	17	46
	BOTTOM SURFACE	486	(70)	420	(61)	17	47
	AVERAGE	510	(74)	442	(64)	16	44
	AVERAGE T/4, 3T/4	513	(74)	442	(64)	17	47
	TYPICAL	–	–	–	–	–	–
	MINIMUM [i]	469	(68)	393	(57)	10	–

TABLE 5. SUMMARY OF TENSILE RESULTS (Concluded)

FOOTNOTES

[a] SPECIMENS TAKEN FROM THE T/2 LOCATION ARE FROM THE CENTER OF THE PLATE THICKNESS AND THOSE FROM THE T/4 AND 3T/4 ARE FROM MIDWAY BETWEEN THE CENTER AND THE TOP SURFACE OR BOTTOM SURFACE, RESPECTIVELY

[b] THE NOMINAL DIAMETER OF THE REDUCED-SECTION OF T/2 SPECIMENS WAS 12.7MM, T/4 AND 3T/4 SPECIMENS WAS 6.4MM, AND SURFACE SPECIMENS WAS 4.1MM

[c] "ALCOA ALLOY X-2020," ALCOA GREEN LETTER, ISSUED JULY 1962

[d] "ALUMINUM STANDARDS AND DATA," THE ALUMINUM ASSOCIATION, 1978

[e] ELONGATION MEASURED OVER 5D

[f] ALCOA ALUMINUM HANDBOOK, 1967

[g] SPECIFIED MINIMUM PROPERTIES

[h] "ALCOA ALLOY 7050," ALCOA GREEN LETTER, ISSUED APRIL 1976

[i] "ALCOA 7475 SHEET AND PLATE," ALCOA GREEN LETTER, ISSUED FEBRUARY 1978

3.4 FRACTURE TOUGHNESS RESULTS

Table 6 contains the results of fracture toughness tests conducted on compact specimens of full plate thickness. All tests were valid per ASTM Standard Test Method E399, except for the 2024-T351 and 7475-T651 alloys. Specified minimum K_{Ic} values are not available for any of the three alloys tested in this phase; however, the fracture toughness values are within the ranges usually encountered for each material.

TABLE 6. FRACTURE TOUGHNESS RESULTS, L-T ORIENTATION

ALLOY AND TEMPER	PLATE THICKNESS mm (in.)	SPECIMEN THICKNESS mm	K_Q MPa $\sqrt{m}$ (ksi $\sqrt{in.}$)	VALID K_{IC} PER ASTM E399	AVERAGE VALID K_{IC} OR MEANINGFUL K_Q MPa $\sqrt{m}$ (ksi $\sqrt{in.}$)
2020-T651	32.5 (1.28)	32.5	24 (21)	YES	
		32.5	24 (22)	YES	24 (21)
2024-T351	31.8 (1.25)	31.8	39 (36)	NO[a]	
		31.8	39 (36)	NO[a]	39 (36)
2024-T851	19.0 (0.75)	18.0	24 (22)	YES	
		18.0	24 (22)	YES	24 (22)
2124-T851	38.1 (1.5)	38.1	33 (30)	YES	
		38.1	33 (30)	YES	33 (30)
2324-T39	31.8 (1.25)	31.8	34 (31)	YES	
		31.8	34 (31)	YES	34 (31)
7050-T73651	25.4 (1.0)	24.8	39 (36)	YES	
		24.8	39 (36)	YES	39 (36)
7075-T651	19.1 (0.75)	19.1	29 (26)	YES	
			28 (26)	YES	29 (26)
7075-T7351	25.4 (1.0)	25.4	32 (29)	YES	
		25.4	32 (29)	YES	32 (29)
7475-T651	19.0 (0.75)	18.0	48 (44)	NO[b]	
		18.0	41 (38)	NO[a]	41 (38)
7475-T7351	38.1 (1.5)	38.1	55 (50)	YES	
		38.1	56 (50)	YES	55 (50)

[a]TEST INVALID PER ASTM E399 SINCE $P_{MAX}/P_Q > 1.10$. HOWEVER, DATA STILL MEANINGFUL, SINCE P_{MAX}/P_Q WAS 1.15

[b]TEST INVALID PER ASTM E399 DUE TO INSUFFICIENT THICKNESS AND FATIGUE CRACK LENGTH

3.5 FATIGUE CRACK GROWTH RESULTS UNDER CONSTANT AMPLITUDE LOADING

Fatigue crack growth data were generated for all alloys from near-threshold (ΔK_{th}) through intermediate ΔK values, with measured near-threshold FCG rates approaching 10^{-10} m/cycle (4×10^{-9} in./cycle). The FCGR data for the three alloys evaluated in this phase are presented in Figures A-1 through A-3 in Appendix A. The FCGR data for the seven alloys evaluated in Phase I are presented in Reference 27, Appendix A. In Figure 16, the da/dN versus ΔK curves for all ten alloys are shown. In addition, the FCGR data are shown in Figure 17 and Table 7 as the stress intensity required to drive a fatigue crack at a specified rate. In Figure 17 the results are grouped into 2000 and 7000 series and within the groups are in descending order of their spectrum fatigue lives (Section 3.6).

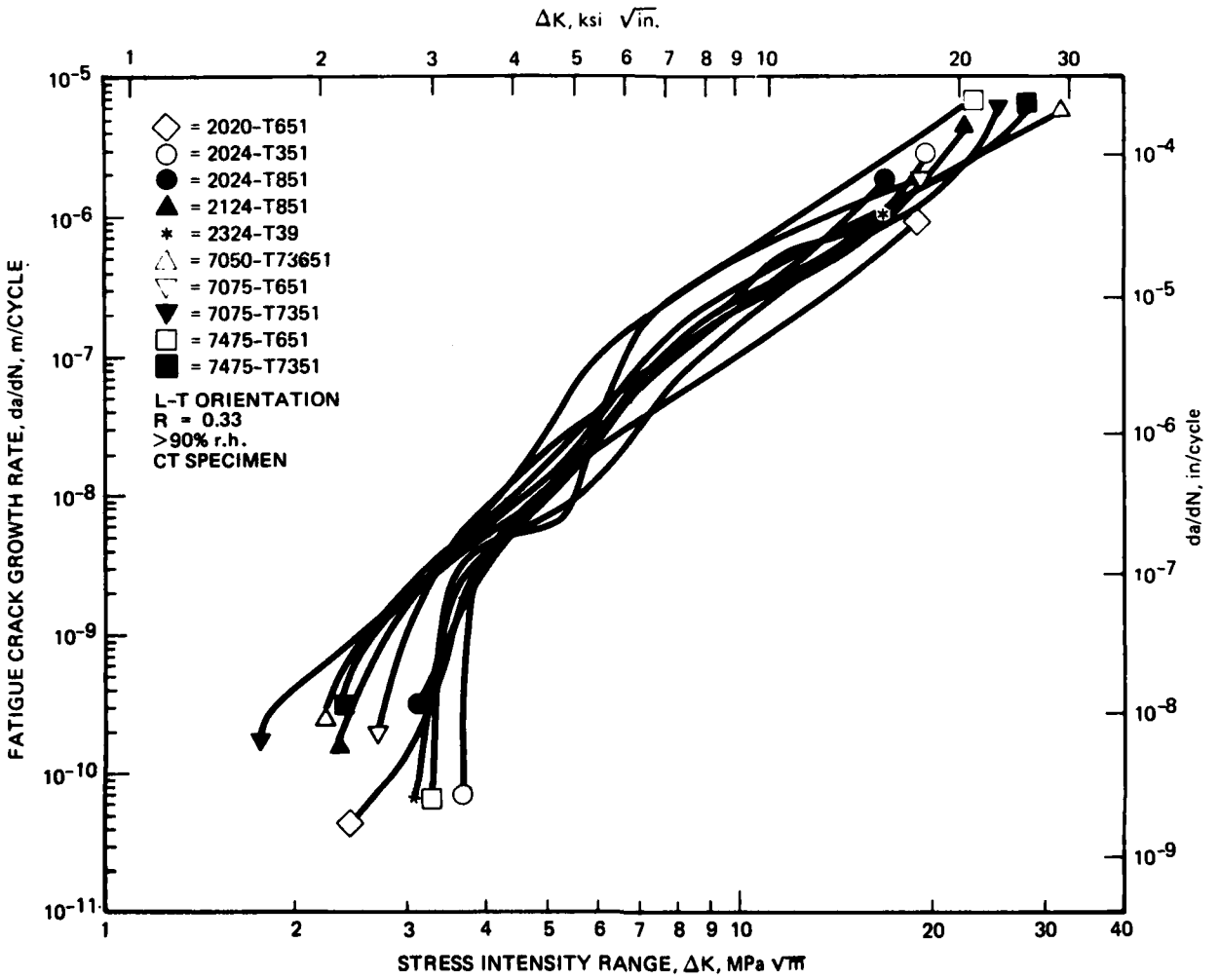

FIGURE 16. COMPARISON OF FATIGUE CRACK GROWTH BEHAVIOR UNDER CONSTANT AMPLITUDE LOADING

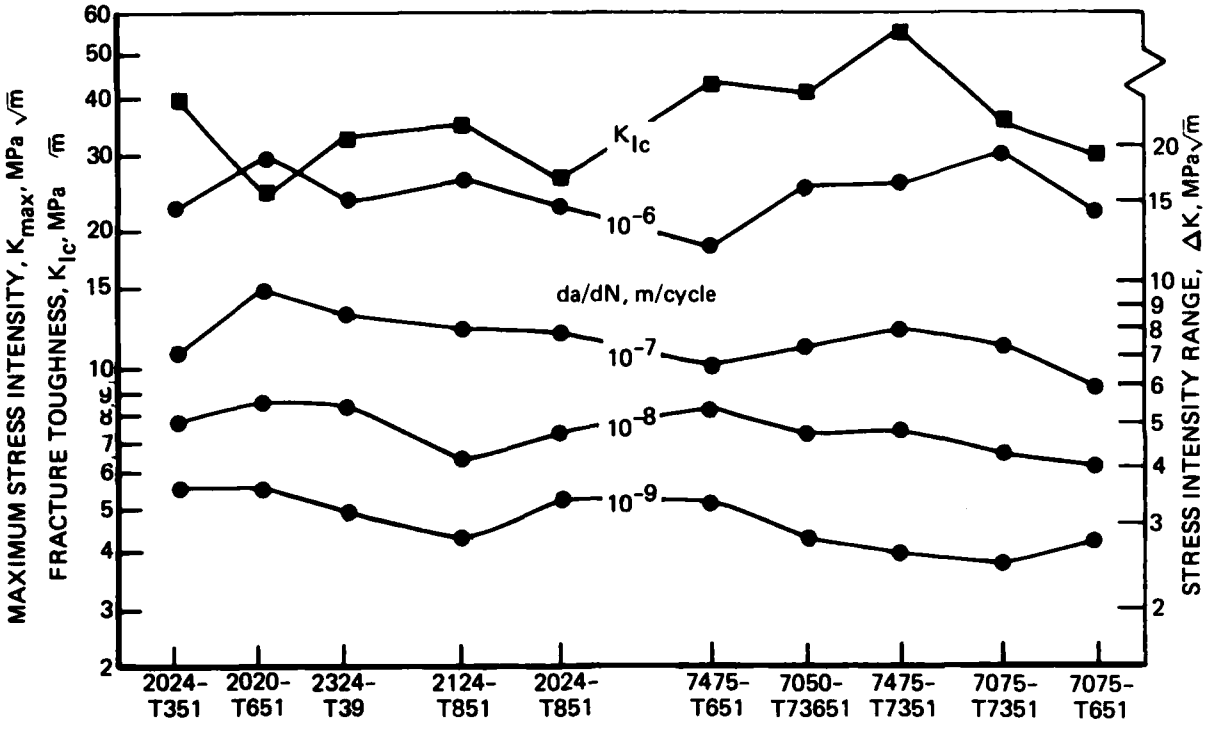

FIGURE 17. STRESS INTENSITY NEEDED TO OBTAIN A GIVEN FATIGUE CRACK GROWTH RATE UNDER CONSTANT AMPLITUDE LOADING. (R = 0.33, > 90% rh, L-T ORIENTATION)

TABLE 7. RANKING OF MATERIALS BY STRESS INTENSITY RANGE TO OBTAIN A GIVEN FATIGUE CRACK GROWTH RATE UNDER CONSTANT AMPLITUDE LOADING

	ΔK, MPa $\sqrt{m}$ (ksi $\sqrt{in.}$) TO OBTAIN A GIVEN FCGR									
FCGR	RANK	10^{-10} m/CYCLE (4×10^{-9} in/CYCLE)	RANK	10^{-9} m/CYCLE (4×10^{-8} in/CYCLE)	RANK	10^{-8} m/CYCLE (4×10^{-7} in/CYCLE)	RANK	10^{-7} m/CYCLE (4×10^{-6} in/CYCLE)	RANK	10^{-6} m/CYCLE (4×10^{-5} in/CYCLE)
MATERIAL 2020-T651	4	2.9 (2.7)	2	3.7 (3.4)	2	5.5 (5.0)	1	10.2 (9.3)	2	18.0 (16.4)
2024-T351	1	2.7 (3.4)	1	3.8 (3.5)	2	5.5 (5.0)	6	7.6 (6.9)	7	16.2 (14.7)
2024-T851	5	2.7 (2.5)[a]	3	3.5 (3.2)	6	4.8 (4.4)	3	8.0 (7.3)	8	15.0 (13.7)
2124-T851	7	2.2 (2.0)[a]	7	2.8 (2.5)	9	4.3 (3.9)	3	8.0 (7.3)	3	17.2 (15.7)
2324-T39	3	3.2 (2.9)	5	3.4 (3.1)	1	5.7 (5.2)	2	8.9 (8.1)	6	16.4 (14.9)
7050-T73651	8	2.1 (1.9)[a]	8	2.7 (2.5)	7	4.7 (4.3)	8	7.2 (6.6)	4	16.9 (15.4)
7075-T651	6	2.6 (2.3)[a]	6	2.9 (2.7)	10	4.2 (3.9)	10	6.0 (5.5)	9	14.0 (12.7)
7075-T7351	10	1.7 (1.6)[a]	10	2.5 (2.3)	8	4.4 (4.0)	6	7.6 (6.9)	1	19.0 (17.3)
7475-T651	2	3.3 (3.0)	4	3.4 (3.1)	4	5.4 (4.9)	9	6.6 (6.0)	10	12.1 (11.0)
7475-T7351	9	2.0 (1.8)[a]	9	2.6 (2.4)	5	4.9 (4.5)	3	8.0 (7.3)	5	16.6 (15.1)

[a] EXTRAPOLATED

The data in Figure 16 show that the variation in FCP resistance among the ten alloys is greatest in the near-threshold regime ($\Delta K \lesssim 4$ MPa $\sqrt{m}$); while for higher ΔK levels, crack growth rates vary by no more than a factor of 5. Further study of Figure 16 reveals that the relative rankings in FCP resistance change with ΔK level; these changes in ranking are listed in Table 7. For example, alloy 7475-T651 has the second highest ΔK_{th} value, indicating excellent low ΔK FCP resistance; in contrast, for $\Delta K > 10$ MPa $\sqrt{m}$ this alloy has the highest growth rates.

Alloys 2020-T651 and 2324-T39 have lower crack growth rates in the intermediate ΔK region (4 MPa $\sqrt{m} \lesssim \Delta K \leq 20$ MPa $\sqrt{m}$) than those for the other eight alloys. Both of these alloys also have relatively high crack growth thresholds. In the case of 2020-T651, however, FCP resistance at high ΔK will be poor as a result of the low fracture toughness of this alloy (24 MPa $\sqrt{m}$). Crack growth rates in 7075-T651 are higher than those for all other alloys in the ΔK range from 4 to 7 MPa $\sqrt{m}$, but are within the band for the other alloys for stress intensities outside that range.

The effects of purity and temper on constant-amplitude FCP were discussed in the Phase I report.[27] The addition of 7075-T651 to the test matrix in this phase reinforces the observation that alloy purity (Fe and Si content) has no effect on near-threshold FCP rates. Rather, increasing purity is expected to decrease crack growth rates at high ΔK levels, concurrent with an increase in fracture toughness,[18] although this is not apparent in the range of fatigue crack growth rates generated herein (Figure 16). (However, as will be discussed later on, the spectrum FCG rates was found to be lower for the higher purity versions of the alloys at high stress intensities.)

The effect of temper in 7XXX alloys varies with ΔK level. At near-threshold levels in both 7075 and 7475, the peak aged T651 temper has significantly lower growth rates than overaged T7351. In contrast, crack growth rates generally are lower for the T7351 temper at intermediate and high ΔK levels, a difference attributed to the greater resistance of an overaged temper to the acceleration of FCP rates in the presence of high humidity.[18] Recent studies [19, 37, 38] also have observed this crossover in fatigue resistance from intermediate to low ΔK levels and have rationalized the

greater near-threshold resistance of the T651 temper in terms of microstructural details such as precipitate morphology and distribution. These same microstrucural features appear to influence spectrum FCP behavior as will be discussed later in Section 3.6.2.

3.6 SPECTRUM TEST RESULTS

The spectrum life results for each test are presented in Table 8. Overall, the results were reproducible, with the maximum difference between the lives of duplicate tests being 21 percent. Crack length versus simulated flight hour data (a versus H) are shown graphically in Appendix B, while results for spectrum crack growth rate versus maximum peak stress intensity (da/dH versus K_{hmax}) are shown in Appendix C. For comparison, spectrum crack growth rate curves (da/dH versus K_{hmax}) for all ten materials are shown in Figure 18a and 18b. For easier comparison of resistance to spectrum crack growth among all ten materials for both spectra, the maximum peak stress intensities to obtain a given crack growth rate are shown in Figure 19 and Table 9 in presentations similar to those for the constant amplitude data in Figure 17 and Table 7.

TABLE 8. SPECTRUM FATIGUE RESULTS – BASELINE SPECTRA

MAXIMUM PEAK STRESS σ_{hmax}	SIMULATED FLIGHT HOURS, H					
	103 MPa (15 ksi)		145 MPa (21 ksi)		169 MPa (24.5 ksi)	
SPECTRUM	TD	TC	TD	TC	TD	TC
CRACK GROWTH REGIME, a_i to a_f	6-13 mm 0.24-0.51 in.	6-13 mm 0.24-0.51 in.	6 mm-F[a] 0.24 in.-F	6 mm-F 0.24 in.-F	18 mm-F 0.71 in.-F	18 mm-F 0.71 in.-F
MATERIAL[b]						
2020-T651	78,416	54,895	17,188	14,575	0[c]	0[c]
	–	–	20,020	11,717	–	–
2024-T351	26,412	24,633	21,719	15,375	2,451	1,092
	28,027	24,035	22,565	15,389	2,363	1,192
			22,122			
2024-T851	18,297	18,299	8,505	7,031	196	0[c]
	19,258	17,824	8,557	7,132	184	0[c]
2124-T851	17,274	15,787	11,244	8,853	851	1,085
	16,769	15,563	11,096	9,314	828	1,245
2324-T39	29,057	24,616	18,148	15,338	2,443	1,159
	–	–	17,547	13,529	–	–
7050-T73651	18,741	19,467	14,496	13,340	2,260	1,638
	18,930	16,217	15,223	12,962	2,455	1,837
7075-T651	14,775	13,886	9,820	8,617	651	380
	–	–	11,945	9,181	–	–
7075-T7351	17,642	16,666	13,517	10,392	1,300	740
	16,910	16,529	12,314	10,934	1,601	781
7475-T651	15,387	15,522	18,303	14,744	3,777	2,661
	15,384	16,624	19,792	15,141	3,197	2,608
7475-T7351	18,241	16,578	15,417	13,410	2,714	2,152
	18,873	17,332	14,661	13,345	2,852	2,256

a. F = FAILURE

b. RESULTS FOR 2020-T651, 2324-T39, AND 7075-7651 ARE FOR PRESENT EFFORT, OTHER RESULTS FROM PHASE I.

c. SPECIMEN FRACTURED BEFORE REACHING INITIAL CRACK LENGTH, a_i, OF 18mm, FOR THESE MPa (24.5 ksi) TESTS, IN FATIGUE

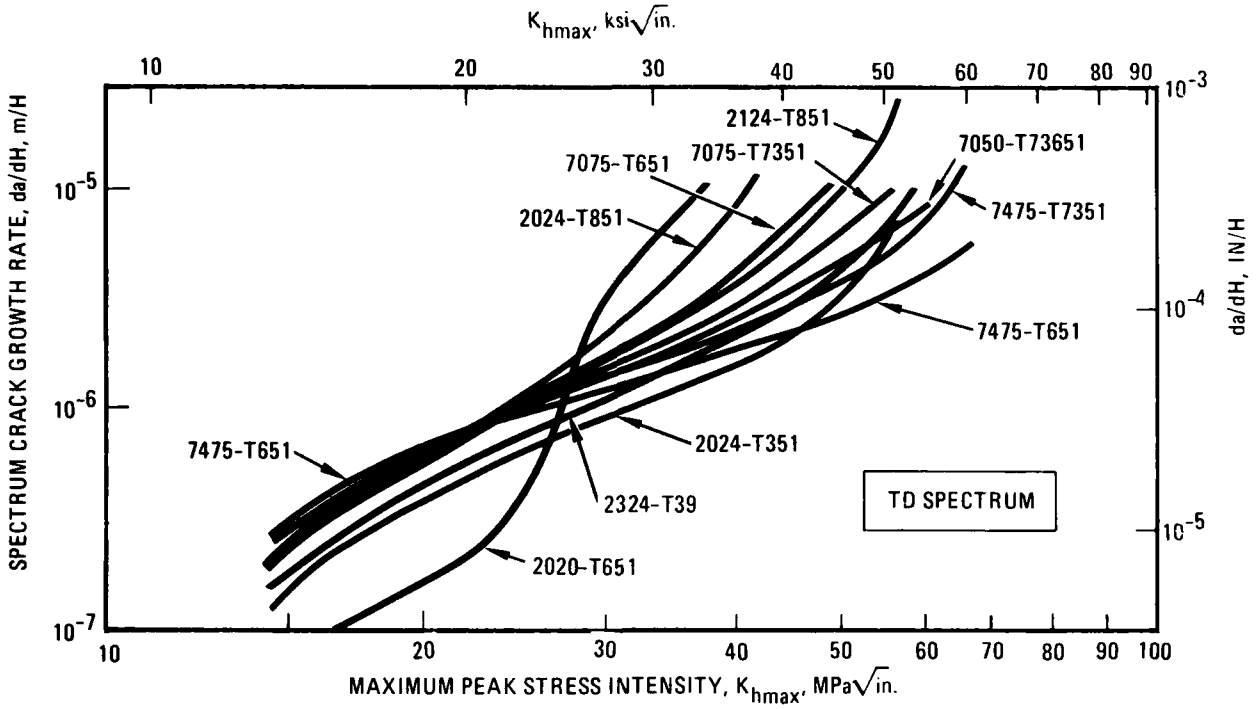

a. TENSION DOMINATED SPECTRUM

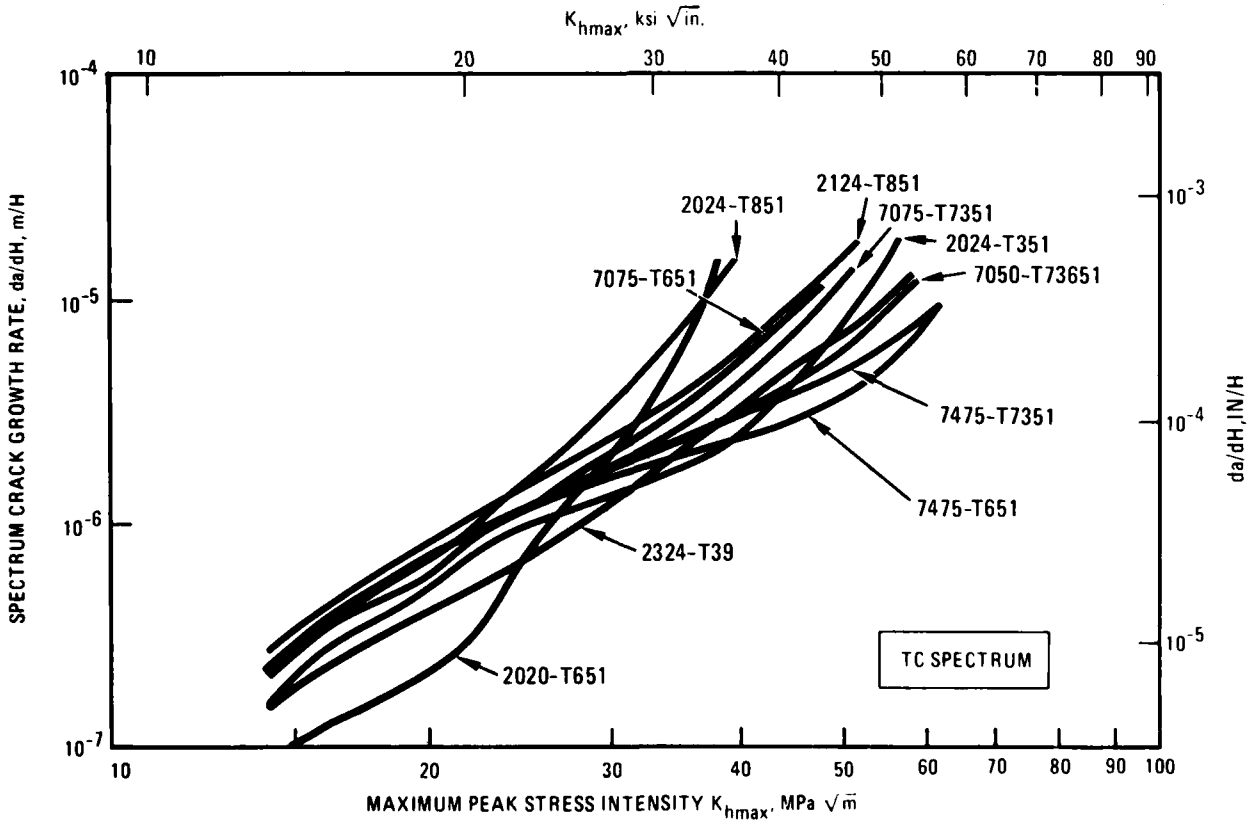

b. TENSION-COMPRESSION SPECTRUM

FIGURE 18. SPECTRUM FCGR CURVES

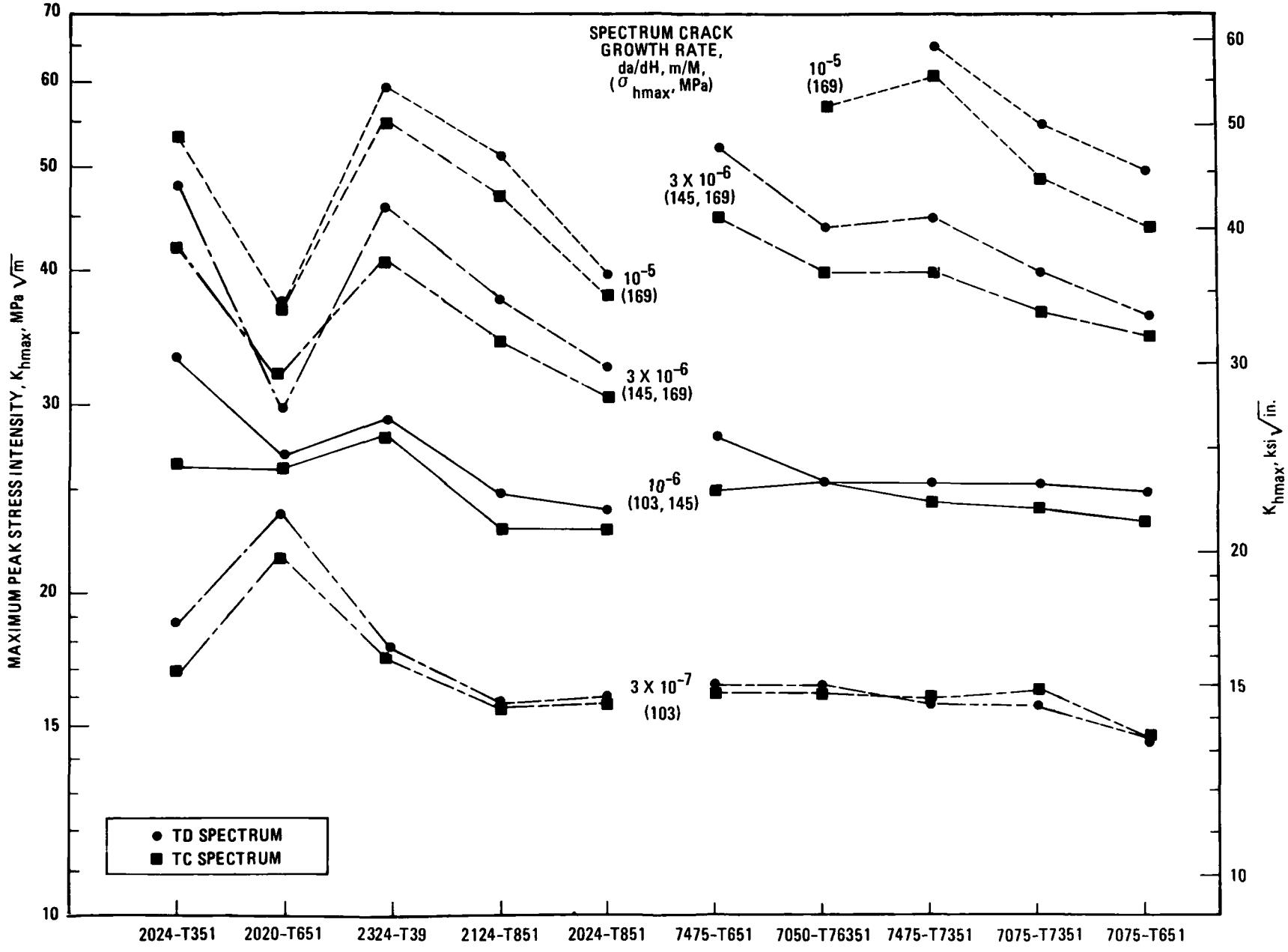

FIGURE 19. MAXIMUM PEAK STRESS INTENSITY NEEDED TO OBTAIN A GIVEN SPECTRUM FCGR FOR TD AND TC SPECTRA

TABLE 9. RANKING OF MATERIALS IN SPECTRUM FATIGUE BY MAXIMUM PEAK STRESS INTENSITY TO OBTAIN A GIVEN FATIGUE CRACK GROWTH RATE

	K_{hmax}, MPa $\sqrt{m}$ (ksi $\sqrt{in.}$) TO OBTAIN A GIVEN SPECTRUM FCGR											
FCGR	3×10^{-7} m/H[a] (1.2×10^{-5} in./H)			10^{-6} m/H (4×10^{-5} in./H)[b]			3×10^{-6} m/H (1.2×10^{-4} in./H)[c]			10^{-5} m/H (4×10^{-4} in./H)[d]		
SPECTRUM	TD	RANK[e]	TC	TD	RANK[e]	TC	TD	RANK[e]	TC	TD	RANK[e]	TC
MATERIAL												
2020-T651	24.1 (22.1)	1	21.9 (19.9)	27.1 (24.9)	3	26.3 (23.9)	30 (28)	9	32 (29)	37 (34)	9	37 (34)
2024-T351	18.8 (17.1)	2	17.0 (15.5)	33.0 (30.0)	1	26.5 (24.1)	48 (44)	2	42 (38)	– –	4	53 (48)
2024-T851	16.0 (14.6)	8	15.9 (14.5)	24.0 (21.8)	10	23.0 (20.9)	32 (29)	9	31 (28)	41 (37)	8	38 (35)
2124-T851	15.8 (14.4)	9	15.7 (14.3)	24.8 (22.6)	9	23.0 (20.9)	38 (35)	7	34 (31)	51 (46)	6	47 (43)
2324-T39	18.1 (16.5)	3	17.5 (15.9)	29.0 (26.4)	2	28.1 (25.6)	47 (43)	3	41 (37)	58 (53)	2	55 (50)
7050-T73651	16.2 (14.7)	4	16.5 (15.0)	25.5 (23.2)	5	25.5 (23.2)	44 (40)	5	40 (36)	– –	3	57 (52)
7075-T651	14.8 (13.5)	10	14.8 (13.5)	24.9 (22.7)	8	23.8 (21.7)	37 (34)	8	35 (32)	50 (46)	7	44 (40)
7075-T7351	16.4 (14.9)	6	15.9 (14.5)	25.5 (23.2)	7	24.2 (22.0)	40 (36)	6	37 (34)	55 (50)	5	49 (45)
7475-T651	16.2 (14.7)	4	16.5 (15.0)	28.0 (25.5)	4	24.7 (22.5)	52 (47)	1	45 (41)	– –	1[f]	– –
7475-T7351	16.0 (14.7)	7	15.9 (14.5)	25.5 (23.2)	6	24.5 (22.3)	45 (41)	4	40 (36)	65 (59)	2	61 (56)

a σ_{hmax} = 103 MPa (15 ksi)

b σ_{hmax} = 103 MPa (15ksi) and 145 MPa (21 ksi)

c σ_{hmax} = 145 MPa (21 ksi

d σ_{hmax} = 145 MPa (21 ksi) and 169 MPa (24.5 ksi)

e BASED ON AVERAGE TD AND TC SPECTRUM

f BASED ON EXTRAPOLATION

In general, for each material, the spectrum FCG curves (Figures 18a and 18b) have the same trends for the two spectra (TD and TC), i.e., the magnitudes are similar and the crossovers are in similar places. Also, the spectrum fatigue crack growth rates (da/dH versus K_{hmax}) for the testing at the three maximum stress levels overlap for the same material and spectrum (see Appendix C). The two exceptions may be 2020-T651 (Figures C-1 and C-2 in Appendix C) and 7475-T651 (Figures C-11 and C-12, Reference 27), but the scatter in data for these two alloys was greater than that for the other alloys, which prevents definite conclusions from being drawn. The 7475-T651 result was discussed in Reference 27. For 2020-T651, for both the TD and TC spectra, the spectrum crack growth rates for tests performed at 103 MPa appear to be somewhat slower than those for tests performed at 145 MPa and 169 MPa.

3.6.1 Ranking of the Materials

The alloys are ranked by their spectrum fatigue lives for each spectrum (average of the two duplicate tests) in Table 10 as the initial step in determining critical material and spectrum parameters. These results are shown graphically in Figure 20. Several observations for the 145 MPa test results ("a" from 6 mm to failure) can be made:

1. The ranking of the ten alloys is the same in the two spectra, except for 2020-T651 for which the ranking under the TC spectrum is considerably lower than under the TD spectrum.
2. For each material the TD spectrum consistently resulted in longer life.
3. The differences in life for the same material between the two spectra were small – not more than 18 percent difference for any of the alloys except 2020-T651 and 2024-T351, which had 34 and 36 percent differences, respectively.

TABLE 10. RANKING OF MATERIALS UNDER SPECTRUM LOADING – BASELINE SPECTRA

AVERAGES OF TWO TESTS ROUNDED TO NEAREST HUNDRED HOURS

a. σ_{hmax} = 103 MPa FROM a = 6 TO 13mm

TD SPECTRUM	
MATERIAL	SIMULATED FLIGHT HOURS
2020-T651	78,400[a]
2324-T39	29,100[a]
2024-T351	27,200
7050-T73651	18,800
2024-T851	18,800
7475-T7351	18,600
7075-T7351	17,300
2124-T851	17,300
7475-T651	15,400
7075-T651	14,800[a]

TC SPECTRUM	
MATERIAL	SIMULATED FLIGHT HOURS
2020-T651	54,900[a]
2324-T39	24,600
2024-T351	24,300[a]
2024-T851	18,100
7050-T73651	17,800
7475-T7351	17,000
7075-T7351	16,600
7475-T651	16,100
2124-T851	15,700
7075-T651	13,900[a]

b. σ_{hmax} = 145 MPa FROM a = 6mm TO FAILURE

TD SPECTRUM	
MATERIAL	SIMULATED FLIGHT HOURS
2024-T351	22,100
7475-T651	19,000
2020-T651	18,500
2324-T39	17,800
7475-T7351	15,000
7050-T73651	14,900
7075-T7351	12,900
2124-T851	11,200
7075-T651	10,800
2024-T851	8,500

TC SPECTRUM	
MATERIAL	SIMULATED FLIGHT HOURS
2024-T351	15,400
7475-T651	14,900
2324-T39	14,400
7475-T7351	13,400
7050-T73651	13,200
2020-T651	13,100
7075-T7351	10,700
2124-T851	9,100
7075-T651	8,900
2024-T851	7,100

c. σ_{hmax} = 169 MPa FROM a = 18mm TO FAILURE

TD SPECTRUM	
MATERIAL	SIMULATED FLIGHT HOURS
7475-T651	3,400
7475-T7351	2,800
2324-T39	2,400[a]
2024-T351	2,400
7050-T73051	2,400
7075-T7351	1,400
2124-T851	800
7075-T651	700[a]
2024-T851	200
2020-T651	0[ab]

TC SPECTRUM	
MATERIAL	SIMULATED FLIGHT HOURS
7475-T651	2,600
7475-T7351	2,200
7050-T73651	1,700
2124-T851	1,200
2324-T39	1,200[a]
2024-T351	1,100
7075-T7351	800
7075-T651	400[a]
2024-T851	0[b]
2020-T651	0[ab]

[a] ONE TEST RESULT

[b] SPECIMEN FRACTURED BEFORE READING INITIAL CRACK LENGTH

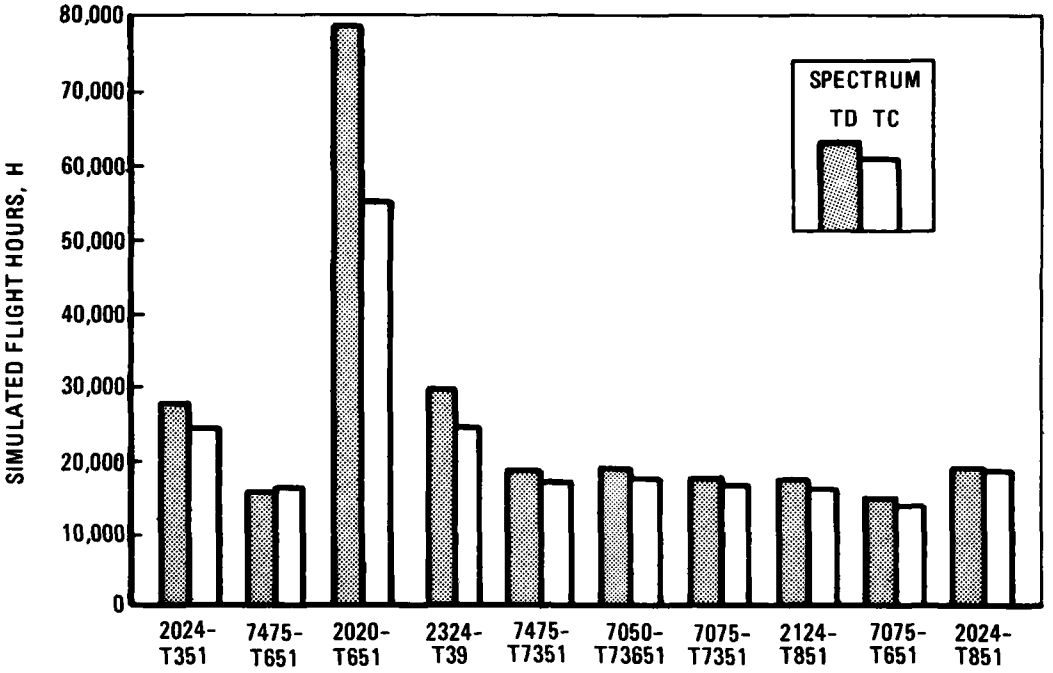

a. SPECTRUM LIFE AT 103 MPa, "a" FROM 6 TO 13MM – THE MATERIALS ARE LISTED IN DESCENDING ORDER FOR LIFE AT 145 MPa

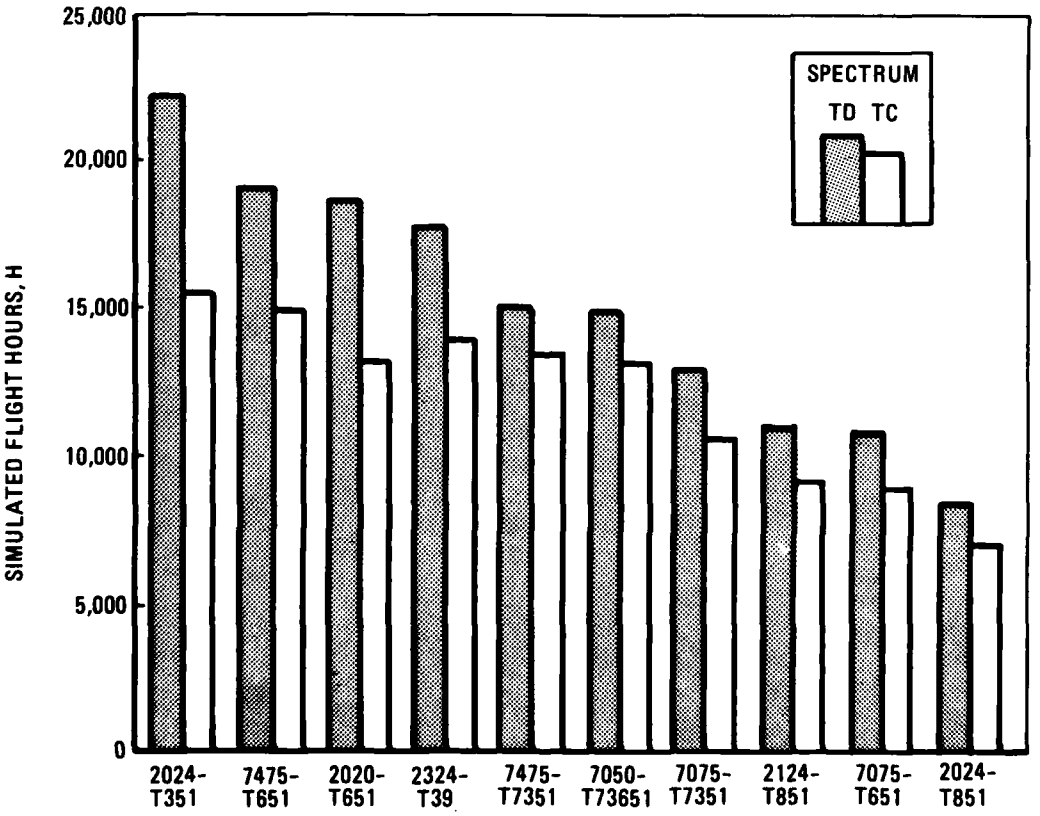

b. SPECTRUM RANKING AT 145 MPa, "a" FROM 6 MM TO FAILURE

FIGURE 20. SPECTRUM FATIGUE LIVES

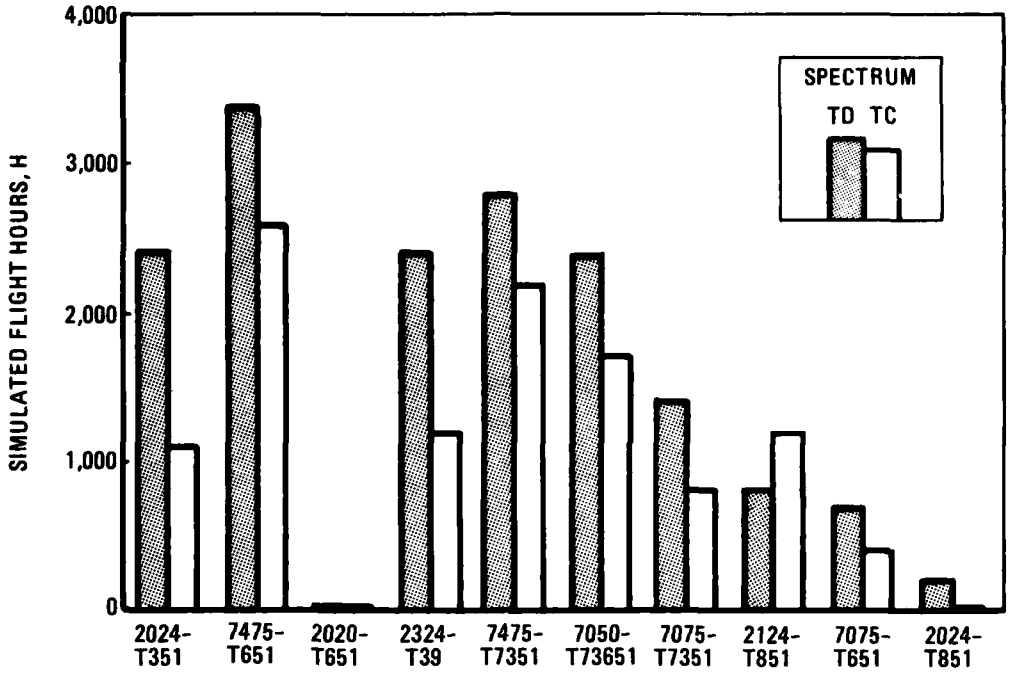

c. SPECTRUM LIFE AT 169 MPa, "a" FROM 18 MM TO FAILURE – THE MATERIALS ARE LISTED IN DESCENDING ORDER FOR LIFE AT 145 MPa

FIGURE 20. SPECTRUM FATIGUE LIVES (Concluded)

4. There were larger differences in lives among the 2XXX materials than among the 7XXX materials, for example, an 84 percent difference for the TD spectrum between the two extremes for 2XXX materials, 2024-T851 and 2024-T351, compared to a 55 percent difference for the TD spectrum between the extremes for 7XXX materials, 7475-T651 and 7075-T651.

5. Comparing the spectrum lives and the spectrum fatigue crack growth rates (Figures 18 and 20) shows that no one regime of spectrum crack growth (or regime of stress intensity) controls the overall spectrum life. This is best shown by 2020-T651 and 7475-T651, which have nearly equal lives, but significantly different spectrum crack growth rate behavior - at low peak stress intensities, 7475-T651 has the fastest SFCGR of all materials evaluated and 2020-T651 has the slowest SFCGR of all materials tested. Whereas, at higher peak stress intensities, 7475-T651 has the slowest SFCGR and 2020-T651 the fastest SFCGR.

Due to the test methodology, the lives of the specimens for the testing at the other two maximum peak stress levels (103 and 169 MPa) represent a much smaller range of crack growth (or range of maximum peak stress intensity).* Specifically, for the 103 MPa testing, the range of maximum peak stress intensity is only from 14.3 to 21.8 MPa $\sqrt{m}$ (see Figures 9 and 10). Several observations from the 103 MPa test results ("a" from 6 to 13 mm) can be made (Figure 20a):

1. The 2XXX alloys 2020-T651, 2324-T39, and 2024-T351 had longer spectrum fatigue lives than the other alloys, and among those, 2020-T651 alloy had a significantly longer spectrum fatigue life.
2. For each alloy, the TD spectrum resulted in a longer spectrum fatigue life than the TC spectrum, except 7475-T651, for which the life for the TD spectrum was slightly shorter.
3. The rankings do not correlate with the rankings for testing at 145 MPa.

For the 169 MPa testing the initial maximum peak stress intensity was 43.6 MPa $\sqrt{m}$ and the test was continued to failure. In comparison to the testing at the other two maximum peak stresses, the lives are an order of magnitude shorter. The lives represent less than one aircraft lifetime and, therefore, are of less value for airframe applications. Nevertheless, several observations from these results ("a" from 18 mm to failure) can be made (Figure 20c and Table 10c) in comparison to the results at 145 MPa:

1. The ranking of the 7XXX materials has improved compared to the 2XXX materials, with 7475-T651 and 7475-T7351 being top ranked for both spectra.
2. The rankings within the 7XXX materials are the same for both spectra.

---

*For the tests at 103 and 169 MPa performed on the three materials in this phase, the entire specimen was spectrum fatigue tested at one maximum peak stress level, therefore spectrum life can be computed for "a" from 6 mm to failure. However, for the seven materials evaluated in Phase I this information is not available (see Section 2.6.5). Therefore comparisons for "a" from 6 mm to failure cannot be made for all ten materials. These results for "a" from 6 mm to failure for the three alloys evaluated in this phase are tabulated in Appendix H.

3. The ranking within the 2XXX materials for the TD spectra is similar except 2020-T651 is lowest ranked compared to second ranked.

4. The ranking within the 2XXX materials for the TC spectra does not correlate.

3.6.2 Effects of Yield Strength and Temper

The spectrum fatigue lives are plotted as a function of yield strength in Figure 21. These data suggest that there is no general relationship between yield strength and spectrum fatigue life at any of the three maximum peak stress levels, an observation made previously in Phase I,[27] nor can any relationship be seen by considering the 2XXX and 7XXX alloys as two separate groups. This absence of a correlation is in contrast to current life prediction models, such as that developed by Willenborg,[20] which assume that decreasing yield strength increases crack growth retardation and lengthens spectrum fatigue life. Of particular note are the data for 2020-T651 at the lowest stress level (Figure 21a); this alloy exhibits significantly longer fatigue lives than any other material in both spectra, despite having nearly the highest yield strength. Clearly, yield strength alone cannot explain differences in retardation and, hence, in spectrum fatigue life among all ten alloys.

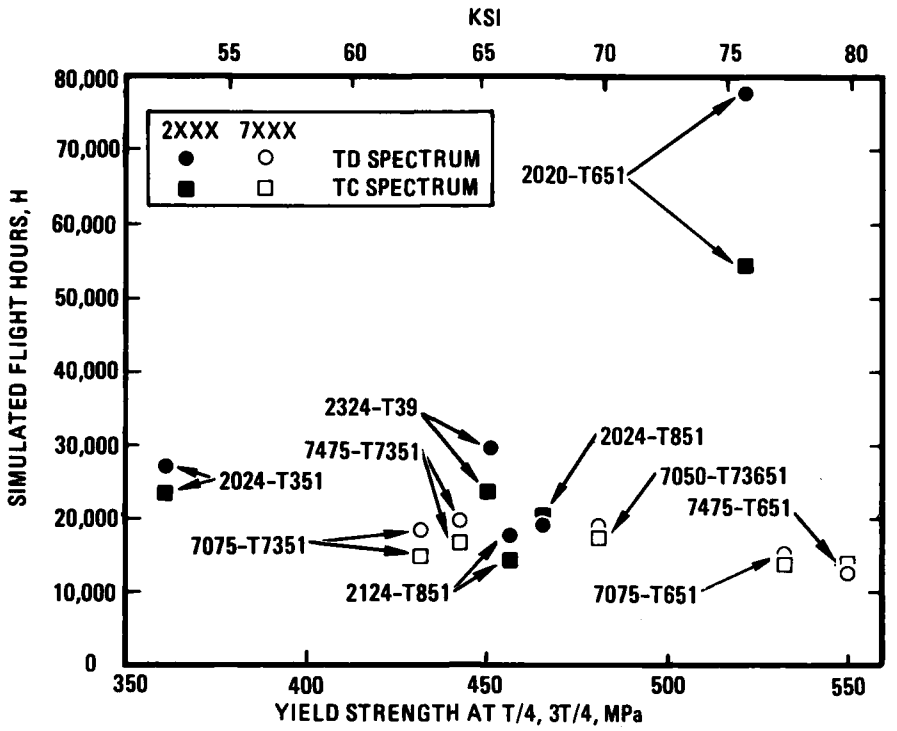

a. σ_{hmax} = 103 MPa, "a" FROM 6 TO 13MM

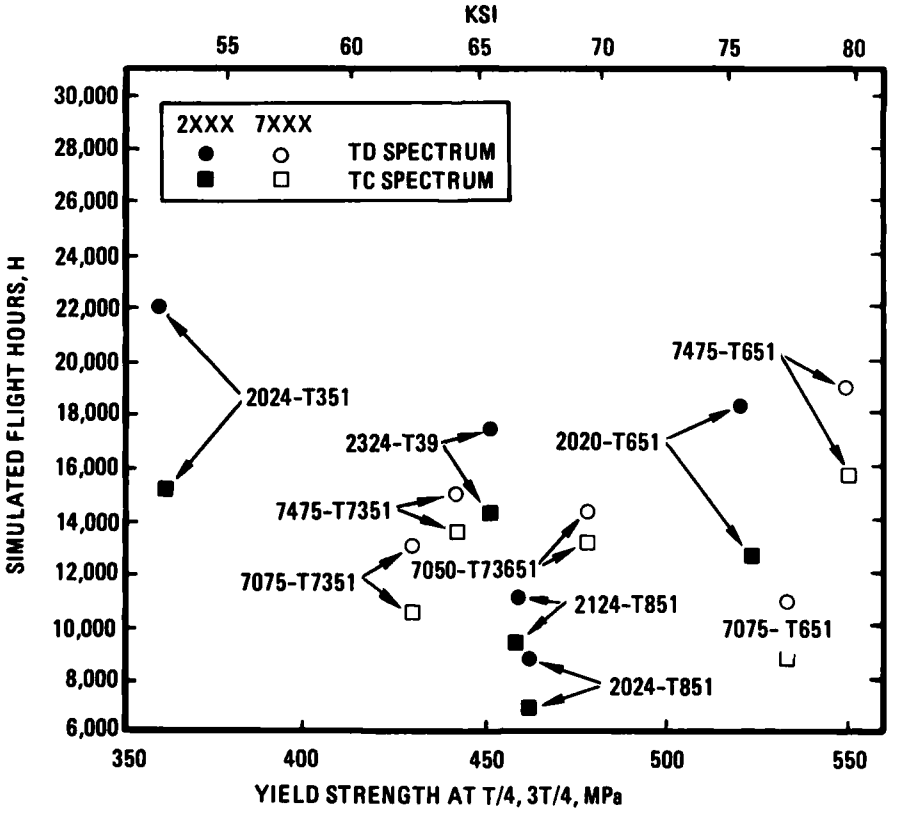

b. σ_{hmax} = 145 MPa (21 ksi), "a" FROM 6MM TO FAILURE

FIGURE 21. SPECTRUM LIFE VS YIELD STRENGTH

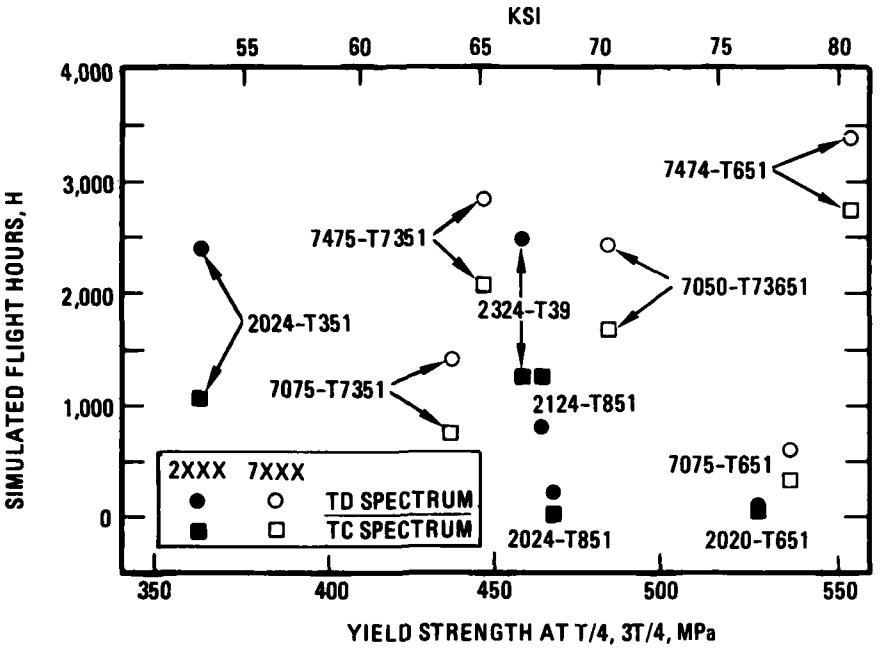

c. σ_{hmax} = 169 MPa, "a" FROM 18MM TO FAILURE

FIGURE 21. SPECTRUM LIFE VS YIELD STRENGTH (Concluded)

The effect of different tempers was investigated by comparing the spectrum fatigue behavior of 2024-T351 with 2024-T851, 7075-T651 with 7075-T351, and 7475-T651 with 7475-T7351. With respect to mechanical properties, temper manifests itself as an inverse relationship between yield strength and toughness, as shown by the solid lines in Figure 22. A clear inverse relationship between yield strength and spectrum life exists at all three maximum peak stress levels for the 2024 alloy, with the lower yield strength T351 condition having twice the life as that of the higher yield strength T851 condition. In terms of spectrum crack growth rates, the lower strength T351 condition (YS = 360 MPa, 52 ksi) has slower crack growth rates than the higher strength T851 condition (YS = 460 MPa, 67 ksi) at all maximum peak stress intensities (Figure 23a). This is consistent with the constant amplitude FCGR results where the lower strength T351 exhibits slower FCGR than the higher strength T851 at almost all stress intensities.

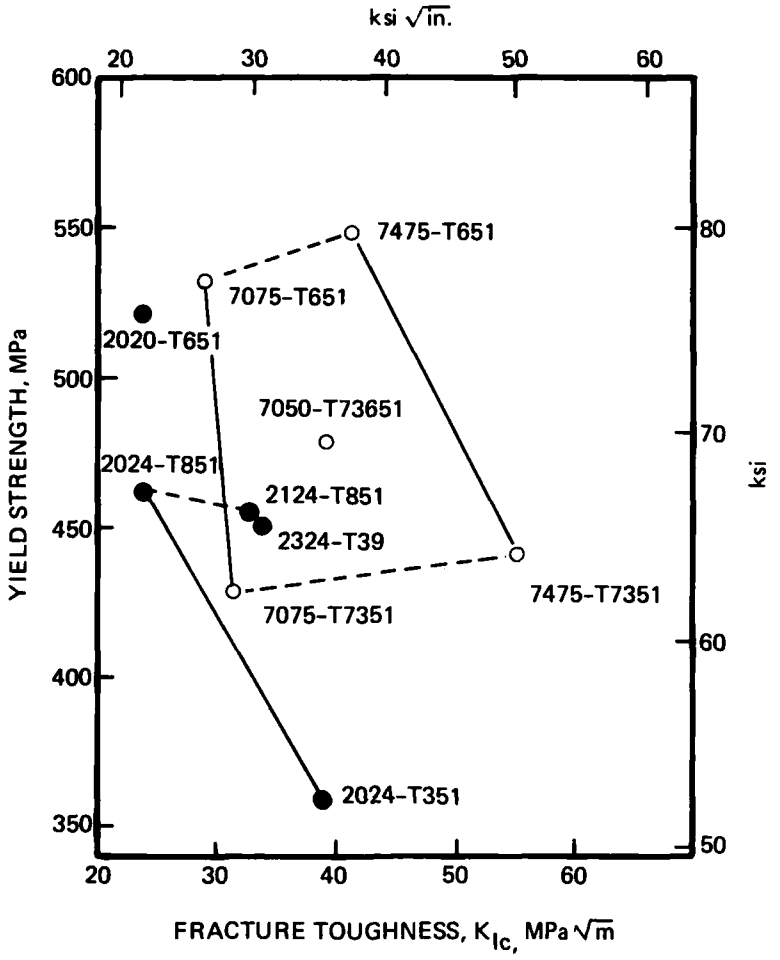

FIGURE 22. RELATIONSHIP BETWEEN YIELD STRENGTH AND FRACTURE TOUGHNESS

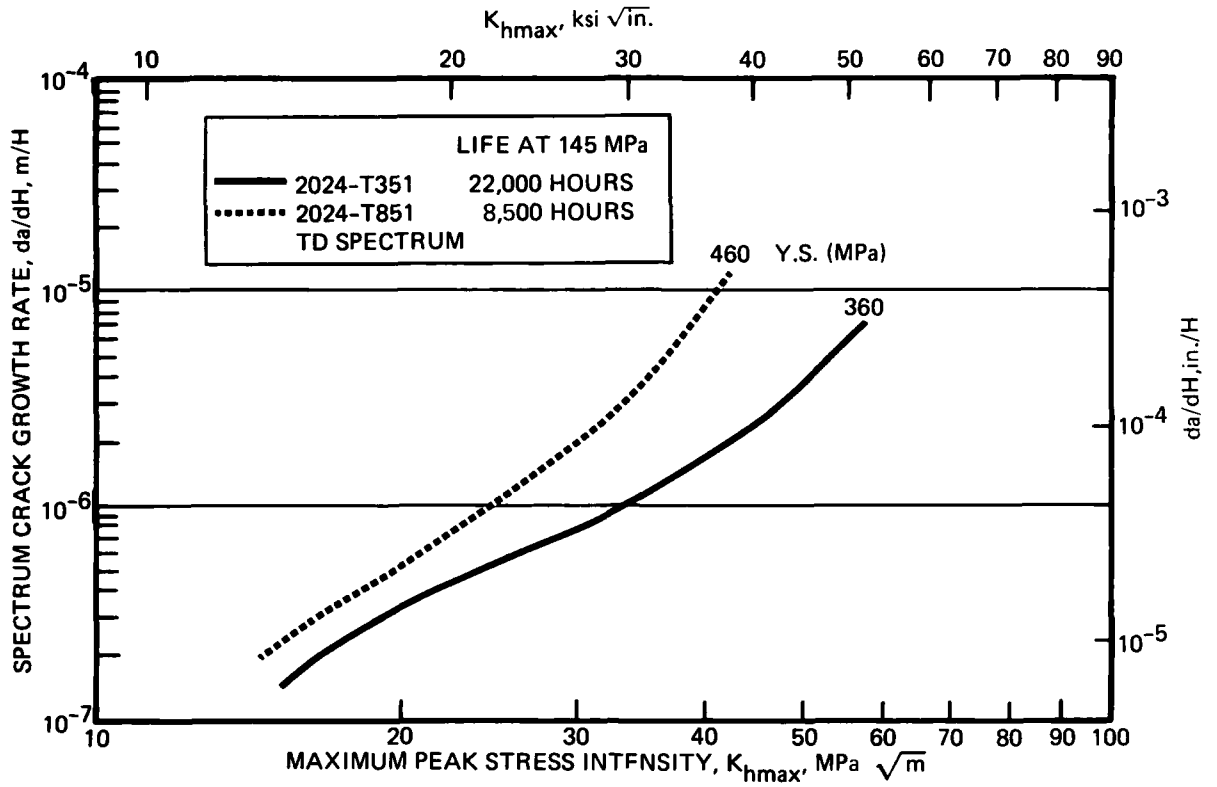

a. 2024-T351 vs T851

FIGURE 23. EFFECT OF PRECIPITATE STRUCTURE (TEMPER) ON SPECTRUM FCGR

The 7075 alloy behaves the same as the 2024 alloy. That is, the lower yield strength T7351 condition has a longer life at all maximum peak stress levels although the differences are not as large as for 2024. The lower strength T7351 condition (YS = 430 MPa, 62 ksi) has slower spectrum fatigue crack growth rates than the higher strength T651 condition (YS = 530 MPa, 77 ksi) at all maximum peak stress intensities (Figure 23b). However, the constant-amplitude curves cross, with the lower strength T7351 having slower crack growth rates except in the near threshold region.

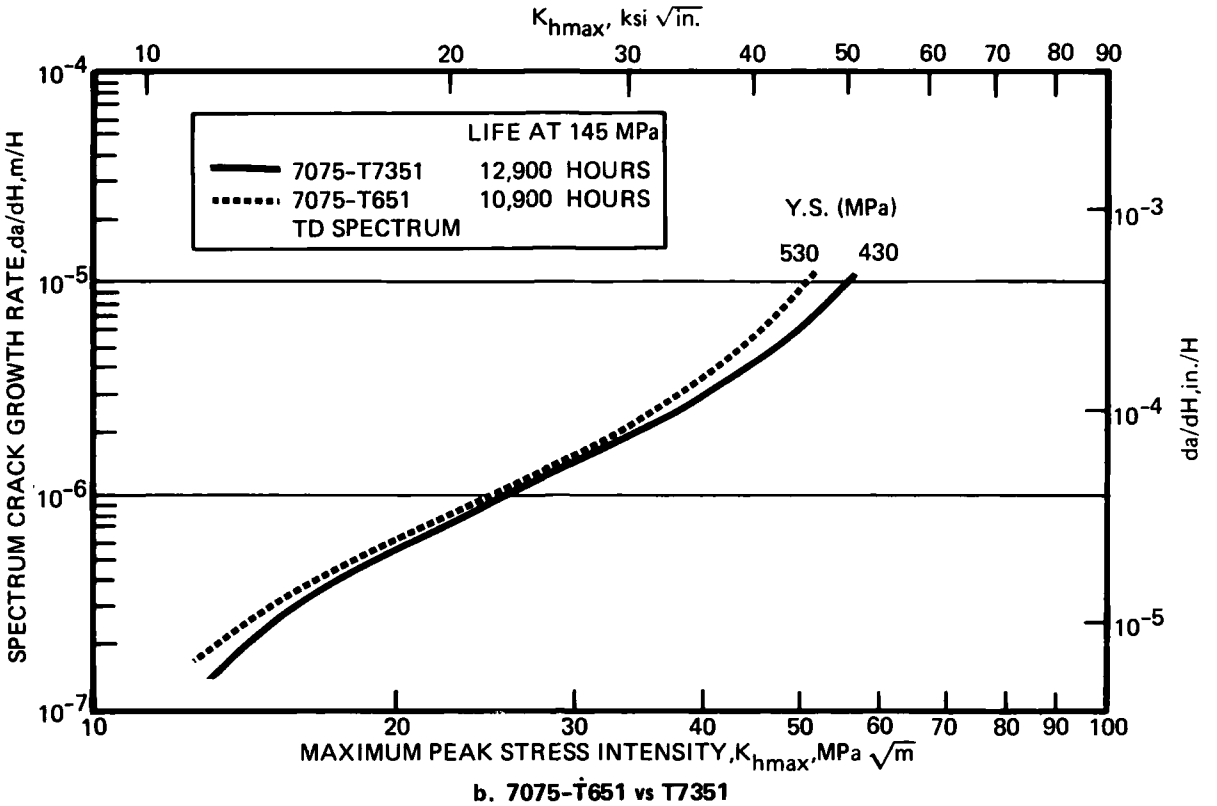

b. 7075-T651 vs T7351

FIGURE 23. EFFECT OF PRECIPITATE STRUCTURE (TEMPER) ON SPECTRUM FCGR (Continued)

The results for the 7475 alloy differ widely from those for 2024 and 7075. The difference in spectrum crack growth rates between the two tempers is smaller and varies depending upon the maximum peak stress intensity (Figure 23c). For the tests at 145 MPa (longest range of crack growth), the higher yield strength T651 condition had a 12 percent longer life (average of both spectra) than the lower yield strength T7351 temper. Similarly, for the testing at 169 MPa, the T651 temper had a 15 percent longer life than that for the T7351 condition. In contrast, over the shorter range of crack growth for testing at 103 MPa, the T651 condition had a 15 percent shorter life than the T7351 condition. The small differences in spectrum FCP behavior for these two tempers are also apparent in the FCGR curves (Figure 23c), which indicates a crossover in ranking at about K_{hmax} = 21 MPa $\sqrt{m}$.

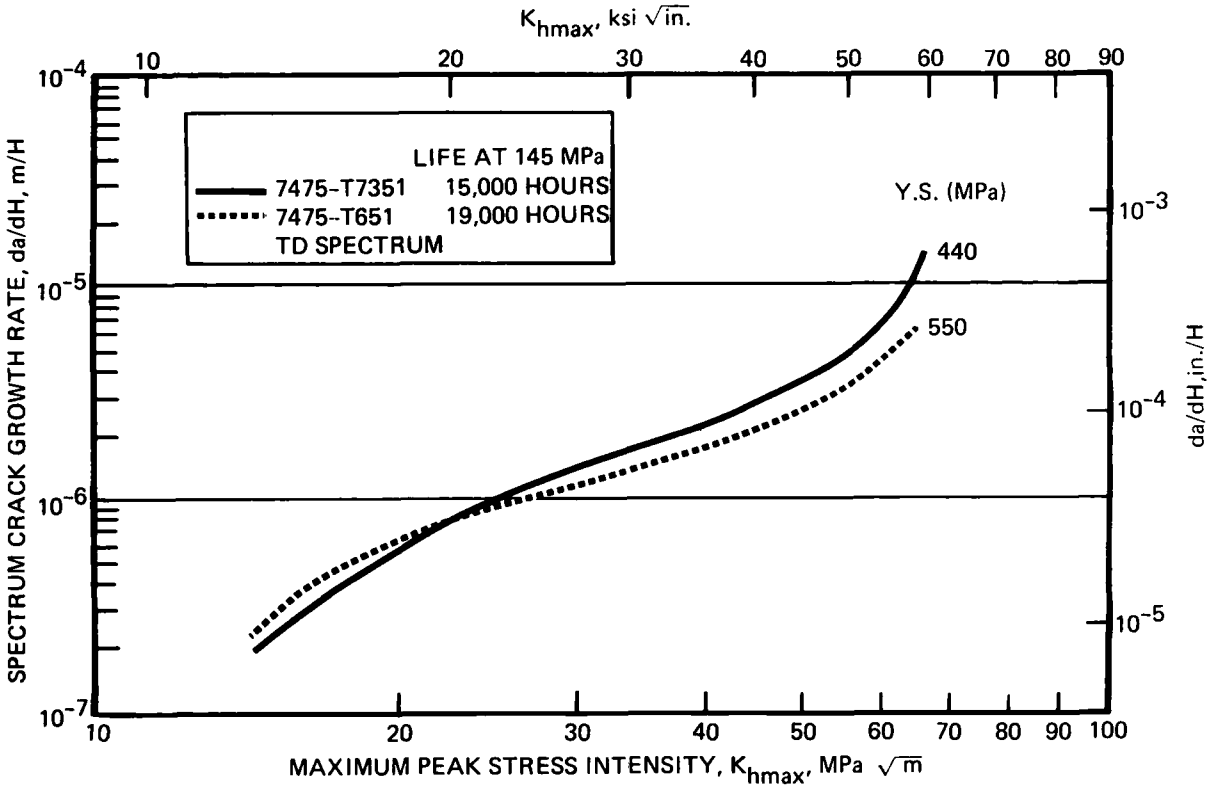

c. 7475-T651 vs T7351

FIGURE 23. EFFECT OF PRECIPITATE STRUCTURE (TEMPER) ON SPECTRUM FCGR (Concluded)

A more illuminating approach to understanding the effects of temper is to consider the deformation mode. The ten alloys can be divided into two groups: (1) those in which dislocation motion tends to be heterogeneous, occurring in planar slip bands (2020-T651, 2024-T351, 2324-T39, and 7X75-T651); and (2) those in which deformation is more homogenous (2X24-T851, 7050-T73651, and 7X75-T7351).[18] Notice in Table 10 that the alloys with the longest spectrum fatigue lives are primarily in the planar slip category; this correlation is particularly strong for the TD spectrum results at σ_{hmax} = 145 MPa. The fact that Al-Li alloys such as 2020-T651 tend to deform heterogeneously also is consistent with the high ranking of this alloy at both the 103 MPa and 145 MPa stress levels.

For constant amplitude fatigue loading, it has been observed[19,29,38,39] that crack growth rates in the near-threshold region ($\Delta K \lesssim 4$ MPa $\sqrt{m}$) decrease as the degree of slip planarity increases. This behavior has been rationalized on the basis of slip reversibility and cyclic hardening,[38] environmental effects,[39] and fracture surface topography.[19] Irrespective of which mechanism is most appropriate, it is obvious

that if the spectrum FCG behavior is sensitive to growth rates in the low ΔK region, then those alloys which deform heterogeneously should have longer spectrum FCG lives than those for which slip is homogeneous. Figure 16 shows that those tempers which deform by planar slip (T3X and T6X) generally do produce lower near-threshold growth rates than do the tempers which deform by homogeneous slip (T8X, T7X). As a final note, it is worth mentioning that the improved FCG resistance at low ΔK levels of tempers which deform by planar slip is opposite to the behavior observed at intermediate and high ΔK levels ($\Delta K > 4$ MPa $\sqrt{m}$), where crack growth rates often are higher for the planar slip tempers.[18,19] In 7XXX alloys, the increased corrosion resistance which accompanies continued aging is responsible for the decrease in FCG rates at intermediate ΔK when tests are conducted in humid environments.[18] As such, the near-threshold behavior cannot be predicted from data at higher growth rates.

The effect of slip planarity on post-overload retardation also has been examined,[38] and the authors concluded that the higher cyclic work hardening which accompanies planar slip results in greater retardation than for alloys which deform homogeneously. Since greater retardation lengthens spectrum fatigue life, the results in Reference 38 are additional evidence that enhanced slip planarity should improve spectrum FCG resistance.

3.6.3 Effects of Fracture Toughness and Purity

The relationship between fracture toughness and spectrum fatigue life is shown in Figure 24. By itself, increased fracture toughness* is expected to lengthen fatigue life by delaying final fracture to a greater crack length. The data in Figures 24b and c reflect this generally increasing fatigue life with higher toughness at stress levels for which crack growth continues to failure (145 and 169 MPa). The correlation is particularly strong at the higher stress (Figure 24c). Notable exceptions are 2020-T651 (at 145 MPa) and 7475-T7351 (at 145 MPa and to a lesser extent at 169 MPa). Even though

*It is recognized that plane strain fracture toughness, K_{Ic}, does not necessarily correlate with the plane stress situation occuring at the longer crack lengths for this testing, but nevertheless, K_{Ic} is the only measure of fracture toughness obtained in this the program and is therefore used for comparison.

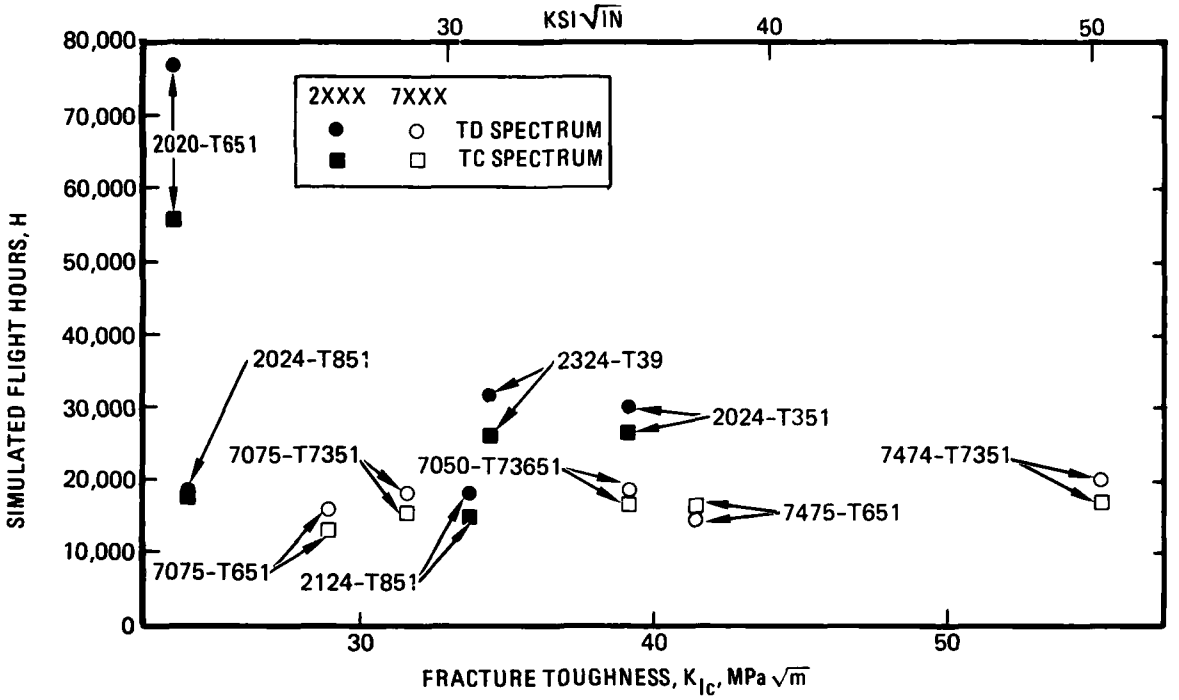

a. σ_{hmax} = 103 MPa, "a" FROM 6 TO 13MM

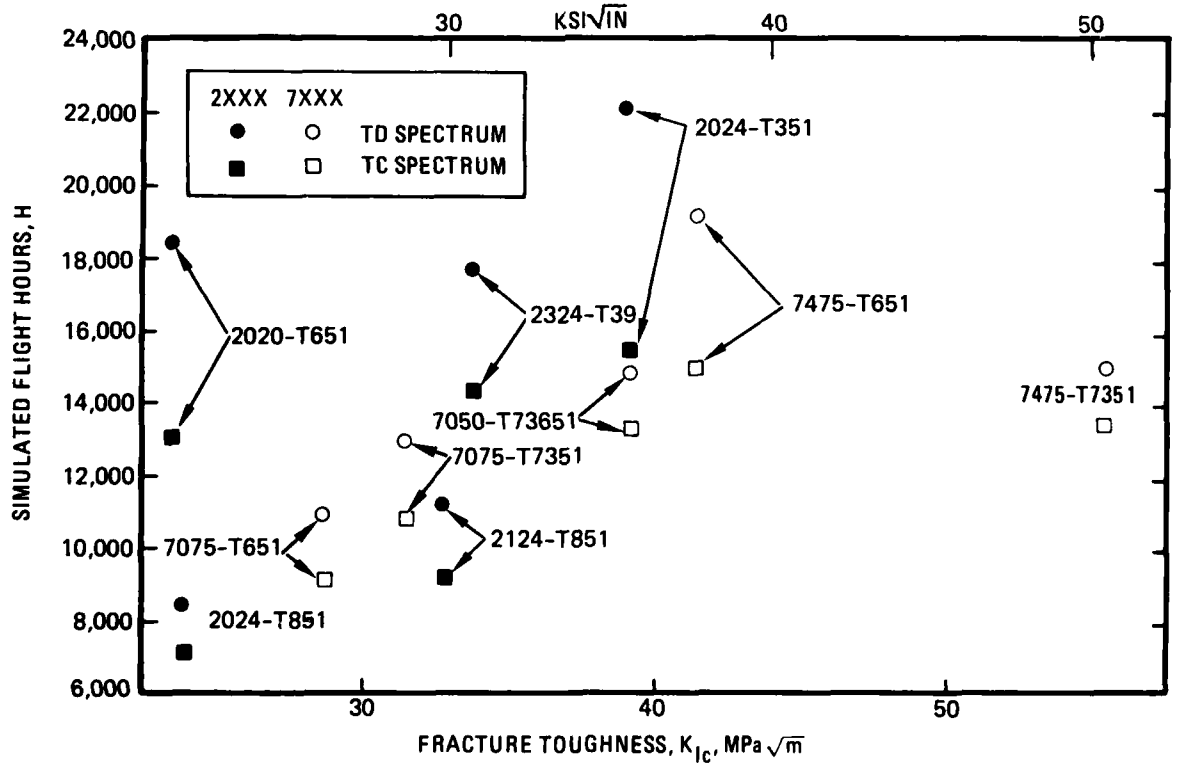

b. σ_{hmax} = 145 MPa, "a" FROM 6MM TO FAILURE

FIGURE 24. SPECTRUM LIFE VS FRACTURE TOUGHNESS

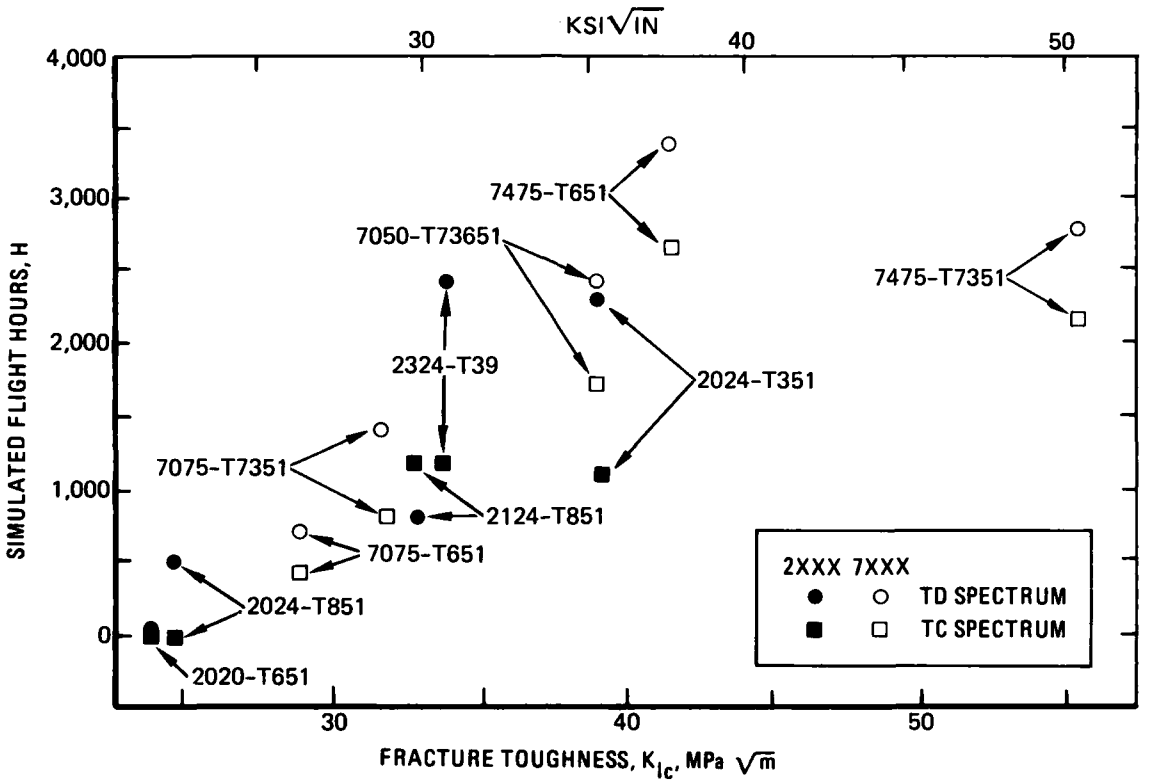

c. σ_{hmax} = 169 MPa , "a" FROM 18 MM TO FAILURE

FIGURE 24. SPECTRUM LIFE VS FRACTURE TOUGHNESS (Concluded)

7475-T7351 has the highest fracture toughness of all the materials in this program, for testing at 145 MPa it had a spectrum life shorter than four other materials for the TD spectrum and three other materials for the TC spectrum. The 7475-T7351 material, with its superior fracture toughness (K_{Ic} = 55 MPa $\sqrt{m}$), does not have a longer life than the 7475-T651 (K_{Ic} = 41 MPa $\sqrt{m}$).

For the 103 MPa tests (with low maximum peak stress intensity relative to the fracture toughness), no correlation exists between fracture toughness and spectrum fatigue life (Figure 24a).

Direct comparisons of the effect of alloy purity on spectrum behavior can be made by comparing 2024-T851 with 2124-T851, 7075-T651 with 7075-T651, and 7475-T7351 with 7475-T7351. The silicon and iron contents of the 2124 and 7475 alloys are significantly lower than those of their standard

counterparts (Table 4), which reduces the volume fraction of coarse constituent particles, thereby increasing alloy toughness. The Phase I report pointed out that the fracture surfaces of the spectrum specimens reflected this purity effect. Particularly at longer crack lengths, the reduced volume fraction of these constituent particles decreased the number of voids on the fatigue fracture surfaces. The fracture toughness values of 2124-T851, 7475-T651, and 7475-T7351, as shown in Table 6, are substantially higher than their lower purity counterparts, while the yield strengths (Table 5) remain about the same (see also Figure 22). All three of the higher purity, higher toughness materials had longer spectrum fatigue lives than their counterparts for tests at 145 MPa (30 percent for 2X24-T851, 72 percent of 7X75-T651, and 20 percent for 7X75-T7351, Figure 24b). Spectrum FCGR curves for these three pairs are shown in Figure 25. For all three pairs, FCGR's are similar at low K_{hmax} values, but become slower for the purer materials at higher values of K_{hmax}.

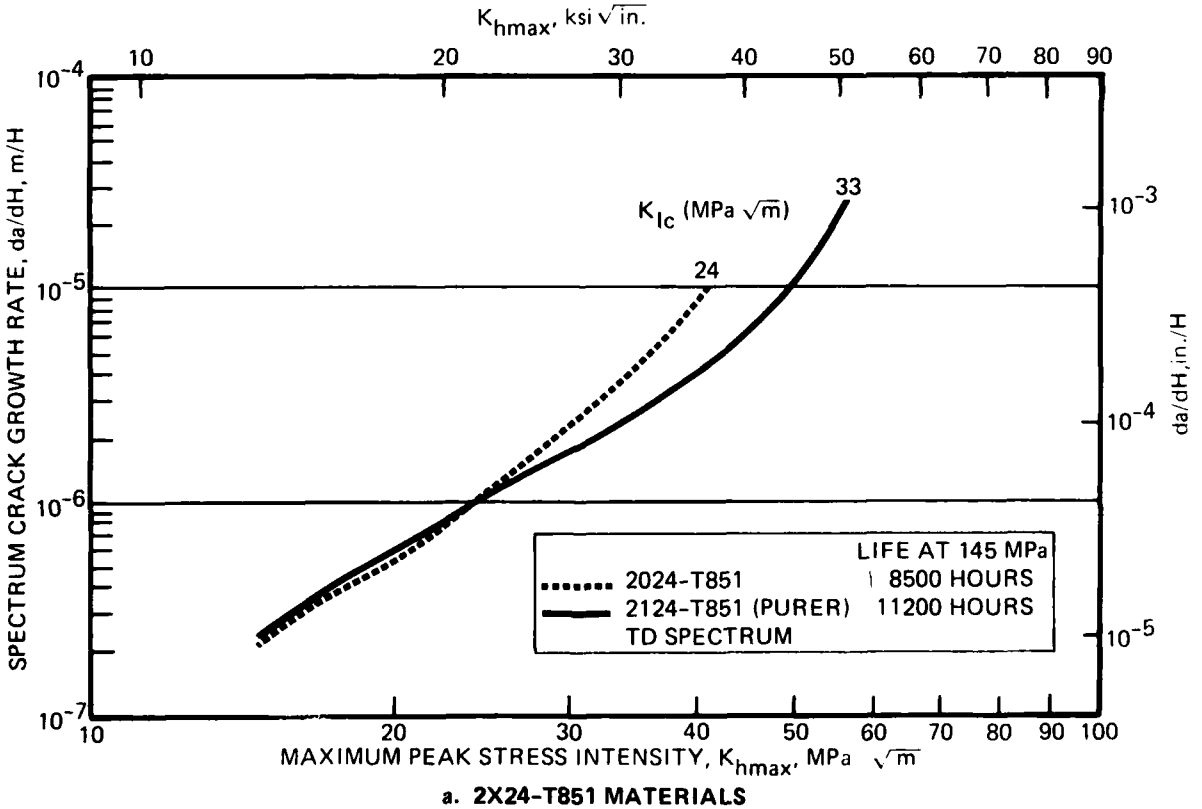

a. 2X24-T851 MATERIALS

FIGURE 25. EFFECT OF PURITY (TOUGHNESS) ON SPECTRUM FCGR

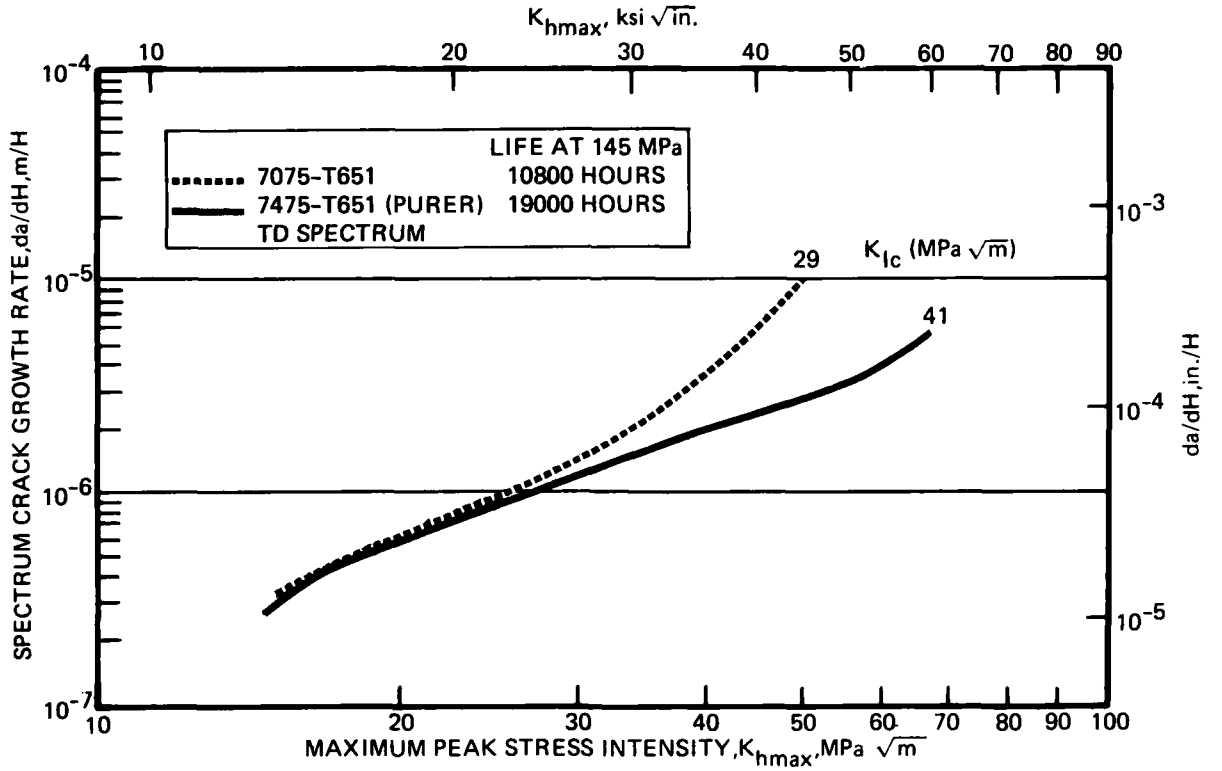

b. 7X75-T651 MATERIALS

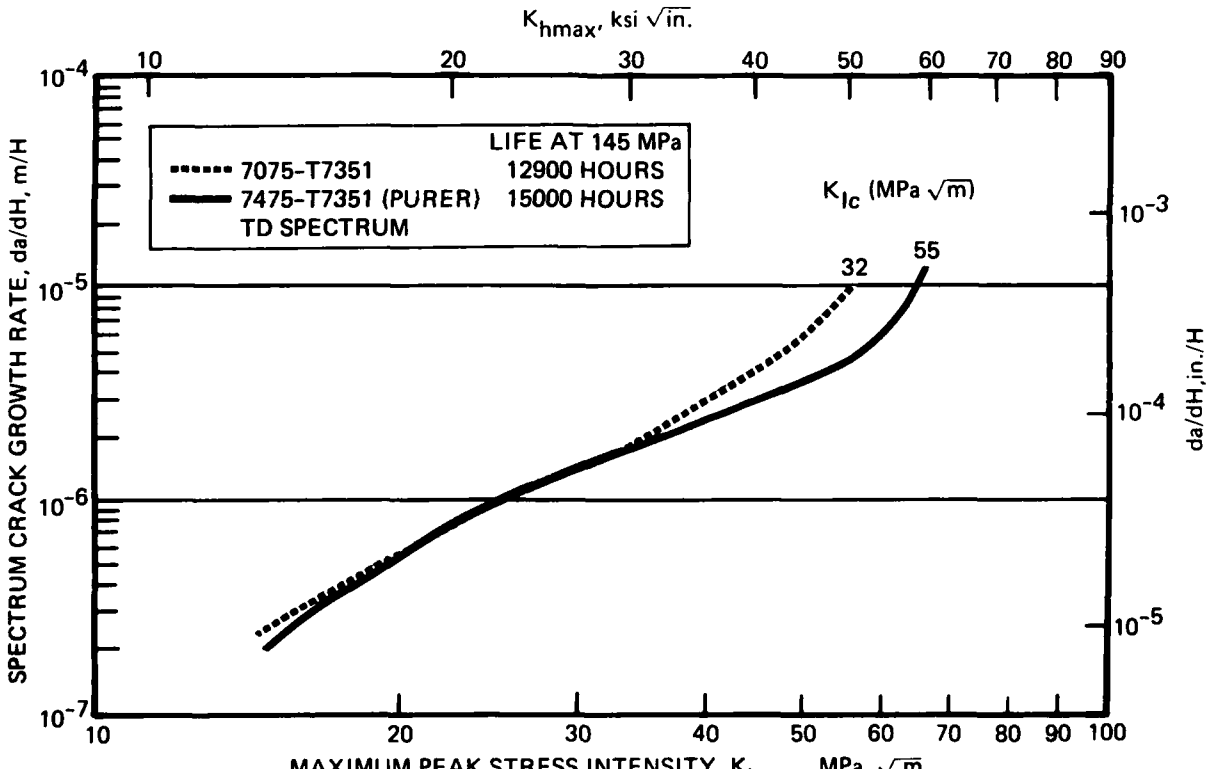

c. 7X75-T7351 MATERIALS

FIGURE 25. EFFECT OF PURITY (TOUGHNESS) ON SPECTRUM FCGR (Concluded)

3.7 MODIFIED SPECTRUM TEST RESULTS

The spectrum life results for the seven materials tested with the modified spectra are presented in Table 11. Crack length versus simulated flight hours data (a vs H) are shown graphically in Appendix D and spectrum crack growth rate versus maximum peak stress intensity data (da/dH vs K_{hmax}) are shown in Appendices E, F, and G. In these latter three appendices the results for the corresponding baseline spectrum are also shown.

TABLE 11. SPECTRUM FATIGUE RESULTS – MODIFIED SPECTRA
MAXIMUM PEAK STRESS, σ_{hmax} = 145 MPa (21 ksi)
CRACK GROWTH FROM 6mm (0.24 in.) TO FAILURE

	SIMULATED FLIGHT HOURS, H		
SPECTRUM	TDR	TCR	TCZ
MATERIAL			
2024-T351	24,899	15,738	34,205 31,090
2024-T851	9,410	7,403	10,258 12,175
7050-T73651	16,787	13,501	19,096 19,346
7075-T651	12,600	9,526	13,039 14,975
7075-T7351	14,179	11,446	17,502 17,595
7475-T651	21,259	19,387	22,630 23,364
7475-T7351	13,785	13,011	19,140 20,268

3.7.1 Racetrack Modified Spectra

The two baseline spectra, TD and TC, were modified using the racetrack technique to determine the effect of small amplitude load excursions and as a first step in developing simplified spectra for materials evaluation. The racetrack modified versions of the tension-dominated spectrum and of the tension-compression spectrum were designated TDR and TCR, respectively. One of the goals of this modification was to preserve the ranking of the alloys based on spectrum fatigue lives. As can be seen in Table 12, this goal was not met. However, the changes in ranking occur based on relatively small differences in life, except for 2024-T351 and 7475-T651 for the TCR and TC spectra combination. The overall significance of these changes are considered below.

The spectrum lives for each of the seven materials evaluated are compared to the lives for the respective baseline spectrum in Table 13 as the ratio of the life for the modified spectrum to the life for the baseline spectrum. Generally the life for the racetrack modified spectrum for each material was slightly longer than the life for the respective baseline spectrum, a 9 percent average increase for the 14 results. Hence, eliminating 43 percent of the smaller amplitude load excursions increased the spectrum life by a relatively small amount – 9 percent. Most of the results are close to the 9 percent average increase – the two exceptions are 7475-T651 for which the life for the TCR spectrum was 30 percent longer than for the TC spectra and the 7475-T7351 for which the life for the TDR spectrum was 8 percent less than for the TD spectrum. The significance of these differences will be considered from two points of view: scatter in the data and what increase in life would be significant in the selection of materials.

First consider the scatter. This may be estimated from the paired tests performed using the TD and TC spectra. The maximum difference between these paired tests was 21 percent which could define a scatter band of ±10.5 percent. All but the two results mentioned above are within 7 percent of the 9 percent average increase, that is, the life of the material for the modified spectrum was from 1.02 to 1.16 times that for the respective base line spectrum. Hence, 12 of the 14 results can be considered to be represented by the 9 percent average increase as they are within the scatter band.

TABLE 12. RANKING OF MATERIALS UNDER SPECTRUM LOADING – MODIFIED SPECTRA

σ_{hmax} = 145MPa from a = 6mm to failure

TDR SPECTRUM		
MATERIAL	SIMULATED FLIGHT HOURS[a]	RANKING UNDER TD SPECTRUM[b]
2024-T351	24,900	1
7475-T651	21,300	2
7050-T73651	16,800	4
7075-T7351	14,200	5
7475-T7351	13,800	3
7075-T651	12,600	6
2024-T851	9,400	7

TCR SPECTRUM		
MATERIAL	SIMULATED FLIGHT HOURS[a]	RANKING UNDER TC SPECTRUM[b]
7475-T651	19,400	2
2024-T351	15,700	1
7050-T73651	13,500	4
7475-T7351	13,000	3
7075-T7351	11,400	5
7075-T651	9,500	6
2024-T851	7,400	7

TCZ SPECTRUM		
MATERIAL	SIMULATED FLIGHT HOURS[c]	RANKING UNDER TC SPECTRUM[b]
2024-T351	32,600	1
7475-T651	23,000	2
7475-T7351	19,700	3
7050-T73651	19,200	4
7075-T7351	17,500	5
7075-T651	14,000	6
2024-T851	11,200	7

a ONE TEST RESULT ROUNDED TO NEAREST HUNDRED HOURS

b CONSIDERING THESE SEVEN ALLOYS

c AVERAGE OF TWO TEST RESULTS ROUNDED TO NEAREST HUNDRED HOURS

TABLE 13. RATIOS OF SPECTRUM FATIGUE LIVES FOR VARIOUS SPECTRA

MAXIMUM PEAK STRESS, σ_{hmax} = 145MPa (21 ksi)
CRACK GROWTH FROM 6mm (0.24 in.) to FAILURE

MATERIAL	RATIO OF SPECTRUM LIVES[a]			
	TD / TC	TCZ / TC	TDR / TD	TCR / TC
2020-T651	1.42	–	–	–
2024-T351	1.44	2.12	1.13	1.02
2024-T851	1.20	1.57	1.10	1.05
2124-T851	1.23	–	–	–
2324-T39	1.24	–	–	–
7050-T73651	1.13	1.46	1.13	1.03
7075-T651	1.22	1.57	1.16	1.07
7075-T7351	1.21	1.65	1.10	1.07
7475-T651	1.27	1.54	1.12	1.30
7475-T7351	1.12	1.47	0.92	1.04

[a]NOTE THAT TWO TESTS FOR EACH MATERIAL WERE PERFORMED FOR THE TD, TC, AND TCZ SPECTRA AND THE AVERAGE OF THESE TWO TESTS WAS USED FOR THE CALCULATION OF THE RATIOS. ONLY ONE TEST FOR EACH MATERIAL WAS PERFORMED FOR THE TDR AND TCR SPECTRA.

Now consider the question, quantitatively what differences in spectrum life are significant? To answer this, the designer's point of view can be taken. The designer wants to know how much the weight can be reduced (or will be increased) by a materials change, therefore his interest is what the increase (or reduction) in stress will be from use of an alternate material. A 10 percent increase in stress can be taken as significant, which is equivalent to a 50 percent increase in life (See Appendix I for the derivation of this

relationship). Therefore, any error in the life due to the racetrack modification of less than 50 percent in life could be taken to be unimportant – based on this criterion the results for the racetrack modified spectra are useful, that is, the racetrack modified spectra results can be used to rate materials for their resistance to fatigue crack growth. It must be noted that this point of view is not the only valid one, and further tests are planned for future phases.

The spectrum crack growth rates for the racetrack modified spectra and the baseline spectra are shown in Appendices E and F*. The only significant differences in spectrum crack growth rates between the racetrack modified spectra and the respective baseline spectra occurred for 7475-T651 for both pairs of spectra (Figures E-6 and F-6 in the Appendices). Of the seven materials tested using the modified spectra, 7475-T651 exhibited the largest differences in spectrum crack growth rates between the duplicate tests performed using the baseline spectra. The cause of this difference might explain the large differences in spectrum crack growth rates between the racetrack modified and baseline spectra, however the cause of the difference is unknown.

Although there are differences in spectrum fatigue crack growth rates between the paired tests for 7475-T651 for the TC spectrum, there was only 3 percent difference in spectrum life for the two tests, considerably less than the 26 percent difference between the lives for the TD and TDR spectra. That is, scatter in crack growth rates does not necessarily explain the differences in spectrum life for the TD and TDR spectra for 7475-T651.

*It should be noted that for the spectrum life comparisons, the initial crack length of 6mm corresponds to a maximum peak stress intensity, K_{hmax}, of 20 MPa$\sqrt{m}$; therefore any differences in spectrum crack growth behavior below this value (due to the differences in test procedures between the results for the baseline spectra performed in Phase I and those for the modified spectra in Phase II) are not a factor in the spectrum fatigue life (see Section 2.6.5).

3.7.2 TCZ Spectrum

To determine the effects of compression loads on spectrum fatigue life, the spectrum with larger magnitude compression loads, the TC spectrum, was modified by setting all negative loads equal to zero. The reduction in load points was small, less than 2 percent (see Section 2.6.2 for details). This spectrum is designated the TCZ spectrum. The ratios of the spectrum life for the TCZ spectrum to the life for the TC spectrum for each of the seven materials tested are listed in Table 12. This modification resulted in similar life increases of from 46 to 65 percent, except for the 112 percent increase for 2024-T351.

Treating the TCZ spectrum as a third spectrum, the results can be compared to the results for the TD and TC spectra (Figure 26). Significantly, the rankings of the alloys are the same as under the other two spectra, although the spectrum lives for the TCZ spectrum are longer than those for both the TC and TD spectra. Note that the TD spectrum has only moderate compressive loads (all greater than -35 percent of σ_{hmax}). These results confirm the damaging effects of compressive loads, even for a very complex, random spectrum. Since the effect of compressive loads is to reduce retardation, and retardation has often been related to yield strength, it is worthwhile to investigate whether there is any relationship between the lives for the TC and TCZ spectra and the yield strength. In Figure 27, these comparisons to yield strength are presented with the ordinate as the ratio of the life for the spectra with less severe compressive stresses to the life for the spectrum with the more severe compressive stresses. No trends are apparent except that 2024-T351 is more sensitive to compressive loads as indicated by higher ratios in each case than those for the other materials.

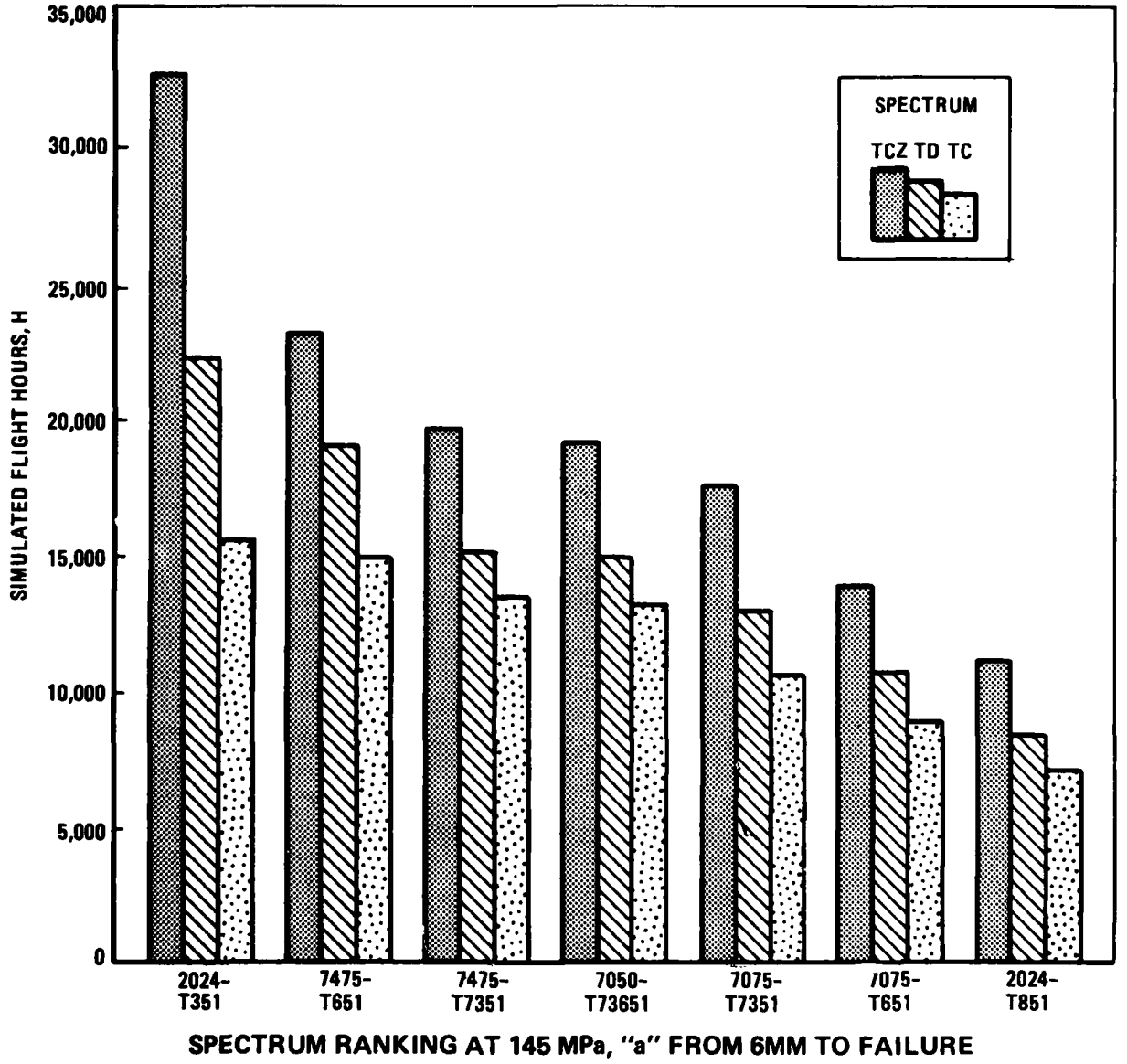

FIGURE 26. SPECTRUM FATIGUE LIVES FOR TCZ, TC, AND TD SPECTRA

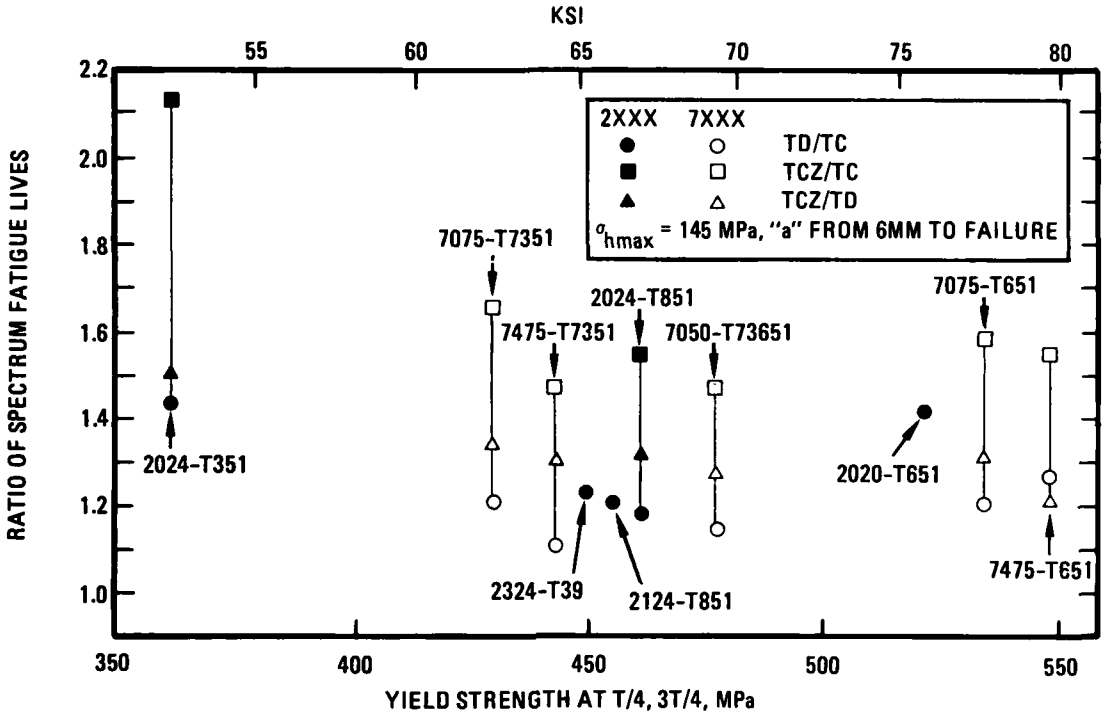

FIGURE 27. RATIOS OF SPECTRUM FATIGUE LIVES VS YIELD STRENGTH

Using presentations similar to those used for the baseline spectra, plots of spectrum life versus yield strength and fracture toughness are shown in Figures 28 and 29. For comparison the maximum peak stress intensity needed to obtain a given spectrum FCGR is shown in Figure 30.

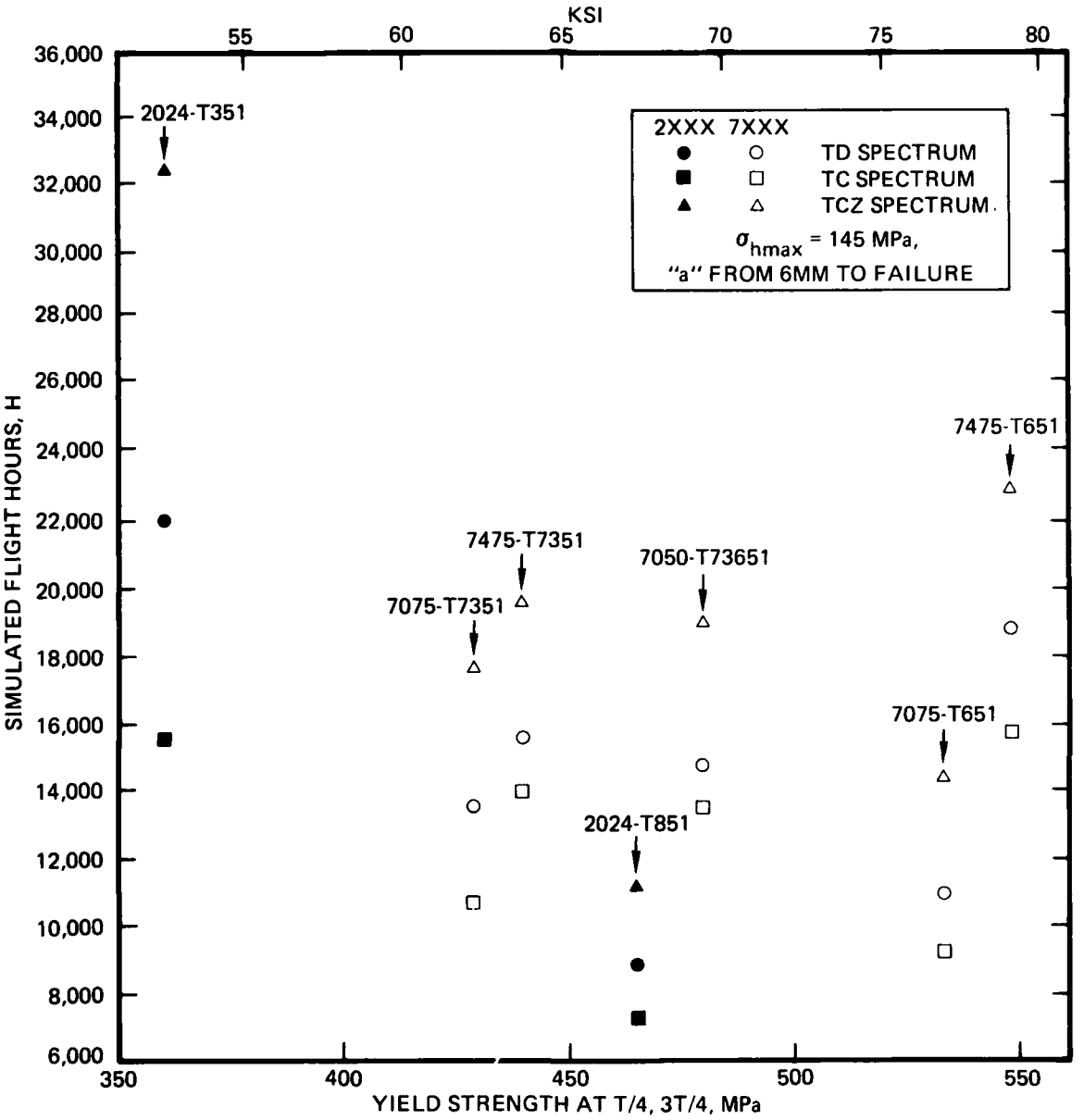

FIGURE 28. SPECTRUM LIFE VS YIELD STRENGTH FOR TCZ, TC AND TD SPECTRA

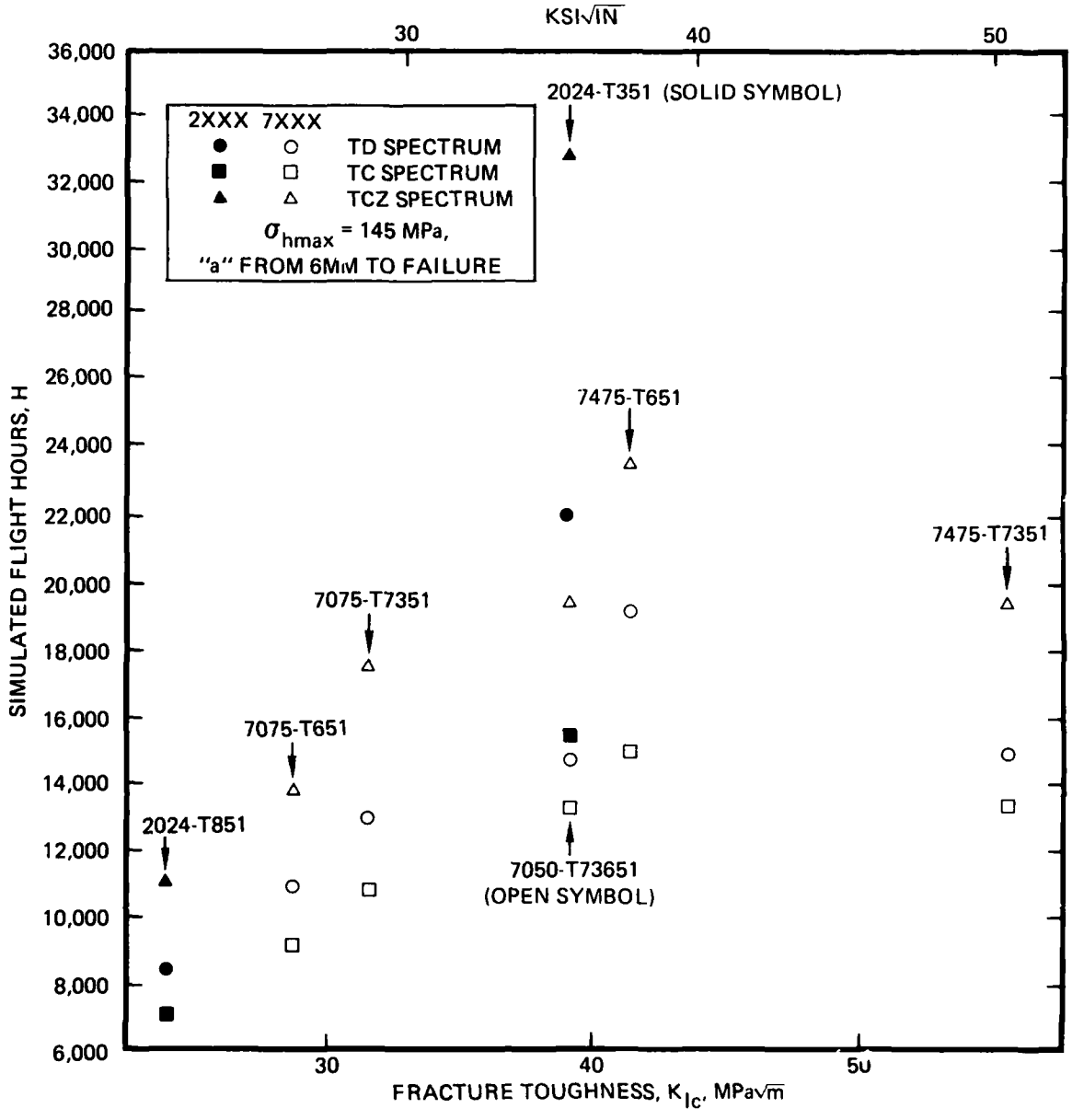

FIGURE 29. SPECTRUM LIFE VS FRACTURE TOUGHNESS FOR TCZ, TC AND TD SPECTRA

AD-A133 206 INVESTIGATION OF FATIGUE CRACK-GROWTH RESISTANCE OF ALUMINUM ALLOYS UNDER.. (U) NORTHROP CORP HAWTHORNE CA AIRCRAFT DIV G V SCARICH ET AL. APR 83 NOR-83-84 2/2

UNCLASSIFIED N00019-81-C-0550 F/G 11/6 NL

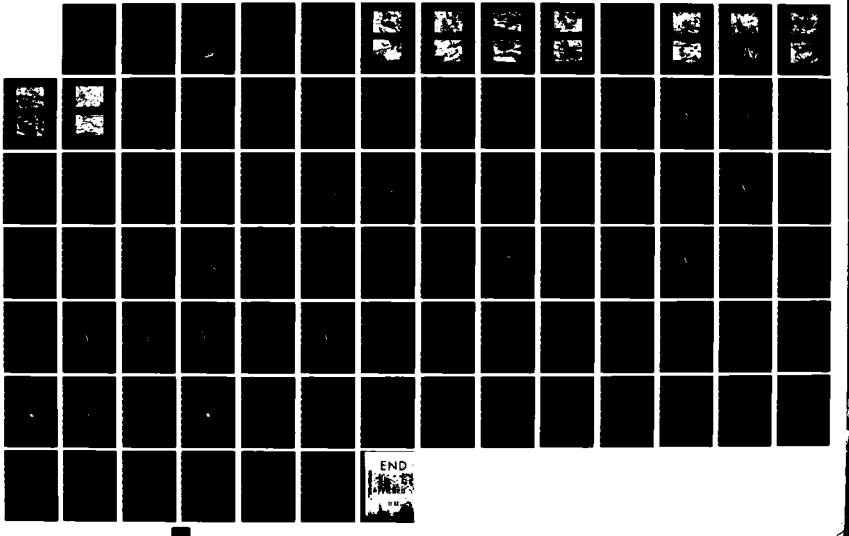

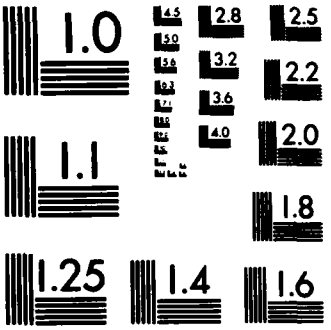

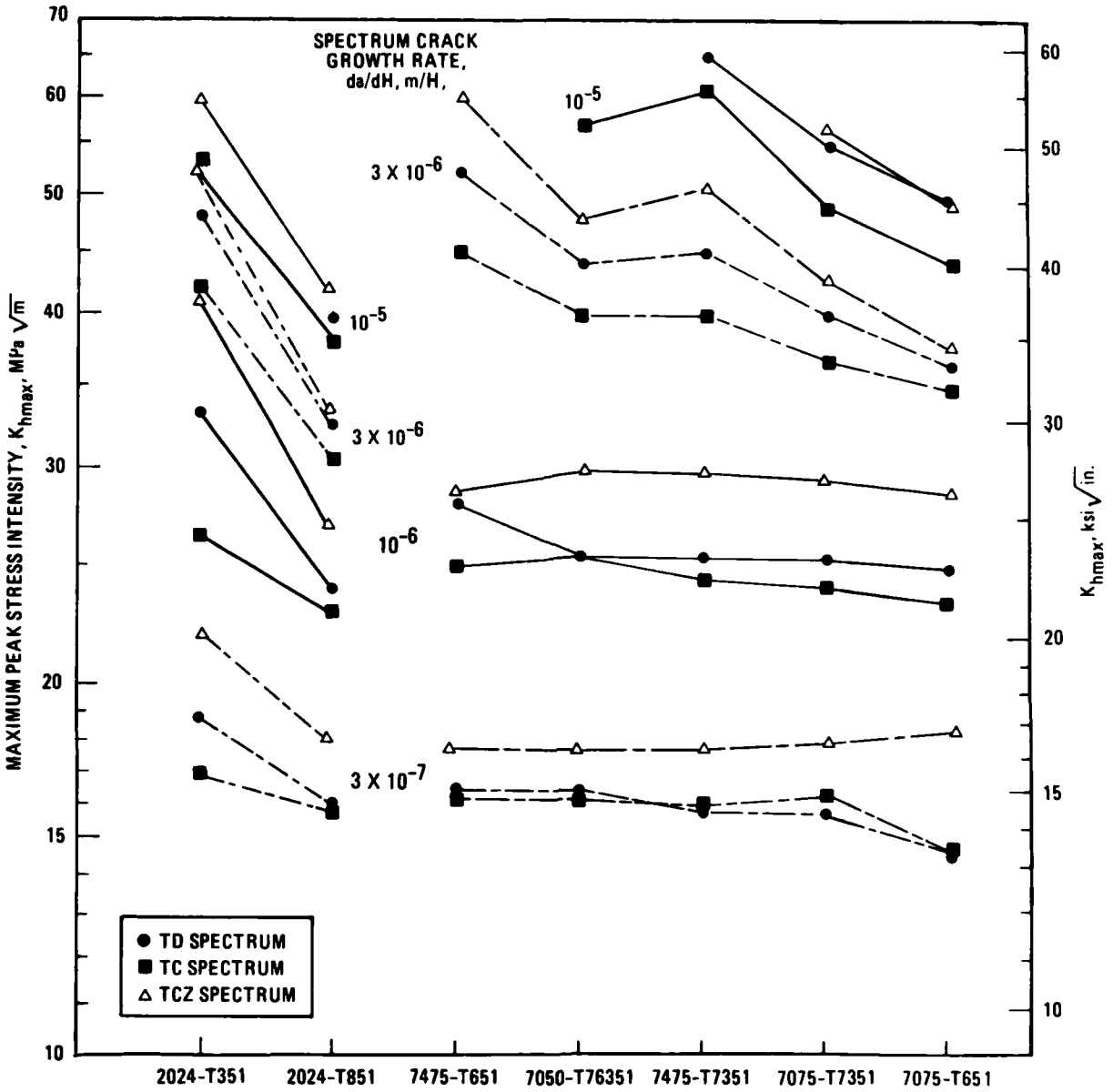

FIGURE 30. MAXIMUM PEAK STRESS INTENSITY NEEDED TO OBTAIN A GIVEN SPECTRUM FCGR FOR TD, TC AND TCZ SPECTRA

3.8 EFFECTS OF LOAD HISTORY

The effects of load history will be considered in more detail in the next phase where the baseline data will be utilized in various life prediction models and correlated with the spectrum FCP results obtained. Some observations that can be made at present follow:

1. For the same material, the crack growth rates are similar for the two baseline spectra at the lower stress intensities (Figure 18 or Figure 19). However, at higher stress intensities the rates for the two spectra generally diverge, with the rates for the TC spectrum faster than those for the TD spectrum. This is shown graphically in Figure 31 as a ratio of the FCG rates for the two spectra at various stress intensities. Alloy 2020-T651 is a major exception with the FCG rate for the TC Spectrum 1.6 times faster than that for the TD spectrum at a K_{hmax} of 20 MPa$\sqrt{m}$.

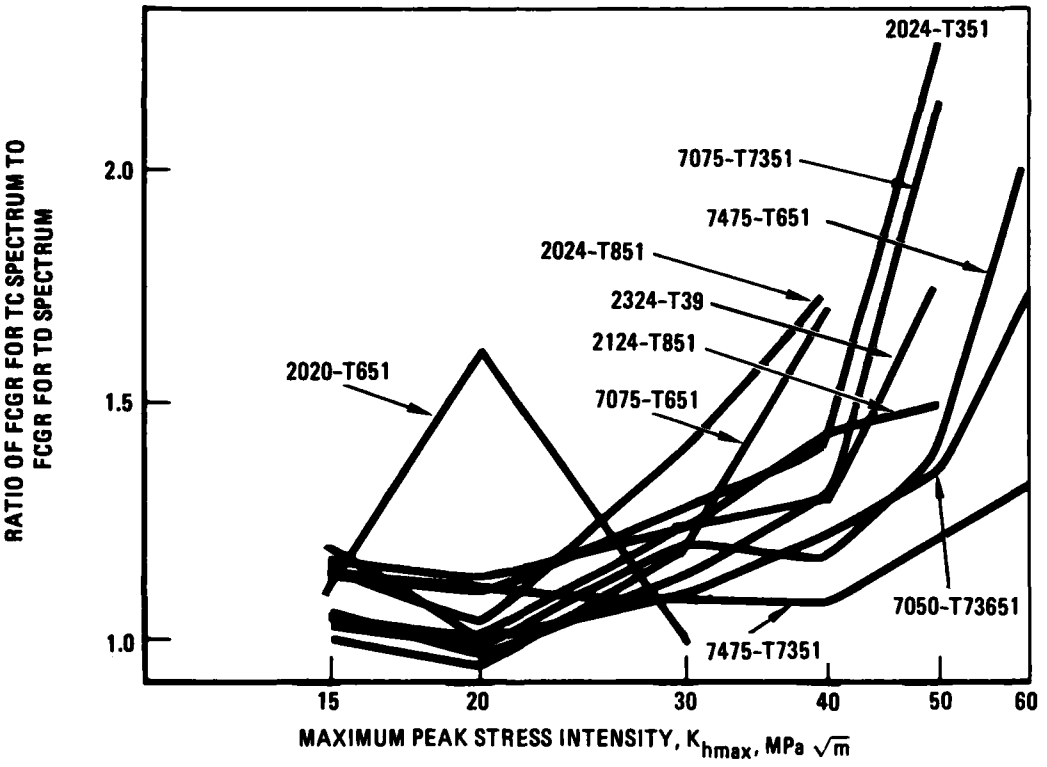

FIGURE 31. RATIO OF THE FCGR'S FOR THE TWO SPECTRA

2. Since a relatively small percentage of the total spectrum life is spent at the higher stress intensities where the maximum difference in the crack growth rates was observed, spectrum fatigue lives are similar for the same materials for the two baseline spectra when tested over a long range of crack growth (i.e., the 145 MPa testing).

3. When the lives for the same material are compared only over the higher stress intensity (i.e., the 169 MPa) testing, the difference in lives between the two baseline spectra are somewhat greater than for the testing at 145 MPa.

4. Eliminating 43 percent of the smaller amplitude load excursions from the two baseline spectra (TD or TC) increased the spectrum life (for TDR or TCR spectra, respectively) by 9 percent. Two exceptions to this were 7475-T651 for the TD/TDR spectra and 7475-T7351 for the TC/TCR spectra (See Section 3.7.1).

5. Eliminating all loads less than zero from the baseline spectrum with the highest magnitude compressive loads (the TC spectrum) increased the spectrum fatigue life for six of the materials evaluated by 46 to 65 percent, and 112 percent for 2024-T351 (See Section 3.7.2). This result confirms the damaging effect of compression loads in spectrum fatigue.

3.9 FRACTOGRAPHY

3.9.1 Macroscopic Appearance

Fracture surfaces from the baseline spectrum fatigue test specimens of 2324-T39 and 7075-T651 change from a flat to a slant fracture mode with increasing crack length. In contrast, a flat mode persists in 2020-T651 for the entire fracture surface. The fracture surfaces of 2020 also are distinctive in that no beach markings, which can be formed during spectrum loading, are visible; for the other two alloys, such markings are quite clear at longer crack lengths for both test spectra. Similar markings were apparent on the fracture surfaces of all seven alloys tested in Phase I.[27]

Another distinction between 2020 and the other alloys has to do with fracture surface roughness. For both spectra, the fracture surface of 2020 is much rougher than that of the other two alloys or, for that matter, any of the seven alloys tested in Phase I. This rough fracture appearance is typical of 2020-T651.[40,41]

3.9.2 Microscopic Fracture Mechanisms

As was the case in Phase I of this program, the microscopic fracture surface appearance of each alloy does not vary substantially between the two spectra, although in alloy 2020 there are subtle differences. In this material, the fracture surface at a = 6.4 mm using the TD spectrum is characterized by a combination of intergranular fracture, ductile striation* formation, and void nucleation and growth (Figure 32). When the TC spectrum is used, void formation is more pronounced, and intergranular fracture less obvious (Figure 33). For both spectra, crack growth at a = 19 mm is predominantly intergranular, although here again greater evidence of void growth is visible for the TC spectrum (compare Figures 34 and 35). Both coarse and very fine voids are present on the fracture surface of 2020.

*The term "striation" is used generically in reference to the fine lines in Figure 32 and elsewhere, since it cannot be proven that these markings represent increments of crack growth during individual load cycles.

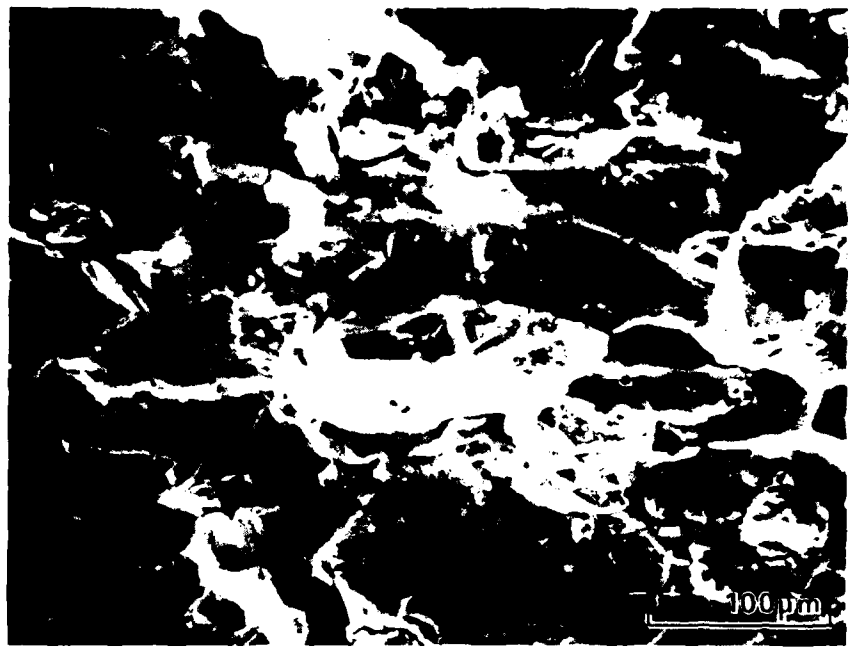

250X

CRACK GROWTH DIRECTION

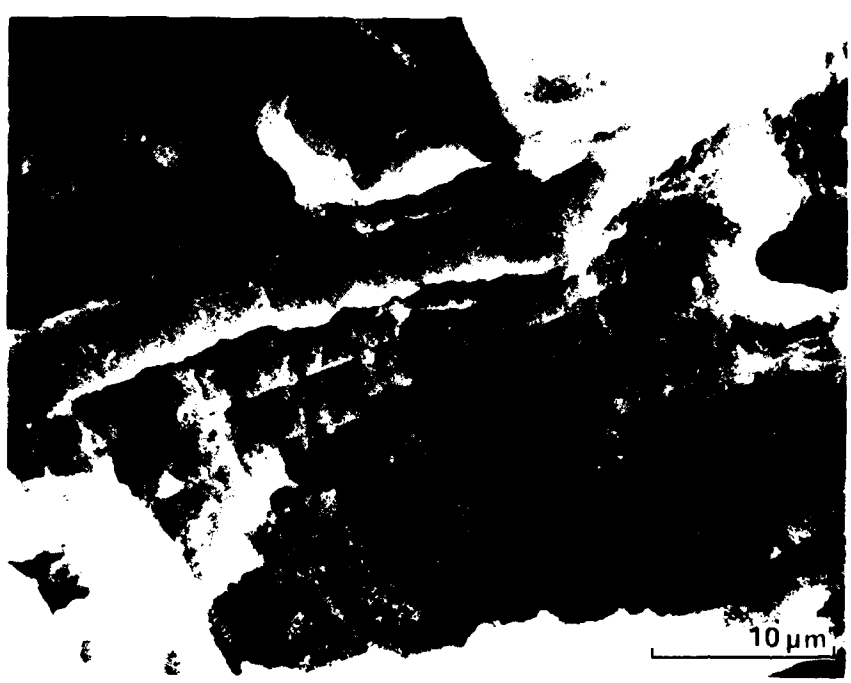

2500X

FIGURE 32. FRACTURE SURFACE OF 2020-T651 TESTED USING TD SPECTRUM AT a = 6.4 MM (0.25 IN.)

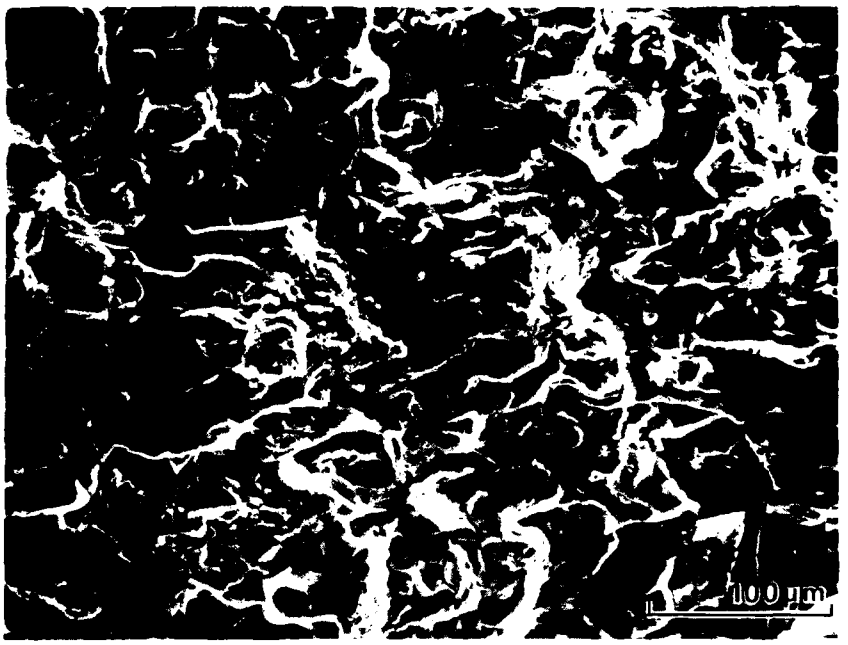

CRACK GROWTH DIRECTION

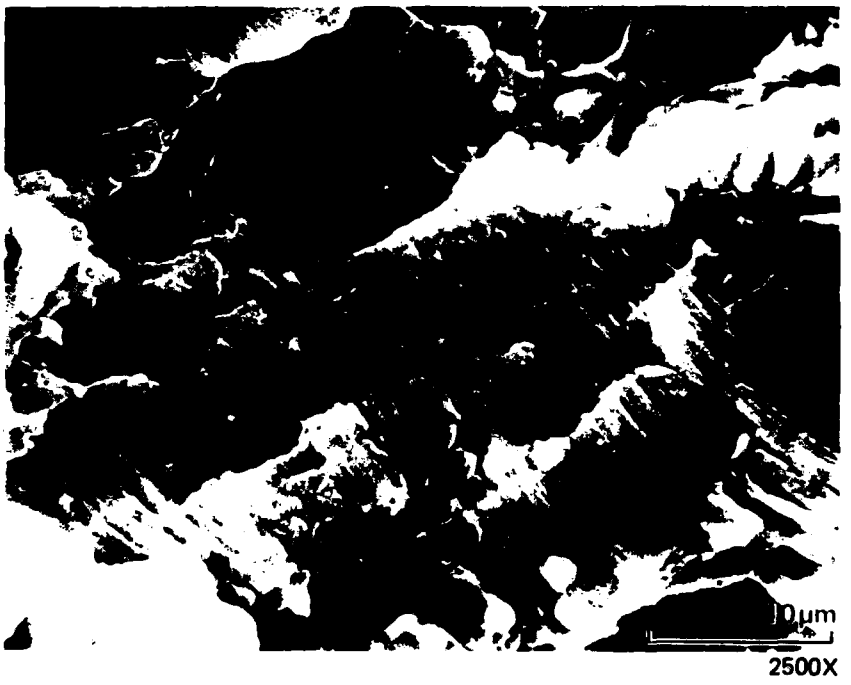

FIGURE 33. FRACTURE SURFACE OF 2020-T651 TESTED USING TC SPECTRUM AT a = 6.4 MM (0.25 IN.)

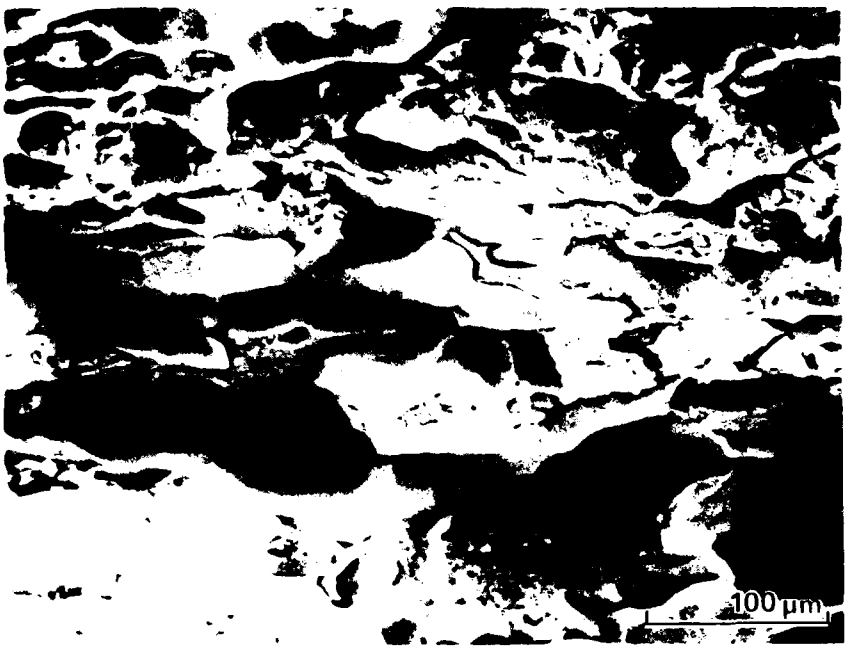

250X

CRACK GROWTH DIRECTION

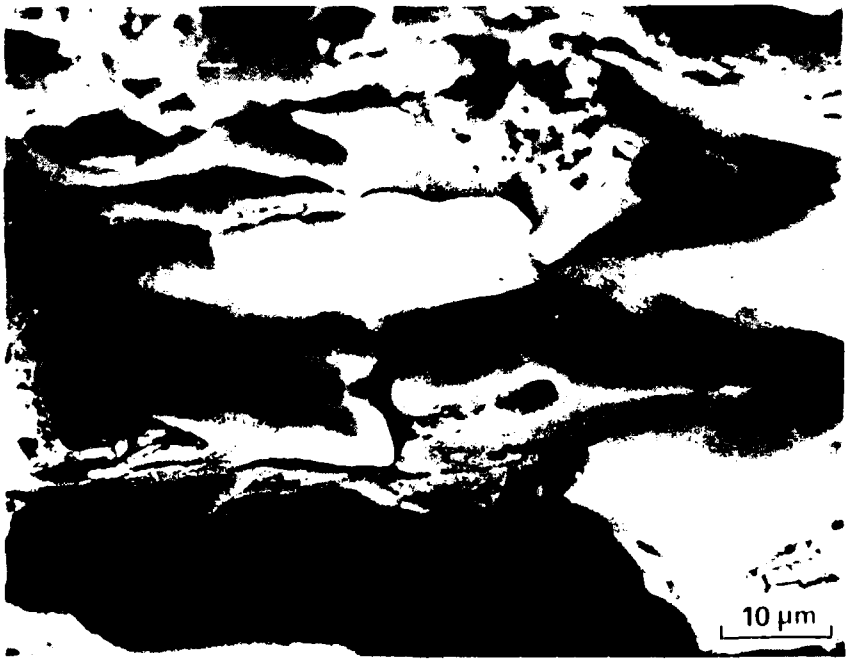

2500X

FIGURE 34. FRACTURE SURFACE OF 2020-T651 TESTED USING TD SPECTRUM AT a = 19 MM (0.75 IN.)

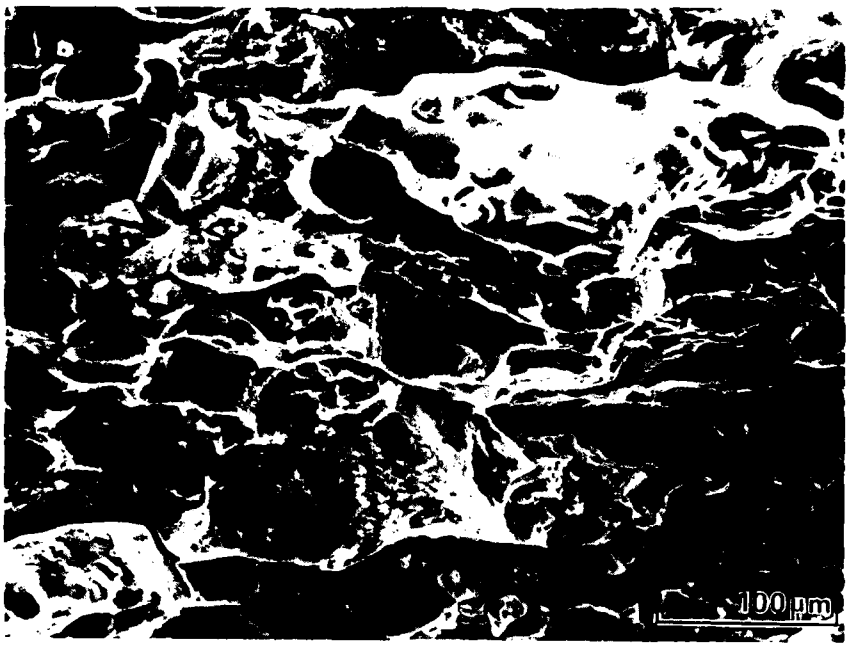

250X

CRACK GROWTH DIRECTION

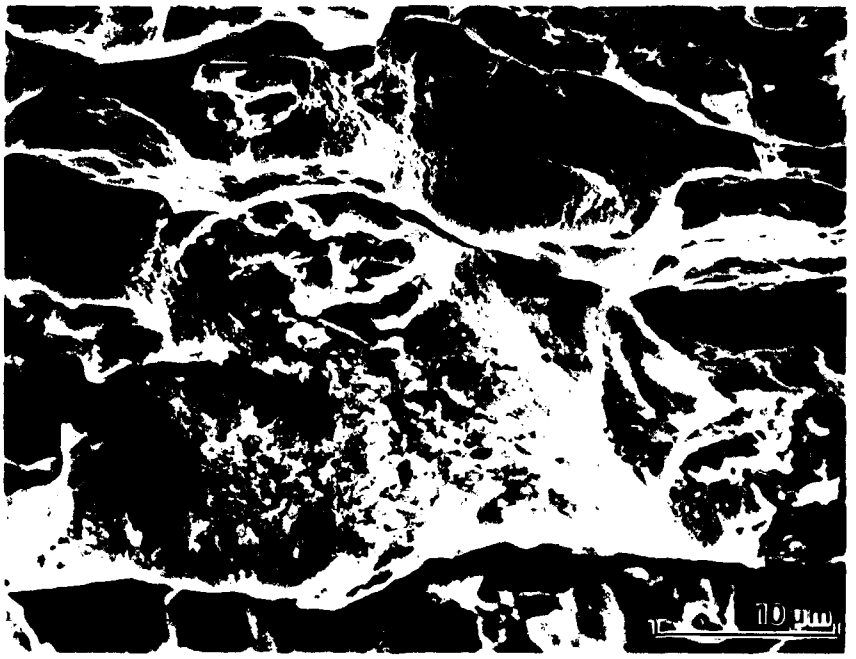

2500X

FIGURE 35. FRACTURE SURFACE OF 2020-T651 TESTED USING TD SPECTRUM AT a = 19 MM (0.75 IN.)

Unlike 2020, the fracture surface of 2324 at a = 6.4 mm, is covered predominantly by ductile striations, with void nucleation from secondary intermetallic particles (Figure 36); this is true for both test spectra. The ductile fracture mode persists to greater crack lengths (Figure 37), although the striations do coarsen and void growth becomes more prevalent. Such fracture details are quite similar to those observed for 2024-T351 in Phase I.

In 7075-T651, striations are not clearly seen for either spectrum; rather, the only distinctive fracture detail even at a = 6.4 mm, is void nucleation (Figures 38 and 39). Also, there are relatively large areas which contain few discernable features, particularly for the TC spectrum (Figure 39). Crack growth at a = 19 mm is almost exclusively by void formation in 7075-T651 (Figure 40), although the fracture surface is highlighted by many short ridges parallel to the rolling direction in the plate. In contrast, though, fatigue fracture at this same crack length in 7075-T7351 (Phase I report) included substantial striation formation in addition to void nucleation and growth.

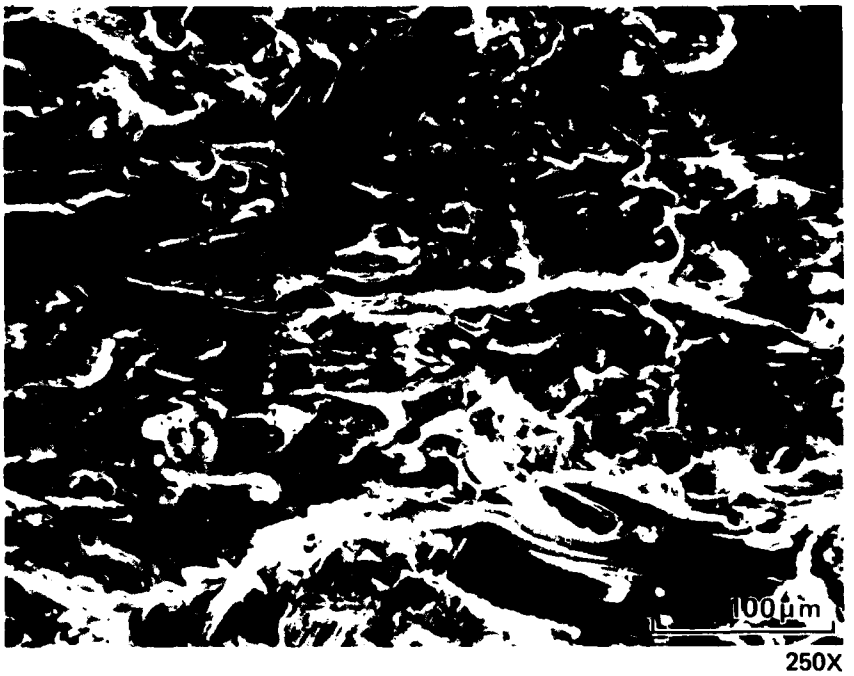

250X

CRACK GROWTH DIRECTION

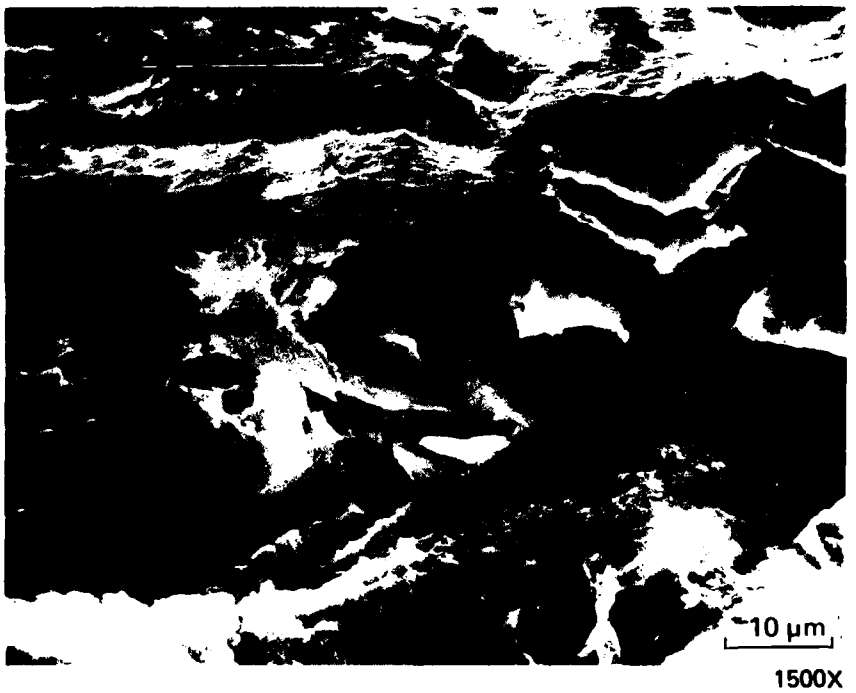

1500X

FIGURE 36. FRACTURE SURFACE OF 2324-T39 TESTED USING TC SPECTRUM AT a = 6.4 MM (0.25 IN.)

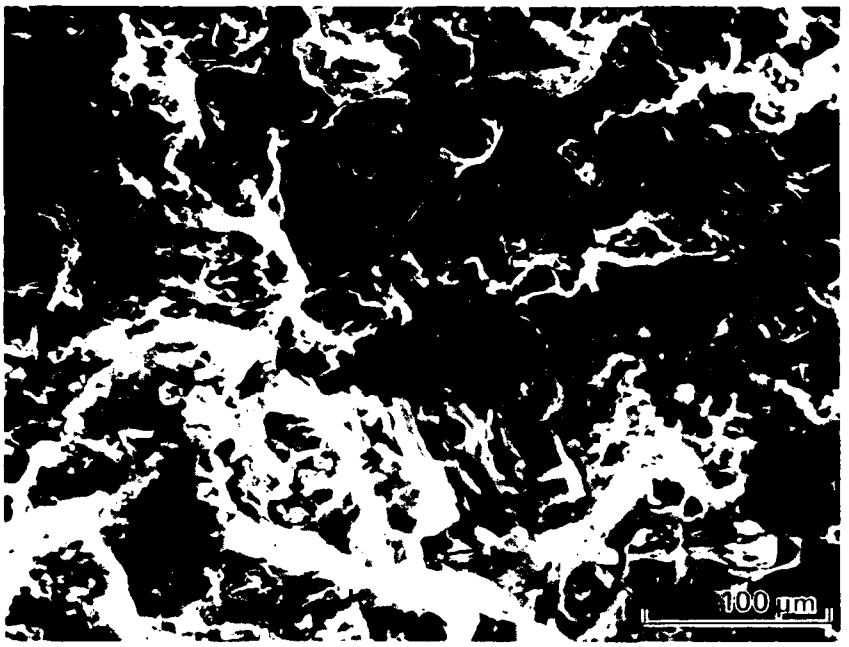

250X

CRACK GROWTH DIRECTION

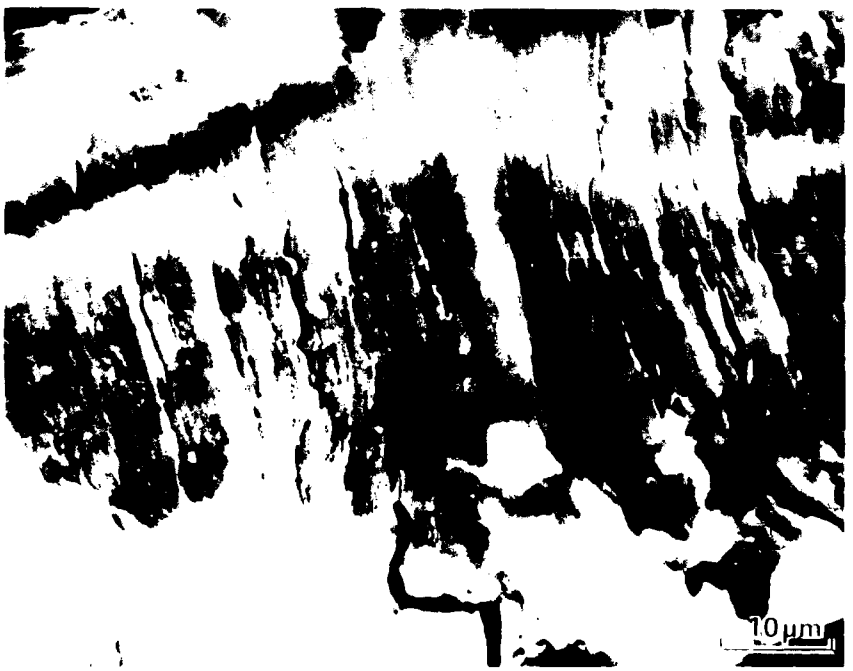

1500X

FIGURE 37. FRACTURE SURFACE OF 2324-T39 TESTED USING TD SPECTRUM AT a = 19 MM (0.75 IN.)

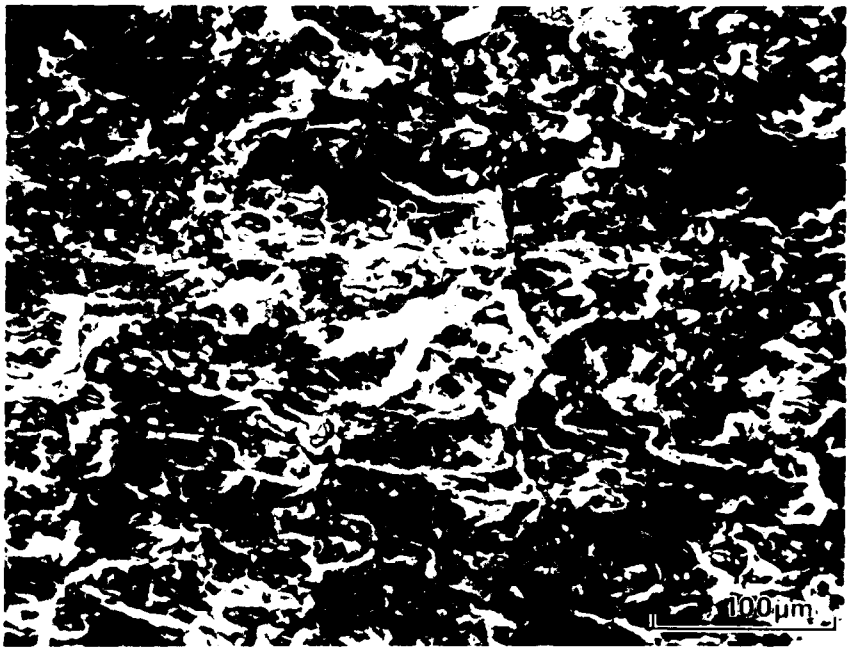

250X

CRACK GROWTH DIRECTION

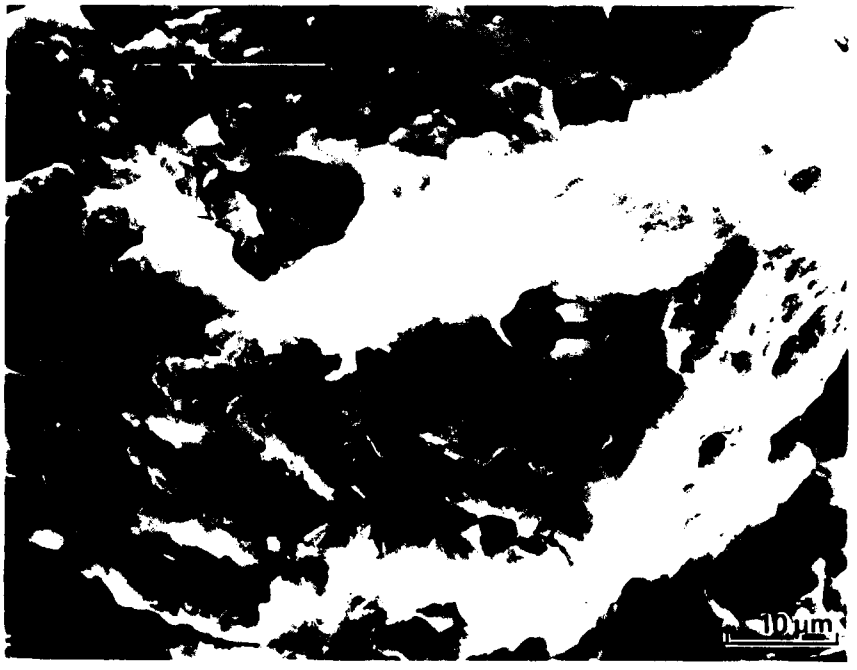

1500X

FIGURE 38. FRACTURE SURFACE OF 7075-T651 TESTED USING TD SPECTRUM AT a = 6.4 MM (0.25 IN.)

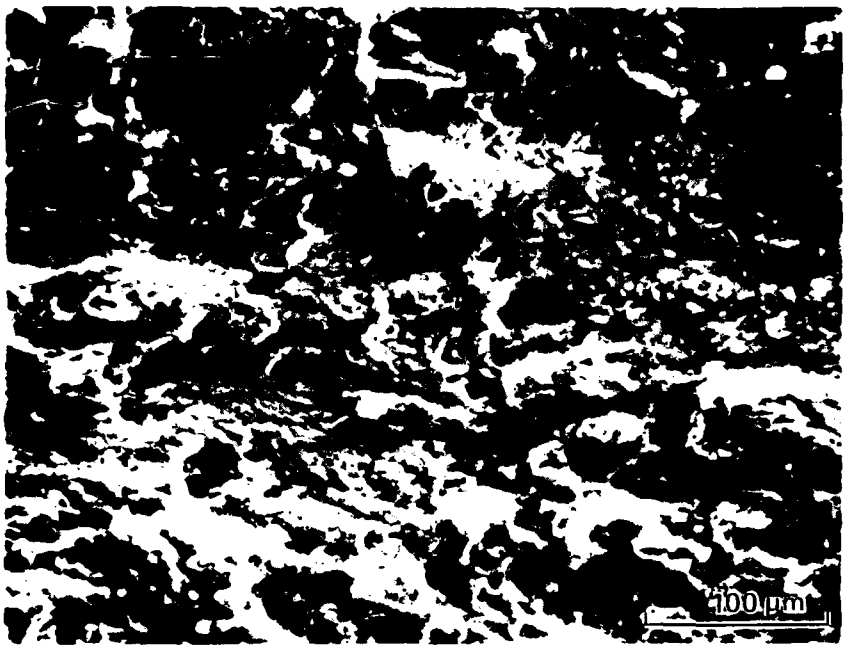

250X

CRACK GROWTH DIRECTION

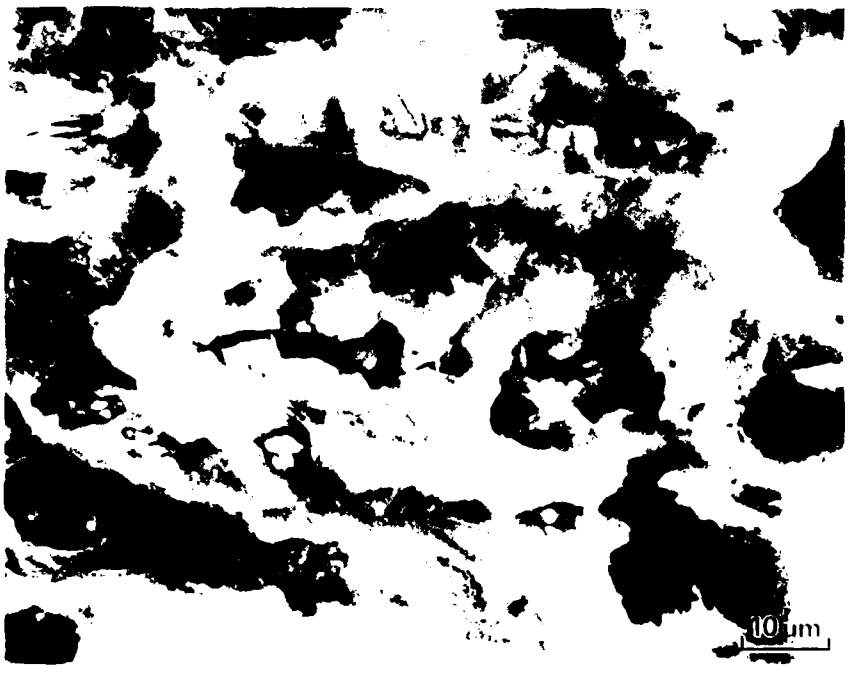

1200X

FIGURE 39. FRACTURE SURFACE OF 7075-T651 TESTED USING TC SPECTRUM AT a = 6.4 MM (0.25 IN.)

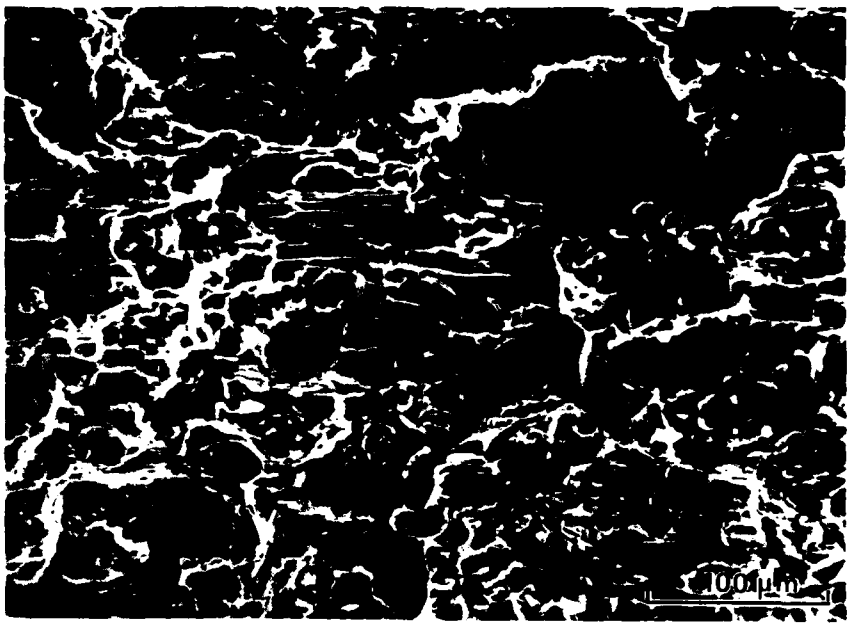

250X

CRACK GROWTH DIRECTION

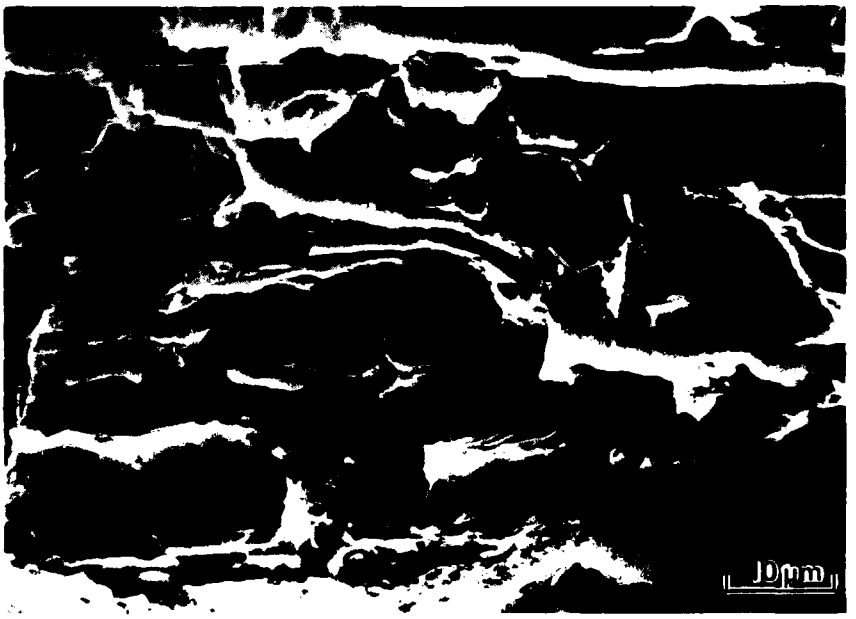

1500X

FIGURE 40. FRACTURE SURFACE OF 7075-T651 TESTED USING TD SPECTRUM AT a = 19 MM (0.75 IN.)

In examining the fracture surfaces, it is apparent that the number and size of voids (which usually nucleate at coarse intermetallic particles) varies among the alloys and with crack length. This, however, does not necessarily imply that intermetallic particles substantially influence the fatigue fracture process. The initial value of K_{hmax} for spectrum tests at a maximum peak stress level of 145 MPa is about 20 MPa$\sqrt{m}$, a stress intensity at which void nucleation and growth is a common constant load amplitude FCP mechanism in both 2XXX (18,42) and 7XXX (18,19) aluminum alloys. The presence of voids on these spectrum fatigue surfaces, particularly at shorter crack lengths (i.e., lower K_{hmax} values), may only reflect the occasional fracture of an intermetallic particle in the crack tip plastic zone during the highest load excursions in each spectrum. In contrast, crack growth may occur primarily by means of a different mechanism during the smaller load-amplitude cycles, with the crack occasionally slicing through a pre-existent void.

IV. SUMMARY AND CONCLUSIONS

An exploratory investigation to determine the important metallurgical factors that influence spectrum fatigue crack propagation in selected high-strength aluminum alloys is being performed. This program is also designed to simplify complex load histories into generic simple spectra and provide information for development and selection of fatigue resistant alloys. The results described in this report represent a baseline characterization of a number of high strength aluminum alloys for use in the investigation as well as the results for tests performed using the first iteration of the simplified spectra.

Ten commercial 2XXX and 7XXX aluminum alloys were chosen for analysis so that the influence of both purity and temper on FCP could be evaluated. The alloys evaluated were 2020-T651, 2024-T351, 2024-T851, 2124-T851, 2324-T39, 7050-T73651, 7075-T651, 7075-T7351, 7475-T651, and 7475-T7351. All ten alloys (seven in Phase I and three in Phase II) have been characterized with respect to chemical composition, microstructure, tensile properties, and fracture toughness. FCP tests were conducted on specimens of each alloy for both constant-amplitude loading (including the low ΔK region) and two F-18 load spectra. The spectrum FCP testing was performed at a maximum peak stress of 145 MPa (21 ksi) as well as limited testing at 103 and 169 MPa (15 and 24.5 ksi) to obtain additional data at the low and high end of the crack-growth range. Seven of the alloys have been evaluated using three simplified spectra. Pertinent fracture surface features were documented on the spectrum fatigue specimens. For completeness, the results from the first phase are included in this summary of the second phase of the program.

The constant load amplitude FCP tests were performed on each material to provide a baseline characterization of steady-state FCP response. These data are necessary as inputs to life prediction models, which will be used to rank alloys in the next phase. Fractographic analyses of these specimens will

be used to help explain the spectrum fatigue results. Several observations can be made about the constant load amplitude FCP behavior of these alloys:

1. Rankings of constant load amplitude FCP resistance among the ten materials are ΔK dependent.
2. At near-threshold ΔK levels (≤ 4 MPa $\sqrt{m}$):
   a. Fatigue crack growth resistance varies more than that at higher ΔK levels.
   b. 2024-T351 has greater crack growth resistance than the other nine alloy-temper combinations.
   c. FCP resistance of 7475-T651 exceeds that of the other four 7XXX alloys: 7075-T651, 7075-T7351, 7050-T73651, and 7475-T7351.
   d. These data confirm that:
      i. increased aging reduces near-threshold FCP resistance.
      ii. purity (Fe, Si content) has little or no effect on near-threshold crack growth rates.
3. At intermediate ΔK levels (4 to 15 MPa $\sqrt{m}$):
   a. The 2XXX alloys, 2020-T651 and 2324-T39, have lower FCG rates than the other alloys.
   b. The peak aged 7XXX alloys, 7075-T651 and 7475-T651 have faster FCG rates than the other alloys.

Spectrum FCP tests were conducted on each of the ten alloys, using two complex F-18 load histories. The performance of each alloy in these spectrum tests and the relative rankings of the alloys represent valuable engineering information; and these results will be used in this program in selecting metallurgical variables that will be systematically evaluated for their effects on fatigue crack growth. Secondly, these results are baseline information for spectrum analyses and spectrum modifications. Several

observations can be made based on the results for testing at the maximum peak stress of 145 MPa (21 ksi):

1. The ranking of the ten alloys is the same for the two spectra, except for 2020-T651 for which the ranking under the tension-compression (TC) spectrum is considerably lower than the tension-dominated (TD) spectrum.

2. For each material the TD spectrum consistently results in longer lives.

3. The differences in life between the two spectra for the same alloy were small – not more than an 18 percent difference for any alloy, except for 2020-T651 and 2024-T351, for which differences were about 35 percent.

4. There were larger differences in lives among the 2XXX alloys than the 7XXX alloys, for example, an 84 percent difference for the TD spectrum between the two extremes for the 2XXX alloys, 2024-T851 and 2024-T351, compared to a 55 percent difference between the extremes for the 7XXX alloys, 7475-T651 and 7075-T651.

5. A comparison of the spectrum lives and fatigue crack growth rates indicates that the overall spectrum life does not appear to be controlled by any particular regime of spectrum crack growth (or stress intensity).

For the spectrum testing at 103 MPa (15 ksi), which was limited to a smaller range of crack growth at lower stress intensities than those for the 145 MPa testing, it was observed that:

1. The 2XXX alloys 2020-T651, 2024-T351, and 2324-T39 had longer spectrum fatigue lives than the other alloys, and among those 2020-T651 alloy had a significantly longer spectrum fatigue life.

2. For each alloy, the TD spectrum resulted in a nearly equal or somewhat longer spectrum fatigue life than the same alloy tested with the TC spectrum, except for 7475-T651.

3. The rankings do not correlate with the rankings for testing at 145 MPa.

The spectrum testing at 169 MPa (24.5 ksi) also represented a smaller range of crack growth than the testing at 145 MPa, but overlapped the higher stress intensities of the testing at 145 MPa. Several observations for these results in comparison to the results at 145 MPa can be made:

1. The ranking of the 7XXX materials has improved compared to the 2XXX materials, with 7475-T651 and 7475-T7351 being top ranked for both spectra.
2. The ranking within the 7XXX materials are the same for both spectra.
3. The ranking within the 2XXX materials for the TD spectrum is similar except 2020-T651 is lowest ranked compared to second ranked.
4. The ranking within the 2XXX materials for the TC spectrum does not correlate.

In general, the spectrum performance rankings could not be correlated with yield strength or constant-amplitude FCP resistance at any ΔK level. However, spectrum performance could be correlated with fracture toughness; specifically for the testing at 145 and 169 MPa, FCP life for both spectra generally increased with increased fracture toughness. Perhaps more significantly, the alloys that deform by planar slip generally had longer spectrum fatigue lives than those that deformed more homogeneously.

Seven of the ten alloys were spectrum fatigue tested using modifications of the baseline spectra. Two different types of modifications were performed independently on the baseline spectra. One modification had two goals:

1. to eliminate low-amplitude cycles to reduce testing time without changing the ranking (relative life) of the alloys
2. to determine the importance of low amplitude cycles on the overall spectrum life.

The racetrack method was used to eliminate 43 percent of the low amplitude cycles. Although the goal of preserving the same ranking as the baseline spectra was not met, the differences in spectrum fatigue lives between the modified and baseline spectra are probably small enough so that the selection of one alloy over another would not be significantly affected.

The second modification was made to determine the importance of compressive load cycles. To accomplish this, all compression load points were eliminated from the TC spectrum. There were significant increases in spectrum lives compared to the baseline spectrum; but surprisingly, the rankings of the seven alloys for this modified spectrum were the same as those for the two baseline spectra.

V. FUTURE PLANS

The effort reported herein represented the first two phases of a planned four-phase effort to achieve the goals outlined in Section I. Some of the significant areas to be evaluated in the following phases include:

1. Produce and evaluate alloys with controlled microstructural variants to elucidate their effects on spectrum fatigue behavior. A discussion of this aspect of the program follows this list.
2. Test additional alloys and tempers to yield additional data on the effects of precipitate structure (temper), grain size, and new alloy approaches (e.g., chemistry modification and powder metallurgy). (See Figure 1.)
3. Use spectrum fatigue crack propagation models to:
   a. Investigate alloy rankings in different load spectra, and identify features of the load history which contribute to spectrum FCP rankings.
   b. Determine the effects of material variables on spectrum FCP behavior.
   c. Simplify the spectra retaining the features that influence spectrum fatigue behavior to obtain a more economical and faster test for evaluation of the spectrum fatigue behavior of high-strength aluminum alloys.
4. Continue the spectrum simplication effort based on present results and results of spectrum fatigue crack growth models (3c above).
5. Identify microstructural, metallurgical factors which can be used to optimize FCGR of high strength aluminum alloys.

The results of Phases I and II suggest that spectrum fatigue life can be lengthened by reducing crack growth rate in any region of the constant-amplitude FCG curve. At high ΔK levels, increasing toughness not only lowers growth rates, but also delays final fracture by increasing the critical

flaw size. The metallurgical characteristics which improve FCG resistance at low and intermediate ΔK levels can lengthen spectrum fatigue life, even in the absence of high fracture toughness. The spectrum fatigue resistance of 2020-T651 is a particularly good example of the beneficial effect of good low/intermediate ΔK FCG performance on fatigue behavior in response to complex load histories.

It is a major goal of the remaining phases of this program to identify those metallurgical characteristics which improve spectrum fatigue resistance. As described in the Section 3.6.2, the degree of slip planarity seems to exert an important influence on fatigue behavior. From the literature, it also is apparent that grain structure strongly influences low ΔK FCG resistance for constant amplitude loading.[43-45] One can assume, therefore, that grain structure or these metallurgical characteristics will affect spectrum fatigue behavior. In fact, since the arguments used to rationalize slip planarity[19,38,39] and grain structure[43-45] effects are very similar, there is reason to believe that an interaction between these metallurgical characteristics should occur.

To examine the effects of these metallurgical characteristics on spectrum fatigue behavior, special heats of alloys in the Al-Li system are planned for production in the next phase. These alloys tend to deform by planar slip, the degree of which can be controlled by different temper conditions. Variations in grain structure can be controlled by fabrication practice. Two alloy compositions are planned for the Phase III study: Al-3Cu-2Li-1Mg and Al-3Cu-2Li. These same alloys currently are under investigation in a separate NAVAIR/Alcoa contract,[46] which is seeking fundamental information on fatigue/microstructure relationships, primarily for constant amplitude loading. Use of the same alloys in both contracts will allow valuable cross-pollination of ideas.

Variants of these first two alloys will be fabricated, including different grain structures and tempers. These alloys will be characterized thoroughly with respect to microstructure, mechanical properties (tensile and toughness), and fatigue crack growth behavior for both constant-amplitude and spectrum loadings. This basic information is an intimate part of the work using simplified load histories to elucidate spectrum fatigue/microstructure relationships.

APPENDIX A

CONSTANT AMPLITUDE FATIGUE CRACK GROWTH RATE, da/dN VERSUS ΔK

The results for the alloys characterized in Phase I were presented in Appendix A, Reference 27.

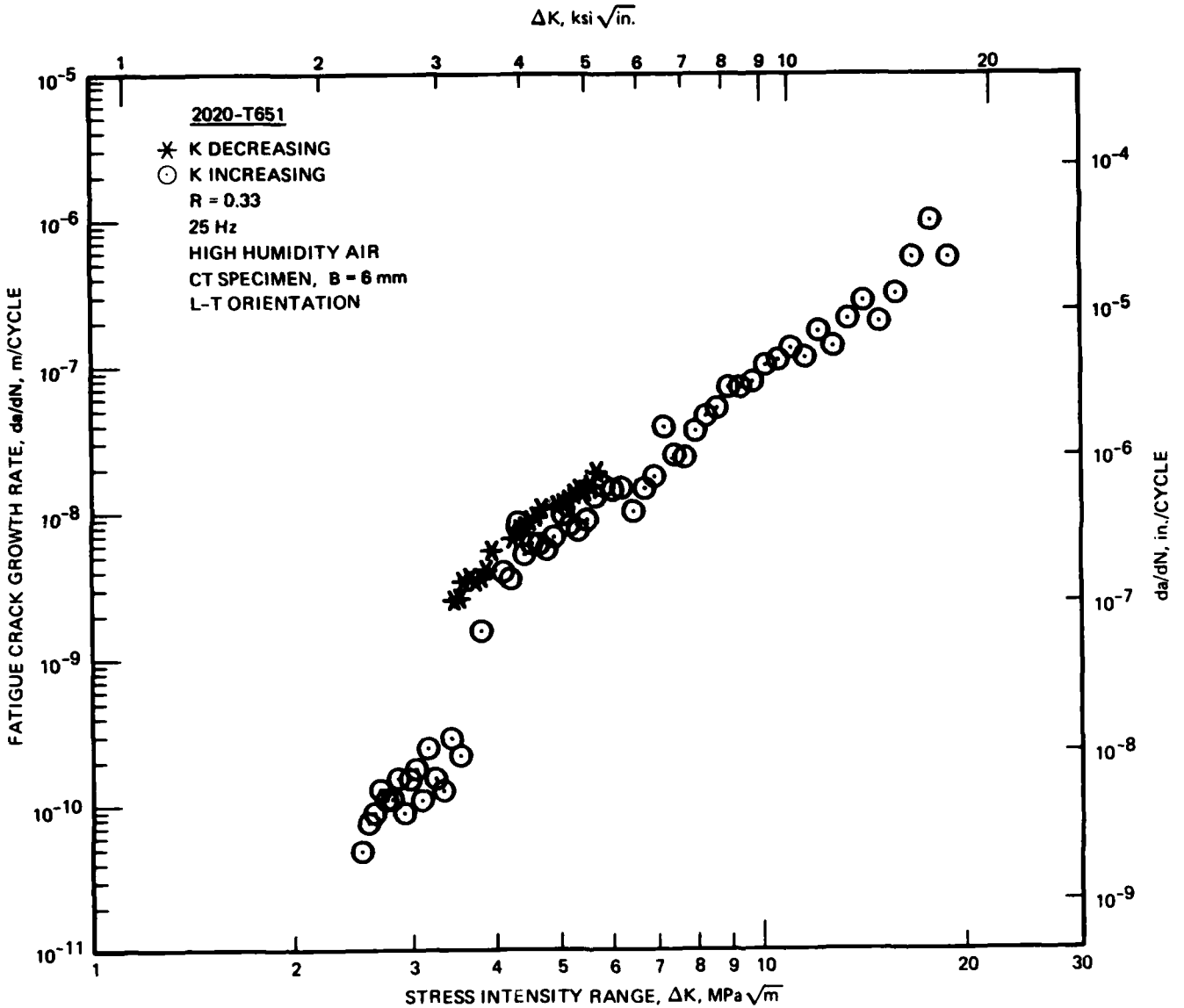

FIGURE A-1. CONSTANT LOAD AMPLITUDE FATIGUE CRACK GROWTH RATE DATA FOR 2020-T651

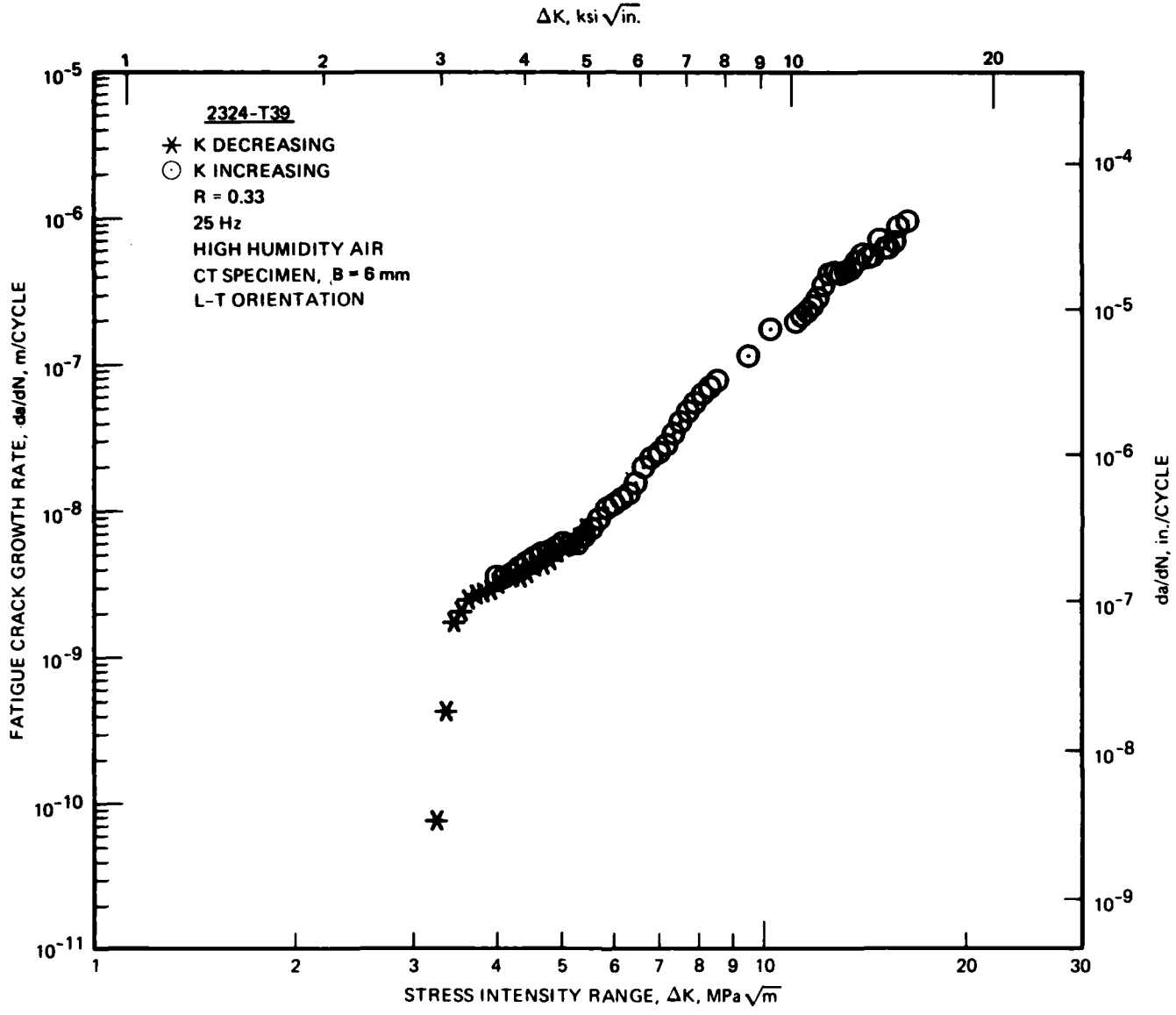

FIGURE A-2. CONSTANT LOAD AMPLITUDE FATIGUE CRACK GROWTH RATE DATA FOR 2324-T39

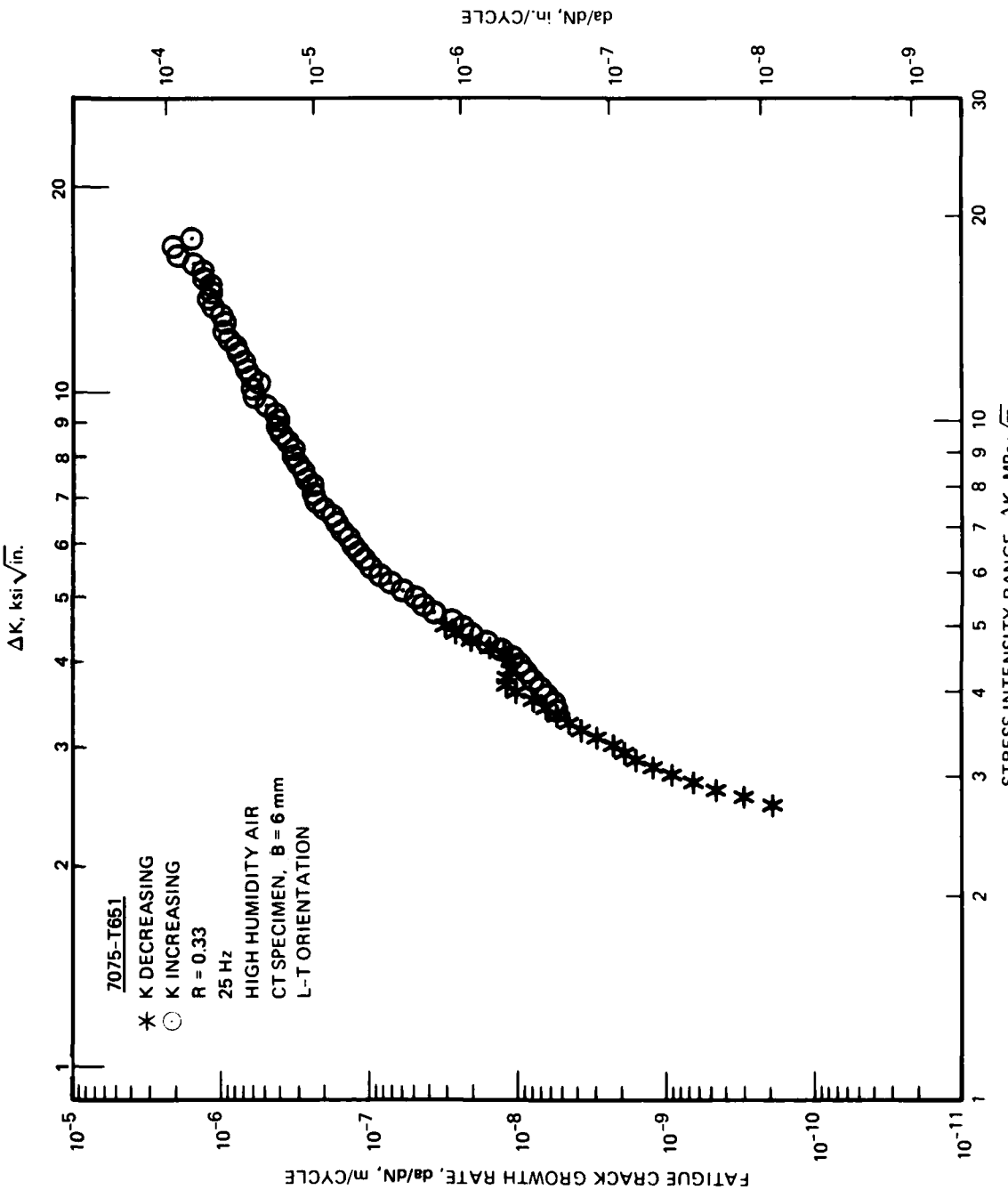

FIGURE A-3. CONSTANT LOAD AMPLITUDE FATIGUE CRACK GROWTH RATE DATA FOR 7075-T651

APPENDIX B

APPENDIX B

CRACK LENGTH VERSUS SIMULATED FLIGHT HOURS FOR BASELINE SPECTRA, a VERSUS H

1. The scale for the ordinate (a) is the same for each graph; the scale for the abscissa (H) varies, and to make comparisons easier, the abscissa was adjusted so that a crack length of 6 mm corresponded to zero simulated flight hours.

2. Two specimens each were tested at 145 MPa, and one each at 103 and 169 MPa.

3. Data are in numerical order by alloy designation with TD spectrum first, then TC spectrum.

4. The tension-dominated (TD) spectrum representing the lower wing root load history of the F-18 is coded C2 at Northrop and the tension-compression (TC) spectrum representing the horizontal hinge tail moment load history is coded E3.

5. Crack length was measured at the end of one or more passes (300 simulated flight hours per pass) of the spectrum, which at the beginning of the 103 and 145 MPa tests resulted in the crack growth increment being less than 0.25 mm which is required by ASTM E647. (Note that ASTM E647 method is a constant amplitude method for fatigue crack growth.) However, in calculating crack growth rates, the 0.25 mm increment requirement was observed. At the higher crack growth rates, the one per pass crack measurement resulted in larger crack growth increments than required by ASTM E647.

6. Graphs were plotted using a Northrop Support Services Laboratory computer program designated $SPECPT from data on files designated .DDN, created from crack length measurement versus pass raw data.

7. The results for the alloys characterized in Phase I were presented in Appendix B, Reference 27.

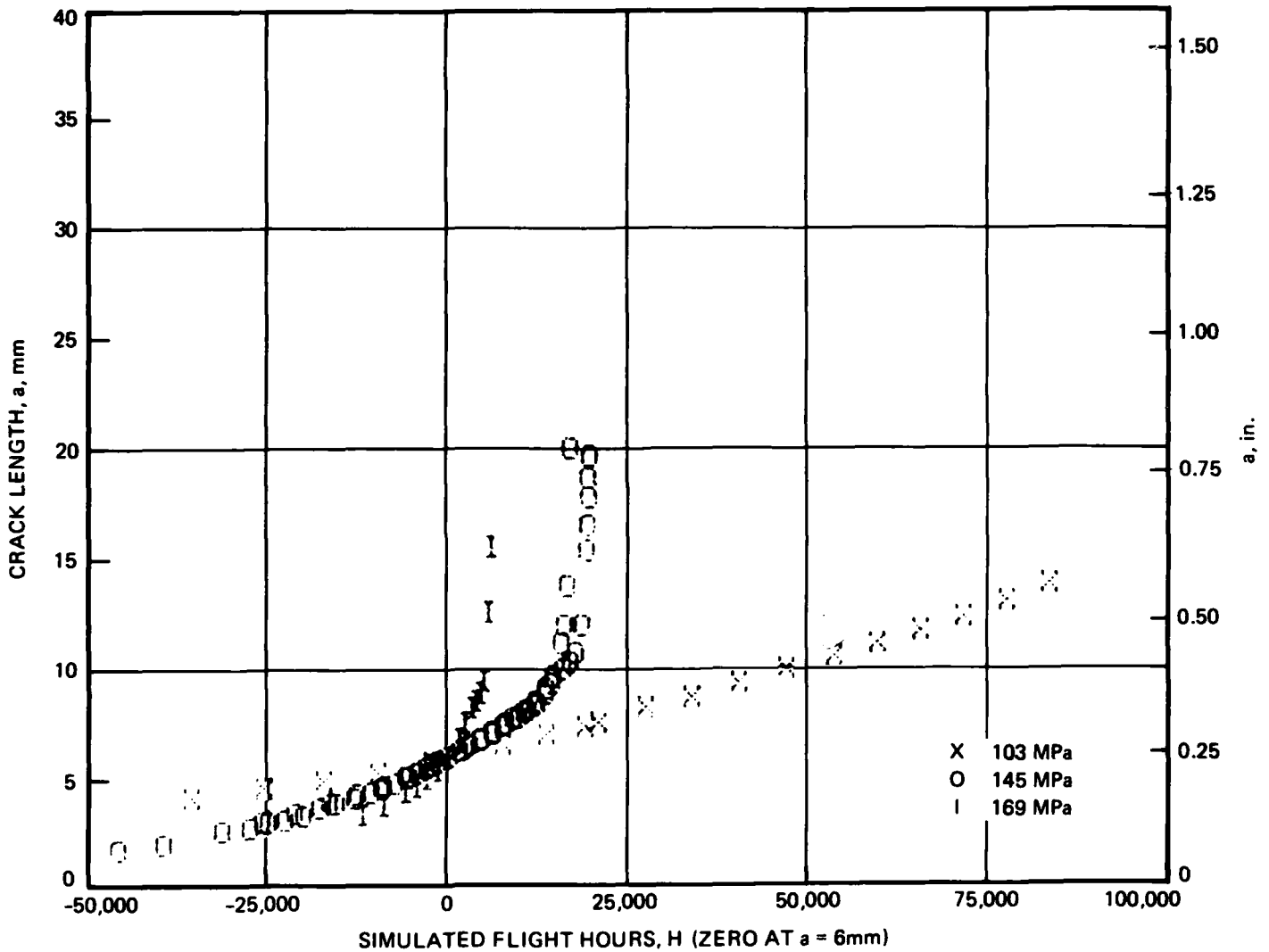

FIGURE B-1. 2020-T651, TD SPECTRUM

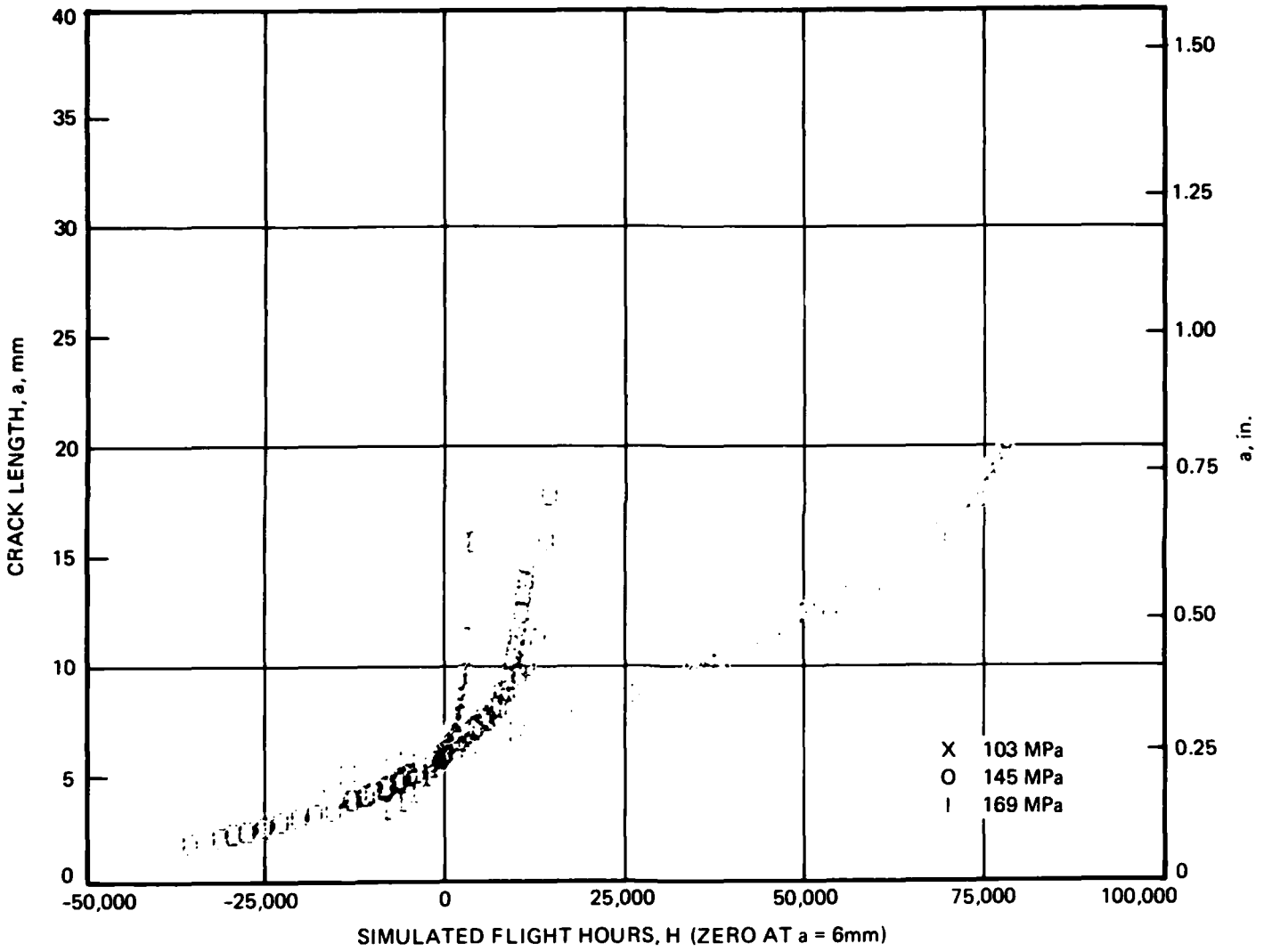

FIGURE B-2. 2020-T651, TC SPECTRUM

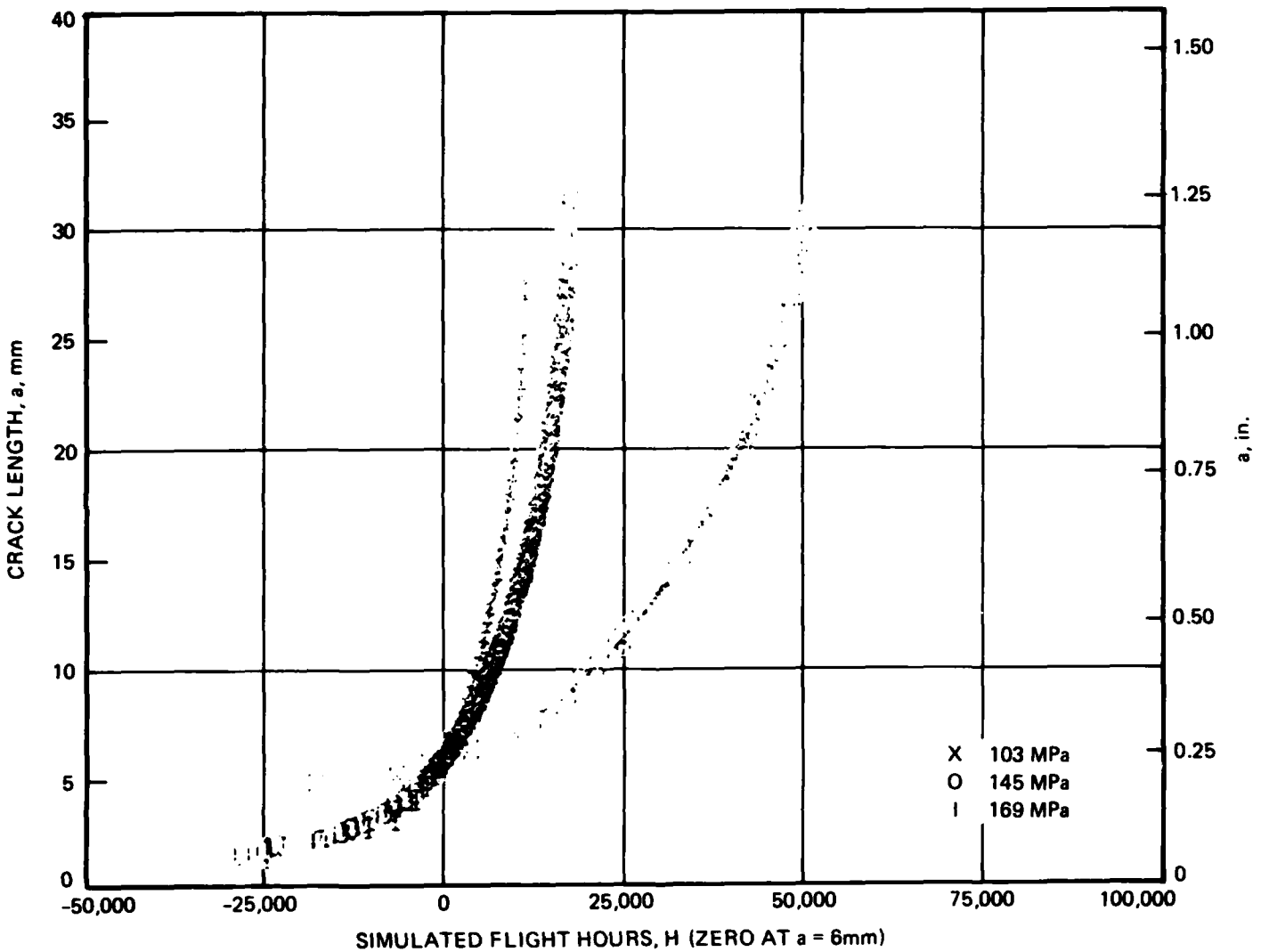

FIGURE B-3. 2324-T39, TD SPECTRUM

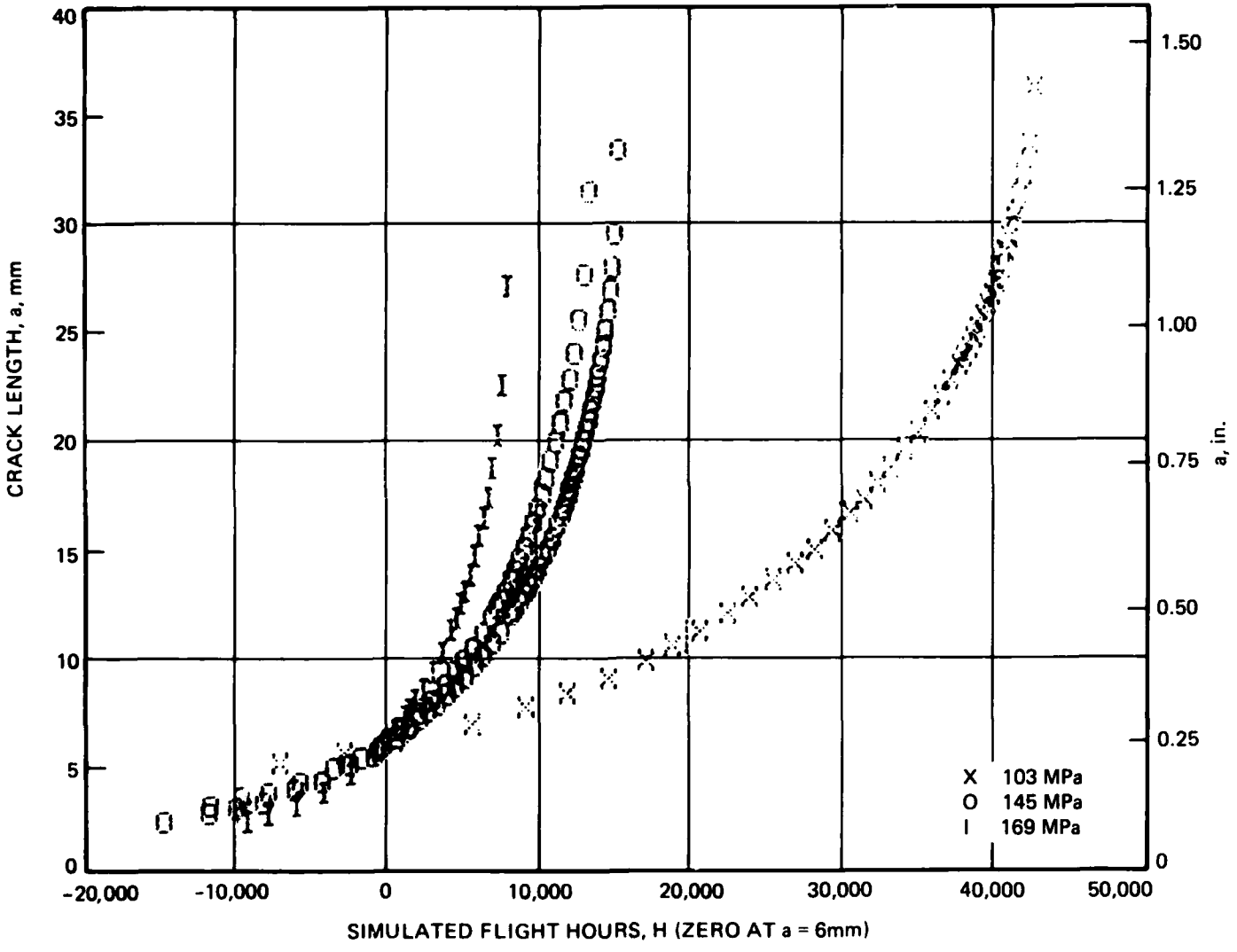

FIGURE B-4. 2324-T39, TC SPECTRUM

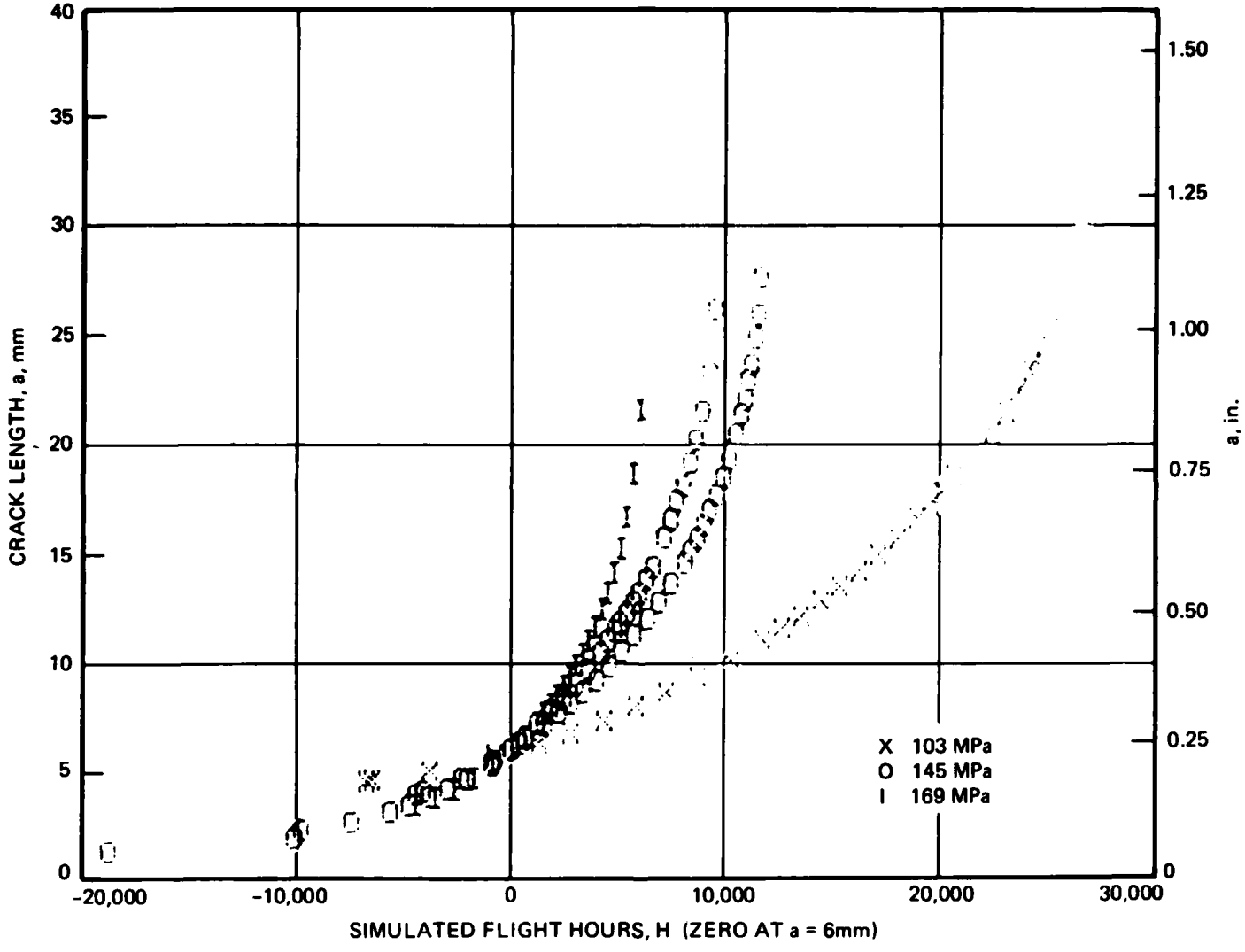

FIGURE B-5. 7075-T651, TD SPECTRUM

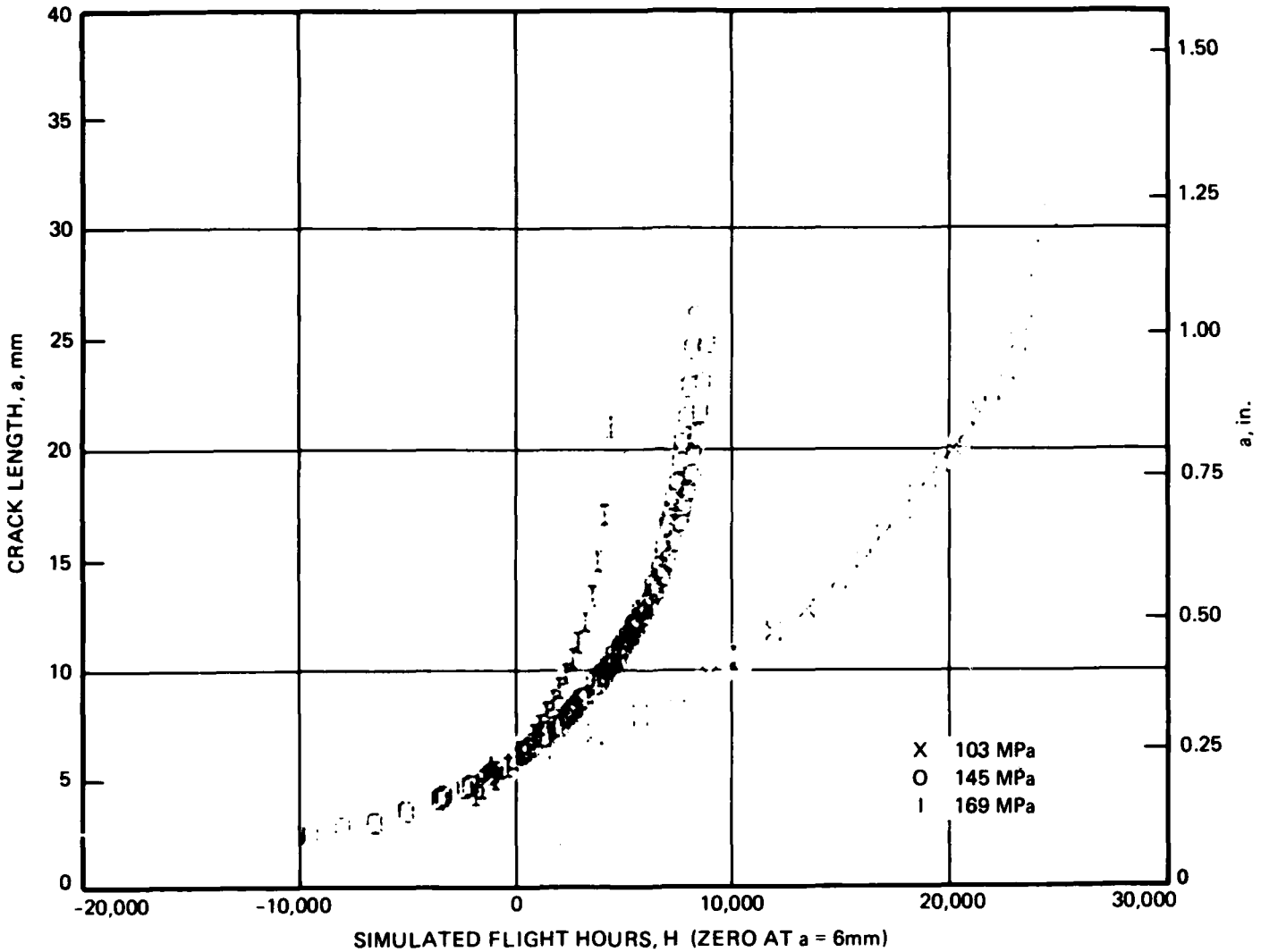

FIGURE B-6. 7075-T651, TC SPECTRUM

APPENDIX C

SPECTRUM CRACK GROWTH RATE VERSUS MAXIMUM PEAK STRESS INTENSITY FOR BASELINE SPECTRA, da/dH VERSUS K_{hmax}

1. The scales for both axes are identical on each graph.
2. There are two tests for the maximum peak stress level of 145 MPa and both are plotted with the same symbol. There is one test each at the maximum peak stresses of 103 MPa and 169 MPa.
3. Crack growth rates are calculated by two-point secant method per ASTM E647 based on the data in Appendix B, and applying the ASTM E647 requirement that the minimum crack growth interval, a, be greater than or equal to 0.25 mm. This is performed using Northrop Support Services Laboratory computer program designated $FITPLT from data on files designated .DDN, created from crack length measurement versus pass raw data.
4. Almost all tests had a crack growth rate which initially decreased for a few data points after precracking, therefore, all data up to the first local minimum crack growth rate were not plotted.
5. The results for the alloys characterized in Phase I were presented in Appendix C, Reference 27.

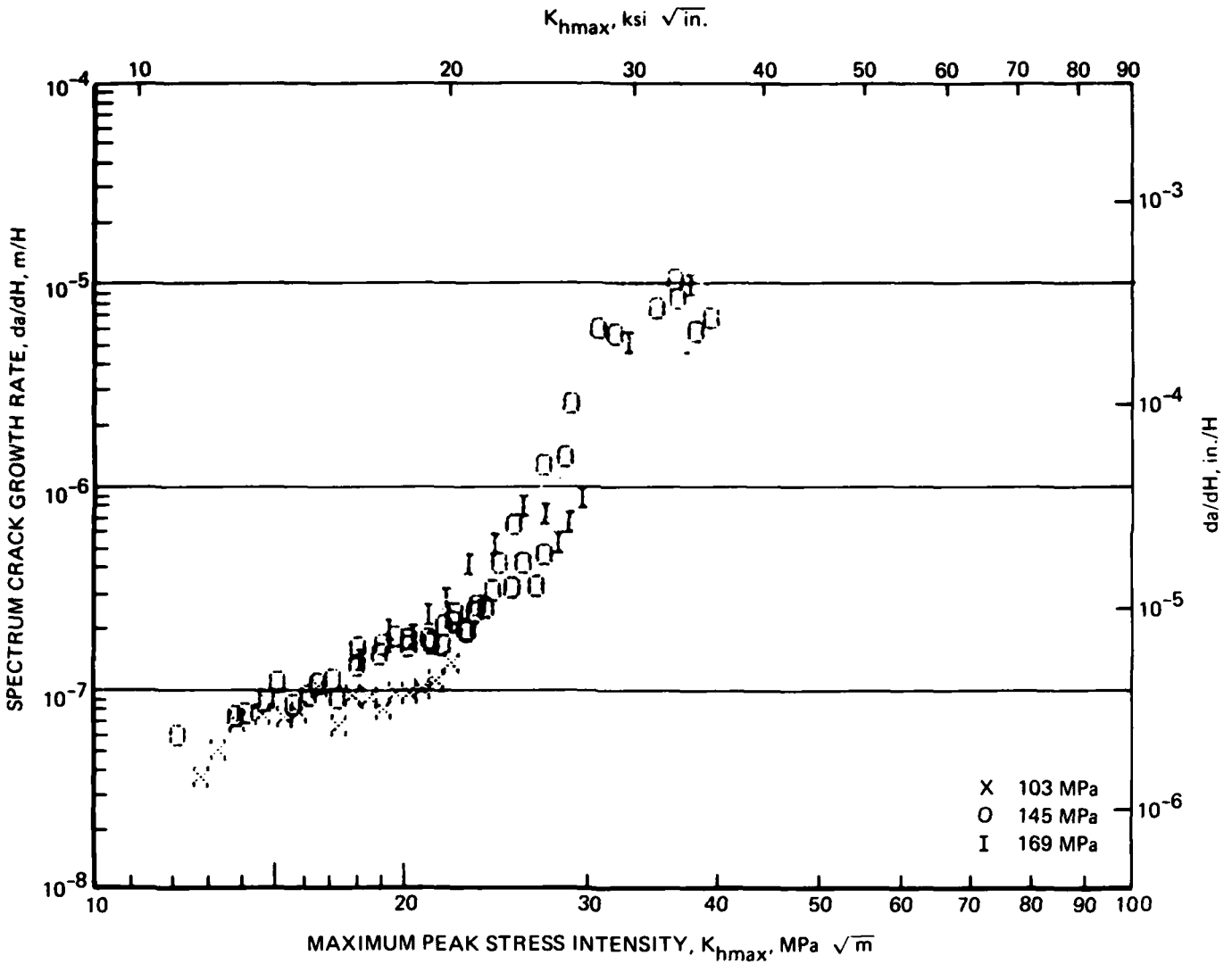

FIGURE C-1. 2020-T651, TD SPECTRUM

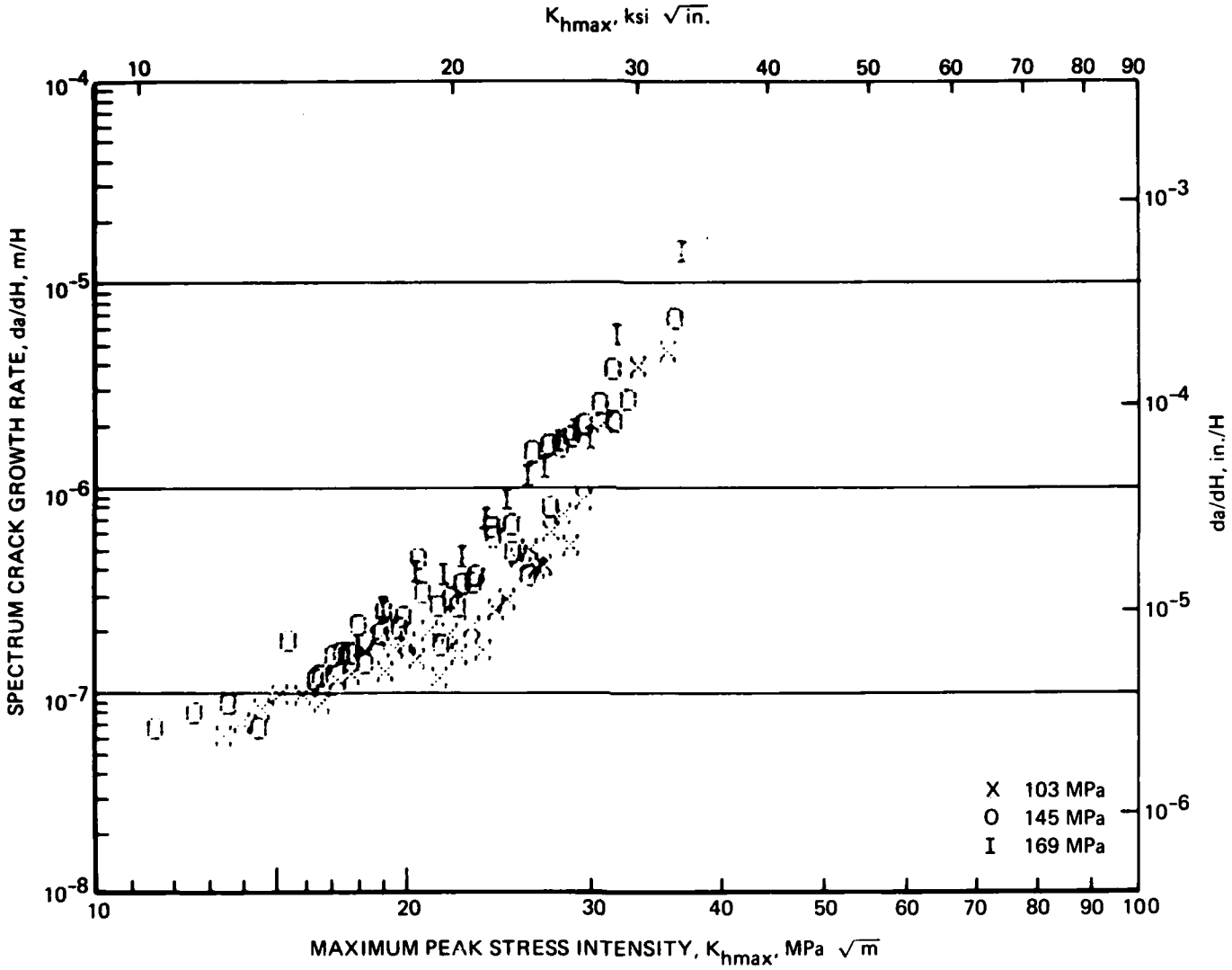

FIGURE C-2. 2020-T651, TC SPECTRUM

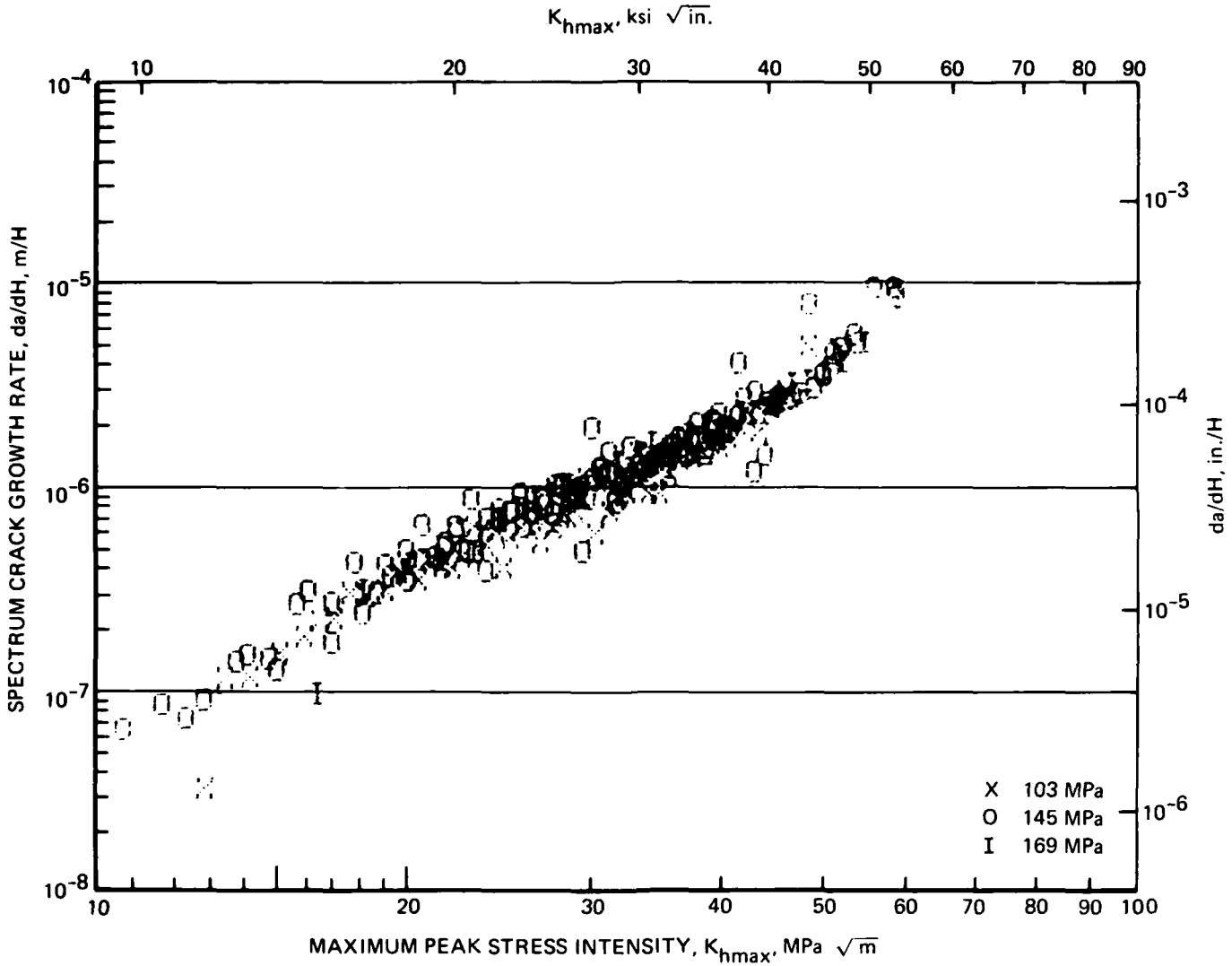

FIGURE C-3. 2324-T39, TD SPECTRUM

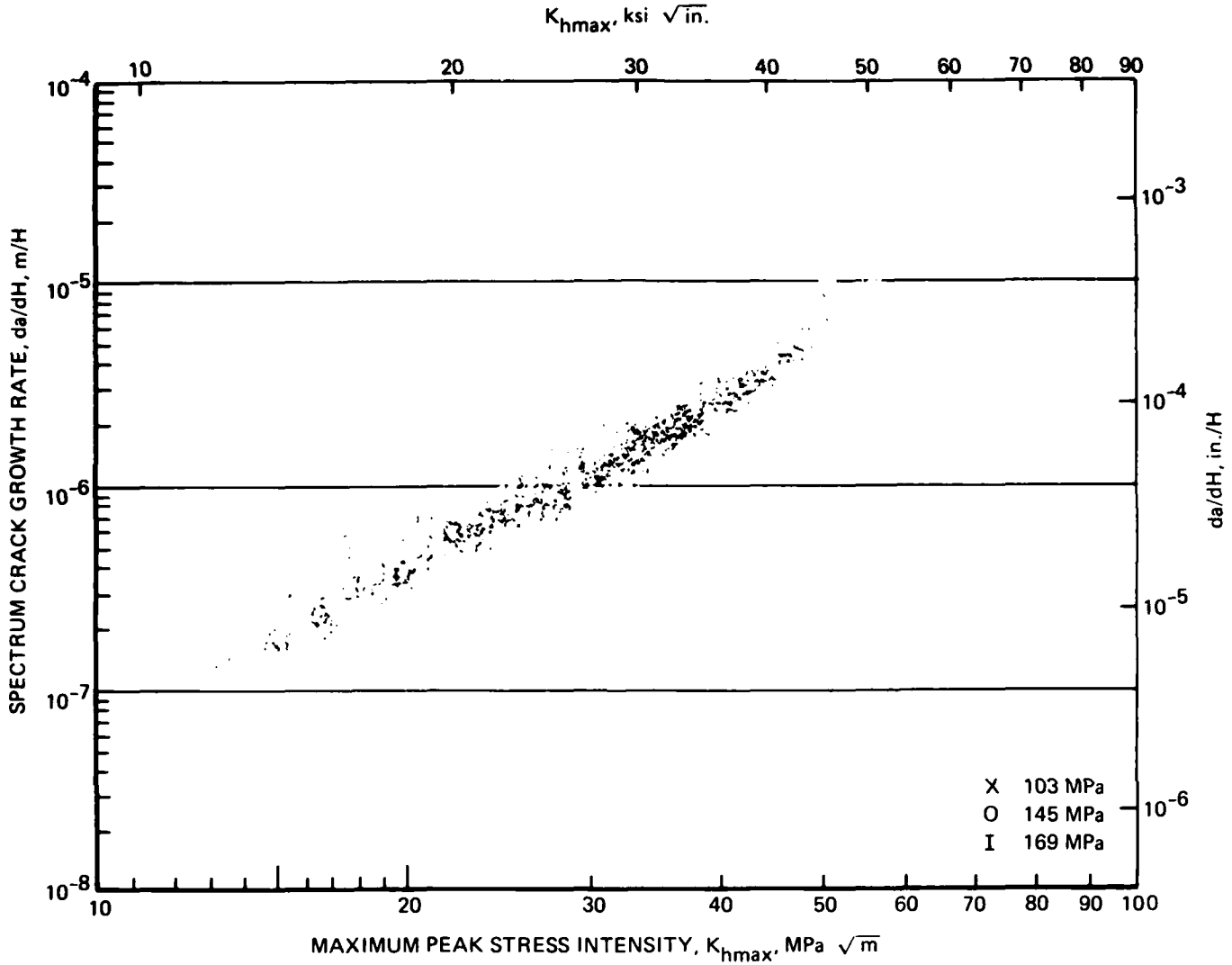

FIGURE C-4. 2324-T39, TC SPECTRUM

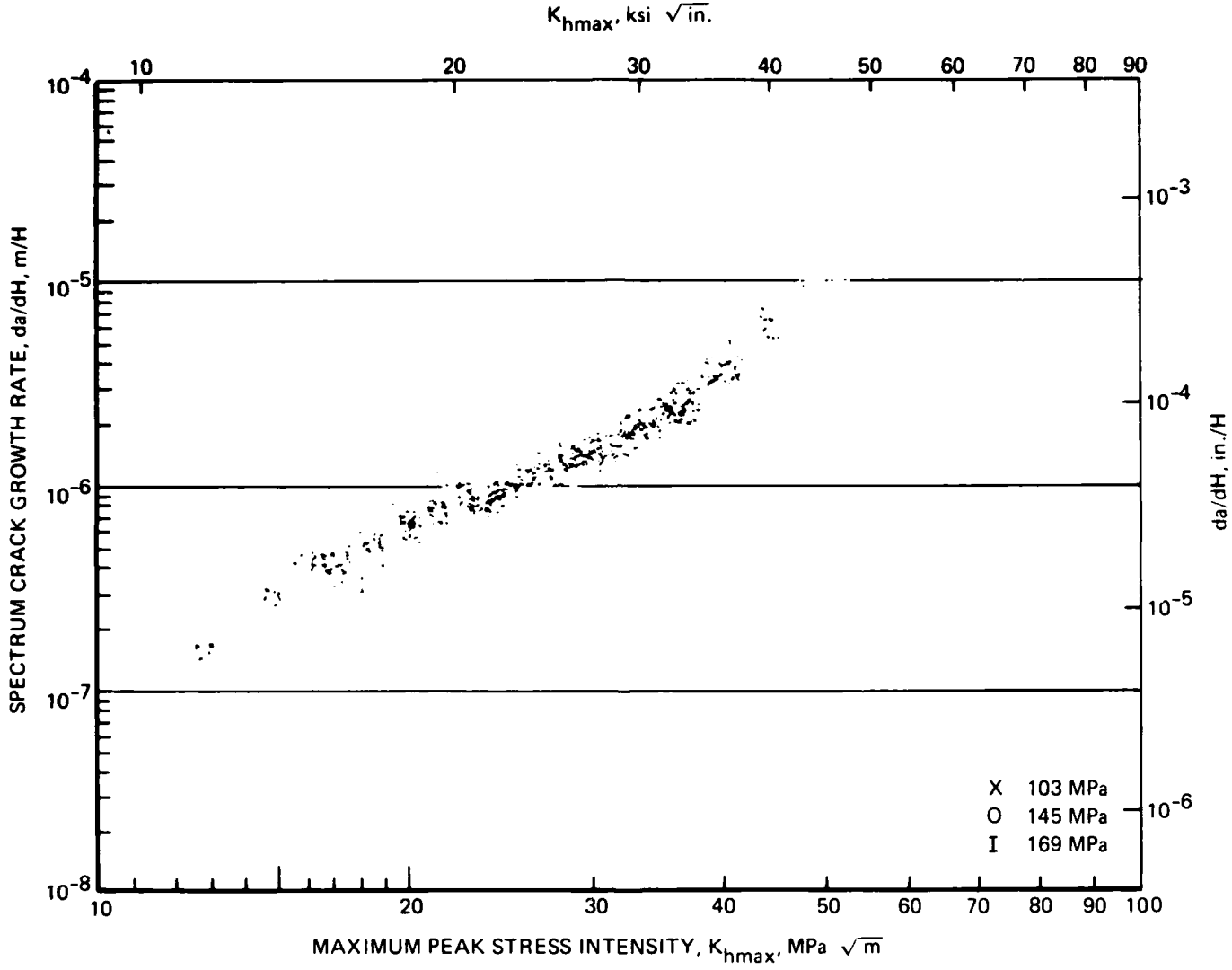

FIGURE C-5. 7075-T651, TD SPECTRUM

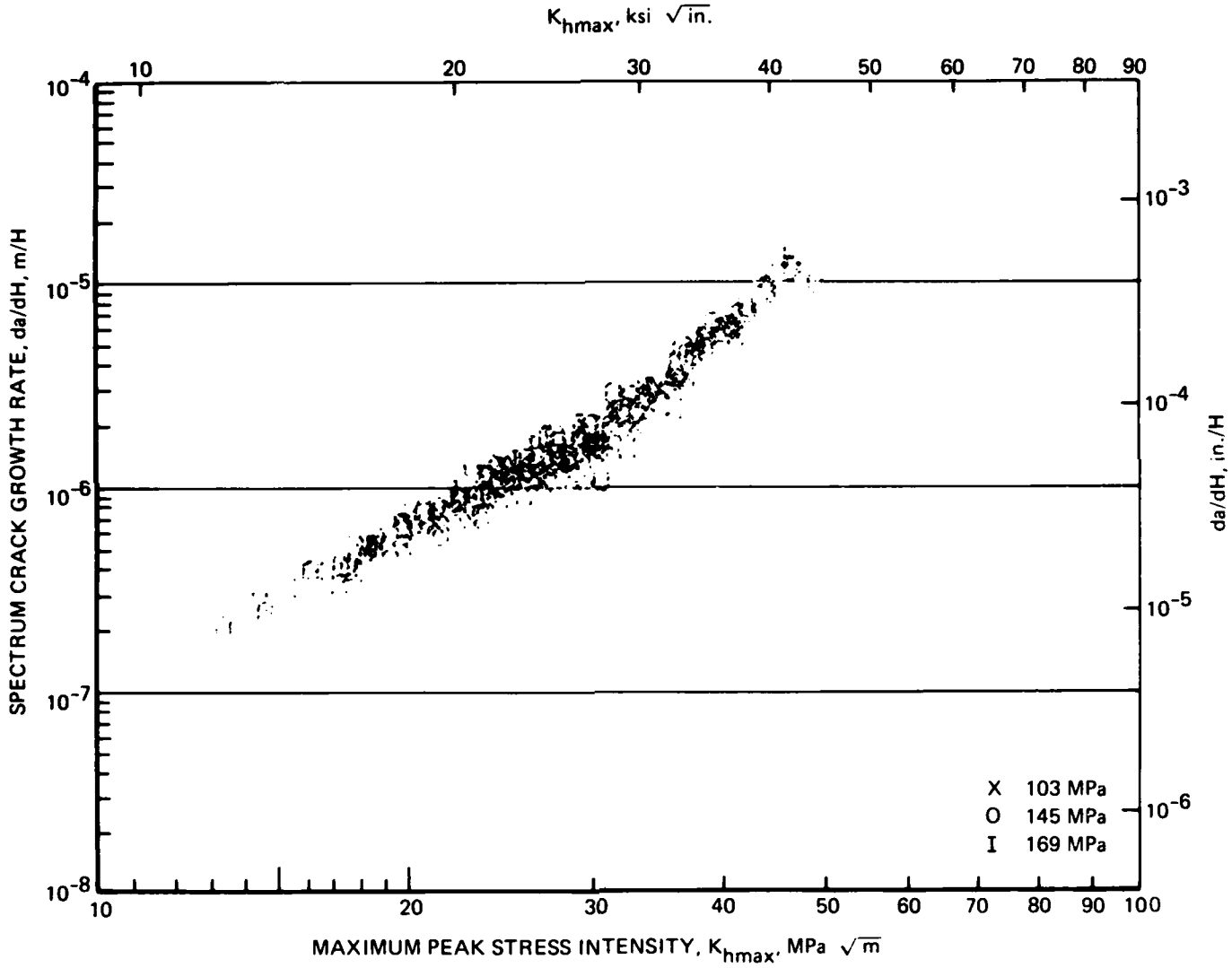

FIGURE C-6. 7075-T651, TC SPECTRUM

APPENDIX D

CRACK LENGTH VERSUS SIMULATED FLIGHT HOURS FOR MODIFIED SPECTRA, a VERSUS H

1. The scale for the ordinate (a) is the same for each graph; the scale for the abscissa (H) varies, and to make comparisons easier, the abscissa was adjusted so that a crack length of 6 mm corresponded to zero simulated flight hours.
2. All testing was at a maximum peak stress of 145 MPa.
3. Data are in numerical order by alloy designation.
4. Two specimens were tested using the TCZ spectrum and one specimen each for the TDR and TCR spectra.
5. The tension-compression-zero (TCZ) spectrum is the tension-compression spectrum with all loads less than zero set equal to zero and is coded F18E3A at Northrop. The tension-dominated-racetrack (TDR) spectrum is the racetrack-modified version of the TD spectrum and is designated SCARC2 at Northrop. The tension-compression-racetrack (TCR) is the racetrack-modified version of the TC spectrum and is designated TDR25 at Northrop.
6. See Appendix B Paragraphs 5 and 6 for other testing notes.

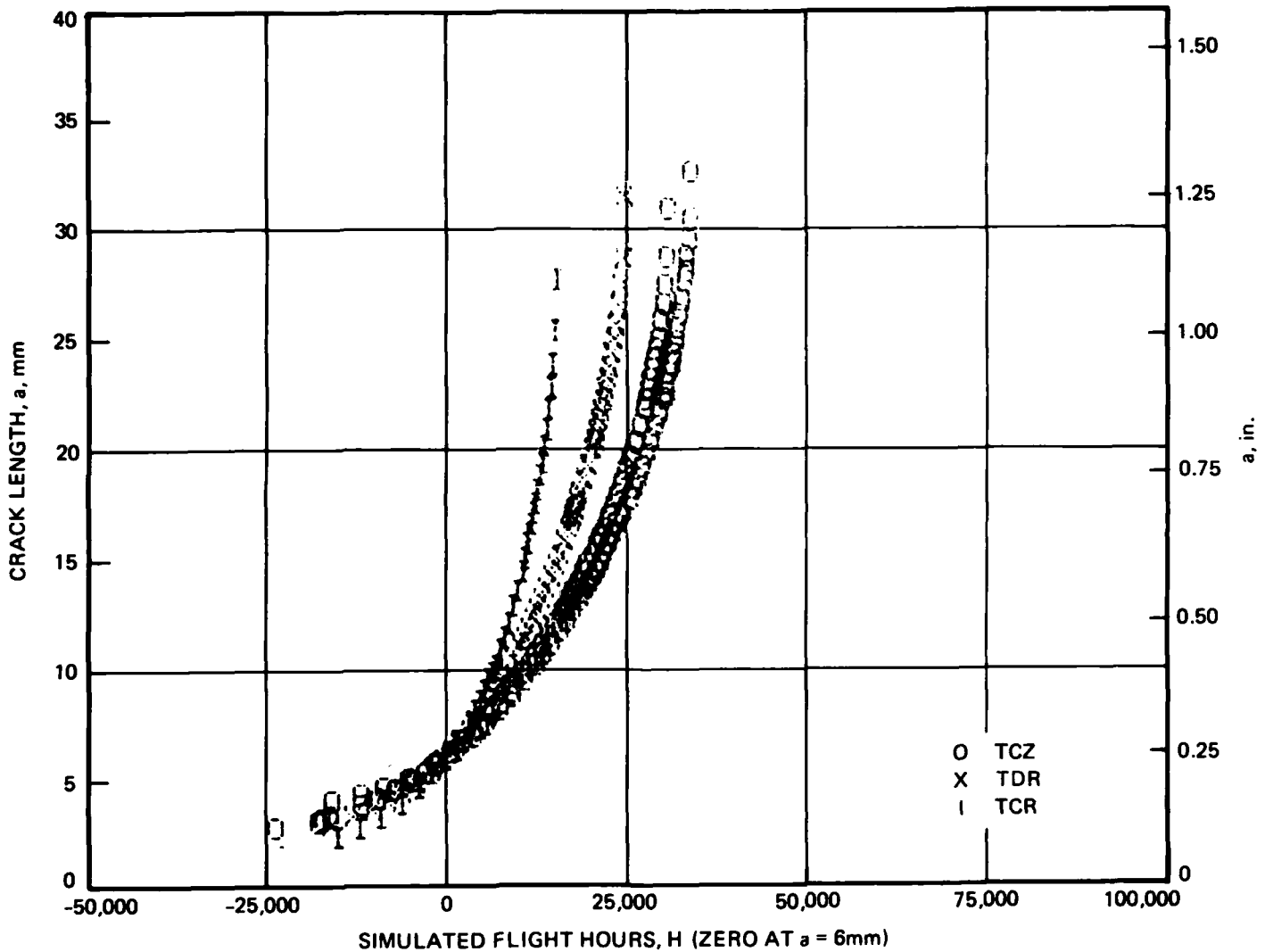

FIGURE D-1. 2024-T351, 145 MPa

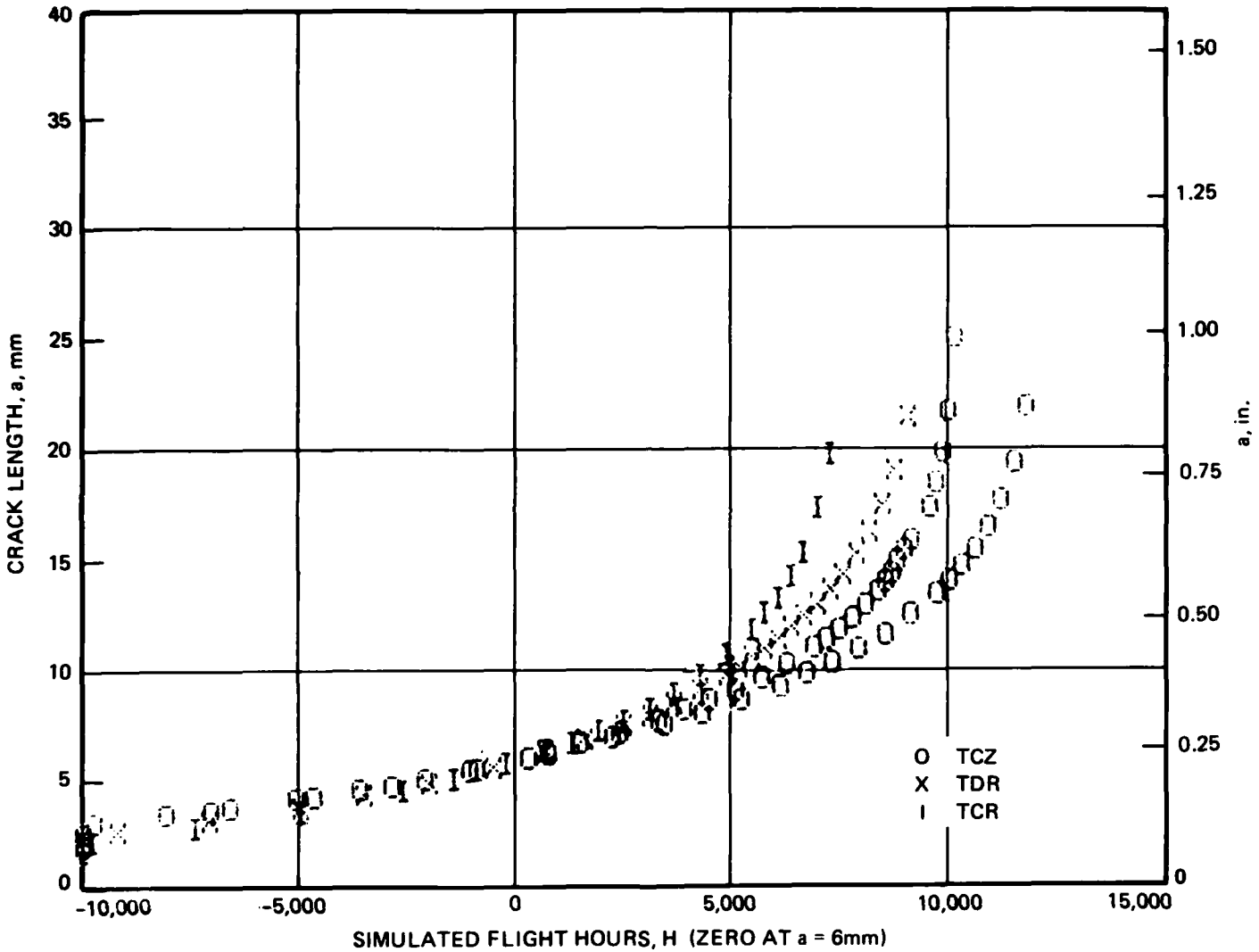

FIGURE D-2. 2024-T851, 145 MPa

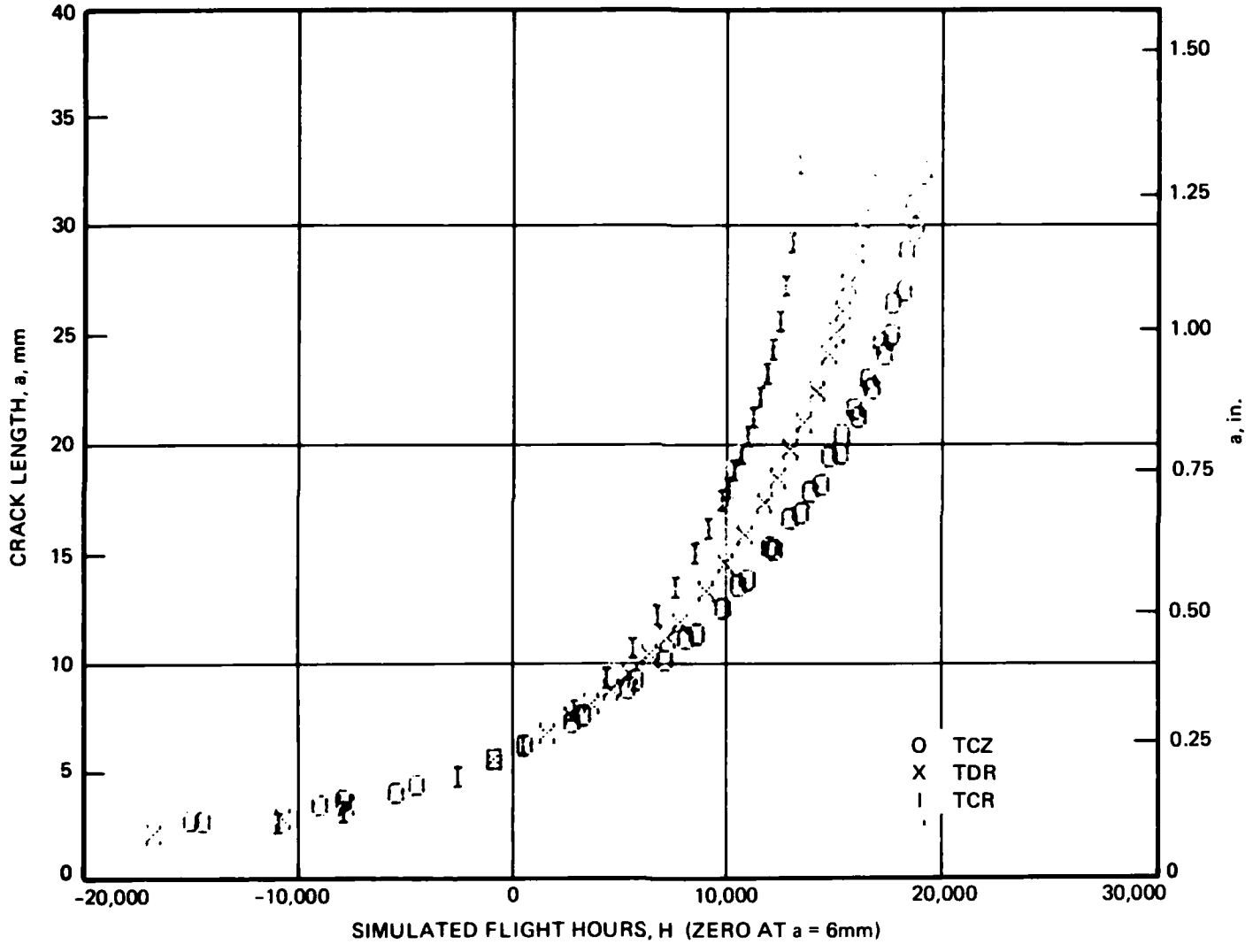

FIGURE D-3. 7050-T73651

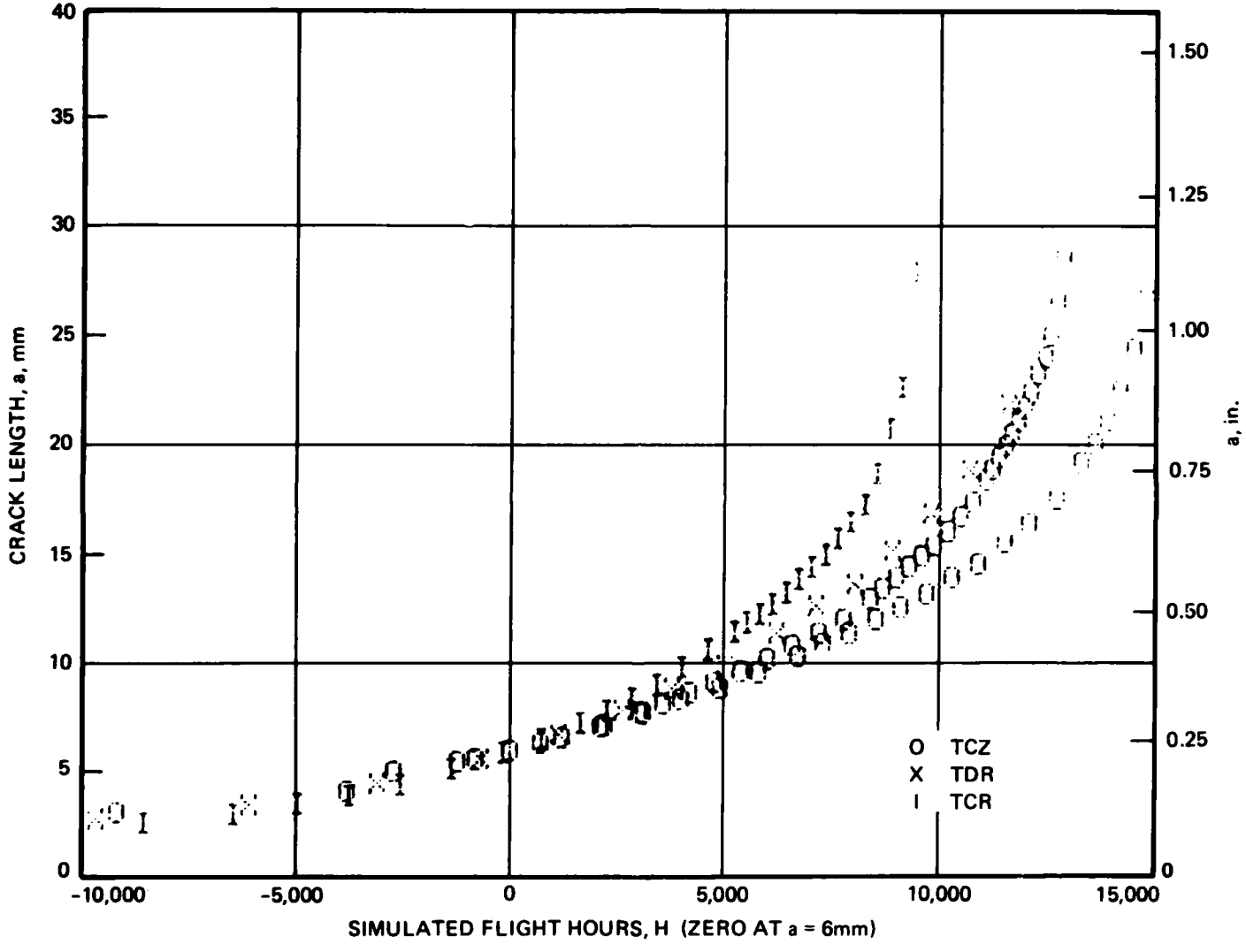

FIGURE D-4. 7075-T651, 145 MPa

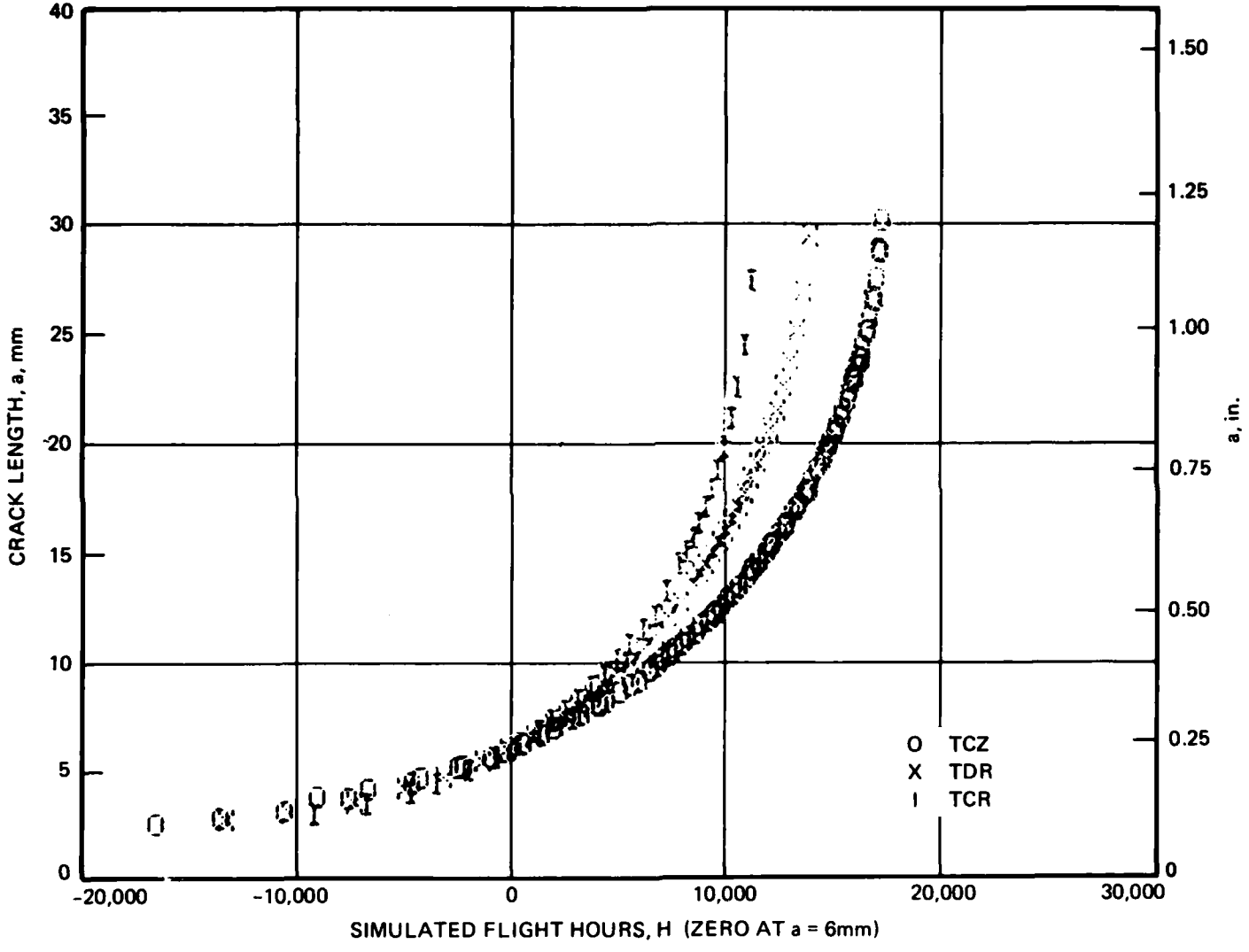

FIGURE D-5. 7075-T7351, 145 MPa

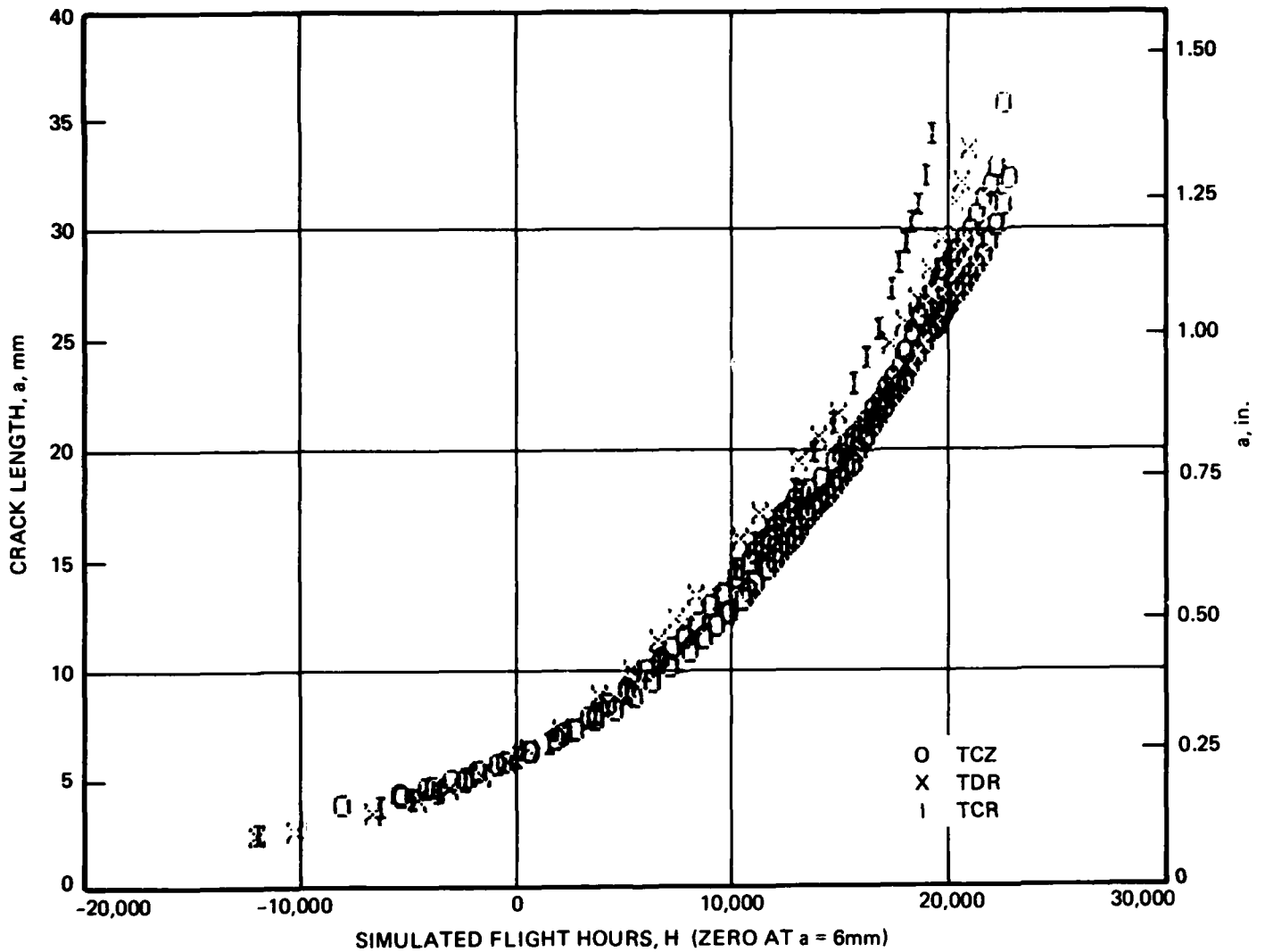

FIGURE D-6. 7475-T651, 145 MPa

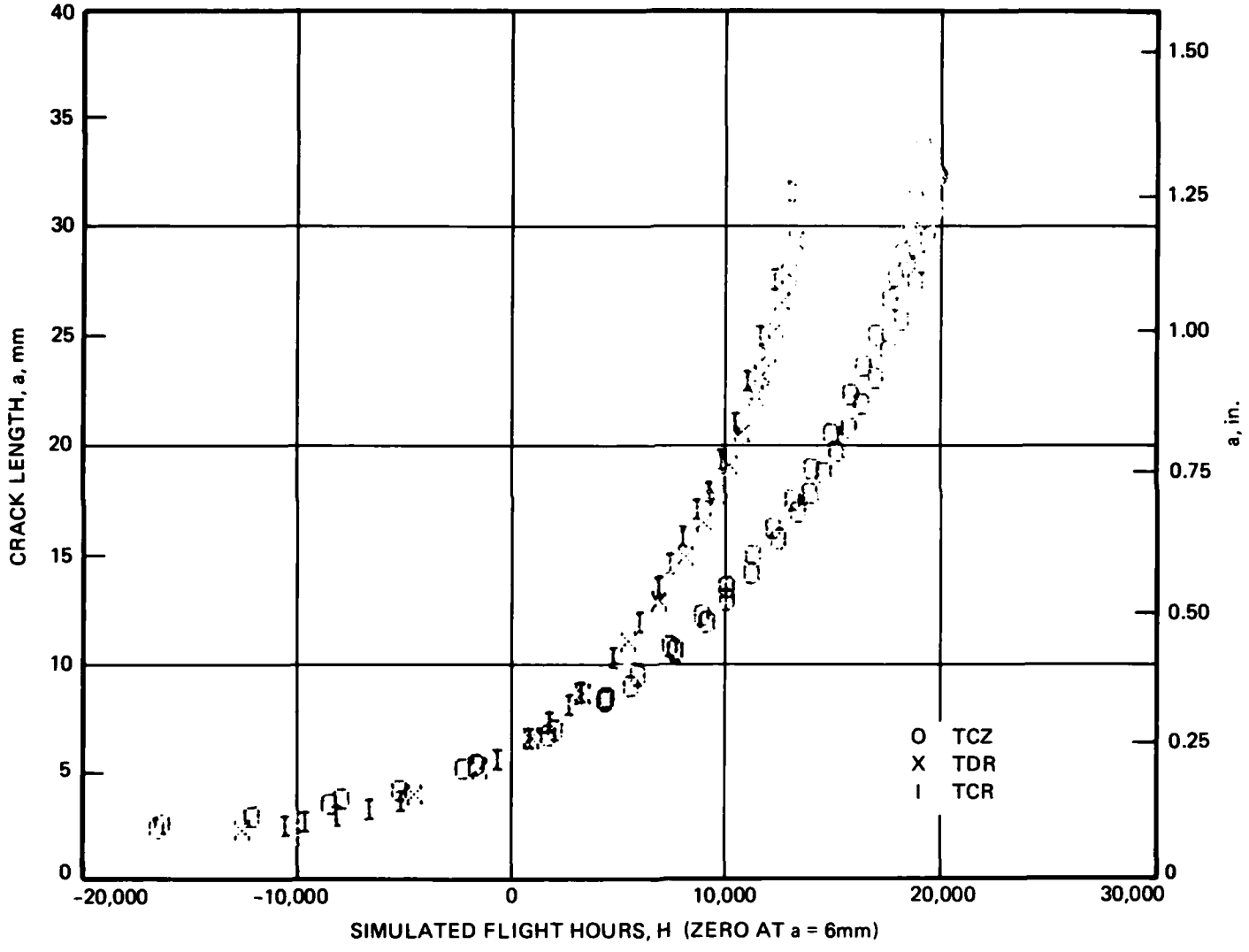

FIGURE D-7. 7475-T7351, 145 MPa

APPENDIX E

SPECTRUM CRACK GROWTH RATE VERSUS MAXIMUM PEAK STRESS INTENSITY FOR RACETRACK-MODIFIED TD SPECTRUM (TDR), da/dH VERSUS K_{hmax}

1. The scales for both axes are identical on each graph.
2. For comparison the results for the TD spectrum at 145 MPa are also shown.
3. Two specimens of each material were tested under the TD spectrum and one specimen of each material was tested under the TDR spectrum. The tests for the TDR spectrum were started at a shorter crack length than for the TD spectrum, therefore spectrum crack growth for lower maximum peak stress intensities was obtained. Also one test for 2024-T351 was started at this shorter crack length.
4. See Appendix C, Paragraphs 3 and 4 for other notes on testing and presentation.

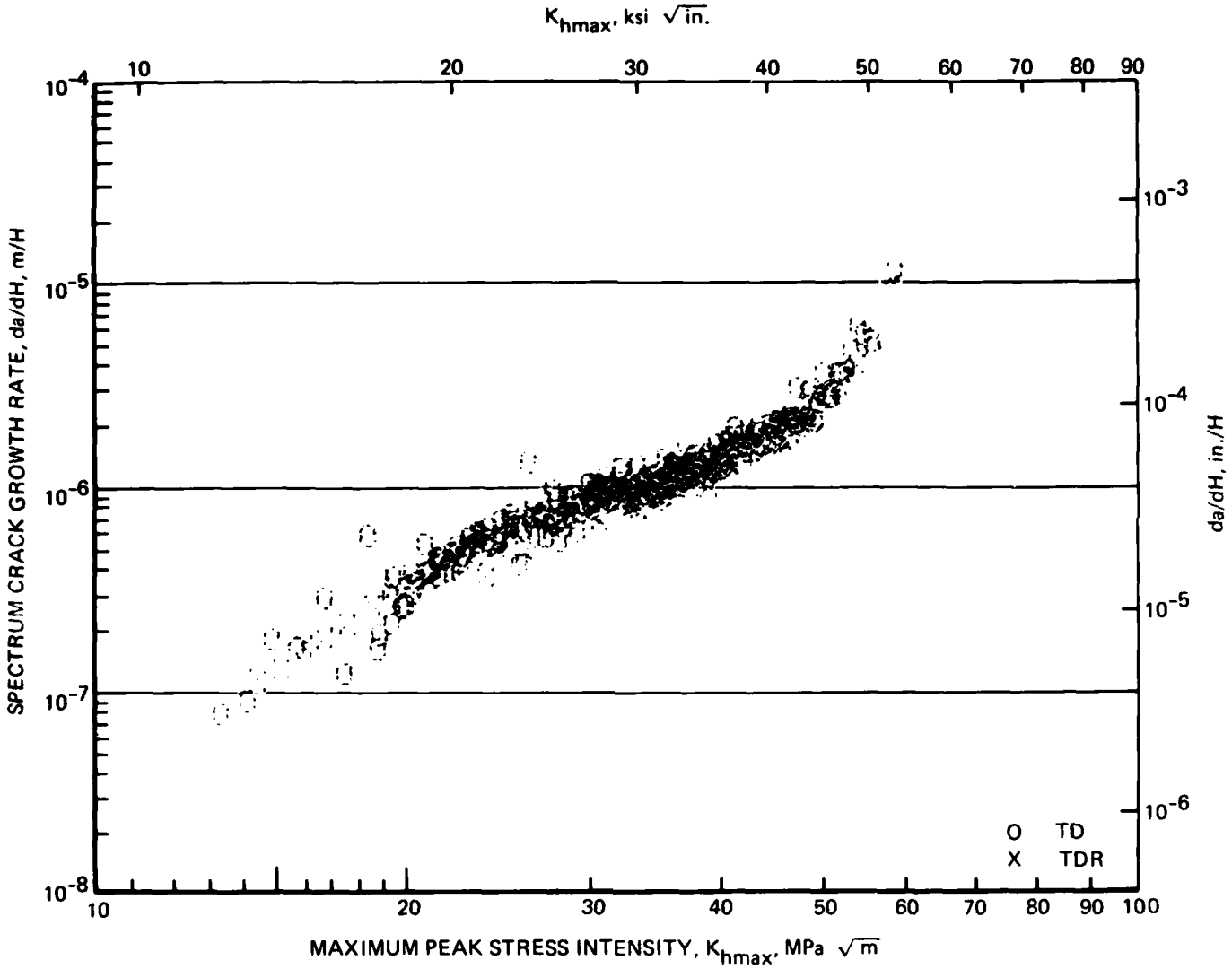

FIGURE E-1. 2024-T351, σ_{hmax} = 145 MPa

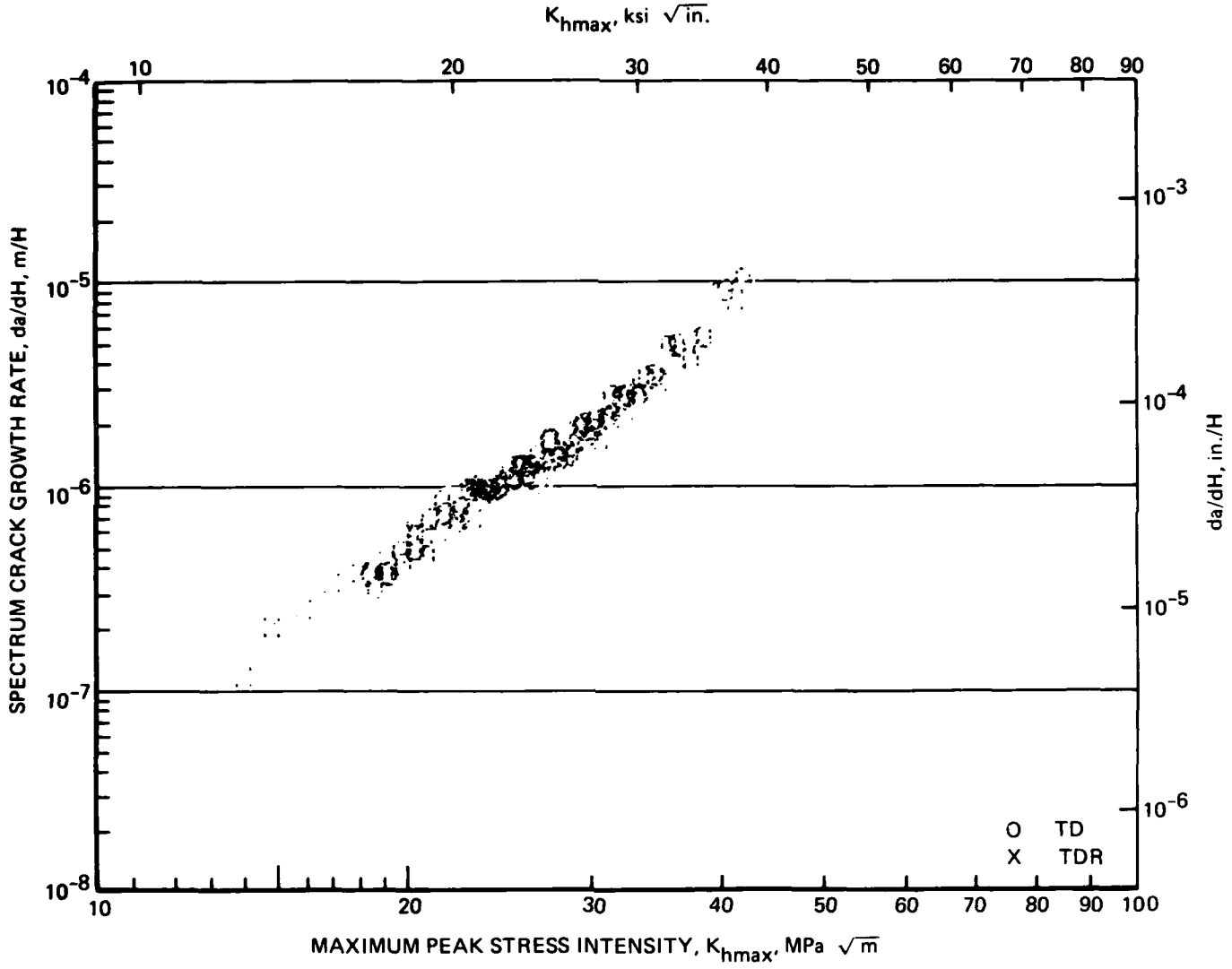

FIGURE E-2. 2024-T851, σ_{hmax} = 145 MPa

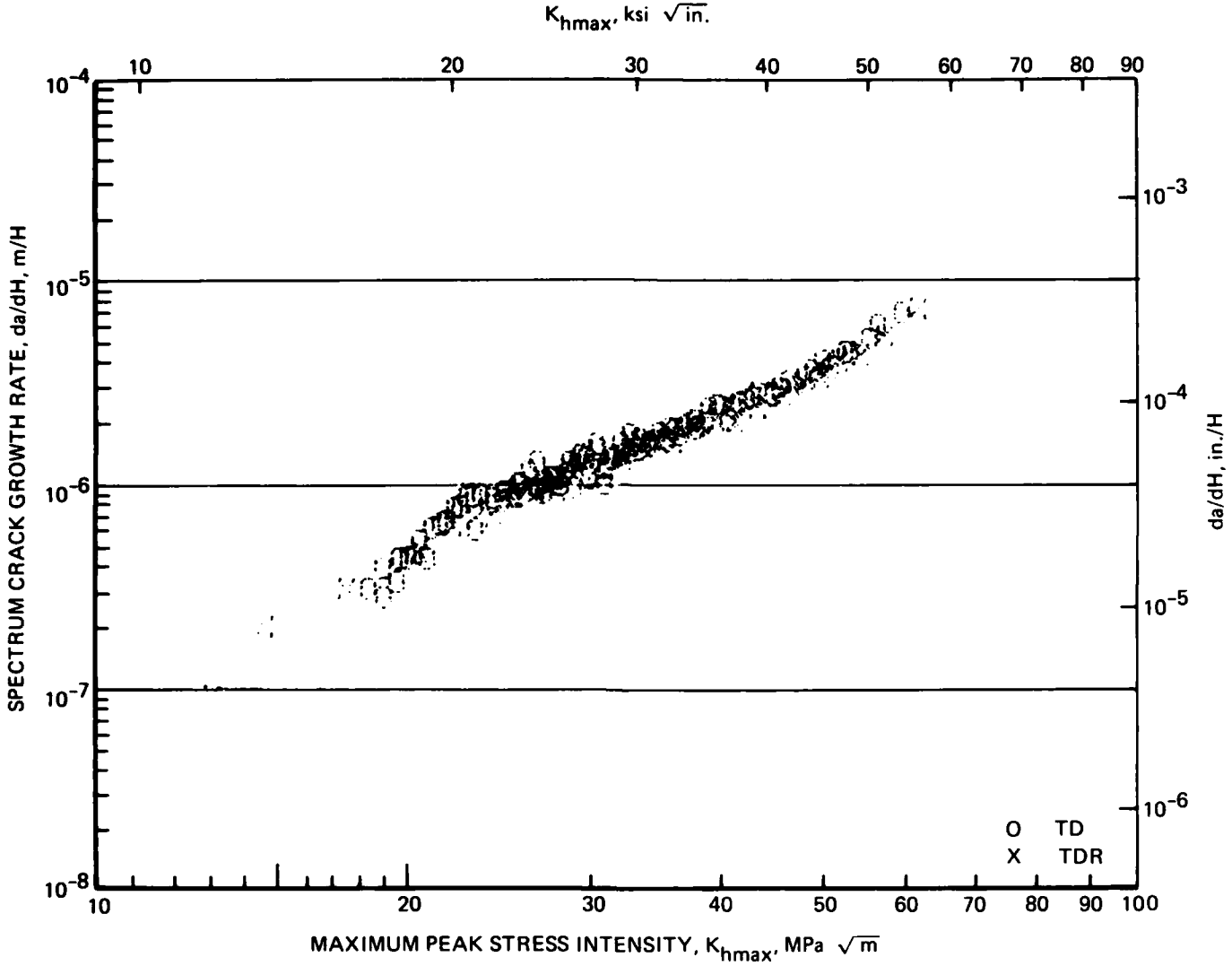

FIGURE E-3. 7050-T73651, σ_{hmax} = 145 MPa

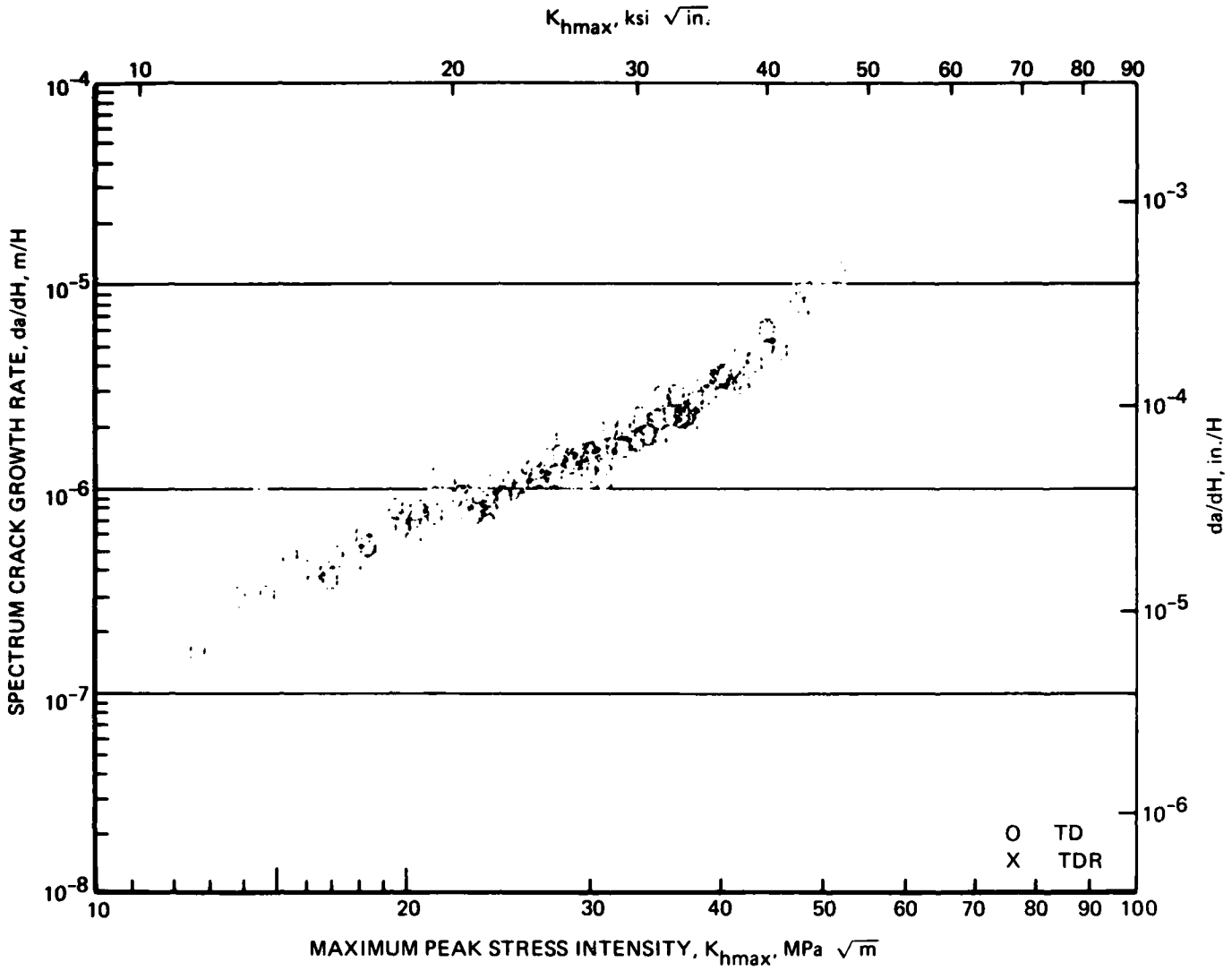

FIGURE E-4. 7075-T651, σ_{hmax} = 145 MPa

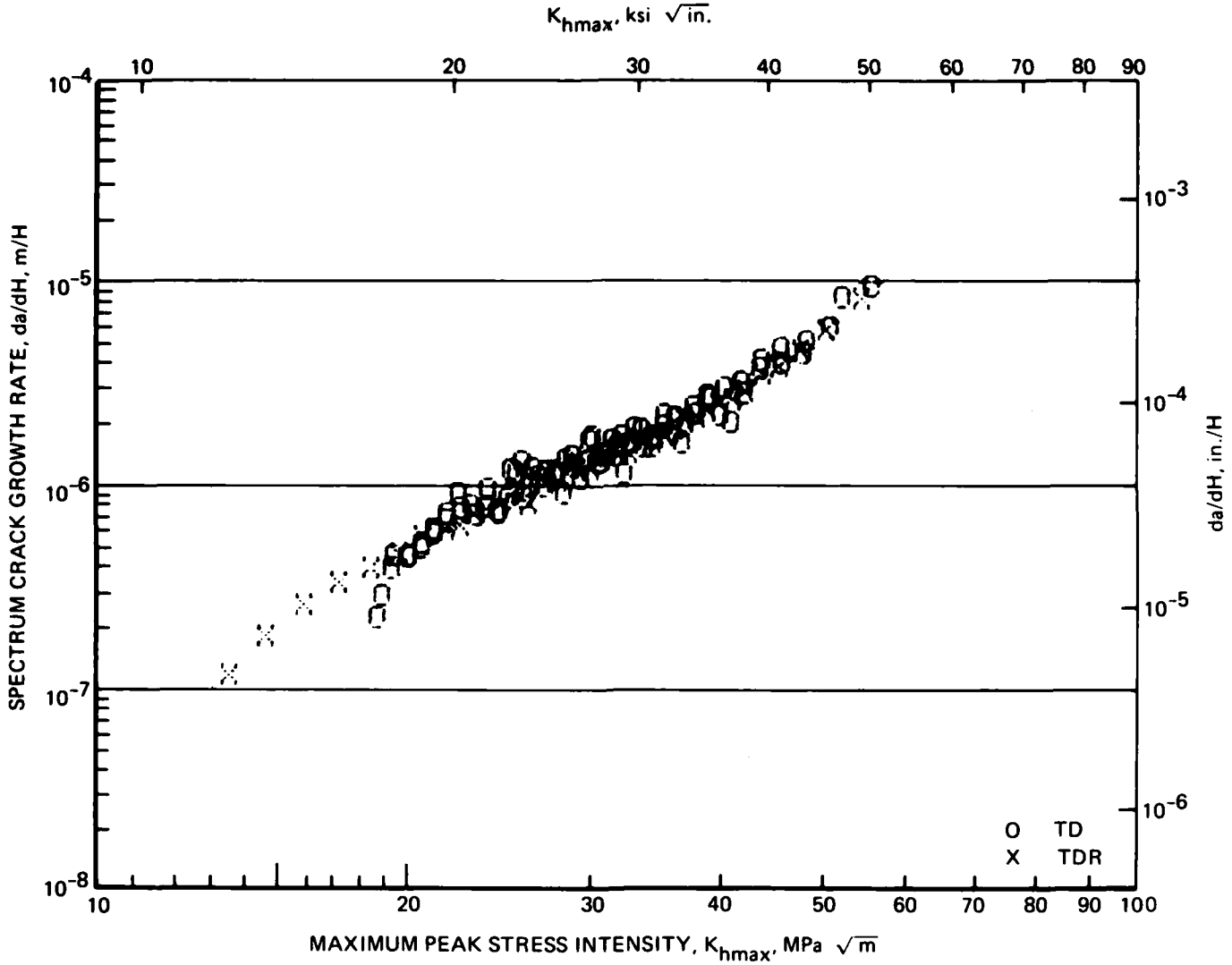

FIGURE E-5. 7075-T7351, σ_{hmax} = 145 MPa

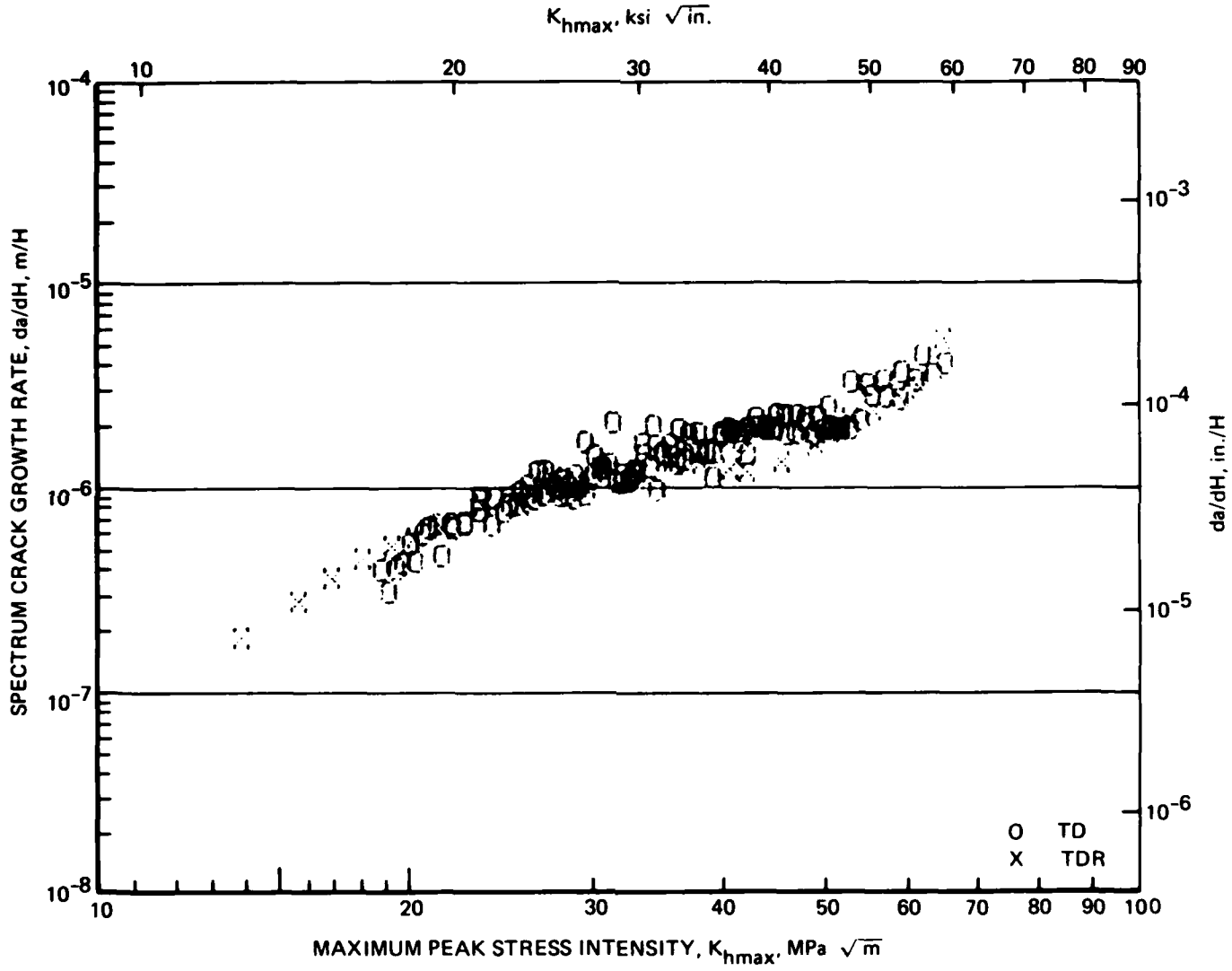

FIGURE E-6. 7475-T651, σ_{hmax} = 145 MPa

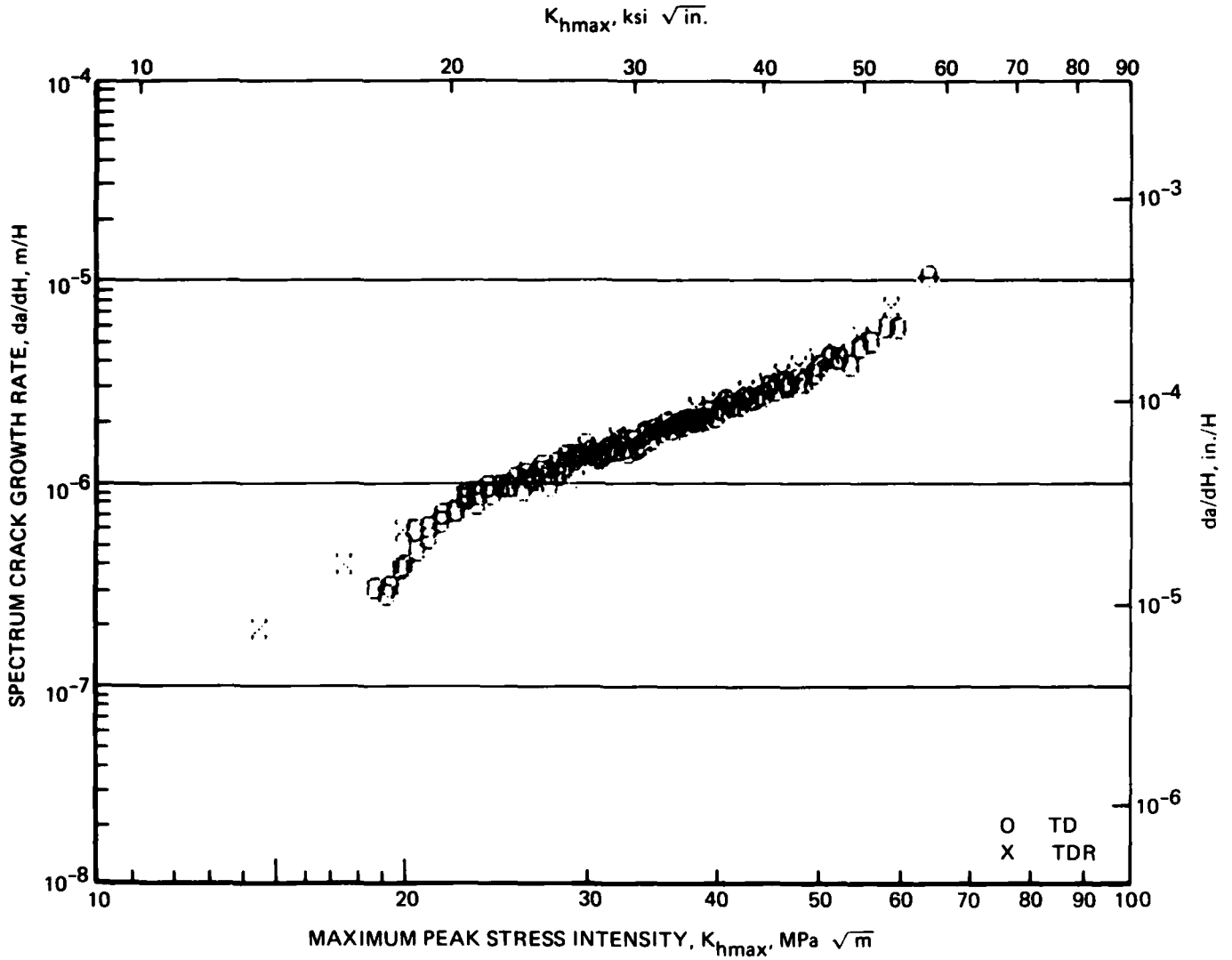

FIGURE E-7. 7474-T7351, σ_{hmax} = 145 MPa

APPENDIX F

SPECTRUM CRACK GROWTH RATE VERSUS MAXIMUM PEAK STRESS INTENSITY FOR RACETRACK-MODIFIED TC SPECTRA (TCR), da/dH VERSUS K_{hmax}

1. The scales for both axes are identical on each graph.
2. For comparison the TC spectrum results at 145 MPa are also presented.
3. Two specimens each were tested under the TC spectrum and one specimen of each material was tested under the TCR spectrum. The tests for the TCR spectrum were started at a shorter crack length than for the TC spectrum, therefore spectrum crack growth for lower maximum peak stress intensities was obtained.
4. See Appendix C, Paragraphs 3 and 4 for other notes on testing and presentation.

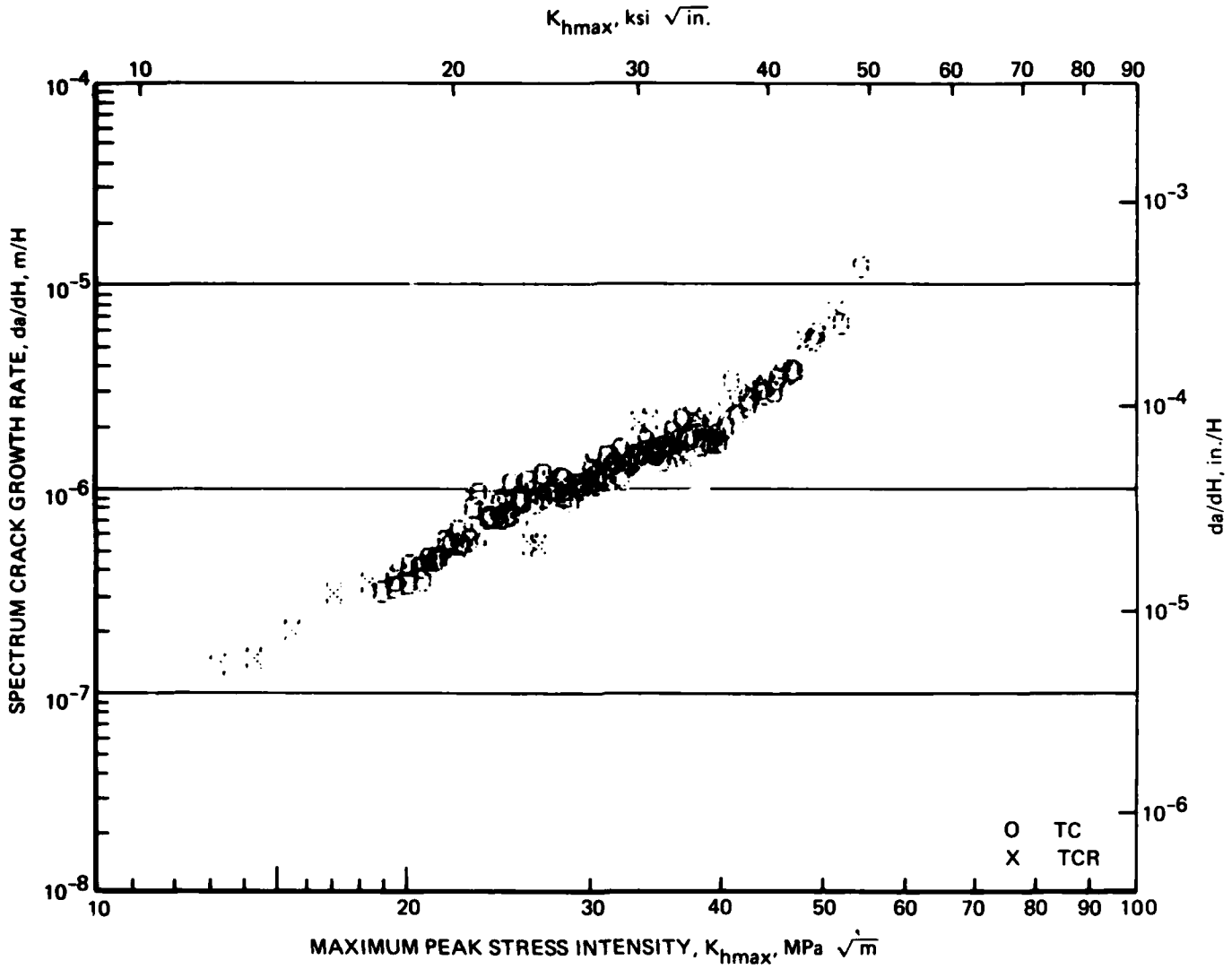

FIGURE F-1. 2024-T351, σ_{hmax} = 145 MPa

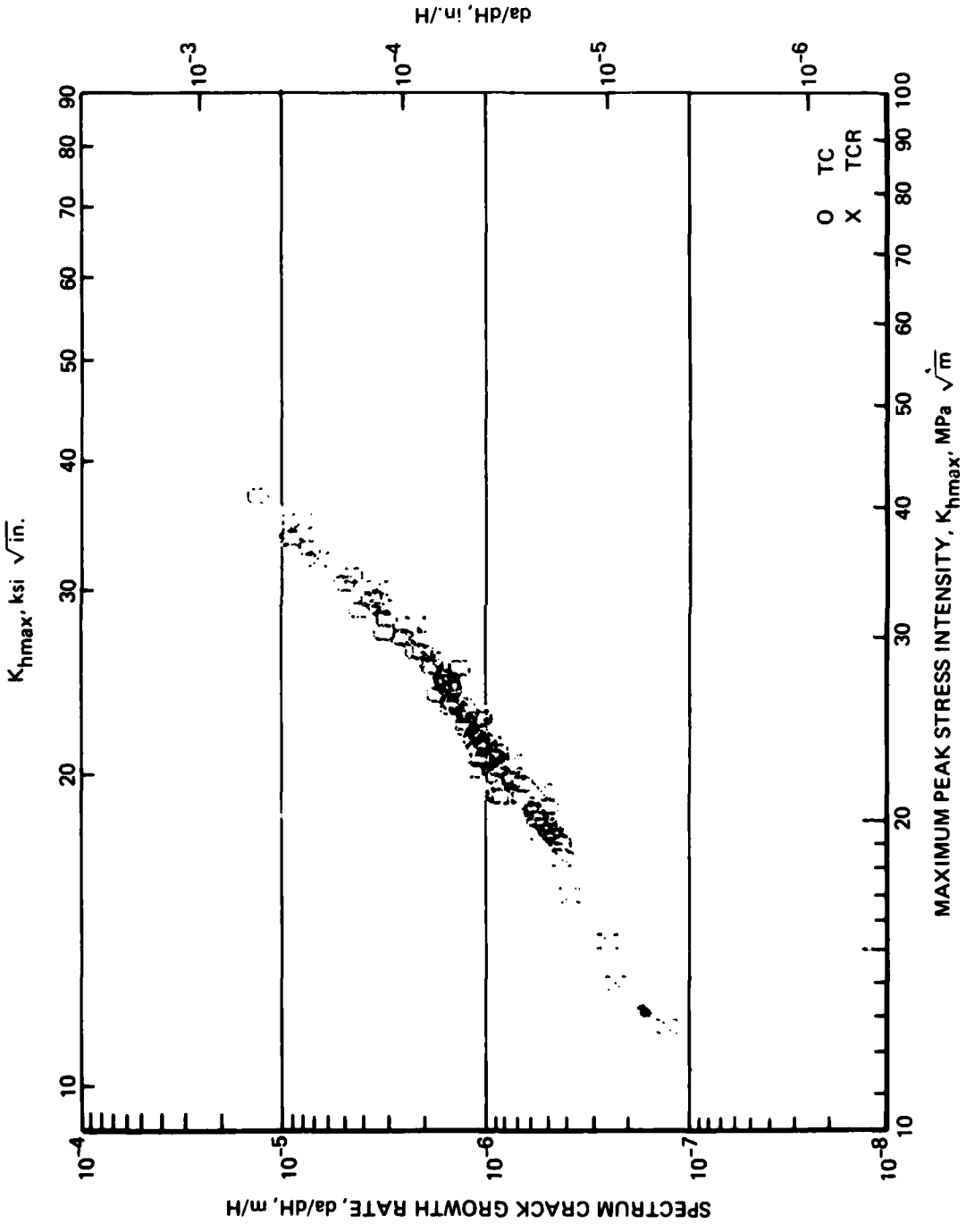

FIGURE F-2. 2024-T851, σ_{hmax} = 145 MPa

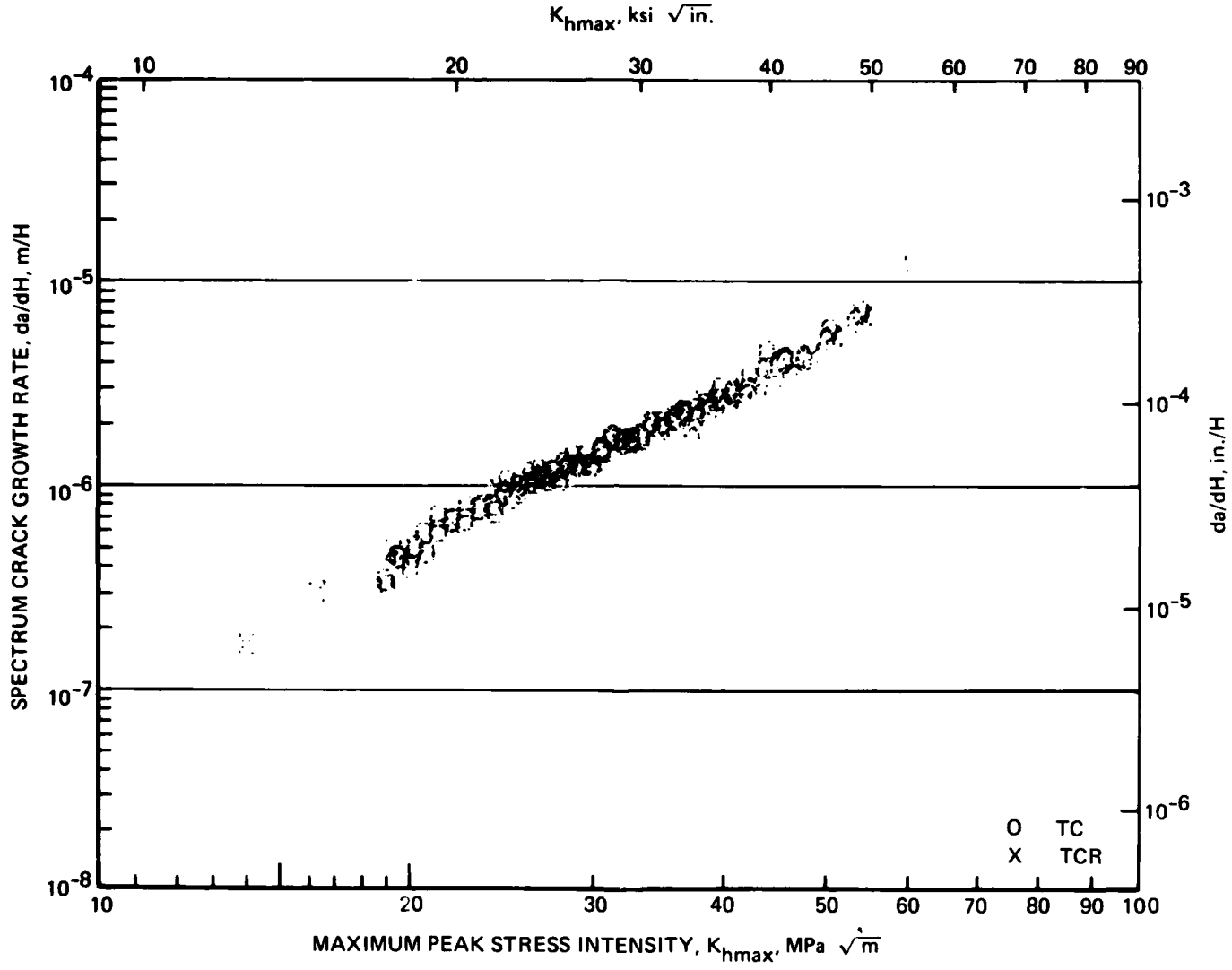

FIGURE F-3. 7050-T73651, σ_{hmax} = 145 MPa

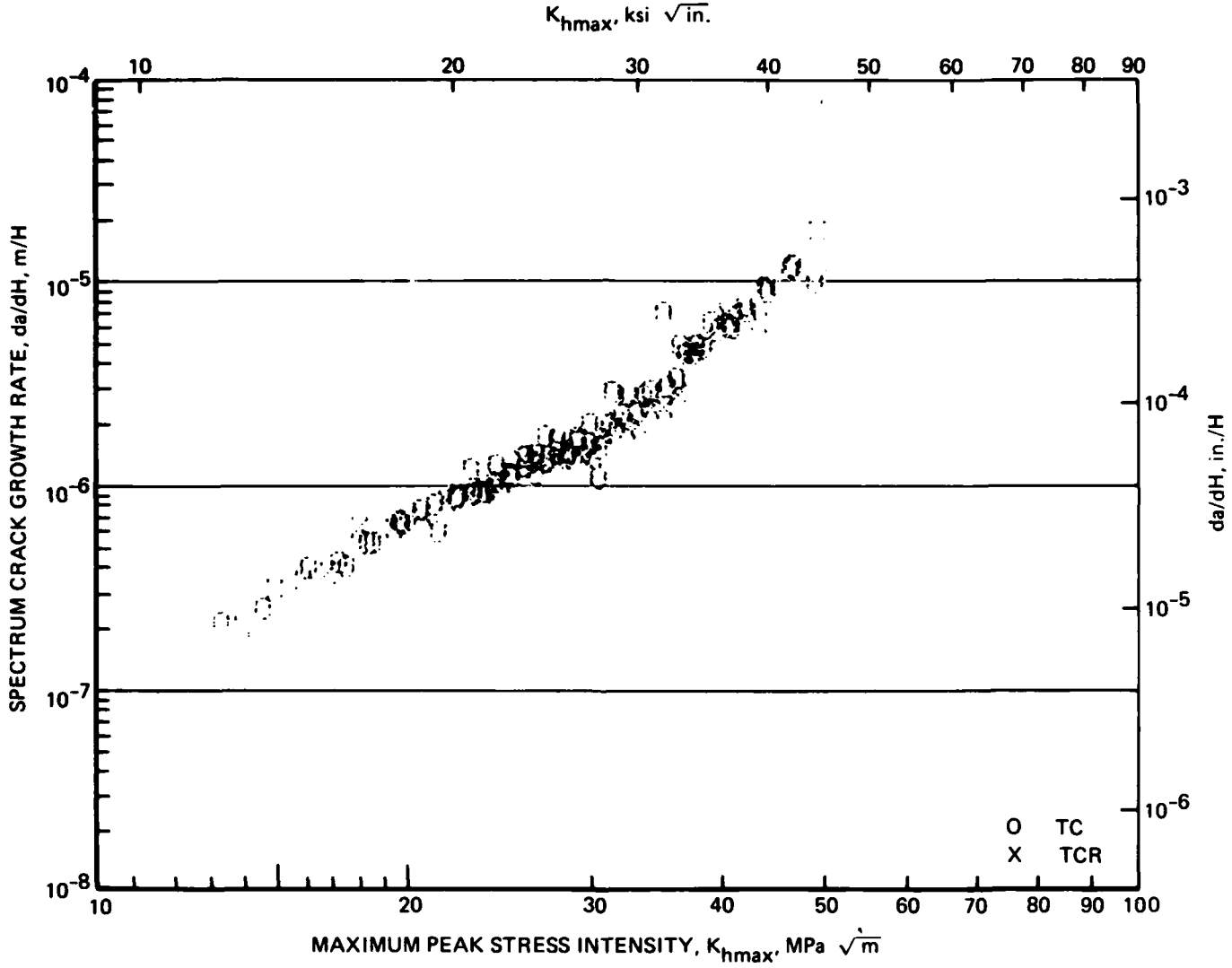

FIGURE F-4. 7075-T651, σ_{hmax} = 145 MPa

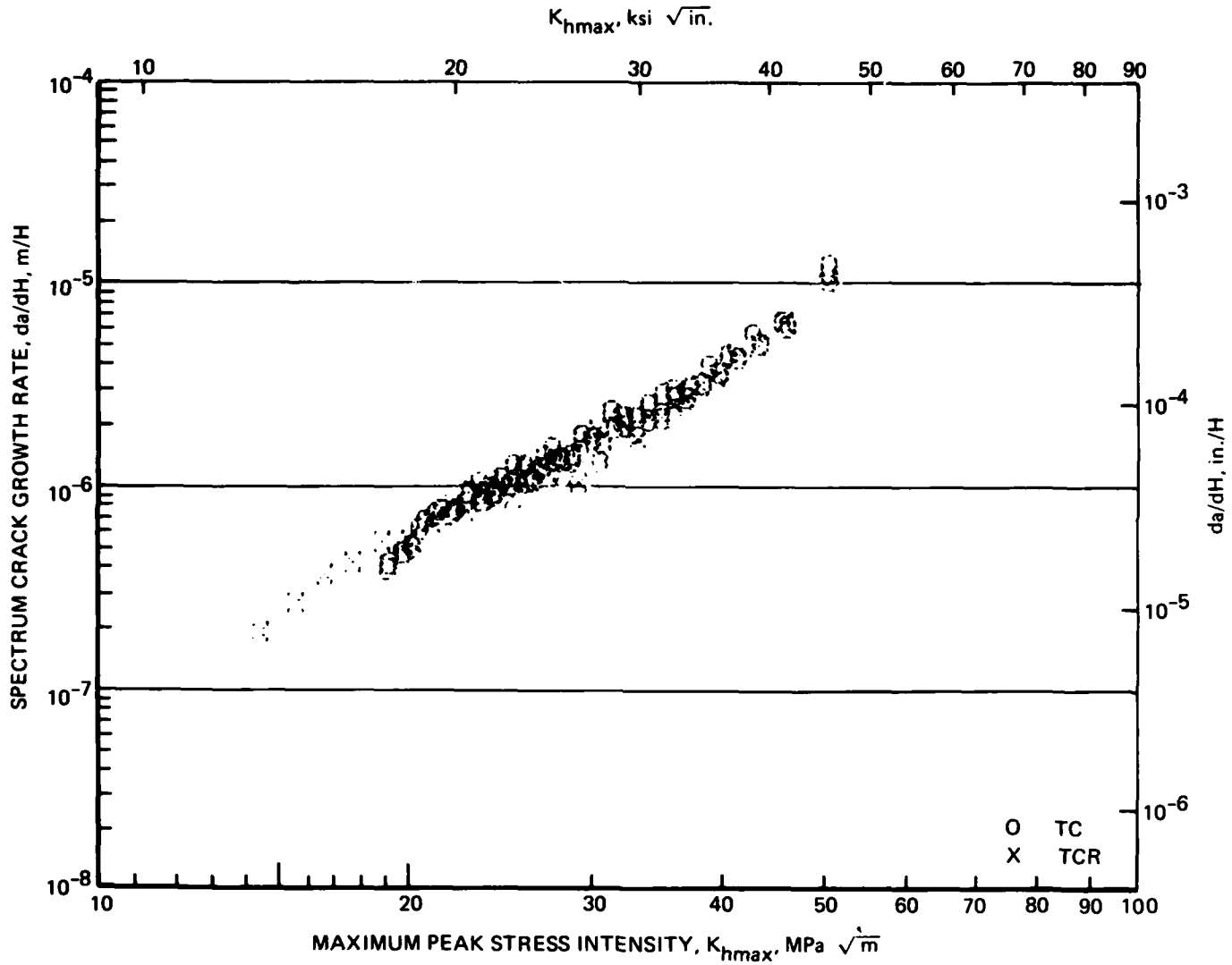

FIGURE F-5. 7075-T7351, σ_{hmax} = 145 MPa

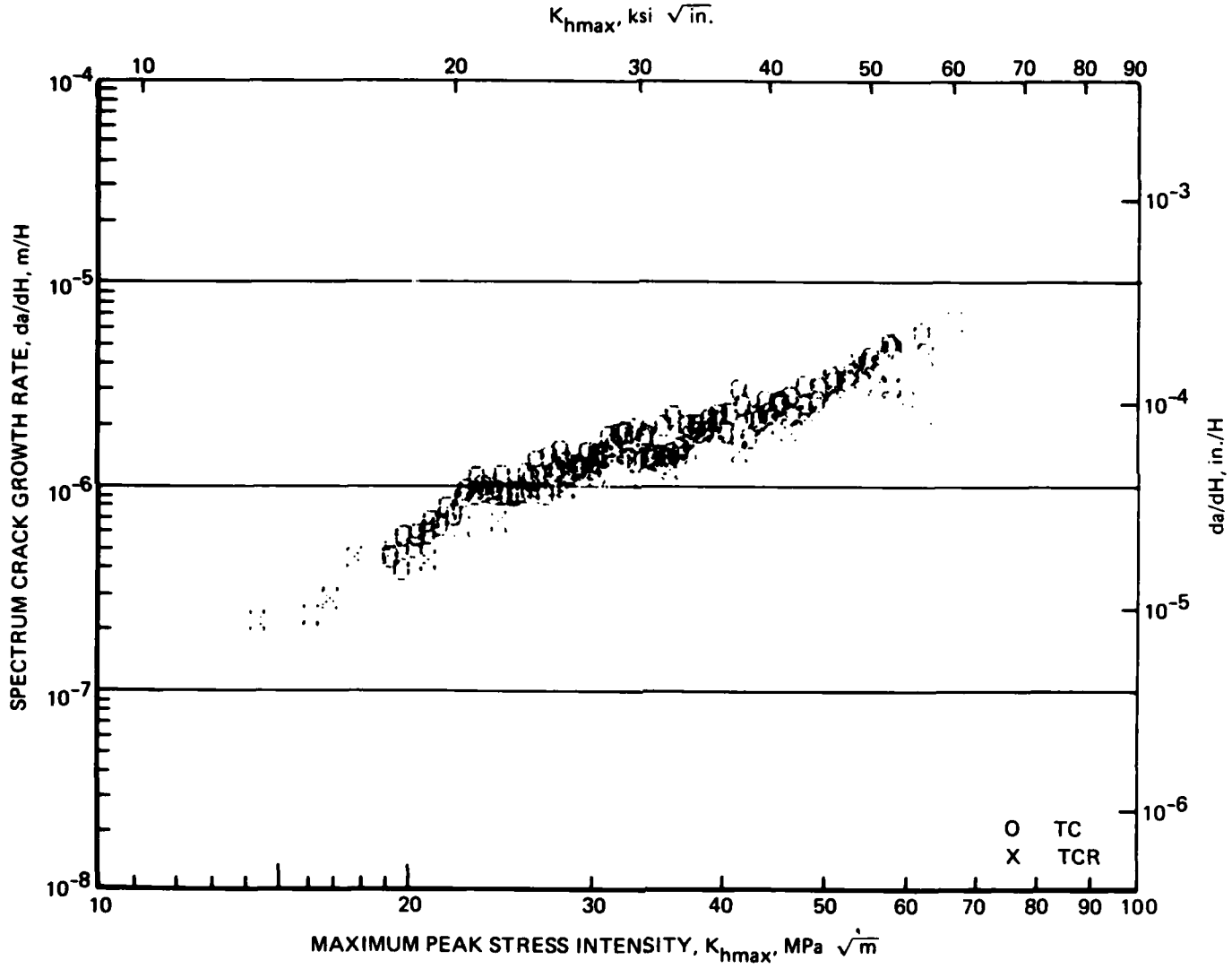

FIGURE F-6. 7475-T651, σ_{hmax} = 145 MPa

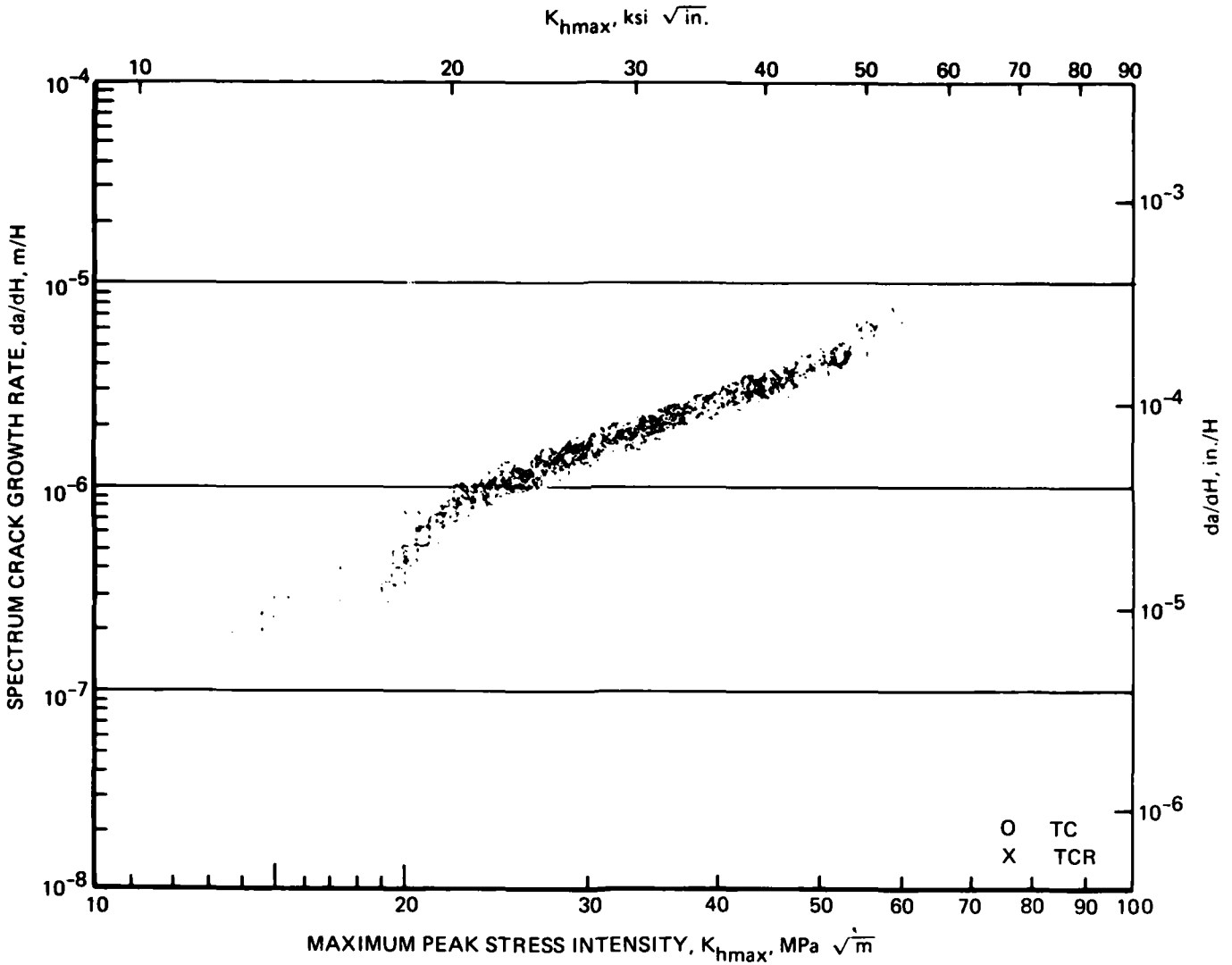

FIGURE F-7. 7475-T7351, σ_{hmax} = 145 MPa

APPENDIX G

SPECTRUM CRACK GROWTH RATE VERSUS MAXIMUM PEAK STRESS INTENSITY FOR TCZ SPECTRUM, da/dH VERSUS K_{hmax}

1. The scales for both axes are identical on each graph.
2. For comparison the results for the TC spectrum at 145 MPa are also shown.
3. Two specimens of each material were tested under the TC spectrum and two specimens of each material were tested under the TCZ spectrum. The tests for the TCZ spectrum were started at a shorter crack length than for the TC spectrum, therefore spectrum crack growth for lower maximum peak stress intensities was obtained.
4. See Appendix C, Paragraphs 3 and 4 for other notes on testing and presentation.

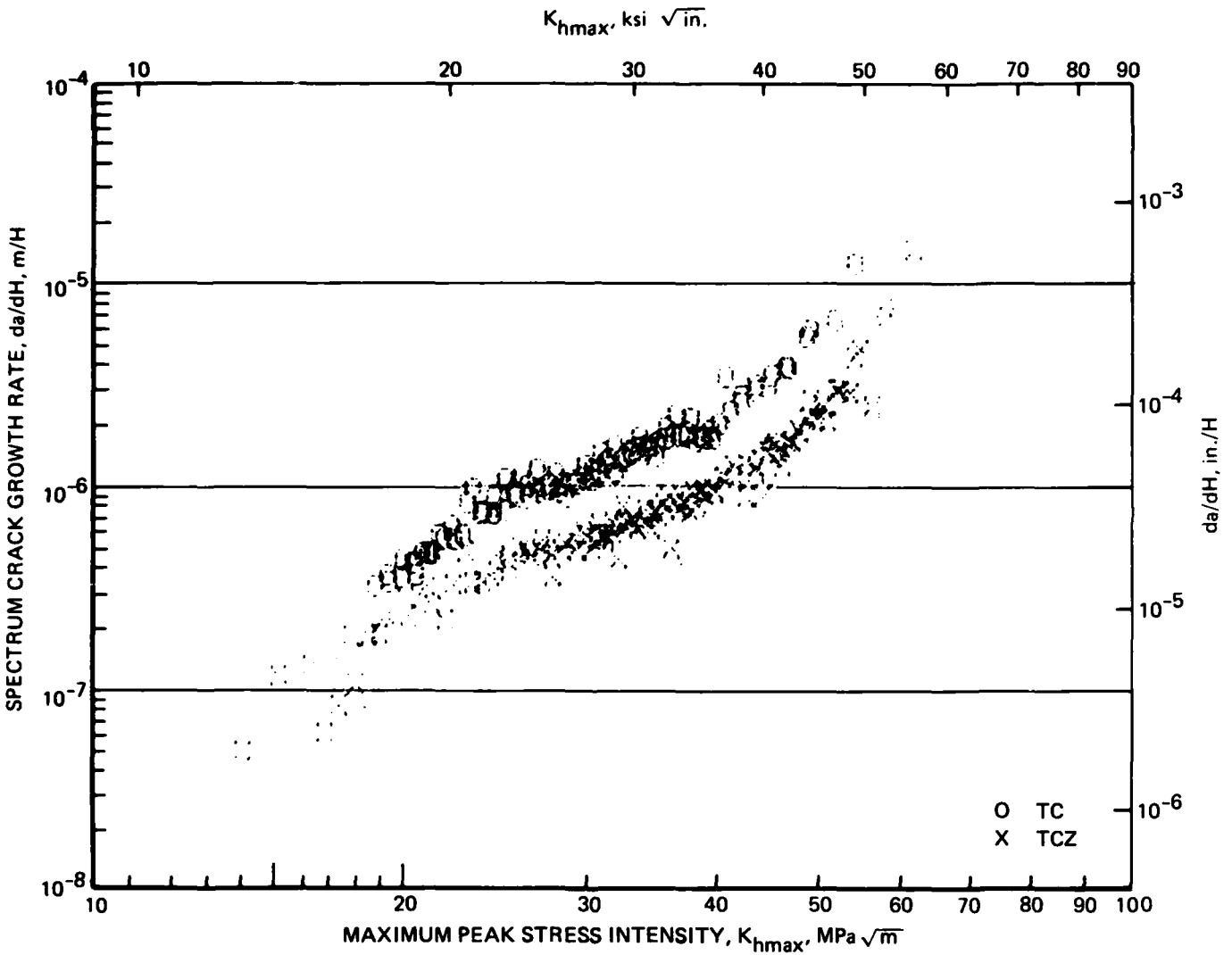

FIGURE G-1. 2024-T351, σ_{hmax} = 145 MPa

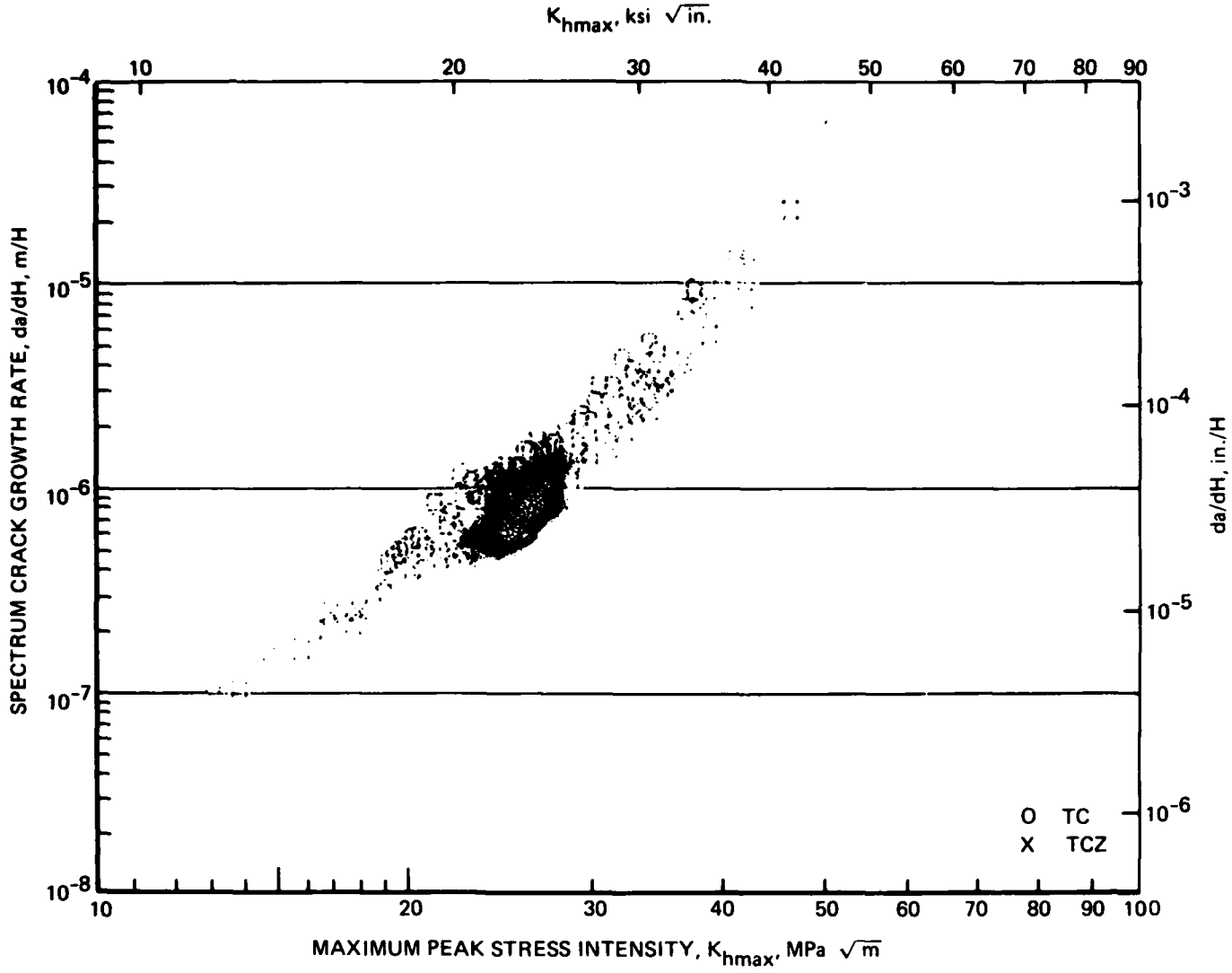

FIGURE G-2. 2024-T851, σ_{hmax} = 145 MPa

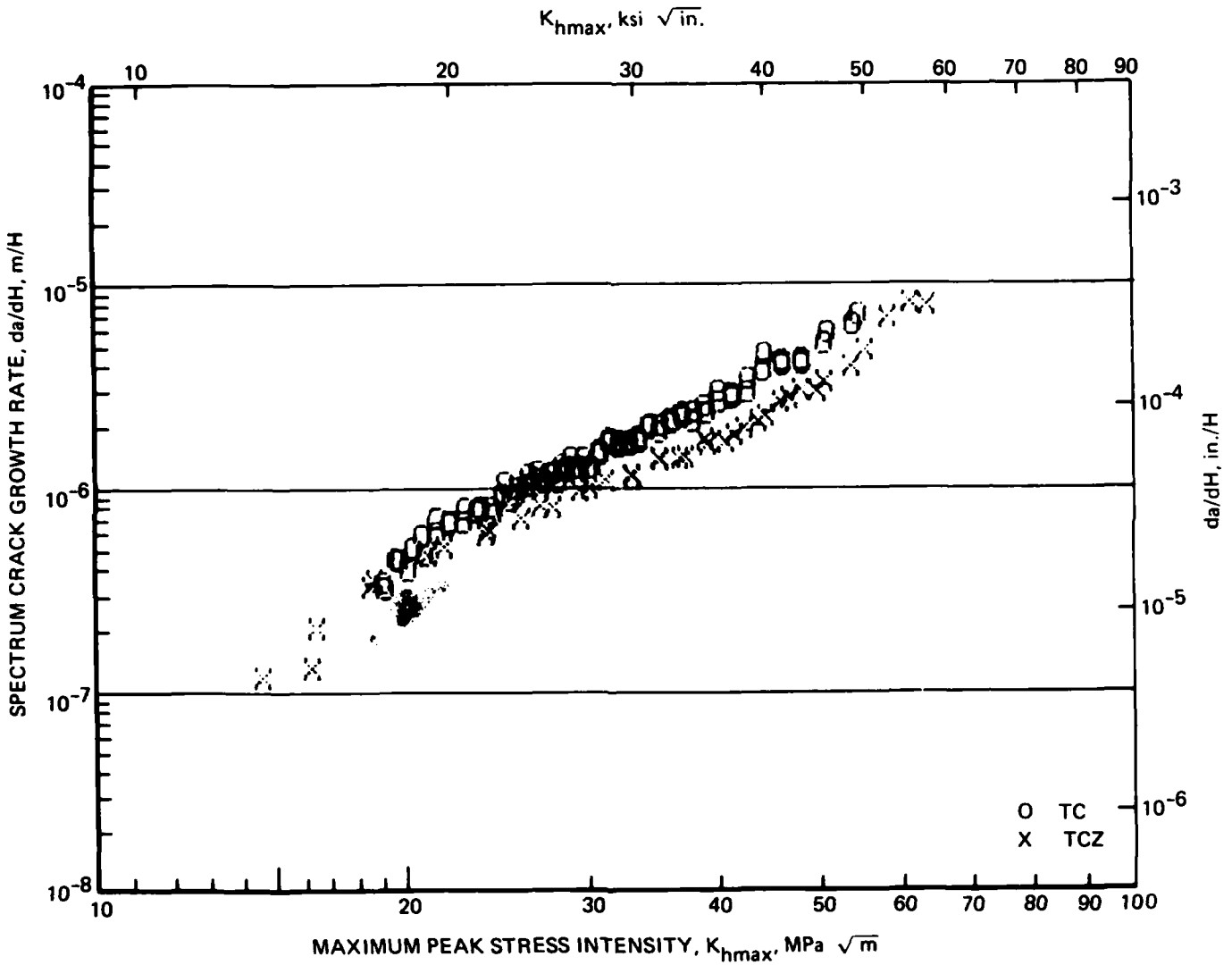

FIGURE G-3. 7050-T73651, σ_{hmax} = 145 MPa

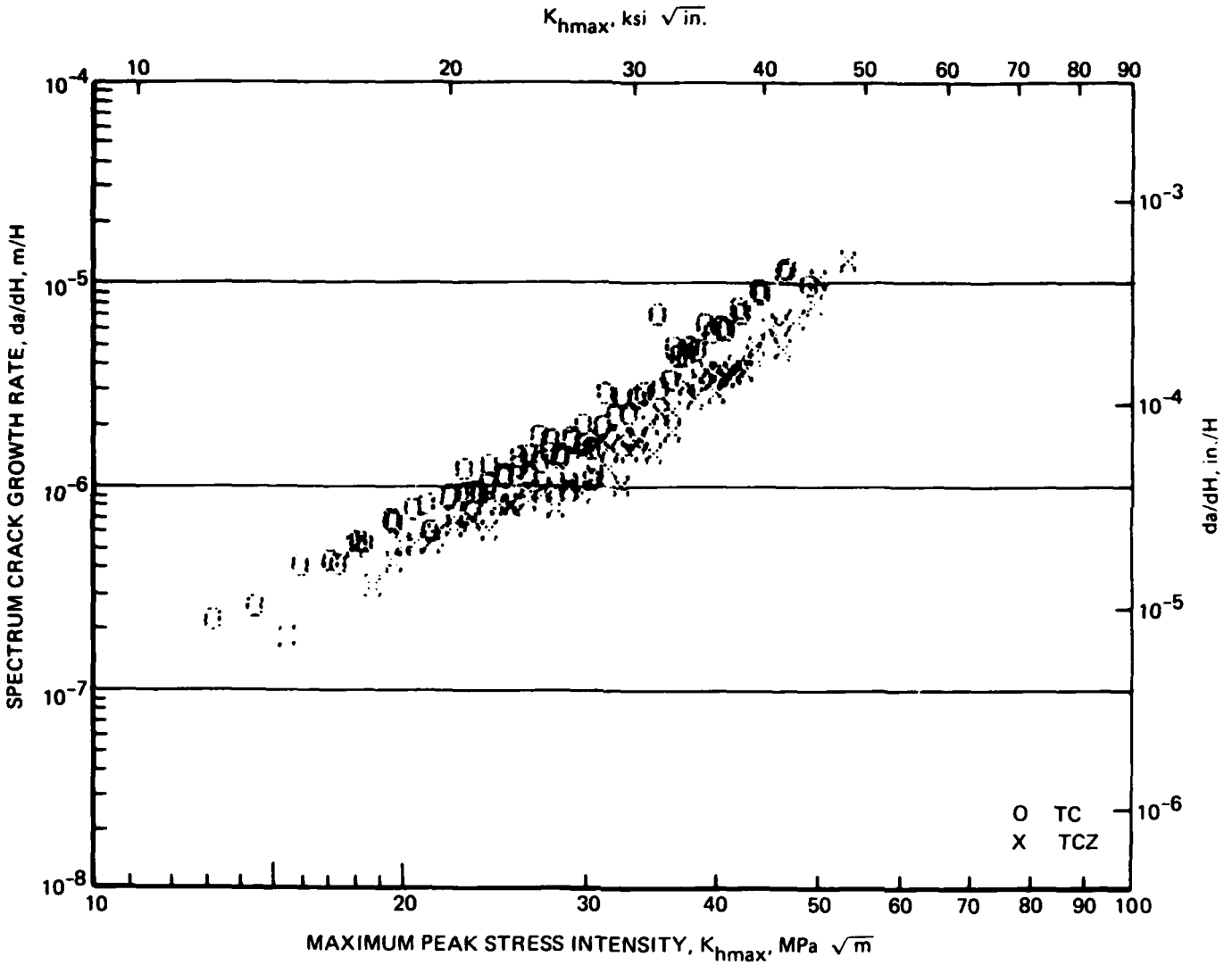

FIGURE G-4. 7075-T651, σ_{hmax} = 145 MPa

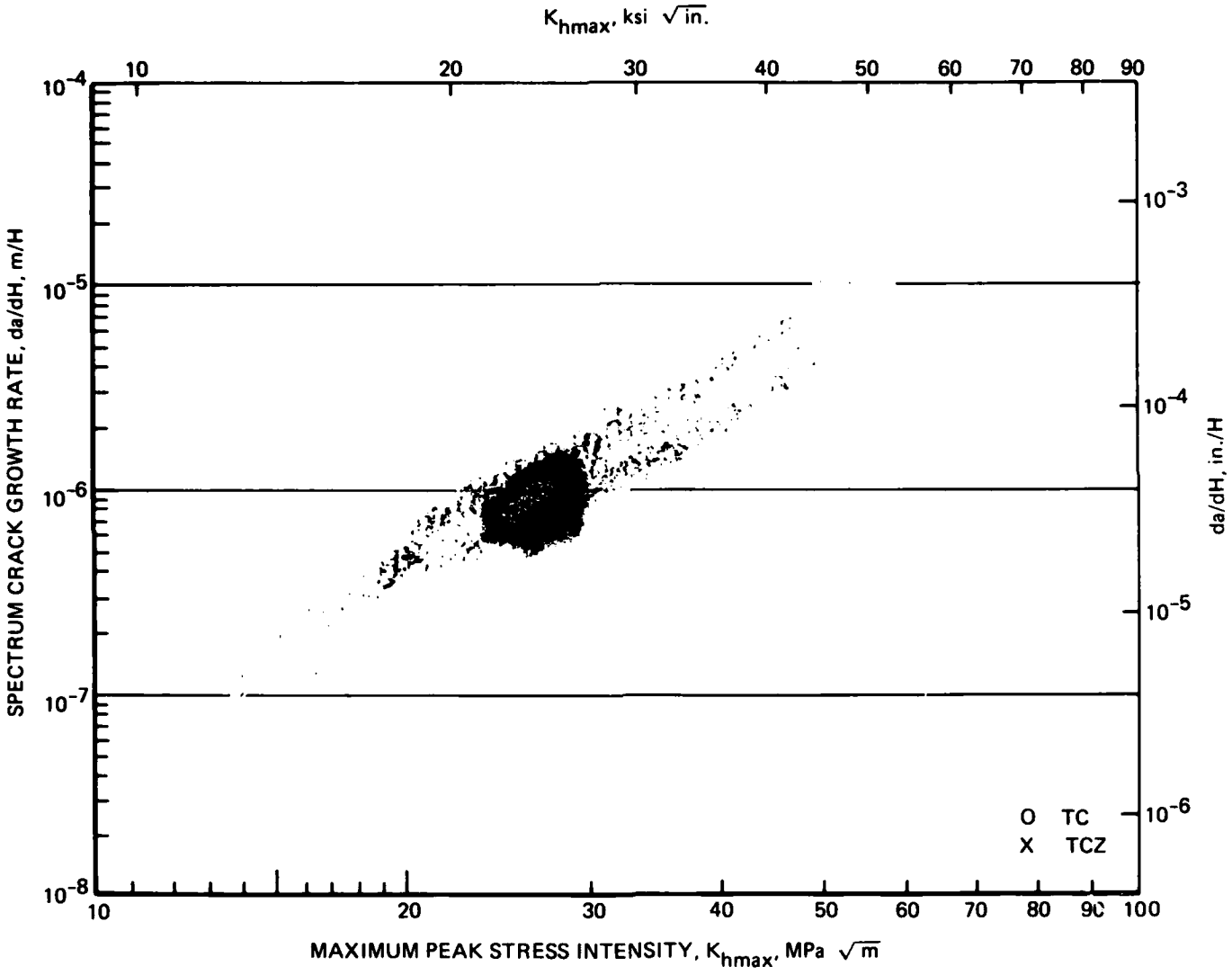

FIGURE G-5. 7075-T7351, σ_{hmax} = 145 MPa

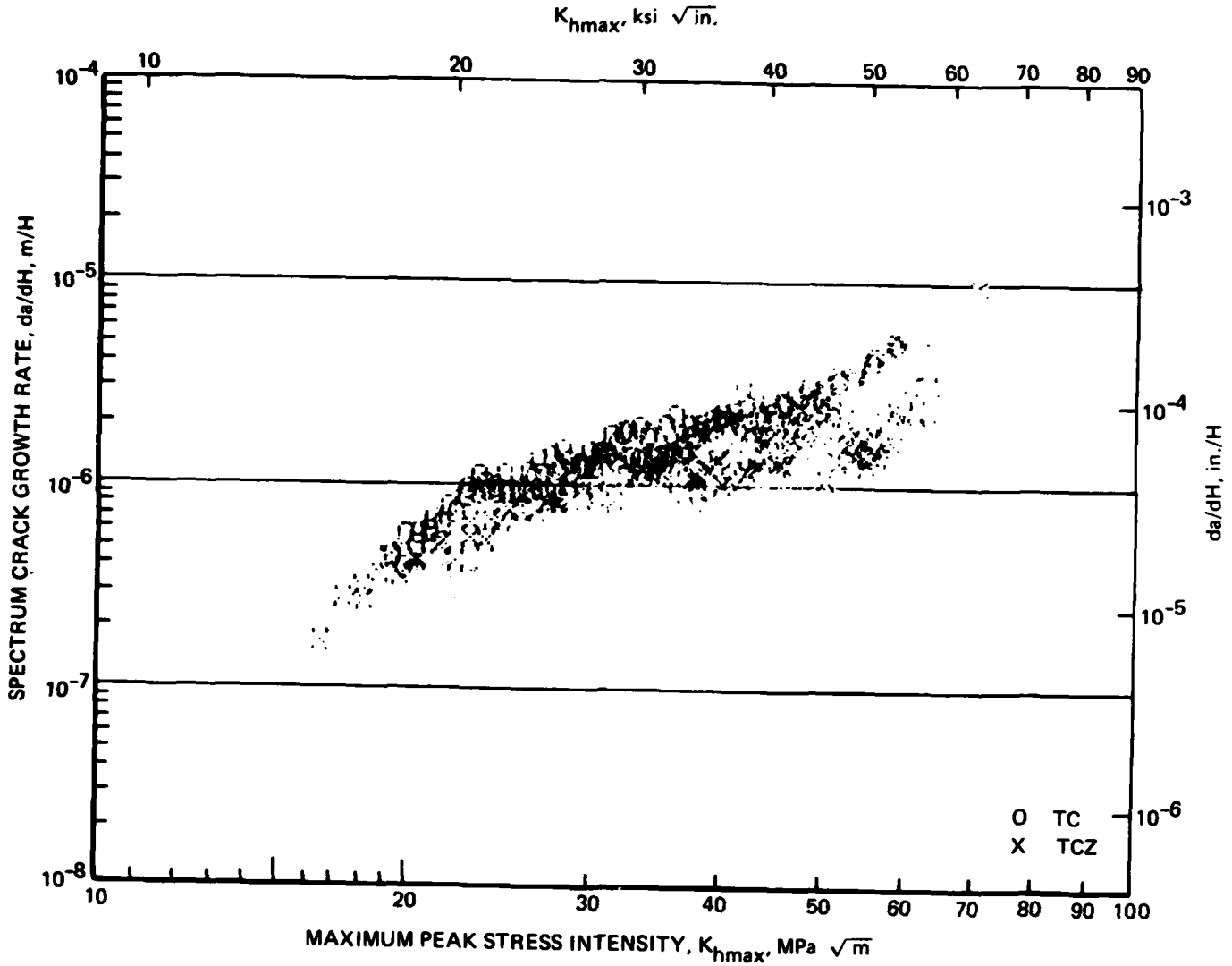

FIGURE G-6. 7475-T651, σ_{hmax} = 145 MPa

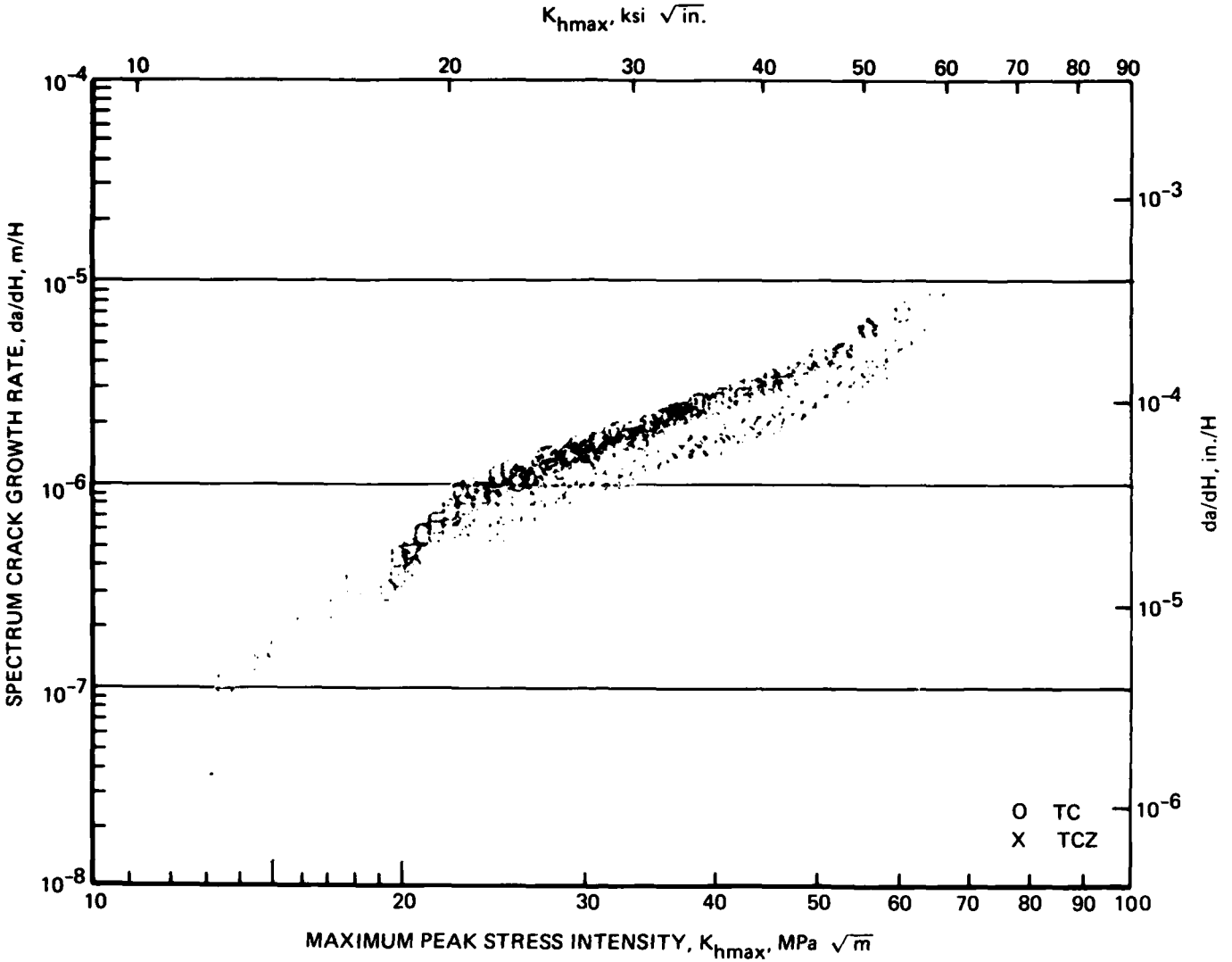

FIGURE G-7. 7475-T7351, σ_{hmax} = 145 MPa

APPENDIX H

SUPPLEMENTARY DATA FOR MATERIALS EVALUATED IN PHASE II

The test procedure was modified for Phase II testing, resulting in data for which no comparisons exist for the materials evaluated in Phase I. These data are presented herein.

TABLE H-1. SPECTRUM FATIGUE LIVES FOR MATERIALS EVALUATION IN PHASE II, FOR "a" FROM 6MM (0.24 IN.) TO FAILURE

MAXIMUM PEAK STRESS σ_{hmax}	SIMULATED FLIGHT HOURS, H			
	103MPa (15 ksi)		169 MPa (24.5 ksi)	
SPECTRUM	TD	TC	TD	TC
MATERIAL				
2020-T651	83,910	80,953	6,217	3,636
2324-T39	53,738	42,939	11,862	8,261
7075-T651	27,341	25,268	6,333	4,612

APPENDIX I

ANALYSIS OF THE SIGNIFICANCE OF AN INCREASE IN SPECTRUM LIFE

To determine the significance of an increase in spectrum life, the perspective of the designer was taken. With respect to fatigue, the designer is usually designing to a fixed life and wants to know what increase in design stress a different material will yield, i.e., the increase in life at a particular stress is usually not of direct interest. Therefore the following analysis was performed to determine what increase in design (maximum peak) stress would result from an increase in life determined from tests performed at a single maximum peak stress. Spectrum life results for three materials (2020-T651, 2324-T39, and 7075-T651) at three maximum peak stress levels (103, 145, and 169 MPa) for the same crack length basis (6 mm to failure) were available from the program (Table H-1 and Table 8) for both the TD and TC spectra. With maximum peak stress as the independent variable, a semilog regression (stress linear, life logarithmic) was performed resulting in a best fit line (Figure I-1). This best fit line established a stress-life relationship for a so called "representative baseline material." A second line was drawn shifted to a 50 percent increase in life beyond that of the "representative" aluminum material (Figure I-2). Using a design life of 24,000 flight hours, a maximum peak stress of 125.7 MPa would be the "design stress" (from the best fit line). For this same life the hypothetical material with a 50 percent longer life would have a design stress of 139.0 MPa, an 11 percent increase over that of the "representative baseline material." A similar analysis was performed for unpublished Northrop results for three aluminum alloys at three maximum peak stress levels using a different spectrum and specimen configuration. The result was that a 50 percent increase in life allowed an 11 percent increase in design stress, which added confidence to the relationship established above. This is a convenient number because an increase in stress of 10 percent is typically the minimum necessary to make it worthwhile to consider a material change. No claim is made that this is a universal relationship, but the relationship is more than adequate for the purpose used in this report.

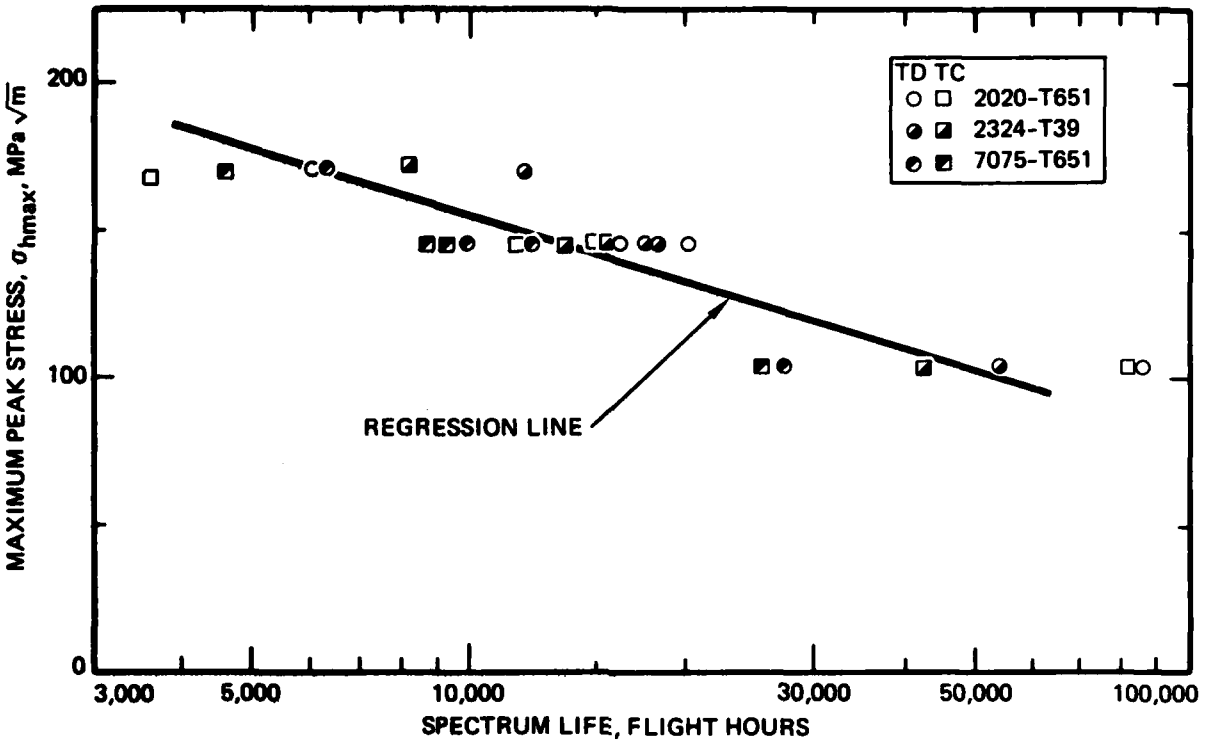

FIGURE I-1. SPECTRUM LIFE VS MAXIMUM PEAK STRESS

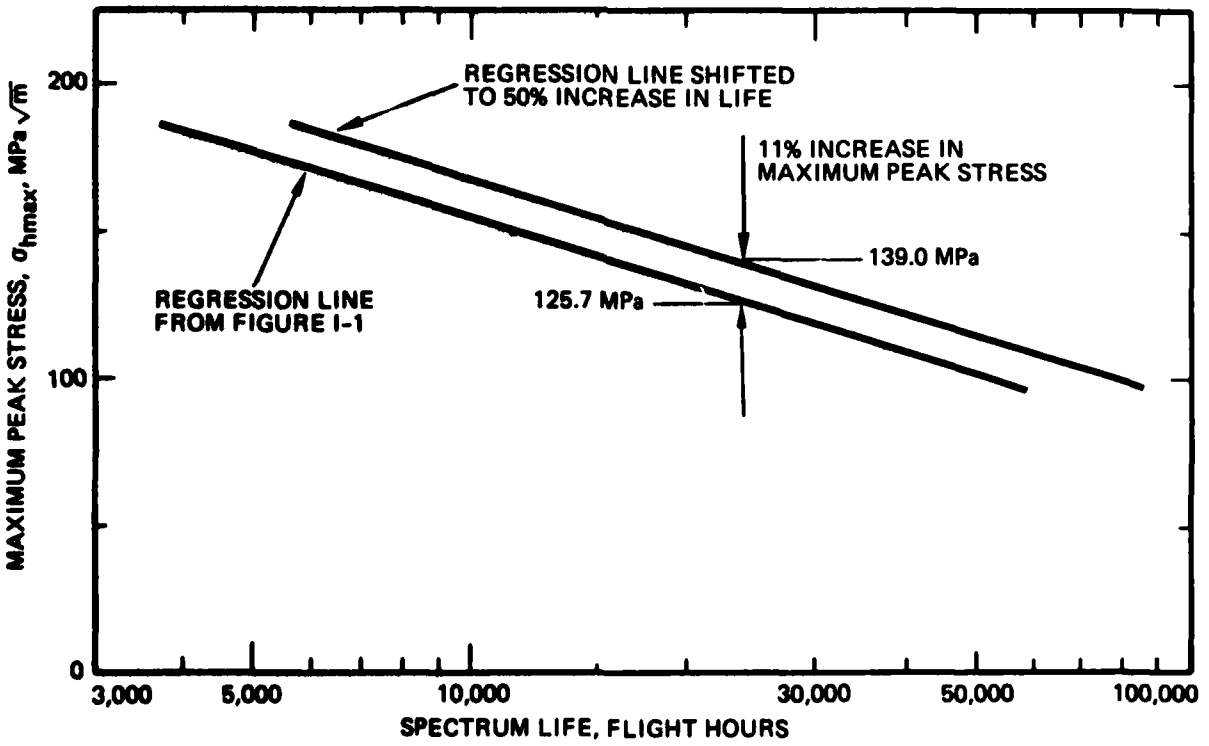

FIGURE I-2. ANALYSIS

REFERENCES

1. G.R. Chanani, "Fundamental Investigation of Fatigue Crack Growth Retardation in Aluminum Alloys," AFML-TR-76-156, 1976.

2. T.H. Sanders, R.R. Sawtell, J.T. Staley, R.J. Bucci, A.B. Thakker, "The Effect of Microstructure on Fatigue Crack Growth of 7XXX Aluminum Alloys Under Constant Amplitude and Spectrum Loading," NADC Contract No. N00019-76-C-0482, 1978.

3. R.J. Bucci, A.B. Thakker, T.H. Sanders, R.R. Sawtell, J.T. Staley, "Ranking 7XXX Aluminum Alloy Fatigue Crack Growth Resistance Under Constant Amplitude and Spectrum Loading," ASTM STP 714, 1980.

4. R.J. Bucci, "Spectrum Loading – A Useful Tool to Screen Effects of Microstructure on Fatigue Crack Growth Resistance," ASTM STP 631, 1977.

5. O. Jonas and R.P. Wei, "An Exploratory Study of Delay in Fatigue-Crack Growth," Int. J. of Fracture Mechanics, Vol. 7, p. 116, 1971.

6. J. Schijve, "Effect of Load Sequences on Crack Propagation Under Random and Program Loading," Eng. Frac. Mech., Vol. 5, p. 269, 1973.

7. R.I. Stephens, D.K. Chen and B.W. Hom, "Fatigue Crack Growth With Negative Stress Ratio Following Single Overloads in 2024-T3 and 7075-T6 Aluminum Alloys," ASTM STP 595, 1976.

8. W.X. Alzos, A.C. Skat, Jr., and B.M. Hillberry, "Effect of Single Overload/Underload Cycles on Fatigue Crack Propagation," ASTM STP 595, 1976.

9. G.R. Chanani, "Effect of Thickness on Retardation Behavior of 7075 and 2024 Aluminum Alloys," ASTM STP 631, 1977.

10. G.R. Chanani, "Investigation of Effects of Saltwater on Retardation Behavior of Aluminum Alloys," ASTM STP 642, 1977.

11. J. Schijve, "Observations on the Prediction of Fatigue Crack Growth Propagation Under Variable-Amplitude Loading," ASTM STP 595, 1976.

12. R.J.H. Wanhill, "Maneuver Spectrum Fatigue Crack Propagation in Aluminum Alloy Sheet Materials," NLR-TR-78091-U, May 1980.

13. H.D. Dill, C.R. Saff and J.M. Potter, "Effects of Fighter Attack Spectrum on Crack Growth," ASTM STP 714, 1980.

14. P.R. Abelkis, "Effect of Transport Aircraft Wing Loads Spectrum Variation on Crack Growth," ASTM STP 714, 1980.

15. J.T. Staley, "Microstructure and Toughness of High Strength Aluminum Alloys," ASTM STP 605, 1976.

16. W.G. Truckner, J.T. Staley, R.J. Bucci, and A.B. Thakker, "Effects of Microstructure on Fatigue Crack Growth of High Strength Aluminum Alloys," AFML-TR-76-169, 1976.

17. J.T. Staley, W.G. Truckner, R.J. Bucci, and A.B. Thakker, "Improving Fatigue Resistance of Aluminum Aircraft Alloys," Aluminum 11, 53, 1977.

18. T.H. Sanders, Jr., and J.T. Staley, "Review of Fatigue and Fracture Research on High-Strength Aluminum Alloys," Fatigue and Microstructure, Metals Park: American Society for Metals, 1979.

19. P.E. Bretz, A.K. Vasudevan, R.J. Bucci, and R.C. Malcolm, "Effect of Microstructure on 7XXX Aluminum Alloy Fatigue Crack Growth Behavior Down to Near-Threshold Rates," Final Report, Naval Air Systems Command, Contract N00019-79-C-0258, 1981.

20. J. Willenborg, R.M. Engle, and H.A. Wood, "A Crack Growth Retardation Model Using an Effective Stress Concept," TM-71-1-FBR, WPAFB, Ohio, 1971.

21. O.E. Wheeler, "Crack Growth Under Spectrum Loading," J. of Basic Eng. Trans. ASME, p. 181, March 1972.

22. W. Elber, "The Significance of Fatigue Crack Closure," ASTM STP 486, 1971.

23. H.D. Dill and C.R. Saff, "Effects of Fighter Attack Spectrum on Crack Growth," AFFDL-TR-76-112, March 1977.

24. G.R. Chanani and B.J. Mays, "Observation of Crack-Closure Behavior After Single Overload Cycles in 7075-T6 SEN Specimens," Eng. Fract. Mech., Vol. 9, p. 65, 1977.

25. G.R. Chanani, "Determination of Plastic-Zone Sites at Fatigue Cracks by Optical Interference Technique," Int. J. of Fracture, Vol. 13, p. 394, 1977.

26. R.L. Jones and T.E. Cagle, "The Mechanical Stress-Corrosion, Fracture Mechanics, and Fatigue Properties of 7050, 7475, and Ti-8Mo-8V-2Fe-3A1 Plate and Sheet Alloys," Report FGT-5791, General Dynamics, 1976.

27. G.R. Chanani, I. Telesman, P.E. Bretz, and G.V. Scarich, "Methodology for Evaluation of Fatigue Crack-Growth Resistance of Aluminum Alloys under Spectrum Loading," Final Report (Phase I Report), Naval Air Systems Command, Contract N00019-80-C-0427, April 1982.

28. A. Saxena, S.J. Hudak, Jr., J.K. Donald, and D.W. Schmidt, "Computer Controlled K-Decreasing Test Technique for Low Rate Fatigue Crack Growth Testing," JETVA, Vol. 6, 1978.

29. R.J. Bucci, "Development of a Proposed Standard Practice for Near-Threshold Fatigue Crack Growth Rate Measurements," ASTM STP 738, 1981.

30. R.M. Wetzel (Ed.), Fatigue Under Complex Loading – Analysis and Experiment, SAE Advances in Engineering, Vol. 6, pp. 159-162, 1977.

31. R. Marrisen, K.H. Trautmann, and H. Nowack, "Analysis of Sequence Effects under Variable Amplitude Loading on the Basis of Recent Crack Propagation Models," Presented at the TMS-AIME Fall Meeting, 24-28 October 1982, St. Louis.

32. W.J. Mills and R.W. Hertzberg, "Load Interaction Effects on Fatigue Crack Progation in 2024-T3 Aluminum Alloy," Eng. Frac. Mech, Vol. 8, p. 657, 1976.

33. J.C. McMillan and R.W. Hertzberg, "Application of Electron Fractography to Fatigue Studies," ASTM STP 436, p. 89, 1968.

34. T.M. Hsu and W.M. McGee, "Effects of Compressive Loads on Spectrum Fatigue Crack Growth Rate," ASTM STP 714, p. 79, 1980.

35. E.A. Starke and F.S. Lin, "The Influence of Grain Structure on the Ductility of the Al-Cu-Li-Mn-Cd Alloy 2020," Met. Trans. A, Vol. 13, p. 2259, 1982.

36. Von K. Schneider and M. Von Heimandahl, Z. Metallkde., "Precipitation Behaviour of a Commercial Aluminium Copper Lithium Alloy Part I; The Microstructure After Isothermal Heat Treatment," Vol. 64, p. 342, 1973.

37. E.J. Coyne, Jr., and E.A. Starke, Jr., "The Effect of Microstructure on Fatigue Crack Growth Behavior of an Al-Zn-Mg-(Zr) Alloy," Int. J. of Fracture, Vol. 15, p. 405, 1979.

38. J.F. Knott and A.C. Pickard, "Effects of Overloads on Fatigue Crack Propagation: Aluminum Alloys," Metal Science, p. 399, 1979.

39. B.R. Kirby and C.J. Beevers, "Slow Fatigue Crack Growth and Threshold Behavior in Air and Vacuum of Commercial Aluminum Alloys," Fatigue of Engr. Matls Str., Vol. 1, p. 203, 1979.

40. R.C. Malcolm, A.K. Vasudevan, R.J. Bucci, and P.E. Bretz, "Evaluation of the Engineering Properties of a Commercially Produced Aluminum Alloy 2020-T651 Plate," Amendment to Naval Air Systems Command Final Report, Contract N00019-79-C-0258, 1981.

41. Alcoa unpublished research.

42. R.W. Hertzberg and W.J. Mills, "Character of Fatigue Fracture Surface Micromorphology in the Ultra-Low Growth Rate Regime," ASTM STP 600, 1976.

43. G.R. Yoder, L.A. Cooley, and T.W. Crooker, "Observations on the Generality of the Grain-Size Effect on Fatigue Crack Growth in Alpha Plus Beta Titanium Alloys," NRL Memorandum Report 4232, Naval Research Laboratory, 1980.

44. G.M. Lin and M.E. Fine, "Effect of Grain Size and Cold Work on the Near Threshold Fatigue Crack Propagation Rate and Crack Closure in Iron," Scripta Met., Vol. 16, p. 1249, 1982.

45. J.I. Petit and P.E. Bretz, "The Effect of Recrystallization on the Microstructure and Fatigue Properties of a 2XXX-Type P/M Alloy," Presented at the AIME 111th Annual Meeting, Dallas, Texas, 17 February 1982.

46. Naval Air Systems Command Contract No. N00019-80-C-0569.

DISTRIBUTION LIST

(One copy unless otherwise noted)

Mr. M. Valentine
AIR-5304B4
Naval Air Systems Command
Washington, D.C. 20361
(10 copies)

Richard Schmidt, Code 320A
Naval Air Systems Command
Washington, D.C. 20361
(2 copies)

Commander
Naval Air Development Center
(Code 302)
Warminster, PA 18974

Naval Sea Systems Command
(Code 03423)
Department of the Navy
Washington, D.C. 20360

Navy Ships Research & Development Center
(Code 2812)
Annapolis, MD 21402

Commander Naval Surface/Weapons Center
(Metallurgy Division)
White Oak
Silver Spring, MD 20910

Director, Naval Research Laboratory
(Codes: 6380, 6384, 6490, 6601, 8430) – 1 each
Washington, D.C. 20390

Office of Naval Research
The Metallurgy Program, Code 471
Arlington, VA 22217

A.P. Divecha, R32
Naval Surface Weapons Center
White Oak, Laboratory
Silver Spring, MD 20910

Naval Surface Weapons Center
Library – X211
White Oak, Silver Spring, MD 20910

Dr. T.R. McNelley
Department of Mechanical Engineering
(Code 59)
Naval Postgraduate School
Monterey, CA 93940

(14 copies) (12 copies for DDC, 2 copies for AIR-954)
Commander, Naval Air Systems Command
AIR-954
Washington, D.C. 20361

Wright-Patterson Air Force Base
Ohio 45433
Attn: W. Griffith, AFWAL/MLLS

Wright-Patterson Air Force Base
Ohio 45433
Attn: A. Gunderson, AFWAL/FIBAA

Wright-Patterson Air Force Base
Ohio 45433
Attn: C.L. Harmsworth, AFWAL/MLSA

Wright-Patterson Air Force Base
Ohio 45433
Attn: G.J. Petrak, AFWAL/MLSA

Wright-Patterson Air Force Base
Ohio 45433
Attn: Dr. T. Ronald, AFWAL/MLLS

Army Materials & Mechanics
Research Center
Watertown, MA 02172
Attn: Dr. A. Gorum

Commanding Officer
Office of Ordnance Research
Box CM, Duke Station
Durham, NC 27706

U.S. Army Armament R&D Command
(ARRADCOM)
Dover, NJ 078901
Attn: Dr. J. Waldman
DRDAR-SCM-P, Bldg. 3409

National Aeronautics & Space Administration
(Code RWM)
600 Independence Avenue, S.W.
Washington, D.C. 20546

National Aeronautics & Space Administration
Langley Research Center
Materials Division, Langley Station
Hampton, VA 23365
Attn: Mr. H.F. Hardrath
Stop 188M

National Aeronautics & Space Administration
Marshall Space Flight Center
Huntsville, AL 35812
Attn: Osmer White
MS-AS246

National Academy of Science
Materials Advisory Board
Washington, D.C. 20418
Attn: Dr. J. Lane

Director
National Bureau of Standards
Washington, D.C. 20234
Attn: Dr. E. Passaglia

Battelle Memorial Institute
505 King Avenue
Columbus, OH 43201
Attn: Mr. Stephan A. Rubin, Mgr.
Information Operations

IIT Research Institute
Metals Research Department
10 West 35th Street
Chicago, IL 60616
Attn: Dr. N. Parikh

General Dynamics Convair Division
P.O. Box 80847
San Diego, CA 92138
Attn: Mr. Jack Christian
Code 643-10

General Dynamics Corporation
Convair Aerospace Division
Fort Worth Operation
P.O. Box 748
Fort Worth, TX 76101
Attn: Tom Coyle
E. Balmuth

Kaman Aerospace Corporation
Old Windsor Road
Bloomfield, CT 06001
Attn: Mr. M.L. White

Rockwell International
Columbus Division
Columbus, OH 43216
Attn: Mr. P. Maynard, Dept. 75
Group 521

Rockwell International
Rocketdyne Division
Canoga Park, CA 91305
Attn: Dr. Al Jacobs
Group Scientist
Materials Branch

Rockwell International
Los Angeles Division
International Airport
Los Angeles, CA 90009
Attn: Gary Keller
Materials Applications

Autonetics Division of Rockwell International
P.O. Box 4173
Anaheim, CA 92803
Attn: Mr. A.G. Gross, Jr.
Dept. 522-92

Rockwell International
P.O. Box 1082
1027 Camino Dos Rios
Thousands Oaks, CA 91320

Lockheed Palo Alto Research Laboratories
Materials Science Laboratory
3251 Hanover Street
Palo Alto, CA 94303
Attn: Dr. Frank A. Crossley
52-31/204

Lockheed California Company
P.O. Box 551
Burbank, CA 91503
Attn: Mr. J.M. VanOrden
Dept. 74-71, Bldg. 221,
Plt. 2

Lockheed-Georgia Company
Marietta, GA 30061
Attn: E. Bateh

Lockheed Missile & Space
Corporation
P.O. Box 504
Sunnyvale, CA 94088
Attn: Mr. G.P. Pinkerton
Bldg. 154, Dept. 8122
Mr. C.D. McIntyre
Bldg. 132, Dept. 84-13
(1 each)

Douglas Aircraft Company
3855 Lakewood Blvd
Long Beach, CA 90808
Attn: M.L. Tonkanian
Mail Code 35-14
Dept. C1-E83

Sikorsky Aircraft
Division of United Aircraft Corp.
Stratford, CT 06497
Attn: Materials Department

United Technologies Research
Laboratories
East Hartford, CT 06108
Attn: Mr. Roy Fanti

Pratt & Whitney Aircraft
Division of United Technologies
Florida Research and Development
Center
P.O. Box 2691
West Palm Beach, FL 33402

Boeing-Vertol Company
Boeing Center
P.O. Box 16858
Philadelphia, PA 19142
Attn: Mr. J.M. Clark

The Boeing Company
Commercial Airplane
P.O. Box 3707
Seattle, WA 98124
Attn: Cecil E. Parsons
MS77-18, ORG. 6-8733
W.E. Quist
MS73-43, ORG. B-8505
(2 copies)

The Boeing Company
12842 72nd Avenue, N.E.
Kirkland, WA 98033
Attn: Mr. W. Spurr

Northrop Corporation
Aircraft Division
One Northrop Avenue
Hawthorne, CA 90250
Attn: Mr. Allan Freedman
Dept. 3871/62

Vought Corporation
P.O. Box 5907
Dallas, TX 75222
Attn: Mr. A. Hohman

Vought Corporation Advanced
Technology Center
P.O. Box 225-9070
Dallas, TX 75265
Attn: S.W. McClaren
MS 220-57

McDonnell Aircraft Company
St. Louis, MO 63166
Attn: Mr. H.J. Siegel
Materials & Processes Division
General Engineering Division

AVCO Lycoming Division
550 S. Main Street
Stratford, CT 06497
Attn: Mr. Barry Goldblatt

Avco Space Systems Division
Lowell Industrial Park
Lowell, MA 01851

Detroit Diesel Allison Division
General Motors Corporation
Materials Laboratories
Indianapolis, IN 46206

AiResearch Manufacturing Company
of America
Sky Harbor Aircraft
402 S. 36th Street
Phoeniz, AZ 85034
Attn: Mr. Jack D. Tree
Dept. 93-35-5M

Solar
2200 Pacific Highway
San Diego, CA 92112
Attn: Dr. A.G. Metcalfe

Teledyne CAE
1330 Laskey Road
Toledo, OH 43601

Dr. Charles Gilmore
Tompkins Hall
George Washington University
Washington, D.C. 20006

Westinghouse Electric Company
Materials & Processing Laboratories
Beulah Road
Pittsburgh, PA 15235
Attn: Don E. Harrison

Dr. John D. Wood
Associate Professor
Lehigh University
Bethlehem, PA 18015

Dr. A.I. Mlavsky
Senior Vice President for Technology
and Director of Corporate
Technology Center
Tyco Laboratories, Inc.
16 Hickory Drive
Waltham, MA 02145

Dr. Howard Bomberger
Reactive Metals, Inc.
Niles, OH 44446

Dr. John A. Schey
Department of Materials Engineering
University of Illinois at Chicago
Circle
P.O. Box 4348
Chicago, IL 60680

P.R. Mallory & Company, Inc.
3029 East Washington Street
Indianapolis, IN 46206
Attn: Technical Librarian

Southwest Research Institute
8500 Culebra Road
P.O. Box 28510
San Antonio, TX 78284
Attn: Dr. C. Gerald Gardner

Brush Wellman, Inc.
17876 St. Clair Avenue
Cleveland, OH 44110
Attn: Mr. Bryce King

Kawecki Berylco Industries
P.O. Box 1462
Reading, PA 19603

Linde Company
Division of Union Carbide
P.O. Box 44
Tonawanda, NY 14152

Midwest Research Institute
425 Volker Boulevard
Kansas City, MO 64110

University of California
Lawrence Radiation Laboratory
P.O. Box 808
Livermore, CA 94550
Attn: Mr. L.W. Roberts

ERDA Division of Reactor Development
and Technology
Washington, D.C. 20545
Attn: Mr. J.M. Simmons, Chief
Metallurgy Section

Dr. W.C. Setzer, Director
Metallurgy & Surface Technology
Consolidated Aluminum Corporation
P.O. Box 14448
St. Louis, MO 63178

Aluminum Company of America
1200 Ring Bldg.
Washington, D.C. 20036
Attn: Mr. G.B. Barthold

Aluminum Company of America
Alcoa Center, PA 15069
Attn: Mr. Paul L. Mehr

Kaiser Aluminum Chemical Corporation
Aluminum Division of Research Center for Technology
P.O. Box 870
Pleasanton, CA 94566
Attn: T.R. Prichett

Reynolds Metals Company
Metallurgical Research Division
4th & Canal Streets
Richmond, VA 23219
Attn: Dr. Grant Spangler

The Dow Metal Products Company
2020 Dow Center
Midland, MI 48640
Attn: Gloria Byrnes
Inorganic Chemicals

Dr. F.N. Mandigo
Olin Metals Research Laboratories
91 Shelton Avenue
New Haven, CT 06515

Martin Marietta Aluminum
19200 South Western Avenue
Torrance, CA 90509
Attn: Mr. Paul E. Anderson
(M/C 5401)

Martin Marietta Corporation
P.O. Box 5837
Orlando, FL 32805
Attn: Dr. Richard C. Hall
Mail Point 275

General Electric Company
Corporate Research & Development
Bldg. 36-441
Schenectady, NY 12345
Attn: Dr. J.H. Westbrook, Manager
Materials Information Services

General Electric Company
Corporate Research & Development
P.O. Box 8
Schenectady, NY 12301
Attn: Dr. D. Wood

General Electric
Missile & Space Division
Materials Science Section
P.O. Box 8555
Philadelphia, PA 91901
Attn: Technical Library

General Electric Company
Turbine Business Group
Bldg. 41, Room 307
Schenectady, NY 12345
Attn: H. Saunders

General Electric Company
Aircraft Engine Group
Materials & Processes Technology Laboratories
Evendale, OH 45315

Dr. E.A. Starke, Jr.
Department of Materials Science
School of Engineering and Applied Science
University of Virginia
Charlottesville, VA 22903

Dr. S.D. Antolovich
School of Chemical Engineering and Metallurgy
Georgia Institute of Technology
Atlanta, GA 30332

Dr. R. Balluffi, Chairman
Department of Materials Science & Engineering
Bard Hall
Cornell University
Ithaca, NY 14853

Dr. D.J. Duquette
Materials Engineering Department
RPI
Troy, NY 12181

S. Suresh
Department of Materials Science and Mineral Engineering and Lawrence Berkeley Laboratory
University of California
Berkeley, CA 94720


FILM